AD-A151 238 CORROSION CONTROL THROUGH A BETTER UNDERSTANDING OF THE METALLIC SUBSTRAT..(U) LEHIGH UNIV BETHLEHEM PA CENTER FOR SURFACE AND COATINGS RESE.. E M ALLEN ET AL. 1/3

UNCLASSIFIED 13 DEC 84 N00014-79-C-0731 F/G 11/3 NL

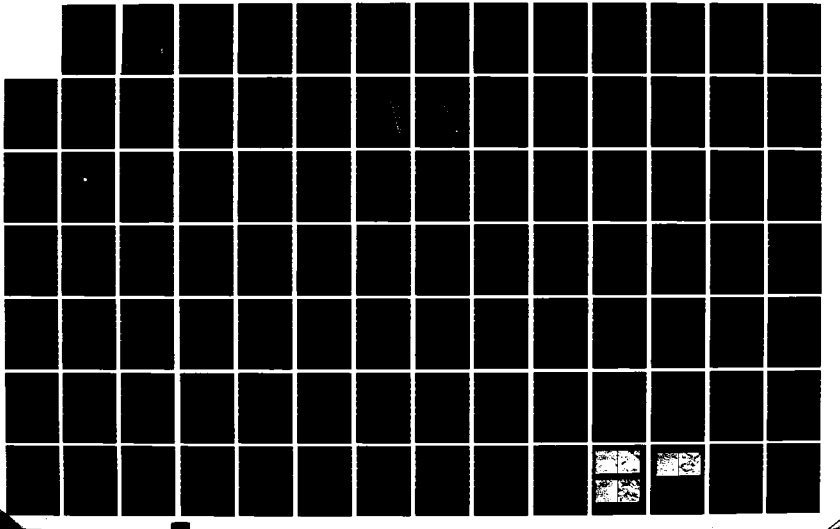

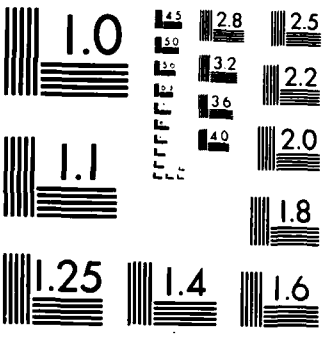

CORROSION CONTROL THROUGH A BETTER UNDERSTANDING OF THE METALLIC SUBSTRATE/ORGANIC COATING/INTERFACE

Agreement No. N00014-79-C-0731

Fifth Annual Report

Covering the Period

October 1, 1983 - September 30, 1984

Sponsor: Office of Naval Research

Washington, D.C.

Principal Investigator: Henry Leidheiser, Jr.

Co-Investigators: Eugene M. Allen
Frederick M. Fowkes
Richard D. Granata
Roland W. Lovejoy
Jack F. McIntyre
John A. Manson
Fortunato J. Micale
Gary W. Simmons

Center for Surface and Coatings Research
Lehigh University
Bethlehem, PA 18015

December 13, 1984

TABLE OF CONTENTS

CONTENTS (Cont'd.)

FOREWORD

This report represents the fifth annual summary of research carried out under Office of Naval Research Contract No. N00014-79-C-0731. The objective of this research is to obtain a better understanding of the metallic substrate/organic coating/interface system so that improvements may be made in corrosion control of metals by painting. The report this year includes a summary of progress made in 14 different components of the program. These activities are concerned with (a) the chemical nature of the oxide on the surface of steel; (b) the loss of adhesion of an organic coating on a metal; (c) chemical modification of the surface of a metal; (d) the detection of water in a coating; and (e) the transport of species through organic coatings. Each of the 14 components has been authored by the co-principal director or an associate and there is a difference in the style of presentation. It should be noted that the material has been organized into a logical sequence of the divisions noted above and the number assigned to a program is not necessarily the same as the number in the fourth annual report. The report has been written so that it is self-standing and there is no need to refer to previous reports.

It is recognized that readers of this report will be interested in the contents for different purposes. In an effort to accommodate to these diverse interests, the report is presented in the following format:

(1) A list of public disclosures of the research. The references may be useful to those who wish to explore the research results in greater detail.

(2) A condensation of the total program. This summary is aimed at those who wish to obtain an overview of the program and the approaches being used.

(3) A more detailed outline of the results generated during the present report period.

SECTION I

A List of Public Disclosures of the Research during the Period, October 1, 1983 - September 30, 1984

Published Papers

"Metal/Flame-Sprayed-Aluminum Inteface as Studied by Emission Mössbauer Spectroscopy," Henry Leidheiser, Jr., Herbert Herman, R. A. Zatorski, Svetozar Musić, and Attila Vértes, J. Electrochem. Soc. 131, 1348-49 (1984).

"The Importance of Alkali Metal Cations in Acid Environments in Contact with Corrosion-Protective Coatings," Henry Leidheiser, Jr., Hyacinth Vedage, Richard D. Granata, and Malcolm L. White, J. Electrochem. Soc. 131, 1460-61 (1984).

"The Improved Corrosion Resistance of Steel in Mild Media after Abrasive Blasting with Alumina," Henry Leidheiser, Jr., Svetozar Musić, and J. F. McIntyre, Corrosion Science 24, 197-208 (1984).

"Corrosion and Coating Delamination Properties of Steel Ion-Implanted with Aluminum and Titanium," R. D. Granata, M. A. DeCrosta and H. Leidheiser, Jr., Proceedings of the International Congress on Metallic Corrosion, Toronto, Canada, June 3-7, 1984, pp. 264-68

"Characterization of Phosphate Conversion Coatings by Laser Raman Spectroscopy," A. J. Sommer and Henry Leidheiser, Jr., Proceedings of the 19th Annual Conference of the Microbeam Analysis Society, Bethlehem, PA., A. D. Romig, Jr., and J. I. Goldstein, Editors, San Francisco Press, Inc., 1984, pp.111-14.

"The Composition and Properties of a Protective Layer Formed on a Steel by Anodizing with 8-Hydroxyquinoline," Hidetaka Konno, Masaichi Nagayama, Henry Leidheiser, Jr., and Richard D. Granata, J. Metal Finishing Soc. of Japan 35, No. 8, 402-08 (1984).

Reprint of paper, "Corrosion of Painted Metals - a Review," Henry Leidheiser, Jr., in the book, "Corrosion Source Book," Seymour K. Coburn, Editor, American Society for Metals and National Association of Corrosion Engineers (1984), pp.215-24.

"A Model for the Quantitative Interpretation of Cathodic Delamination," Wendy Wang and Henry Leidheiser, Jr., in Proceedings of an International Symposium Honoring Marcel Pourbaix on His Eightieth Birthday, "Equilibrium Diagrams Localized Corrosion," R. P. Frankenthal and J. Kruger, Eds., Proceedings Vol. 84-9, The Electrochemical Society, Pennington, NJ, 1984, pp.255-66.

"Migration of Ionic Species through Organic Coatings and Its Relationship to Cathodic Delamination," Jeffrey Parks and Henry Leidheiser, Jr., Proceedings of XVII. FATIPEC Lugano (Switzerland), Vol III 1984, Nr. 70, pp. S.517-35.

"Environmental Control or Coatings Composition As a Means for Reducing Cathodic Delamination of Organic Coatings," Henry Leidheiser, Jr., Wendy Wang, Richard D. Granata, Hyacinth Vedage, and Malcolm L. White, J. Coatings Tech. 56, No. 717, October 1984, pp. 55-56.

"A Mössbauer Spectroscopic Study of Rust Formed during Simulated Atmospheric Corrosion," Henry Leidheiser, Jr., and Ilona Czakó-Nagy, Corrosion Science 24(7), 569-77 (1984).

"Protective Organic Coatings and the Coating/Metal Interface," Henry Leidheiser, Jr., In Proceedings - INTERFINISH '84, 11th World Congress on Metal Finishing, Jerusalem, Israel, October 21-26, 1984, pp.23-27.

"A Model for the Quantitative Interpretation of Cathodic Delamination," Wendy Wang and Henry Leidheiser, Jr., In Proceedings - INTERFINISH '84, 11th World Congress on Metal Finishing, Jerusalem, Israel, October 21-26, 1984, pp. 262-69.

"Inhibition Methods for Semiconducting Protective Oxides on Mild Steel," R. D. Granata, Paper No. 124, National Association of Corrosion Engineers, Corrosion '84 Conference, 1984.

"Acid-Base Contributions to Polymer-Filler Interactions," Rubber Chem. & Tech. 57, 328-43 (1984).

"Drying and Curing of Epoxy Resin-Curing Agent Systems," Ata-ur Rahman, M.S. Report, Polymer Science & Engineering, October 1983.

"Some Effects of Acid-Base Interactions," A. C. Tiburcio, M.S. Report, Chemical Engineering, October 1983.

"Cathodic Blistering," Valmore Rodriguez, M.S. Report, Chemical Engineering, January 1985.

"The Mechanism for Cathodic Delamination Process at the Organic Coating/Metal Substrate Interface," Wendy, Ching-Yung Wang, Ph.D. Thesis, Chemical Engineering, January 1984.

"Characterization of Acid-Base Properties of the Hydrated Iron Oxide and Titanium Oxide on Metal Surfaces by XPS and AES," Bruce C. Beard, Ph.D. Thesis, Chemistry, June 1984.

"Characterization of the Acidic Surface Sites on -Ferric Oxide Using Flow Microcalorimetry," Sara T. Joslin, Ph.D. Thesis, Polymer Science and Engineering, October 1984.

"Development and Application of High Frequency Dielectric Spectroscopy in Studies of Water in Organic Coatings," Douglas J. Eadline, Ph.D. Thesis, Chemistry, October 1984.

"Water and Ion Diffusion through Organic Coatings on Steel and the Cathodic Delamination Process," Jeffrey M. Parks, Ph.D. Thesis, Physical Chemistry, January 1985.

Papers Submitted, Accepted or in Press

"A Mathematical Model for the Cathodic Delamination of Organic Coatings," Wendy Wang and Henry Leidheiser, Jr., Submitted to I&EC Prod. R&D.

"Oxygen Diffusion through Organic Free Films Exposed to Aqueous Solutions," Wayne Bilder and Henry Leidheiser, Jr., Submitted to I&EC Prod. R&D.

"Resistance Measurements on Thin Film Substrates as a Technique for Studying the Deterioration of Coated Metals," J. F. McIntyre and H. Leidheiser, Jr., Submitted to I&EC Prod. R&D.

"Ionic Diffusion through Organic Coatings and Its Consequences to Corrosion," J. Parks and H. Leidheiser, Jr., Submitted to I&EC Prod. R&D.

"Acid-Base Effects in Glass-Bead/Phenoxy Model Coating Systems," Astrophel C. Tiburcio and John A. Manson, Submitted to I&EC Prod. R&D.

"Laser Raman Study of the Homogeneity of Epoxy-Amine Coatings," Eugene M. Allen, Submitted to I&EC Prod. R&D.

"Surface Acidity of Ferric Oxides Studied by Flow Microcalorimetry," Sara T. Joslin and Frederick M. Fowkes, Submitted to I&EC Prod. R&D.

"High Frequency Time Domain Dielectric Spectrometer for the Determination of Water in Polymer Coatings on Metal Substrates," Douglas J. Eadline and Henry Leidheiser, Jr., Submitted to Review of Scientific Instruments.

"Corrosion beneath Polymeric Coatings on Thin Metal Films as Studied Using Concurrent AC Impedance and Parallel DC Resistance Measurements," J. F. McIntyre and H. Leidheiser, Jr., Submitted to J. Electrochem. Soc.

"Characterization of Acid-Base Properties of the Hydrated Iron Oxide and Titanium Oxide on Metal Surfaces by XPS and AES," Bruce C. Beard and Gary W. Simmons, to be submitted.

"Characterization of Surface Properties of Iron Oxides," F. J. Micale, D. J. Kiernan, A. C. Zettlemoyer, Submitted to J. Colloid Interface Sci.

SECTION 2

A Summary of the Experimental Results Obtained during the Period, October 1, 1983 - September 30, 1984

A summary is given herein of the total research program, the components of which are directed by 7 Lehigh faculty members, a research scientist and a research associate. Detailed summaries of the programs are given in the body of the report.

The research efforts are directed towards a better understanding of the metal substrate, the interface between the metal and the coating, and the organic coating.

The interaction between an organic coating and a steel substrate and the interaction of inorganic fillers and pigments with the organic matrix are determined in good part by acid/base interactions. Three studies have been carried out in order to increase our understanding of these effects.

The properties of large-area iron oxides were investigated as model corrosion products or model oxide-covered iron surfaces. All the iron oxides are hydrophilic and contain high concentrations of hydroxyl groups. These surface hydroxyls can be used to interact quantitatively with hydrophobing agents such as dimethyldisilazane (HMDS) or other coupling agents capable of interacting with protective coatings for the purpose of promoting adhesion. Methanol is a very efficient hydrophobing agent for α-Fe_2O_3 when the oxide is previously heated at 400°C in vacuum.

The acid/base nature of α-Fe_2O_3 was studied using adsorption of nitrogen and oxygen bases from neutral hydrocarbons onto the surface sites. The technique utilized was flow calorimetry. The heats of adsorption were critically dependent on the amount of adsorbed moisture. The acidic surface FeOH sites were found to be hard acids with a range of acid strengths in agreement with studies based on electrophoretic measurements.

The studies with high-area iron oxides were complemented with a study of the hydroxyl groups on the oxide present on iron panels. High resolution oxygen spectra of the hydrated oxide on iron indicated the presence of hydroxyls with concentrations of 2-4 hydroxyls/nm^2. The surface hydroxyls exchanged with potassium as a function of pH at high pH and with phosphate in the neutral to slightly alkaline pH range. These data were utilized to determine the equilibrium for surface $FeOH_2^+$ groups.

The major damage on a coated metal exposed to an aggressive environment occurs in the interfacial region between the metal and the coating and is a result of the cathodic reaction which generates hydroxyl ions. The local strong alkalinity leads to dissolution of material in the interfacial region or attack of the polymer with a consequent loss in adhesion of the coating. Three studies are being carried out in an effort to modify the metal surface such that it is a poor catalyst for the cathodic oxygen reduction reaction.

One of these is concerned with modifying the surface by abrasive blasting and the other two are concerned with changing the surface character by reaction of materials with the -OH groups on the iron oxide that normally is present on the surface of iron on exposure to the atmosphere.

Steel surfaces, coated with a thin layer of evaporated second metal, were abrasively blasted in efforts to modify the surface chemistry of the steel. Changes in the electrochemical properties of such surfaces were attributed to variations in surface profile, alterations in the stress state of the surface, and chemical changes in the oxides or other surface species. In general, abrasively blasted steel surfaces have a higher corrosion resistance in mild media than non-abrasively treated surfaces. Unusual, and unexplained, corrosion resistance was observed when steel surfaces were abrasively blasted with glass beads coated with sodium benzoate.

Two techniques for modifying the surface of iron look promising, one based on anodization in the presence of aluminum cations and the other based on reaction with a titanium coupling agent. Two-step anodizations yield surfaces of iron with slightly modified surface activities. The oxide film in both cases appears to be more stable. Silanation of iron surfaces by simple dipping in aqueous solutions also shows promise as a means for modifying the corrosion and catalytic properties of iron.

Commercial metal surfaces are often modified by coating the surface with a phosphate, the most common of which is a zinc phosphate. Solution studies, Raman microprobe spectroscopy and electron microprobe analyses have shown that dissolution rates of the phosphate increase with increase in pH and that precipitation of a zinc oxide or zinc hydroxy carbonate occurs on the surface of the phosphate. The rate of dissolution of the phosphate was a function of the alkali metal ion in the solution and the rate increased in the order: LiOH, CsOH, KOH, NaOH.

A sensitive technique was developed for following changes in the metallic substrate in the case of a coated metal exposed to an aqueous environment. A coating is applied to a thin metal film on glass and the parallel DC conductivity of the metal is followed by a variation of the four-point probe method. Impedance measurements and microscopic studies of the interface through the glass backing were made simultaneously with the parallel DC measurements. The technique is very sensitive and changes in the parallel DC conductivity are observed before corrosion is signaled by the AC impedance values.

Phosphate coatings provide improved resistance to cathodic delamination, i.e., the loss of adherence that occurs when metal with a defect is subjected to an applied cathodic potential. The rate of cathodic delamination of an epoxy coating on steel is strongly a function of the alkali metal cation present in the medium and increases in the order, lithium, sodium, cesium and potassium. This order is interpreted in terms of an integration of the rate of diffusion of the alkali metal to the delaminating front and the rate of dissolution of the phosphate.

New ways are being sought to determine the presence of aqueous phase water at the coating/metal interface, since aqueous phase water is the

precursor to corrosion at the interface. Two methods are being explored. First, the incorporation of a probe molecule such as 2,2'-bipyridine at the coating/metal interface looks promising as a water detection technique. This molecule upon reaction with ferrous ion yields a complex when dissolved in water that has a resonance Raman band of very high intensity. The method will be useful with transparent coatings. Second, high frequency dielectric spectroscopy at 10^8 to 10^{10} Hz may be used to detect water in an organic coating. The method has proven to be sensitive to the presence of water in all coatings studied to date, including a vinyl ester, an acrylic and an alkyd. More work remains to be done in order to deconvolute the spectra such that the aqueous phase portion can be differentiated from the mobile or gas-like water in the coating.

Reactions at the metal/organic coating interface are dependent upon the rate at which reactive species, such as anions, cations, water and oxygen reach the interface. The diffusion rates of sodium, chloride and cesium ions through an alkyd topcoat, an alkyd topcoat plus primer and polybutadiene on steel were determined. Cathodic polarization resulted in a 3- to 28-fold increase in the rate of ion uptake, and presumably ion migration, th· the coating. The major pathway for ionic diffusion under cathodic riza· tion conditions was through the coating. Lateral diffusion from t _ defect to the delamination front appeared to be the principal transport pathva· at open circuit. The ion flux was sufficient to account for the observe· _- lamination rate under cathodic polarization when certain assumptions were made.

Oxygen diffusion through a polyethylene film under conditions designed to reflect conditions existing during cathodic polarization of a coated metal was a function of the cation in the chloride solution and increased in the order, lithium, sodium, potassium. The differences in the rate of oxygen diffusion did not appear large enough to explain the strong cation dependence observed in cathodic delamination.

Inhomogeneities in a coating is a possible explanation for regions of high water migration through a coating. A laser Raman microprobe method was developed for determining the uniformity of distribution of the epoxy and amine components in an electrodeposited coating. A peak ratio method was suggested for determining the mol fraction of amine in the coating. Unwanted fluorescence was minimized by heating the sample while obtaining the spectrum.

A model system consisting of glass beads (to represent a filler or a pigment) and a linear high molecular weight phenoxy as binder was utilized to determine the effects of pigment/binder interaction on the permeability and other properties of coatings used for corrosion resistance. The enthalpy of adsorption of 6 organic compounds on glass beads was determined using an inverse gas chromatographic technique. The glass beads were observed to contain active sites with varying degrees of acidity. Untreated glass beads exhibited higher permeability to water vapor at 50°C than glass beads having adsorbed components on the surface. The treated glass/matrix system exhibited a higher permeability than the behavior predicted for the limiting case of good adhesion with an impermeable filler. The role of the solvent in determining the permeability characteristics is emphasized.

SECTION 3

INDIVIDUAL PROGRAMS

Program #1

Characterization of the Surface Properties of Iron Oxides

Principal Investigator: F. M. Micale
Prof. of Chemistry

Associate: Dennis Kiernan
Graduate Student

INTRODUCTION

The development of protective coatings for corrosive materials requires a knowledge not only of the physical properties of the coating, but also the nature of the interaction of the coating with the substrate and the affinity of the metal oxide/coating interface for water. Water plays an essential role in the corrosion of iron [1]. The growth of rust layers on ferrous metals in the atmosphere where water vapor is present, or the retention of water by certain soils are additional examples of the importance of the interaction of iron oxide with water. In addition, an understanding of the iron oxide-water system should provide insight into the broader problem involving adsorption of polar gas on an ionic solid. The experimental approaches used to study the surface properties of materials require high-surface-area, small-particle-size samples. Mössbauer spectroscopic and X-ray diffraction techniques have shown that α-Fe_2O_3, Fe_3O_4, γ-FeOOH, and β-FeOOH, among others, are present as corrosion products on iron exposed to the atmosphere [2].

Although a large body of literature exists in the area of gas adsorption on metal oxide surfaces, relatively little has been published for the adsorption of gases on iron oxides. Previous investigations in this laboratory by McCafferty and Zettlemoyer [3] studied the interaction of water vapor with α-Fe_2O_3 using heat of immersion [4], dielectric techniques [5,6], and adsorption thermodynamics. They concluded [7] that water vapor chemisorbs on bare α-Fe_2O_3 by a dissociative mechanism to form two hydroxyls per water molecule, the hydroxyl group adsorbing on a surface Fe^{3+} ion and the proton forming a second hydroxyl with an adjacent surface O^{2-} ion. The first layer of

physically adsorbed water vapor on the hydroxylated substrate is localized by double hydrogen bonding of a single water molecule to adjacent hydroxyl groups, as was shown by energetic, thermodynamic, and dielectric arguments. The multilayer adsorption was proposed to develop in an ordered ice-like structure. Blyholder and Richardson [8] applied infrared spectroscopy to the investigation of the α-Fe_2O_3/water system. They concluded that physically adsorbed water was completely removed by prolonged outgassing at 25°C and that underlying surface hydroxyls were totally removed at 475°C. Jurinak [9] investigated the interaction of water with α-Fe_2O_3 at various activation temperatures. He showed that about 1/3 of the α-Fe_2O_3 surface is covered with chemisorbed or strongly adsorbed water which, unless removed by high temperature activation, blocks water adsorption sites on the surface. Morimoto et al. [10] studied the amounts of chemisorbed and physisorbed water on α-Fe_2O_3. They took the hydroxyl groups remaining on the oxide surface into account and reported the ratio of the number of water molecules in the first physisorption layer to that of underlying hydroxyl groups to be about 1:2.

Modifications of surface properties by addition of surface-active materials to the surface hydroxyls of silica are relatively common. Hexamethyldisilazane (HMDS) was chosen for this investigation because it reacts quantitatively with surface hydroxyls from the vapor phase even at room temperature. The interaction of HMDS was first reported by Stark et al. [11] and the reaction kinetics have been explored by Hertl and Hair [12,13]. Kiselev and his co-workers [14] examined the reaction of trimethylchlorosilane (TMCS) with silica, as did Hair and Hertl [15] for all the methyl chlorosilanes. Zettlemoyer and Hsing [16,17] first examined water interaction with silane-treated silica by a NIR technique. They explored the possibility of the NH_3 adsorption of HMDS-treated silica. Kiselev and co-workers [18] also investigated the interaction of water with TMCS-treated silicas.

Although silane-type coupling agents exhibit the desirable property of interacting quantitatively with surface hydroxyl groups, they have the undesirable feature of being relatively large. The cross-sectional area of surface hydroxyls is about 10 $Å^2$, whereas the effective cross-sectional area of a trimethyl silicon group, which results from the chemisorption of HMDS, appears from previous work in this investigation to be in the range of 30-40 $Å^2$. When silanes are performing the function of coupling agents, the steric factor which limits adsorption is not important. When the function, however, is to hydrophobe the surface, the objective is to completely hydrophobe the surface, and in this application surface concentration potential becomes important. Although very little work has been carried out successfully to chemically interact lower alcohols, and especially methanol, with surface hydroxyls [19,20], a major effort has been attempted in the investigation to hydrophobe the surface of iron oxides by means of chemisorption of methanol on surface hydroxyls. One of the objectives of this phase of the program, therefore, is to hydrophobe the surfaces of the iron oxides, which have been identified as corrosion products, and which have been characterized as containing high concentrations of surface hydroxyls.

EXPERIMENTAL

Gas adsorption measurements are the primary technique used to evaluate the concentration of surface polar groups and the effectiveness of different surface modifications. Additional experimental techniques, such as heats of immersion, electrophoresis, and near infrared reflectance spectroscopy, have been used in this investigation in order to determine the nature of these polar groups under different conditions.

The iron oxide samples used in this investigation, α-Fe_2O_3, α-FeOOH, and γ-FeOOH, were precipitated from solution according to experimental techniques described in the Second Annual Report, page 161, November 1, 1981. Previous work had investigated Fe_3O_4 and α-Fe_2O_3 obtained from Pfizer Inc. The current and future experiments are expected to investigate iron oxide samples prepared and characterized in this laboratory.

The argon gas adsorption isotherms for specific area determination were obtained at liquid nitrogen temperatures using a classical BET volumetric vacuum rig. The residual pressure of 10^{-6} torr differential pressure transducer (Datametrics, Inc.) was used to measure the argon gas pressure with a sensitivity of 10^{-3} torr. Specific areas were calculated for argon molecular cross-section of 17 $Å^2$. The water adsorption isotherms were measured on a quartz spring (Worden Quartz Co.) balance with a sensitivity of 10 µg/g of sample. The equilibrium water vapor pressure was measured with a 100 torr capacitive differential manometer (Datametrics, Inc.).

RESULTS AND DISCUSSION

Water adsorption results had previously been reported on α-Fe_2O_3 and Fe_3O_4 samples obtained from Pfizer Inc. and on α-Fe_2O_3, γ-FeOOH, and α-FeOOH prepared in this laboratory. The approach has been to characterize the hydrophilic character of the different iron oxide samples, which have been identified as corrosion products, as a function of pretreatment conditions such as high temperature activation and chemisorption of trimethylsilicon with surface hydroxyls via interaction with hexamethyldisilazane, HMDS. This approach has been continued by determining the experimental conditions which would result in the chemisorption of a single methyl group on the proton of the surface hydroxyl via interaction of methanol with surface hydroxyls.

The experimental approach adopted here, which utilizes gravimetric techniques for measuring water adsorption isotherms, is designed to determine the degree of surface hydrophilicity of iron oxides as a function of activation temperature in the range of 25° to 400°C under high vacuum, and after hydrophobing the surface with HMDS and methanol. The procedure measures the weight loss as a function of activation temperature, the water adsorption isotherms at 25°C after activation at the specified elevated temperature, and a second series of isotherms which follows the previous series after activation at 25°C. The intent is to compare the weight loss results to the amount of

irreversibly adsorbed water after each isotherm, and also the decrease in monolayer capacity of the second isotherm activated at 25°C compared to the first isotherm which was activated at the elevated temperature. Since the intrinsic surface properties of the iron oxide sample are sought in this approach, the specific surface area, as determined from a BET analysis of argon adsorption isotherms at -195°C, was measured as a function of activation temperature.

The approach which has been used to hydrophobe iron oxide is by chemical treatment of HMDS with the surface. Since surface hydroxyl groups on iron oxides are primarily responsible for the adsorption of water, the approach was to treat chemically these hydroxyls so as to render them hydrophobic. Silanes, in general, are known to react with the proton of hydroxyls whether they are part of the surface or of an organic or inorganic molecule. Hexamethyldisilizane, HMDS, was used to treat α-Fe_2O_3, α-FeOOH and Fe_3O_4 according to the following reaction:

$$2ROH + (CH_3)_3\,Si\text{-}\overset{\overset{H}{|}}{N}\text{-}Si(CH_3)_3 \longrightarrow NH_3 + 2ROSi(CH_3)_3$$

where, R represents the iron oxide surface. HMDS adsorption isotherms were measured on α-Fe_2O_3 and γ-FeOOH at 25°C after sample activation at 400°C. The amount of irreversibly adsorbed HMDS, after subsequent activation at 25°C and 10^{-6} torr, was assumed to be due to the above chemical reaction where one molecule of HMDS reacts with two surface hydroxyl groups to yield two molecules of chemisorbed trimethylsilicon and one molecule of ammonia. The results show that the concentration of adsorbed trimethylsilicon was 1.5 and 2.5 groups/100 $Å^2$ for α-Fe_2O_3 and γ-FeOOH, respectively. Since the cross-sectional area of trimethylsilicon is expected to be about 40 $Å^2$, 2.5 groups/100 $Å^2$ represents close packing and hence a maximum value.

The HMDS treatment has been shown to have a measurable effect on decreasing the surface hydrophilicity of α-Fe_2O_3, γ-FeOOH, α-FeOOH and Fe_3O_4. The proposed mechanism for this HMDS interaction is chemisorption of the trimethylsilicon group with the oxygen of the surface OH. Although both α-Fe_2O_3 and δ-FeOOH exhibited about the same degree of surface hydrophilicity from water adsorption isotherm results, α-Fe_2O_3 irreversibly adsorbed 1.5 trimethylsilicon groups/100 $Å^2$ as compared to 2.5 trimethylsilicon groups/100 $Å^2$ for γ-FeOOH. Since the cross sectional area of trimethylsilicon is of the order of 40 $Å^2$, the value of 2.5 groups/100 $Å^2$ represents a maximum value due to close packing. The interpretation of these results is that the surface OH groups are more randomly distributed on γ-FeOOH as compared to α-Fe_2O_3. This interpretation is consistent with previously reported electrophoretic mobility results at a pH value of 1.8 where γ-FeOOH exhibits a higher positive charge than α-Fe_2O_3, where the latter contains clusters of surface OH groups and proton adsorption is limited by localized coulombic repulsion.

All of the iron oxide surfaces investigated thus far interact with HMDS to yield chemisorbed trimethylsilicon which effectively hydrophobes the surfaces to varying degrees. There is no doubt that this silane type interaction, which is basically replacement of the OH proton with a silicon-containing

group, will occur on a corroded iron oxide surface with a variety of different silane molecules containing different functional groups. The implication is that this type of chemisorption can be used to decrease surface hydrophilicity of iron oxide and, at the same time, increase adhesion of a protective coating through selection of the appropriate silane molecule. The limitation is the degree to which surface hydrophilicity can be reduced by a molecule which is significantly larger than the cross-sectional area of a surface hydroxyl group. This limitation is especially serious because the silane type molecules which are available are, by their nature, large compared to surface hydroxyl groups.

An experimental approach was attempted for chemisorbing methanol on surface hydroxyls, where the methanol would have a comparable cross-sectional area, according to the following proposed mechanism:

$$CH_3OH + ROH \longrightarrow ROCH + H_2O$$

where, R would represent the iron oxide surface. There is no question that an activation energy would be required for this reaction to proceed. For example, methanol will adsorb physically and reversibly at 25°C. A necessary requirement is that the methanol adsorb chemically under the appropriate activation temperature conditions, and that the adsorption be irreversible under room temperature conditions and in the presence of water.

Both α-Fe_2O_3 and α-FeOOH were treated with methanol under the following conditions. The samples were activated at 400°C overnight followed by methanol adsorption isotherm measurements at 25°C. The results, Figure 1, show a sharp inflection, indicating relatively high energy adsorption for both samples at levels of 3 to 4 molecules/100 $Å^2$, followed by a relatively flat plateau region up to high relative pressures, indicating low energy adsorption as expected for a methylated surface. Both samples were subsequently outgassed at 25°C and the irreversibly adsorbed methanol for α-Fe_2O_3 and α-FeOOH was 2.5 and 3.4 molecules/100 $Å^2$, respectively. A series of water adsorption isotherms were subsequently measured on both iron oxide samples as a function of activation temperature. An additional experimental technique was used to chemisorb methanol on α-Fe_2O_3. The sample was heated to 400°C, exposed to methanol vapor at 70 torr, cooled in the presence of methanol vapor, and finally outgassed at 25°C. Water adsorption isotherms were then measured on this sample both before and after exposure to water vapor to determine the extent of irreversibility of the methylated surface.

The water adsorption isotherm results as a function of pretreatment conditions are presented in Figures 2 and 3 for α-Fe_2O_3 and α-FeOOH, respectively. Table I summarizes the recent and previously reported water adsorption results for α-Fe_2O_3 and α-FeOOH. As reported previously, the iron oxide samples in general exhibit a high degree of surface hydrophilicity and frequently approach a close-packed hydroxyl concentration of 10 molecules/100 $Å^2$. Activation of the surface at 400°C has the effect of partially dehydroxylating the surface and rendering it somewhat more hydrophobic. There is reason to believe, however, that the surface will slowly rehydroxylate. The HMDS treatment is somewhat more effective in hydrophobing the surface, and apparently irreversible.

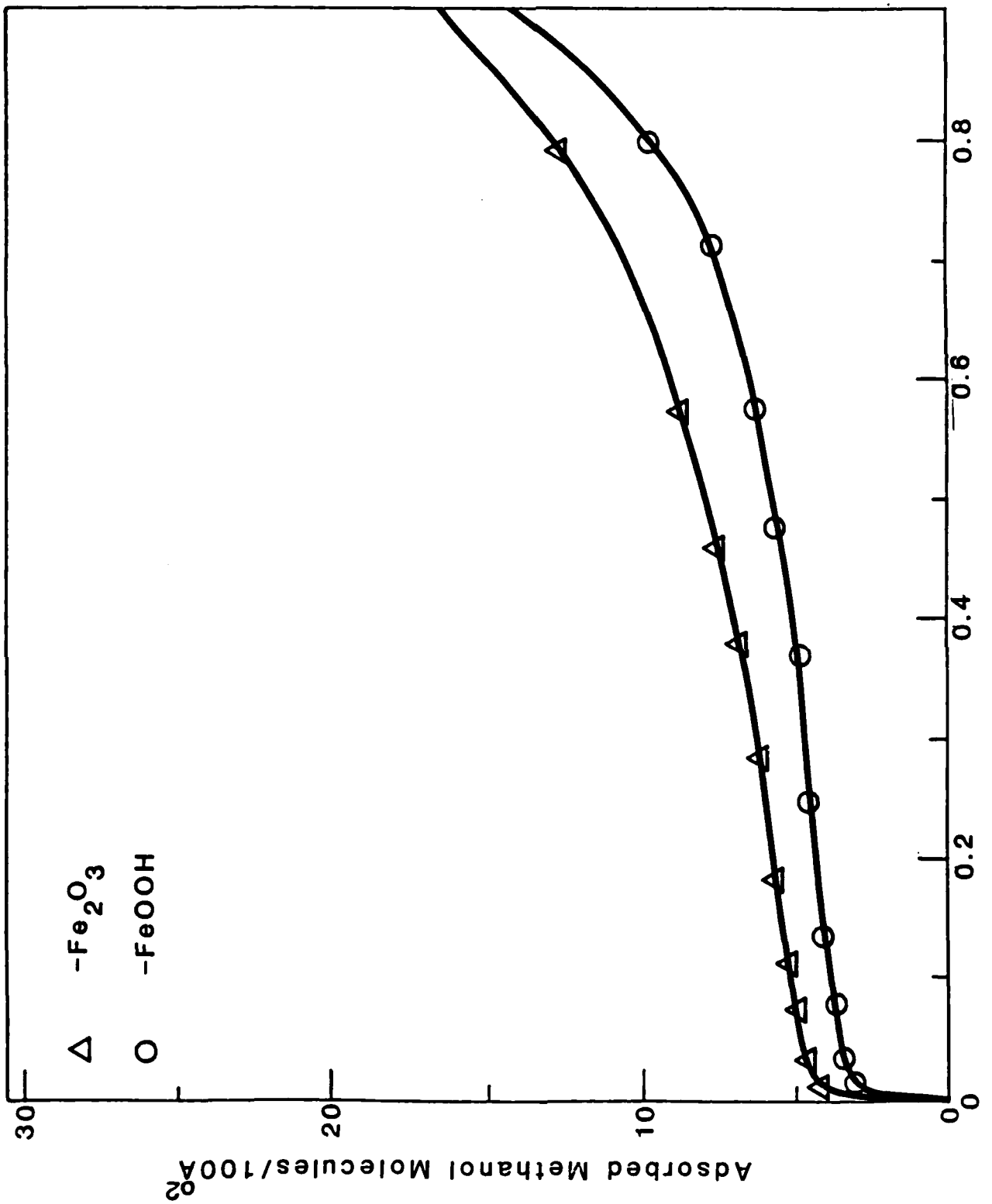

Figure 1. Methanol adsorption isotherms at 25°C on α-Fe_2O_3 and α-FeOOH after activation at 400°C.

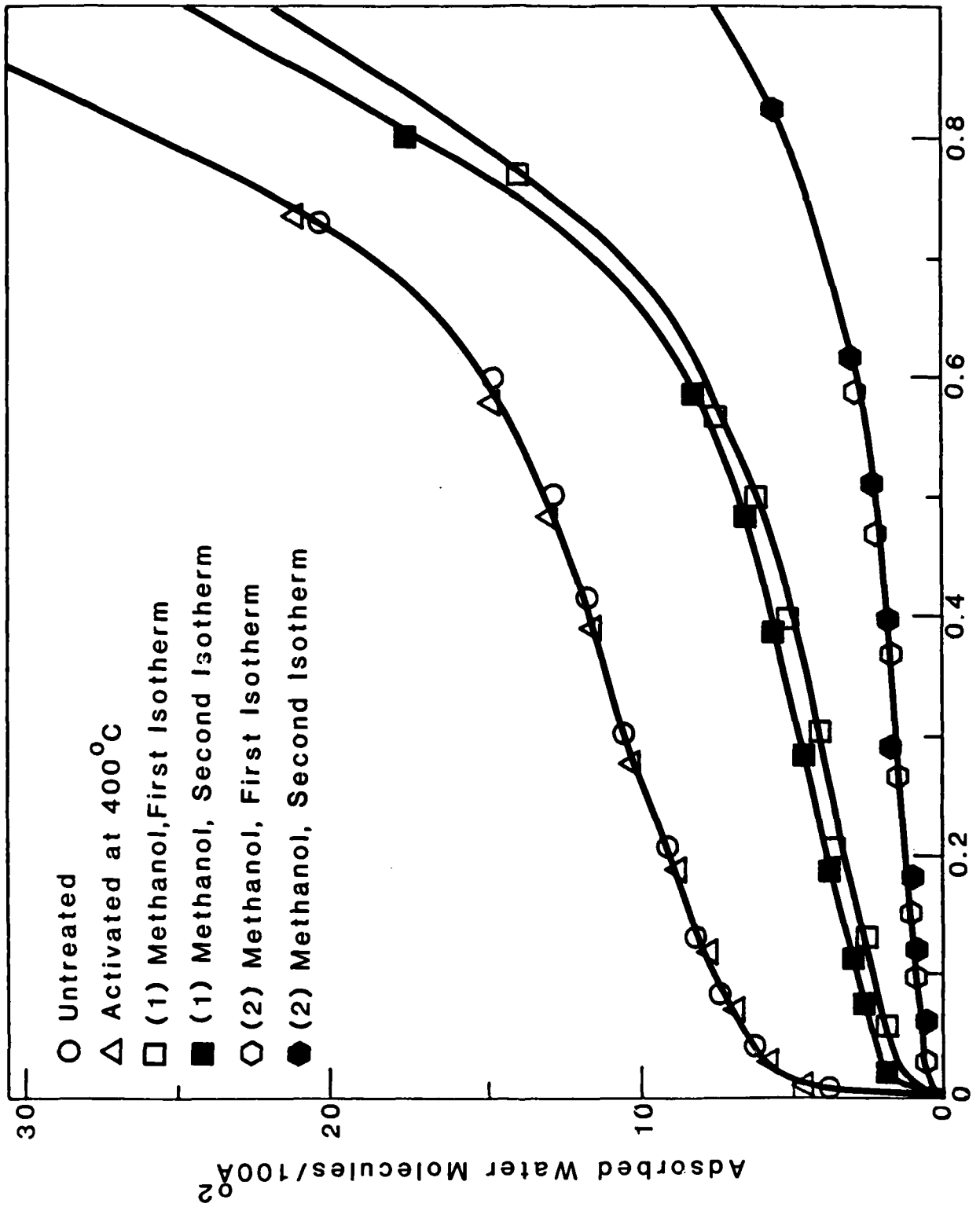

Figure 2. Water adsorption isotherm at 25°C on α-Fe_2O_3.

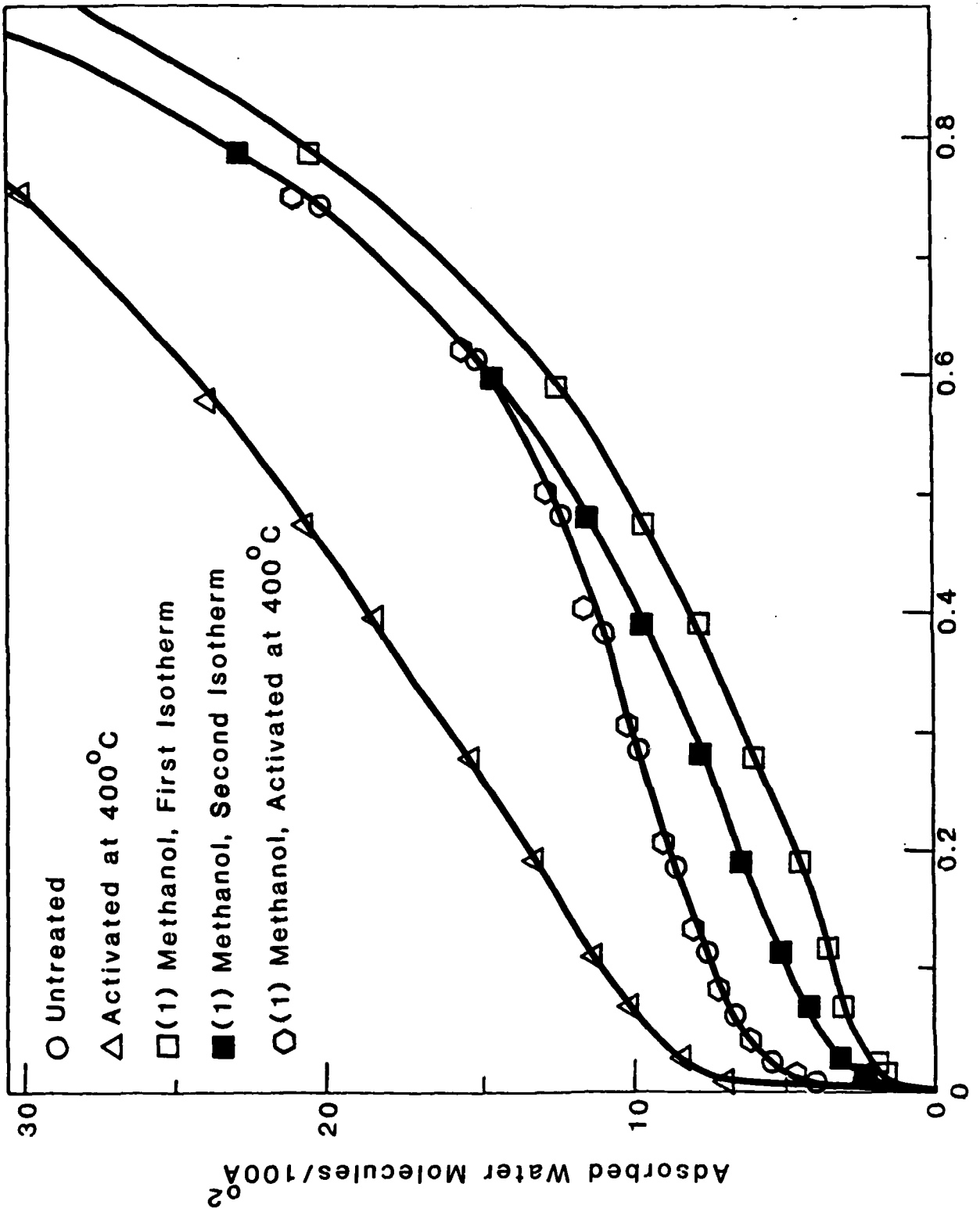

Figure 3. Water adsorption isotherms at 25°C on α-FeOOH.

Table I

Gas Adsorption Results on α-Fe_2O_3 and α-FeOOH

Sample	Pretreatment	Activation Temperature, °C	Molecules/100 Å^2			
			W_{m1}	W_{m2}	$W_{m1}-W_{m2}$	Irreversibly Adsorbed Water
α-Fe_2O_3	None	25	7.8	---	---	---
	None	400	8.3	7.1	1.2	2.7
	HMDS	25	4.9	4.7	0.2	1.1
	HMDS	400	7.5	5.2	2.3	3.7
	(1)Methanol	25	2.0	2.4	-0.4	0
	(1)Methanol	400	2.6	1.6	1.0	1.4
	(2)Methanol	25	0.6	0.4	0.2	0.3
α-FeOOH	None	25	10.0	---	---	---
	None	400	5.6	4.0	1.6	1.9
	HMDS	25	5.8	6.0	-0.2	0.9
	HMDS	400	5.6	4.0	2.6	5.7
	(1)Methanol	25	3.2	4.7	-1.5	0
	(1)Methanol	400	7.2	---	---	3.7

W_{m1} - First water adsorption isotherm at 25°C after indicated activation temperature.

W_{m1} - Second water adsorption isotherm at 25°C after activation at 25°C.

(1)Methanol - Exposure of methanol to sample at 25°C after 400°C activation.

(2)Methanol - Exposure of methanol to sample at 400°C and cooled in presence of methanol.

The limitation with this treatment is the size of the trimethylsilicon group which is large relative to the hydroxyl, and which limits interaction to only about one out of every three surface hydroxyls. There is no question, however, that HMDS and silane-type coupling agents can be used to modify the surface of iron oxides with functional groups which would be capable of specific interactions with protective coatings.

Methanol is unique in terms of surface modification because of its relatively small size and the fact that it requires an activated surface or activation conditions to undergo chemisorption. The results on both α-Fe_2O_3 and α-FeOOH suggest that after activation at 400°C the extent to which the surface is dehydroxylated will control the extent to which methanol will chemically interact with the surface at 25°C to yield one methylated oxygen and one hydroxyl per methanol molecule. This method of methanol treatment is identified as "(1)methanol" in Figures 1 and 2 and Table I where it is observed that this methanol treatment is twice as efficient for hydrophobing the surface compared to the HMDS treatment. The methanol treatment identified as "(2)methanol" resulted in exposure of the surface of α-Fe_2O_3 to methanol at 400°C and subsequent cooling to room temperature in the presence of methanol. This method has been demonstrated as being much more efficient for hydrophobing the surface as indicated by the surface hydroxyl concentration being less than one molecule/100 $Å^2$ before treatment. Although there is no indication that this hydrophobed surface will rehydoxylate at 25°C in the presence of water vapor for short periods of time, i.e., 48 hours at 80% relative humidity, it remains to be demonstrated to what extent slow rehydoxylation will occur on the methylated surface.

CONCLUSIONS

All of the iron oxides which have been investigated, and which have been identified as corrosion products, are hydrophilic and contain high concentrations of surface hydroxyls. These surface hydroxyls can be used to interact quantitatively with hydrophobing agents, such as HMDS, and silane coupling agents containing functional groups which are capable of interacting with protective coatings for the purpose of promoting adhesion. The efficiency for hydrophobing, however, is limited by the steric factors inherent in these types of molecules. Methanol, however, has been demonstrated to be very efficient for hydrophobing α-Fe_2O_3 when the exposure occurs under activated conditions, i.e., 400°C activation. This technique for hydrophobing iron oxide surfaces must be pursued further in order to determine the permanent nature of this type of treatment and how it might be used in conjunction with silane treatments.

REFERENCES

[1] T. A. Banfield, Progress in Organic Coatings 7, 253 (1979).

[2] M. J. Graham and M. Cohen, Corrosion 32, 432 (1976).

[3] E. McCafferty and A. C. Zettlemoyer, J. Colloid Interface Sci. 34, 452 (1970).

[4] A. C. Zettlemoyer and E. McCafferty, Z. Phys. Chem. N. F. 64, 41 (1969).

[5] E. McCafferty and A. C. Zettlemoyer, Trans. Faraday Soc. 66, 1720 (1970).

[6] E. McCafferty and A. C. Zettlemoyer, Trans. Faraday Soc. 66, 1732 (1970).

[7] E. McCafferty and A. C. Zettlemoyer, Disc. Faraday Soc. 52, 239 (1971).

[8] G. Blyholder and E. A. Richardson, J. Phys. Chem. 66, 2597 (1962).

[9] J. J. Jurinak, J. Colloid Sci. 19, 477 (1964).

[10] T. Morimoto, M. Nagao, and F. Tokuda, J. Phys. Chem. 73, 243 (1968).

[11] F. O. Stark, O. K. Johannson, G. E. Vogel, R. G. Chaffee, and R. M. Lacefield, J. Phys. Chem. 72, 2750 (1968).

[12] W. Hertal and M. L. Hair, J. Phys. Chem. 75, 181 (1971).

[13] M. L. Hair, J. Colloid Interface Sci. 60, 154 (1977).

[14] V. Y. Davydov, A. V. Kiselev, and L. T. Zhuravlev, Trans. Faraday Soc. 60, 2254 (1964).

[15] M. L. Hair and W. Hertl, J. Phys. Chem. 73, 2372 (1969).

[16] A. C. Zettlemoyer and H. H. Hsing, J. Colloid Interface Sci. 55, 637 (1976).

[17] A. C. Zettlemoyer and H. H. Hsing, J. Colloid Interface Sci. 58, 263 (1977).

[18] A. V. Kiselev, B. V. Kuzhetsov, and S. N. Lanin, J. Colloid Interface Sci. 69, 148 (1979).

[19] M. Magao and T. Morimoto, J. Phys. Chem. 84, 2054 (1980).

[20] T. Morimoto, M. Kiriki and M. Nagao, J. Phys. Chem. 84, 2058 (1980).

Program #2

Surface Acidity of Ferric Oxides as Studied by Flow Microcalorimetry

Principal Investigator: Frederick M. Fowkes
Prof. of Chemistry

Associates: Sara T. Joslin (Ph.D. awarded)
Mary Jo Kulp, Graduate Student

ABSTRACT

The molar heats of adsorption of nitrogen and oxygen bases from neutral hydrocarbons onto the surface sites of alpha ferric oxides have been determined by using a UV concentration detector in series with a flow microcalorimeter. Since the strongest sites are neutralized first, the distribution of molar heats of adsorption is determined by their time-dependence. Molar heats of adsorption for nitrogen and oxygen bases depended very strongly on the amount of adsorbed moisture, so the development of methods for controlling moisture levels in the liquids and on the solids of these studies became an important issue.

The acidic surface FeOH sites were found to be hard acids with a range of acid strengths. The stronger acid sites had a concentration of about one micromole per square meter, and their Drago E and C constants were found (by the heats of adsorption of pyridine, trimethylamine and ethyl acetate) to be: $C_A = 0.8 \pm 0.2$, and $E_A = 4.5 \pm 1.1$ $(\text{kcal/mole})^{\frac{1}{2}}$.

The adsorption of polyvinylpyridine was found to occur quantitatively as a 0.1% solution in benzene flowed through the bed. 68% of the acidic surface sites of the ferric oxide were occupied by the polymer, as determined by subsequent adsorption of pyridine, and 52% of the pyridine groups of the polymer were bound to the surface.

INTRODUCTION

Intermolecular interactions such as adsorption have been described as polar and non-polar, following the principle that polar groups bond to polar surfaces and that non-polar groups develop "hydrophobic bonds" to non-polar surfaces; thus we have the old rule that "like bonds to like." Current studies of polar interactions, however, have found that all polar interactions are actually Lewis acid-base interactions, that all substances except saturated hydrocarbons are Lewis acids or bases, and that the rule of polar bonding should actually be "acids bond to bases" [1,2].

Quantitative calorimetric and spectrometric studies of the interactions of simple organic liquids by Drago and co-workers [3,4] showed that the heats of mixing of organic liquids (ΔH_M) are entirely predictable as Lewis acid-base interactions between electron-donors (such as nitrogen, oxygen, sulfur or pi-electron bases) and electron acceptors (such as the "active" hydrogens of alcohols, phenols, carboxyls or of partially halogenated hydrocarbons; or the non-Bronsted acids such as iodine and the chlorides or alkyls of boron, aluminum, antimony, etc.). A quantitative correlation of heats of mixing,

$$\Delta H_M = C_A C_B + E_A E_B , \qquad (1)$$

was shown to predict heats of mixing generally to within 0.1-0.2 kcals/mole, except for situations where steric factors prevent optimum donor-acceptor bond angles and bond distances.

The adsorption and adhesion of polymers to inorganic substrates has also been shown to be entirely governed by acid-base interactions between acidic or basic sites of the polymer and of the inorganic substrate. Basic polymers include polystyrene, polyesters, polyamides, polyethers, polyamines and polycarbonates, while acidic polymers include halogenated polyolefins, polymers of vinyl halides, and polymers with "active" hydrogens such as polyvinylbutyral. The E and C constants for polymers such as polymethylmethacrylate (PMMA) are easily measured by infrared spectral shifts [1] and the E and C constants for inorganic substrates such as silica and titania have been measured with high surface-area powders by calorimetry or by infrared spectral shifts [5]. We can therefore predict with precision the heats of adsorption of polymers per adsorption site on silica and titania, but must have further information on the number of sites adsorbed to determine the heats of polymer adsorption per mole of polymer.

The heats of polymer adsorption per site are important parameters for understanding the conformation of adsorbed polymers. The heats of acid-base interaction of polymers with inorganic substrates are often large multiples of kT per site; for PMMA on silica or titania the heats of adsorption per site are about -7 kT. As Silberberg [6] has just made clear, such heats of adsorption cause a large fraction of the adsorbed polymer chains to be in the adsorbed "trains", and a smaller fraction to be in "loops" and "tails". Such conformations are believed to lead to strong adhesive bonding.

This program is concerned with the principles governing the adhesion of polymers to the surface of steel, where acid-base interactions determine the energy of adsorption. Iron oxides can bond to acids or to bases, but this study is limited to the interactions of basic polymer groups with the acidic FeOH sites. The acid strength of these sites has been determined by measuring the heats of adsorption of test bases (pyridine, triethylamine, ethyl acetate), and Drago E and C constants were determined for these sites. Most of the studies have been done with a commercial alpha iron oxide, but some were also done with a gamma iron oxide. Much of the effort in these studies concerned controlling the water content of the oxides, the solvents, and the test bases. Water is both an acid and a base; it adsorbs as a base onto the acidic FeOH sites and can very appreciably reduce the acidity. Our concern was not to make the oxides as dry as possible and thereby maximize their acidity, but to work with controlled water activities in the dryer part of the range normally encountered in polymer coating technology.

The technique used in these studies was a novel combination of flow microcalorimetry with a flow concentration detector suggested to us by George Salensky of Union Carbide. As a solution of the test base is pumped through the iron oxide powder bed, the heat of adsorption is measured by thermistors, and when the solution is pumped on through the flow UV detector, the depletion of base due to adsorption is measured; the combination of these two sensings allows determination of the heat of adsorption of the test base in kcal/mole. Furthermore, because dilute solutions of base are pumped through the bed and the rates of adsorption are fast, the stronger acidic sites are neutralized first and the weaker last, so that the time-distribution of heats of adsorption is a good site-distribution of heats of adsorption. An unexpected bonus of this approach was that after adsorbing polymers onto the oxide we could measure the surface concentration of bare sites directly (with a solution of test base in the same solvent), and thus determine what fraction of the basic sites of the polymers was bound to the acidic sites of the ferric oxide.

EXPERIMENTAL

Oxides and Reagents

Most of the experiments were done with a single sample of an alpha ferric oxide reported to be free of any flocculants or surface-modifiers (R-1299, Lot E9036, from Charles Pfizer, Inc., Easton, PA) having 9.9 sq.m./g of surface area by BET analysis of argon adsorption data (courtesy of Vital and Micale), and a sulfur concentration of about 0.5% in the surface region, as determined by ESCA (courtesy of Prof. David W. Dwight of VPI). After laboratory techniques were developed on the large batch of commercial alpha ferric oxide, a few measurements were made on a small batch of gamma ferric oxide synthesized at Lehigh by T. C. Huang, and which had a BET surface area from argon adsorption of 68.9 sq.m./g [7].

The principal solvent for these studies was HPLC grade cyclohexane from Fisher Scientific, but some additional work was done with decalin (mixed

decahydronaphthalenes) from Aldrich Chemical, with 99% mole purity n-hexane from Fisher Scientific, with HPLC grade n-heptane from Fisher Scientific and with Reagent grade benzene from J. T. Baker, distilled before use to minimize thiophene. Solvents were dried with 8-12 mesh Davison 3-A molecular sieves (activated for at least one hour under vacuum at 250°C), stored under Drierite-dried nitrogen, and dispensed through a sealed buret into HPLC delivery syringes or into adsorption study vials with syringe needles through septa shields for the vials, so as to eliminate any contact of the dried solvent or solutions with air. All glassware was oven-dried for at least 16 hours at 50°C immediately prior to use, and the water content of the solvents was monitored with an Aquatest IV automatic Karl Fischer titrimeter (Photovolt Corp., NY). Solvents were stored over freshly activated molecular sieves, but not for longer than two weeks, for in that time enough water entered from the glass to raise the dissolved water content despite the presence of molecular sieves. Solutions were made fresh daily.

The organic bases used for titration of surface acidity included pyridine (99+% mole purity, Aldrich Chemical), triethylamine (99 mole % from Aldrich Chemical), ethyl acetate (Certified A.C.S. grade from Fisher Scientific), and poly(2-vinyl pyridine) with M(W) of 92,000 and M(N) of 89,000 supplied by Scientific Polymer Products of Ontario, NY. Measurements were also made with n-butanol (Certified A.C.S. grade from Fisher Scientific).

Flow Calorimeter

The flow calorimeter (Microscal Ltd., London, U.K.) has a central stainless steel block with a long 6 mm. diameter cylindrical cavity in which a 6 mm. deep adsorption bed is enclosed between inlet and outlet tubes. The two thermistors which project into the bed and the two in the block are in a Wheatstone bridge circuit which is very sensitive to the bed temperature. The efficiency of the calorimeter depends on the degree of filling of the bed; maximum efficiency was found with 150 mg of iron oxide, thus leaving about 120 microliters of pore space in the bed. The unit is operated just like an HPLC unit (see Figure 1) with syringe pumps for pumping solvent or solution (usually at 100 microliters per minute) and with two Valco HPLC valves (with loops) for switching from solvent to solution and back again. The liquid that flowed through the bed was conveyed directly into a Perkin Elmer LC-75 UV detector by HPLC Teflon tubing, so that the UV absorbance (and concentration) of solutes could be determined, thereby allowing quantitative measurement of solute adsorption.

The calorimeter was equipped for evacuation of the bed with a vacuum pump and liquid nitrogen trap attached through the bed outlet. We attached a Hastings gauge just upstream of the inlet on a "T" into the Teflon tubing connecting the Valco valves to the bed, and the pressures measured there during bed evacuation were a bit higher, but considered indicative of those attained in the bed. During pump-down of a freshly loaded bed of 150 mg of alpha ferric oxide, the decrease in pressure at the Hastings gauge is monitored. However, during pump-down we also observed a marked endotherm sensed by the thermistors, resulting from evaporative cooling of the bed as traces of adsorbed water evaporate (Figure 2). Reproducibly low moisture

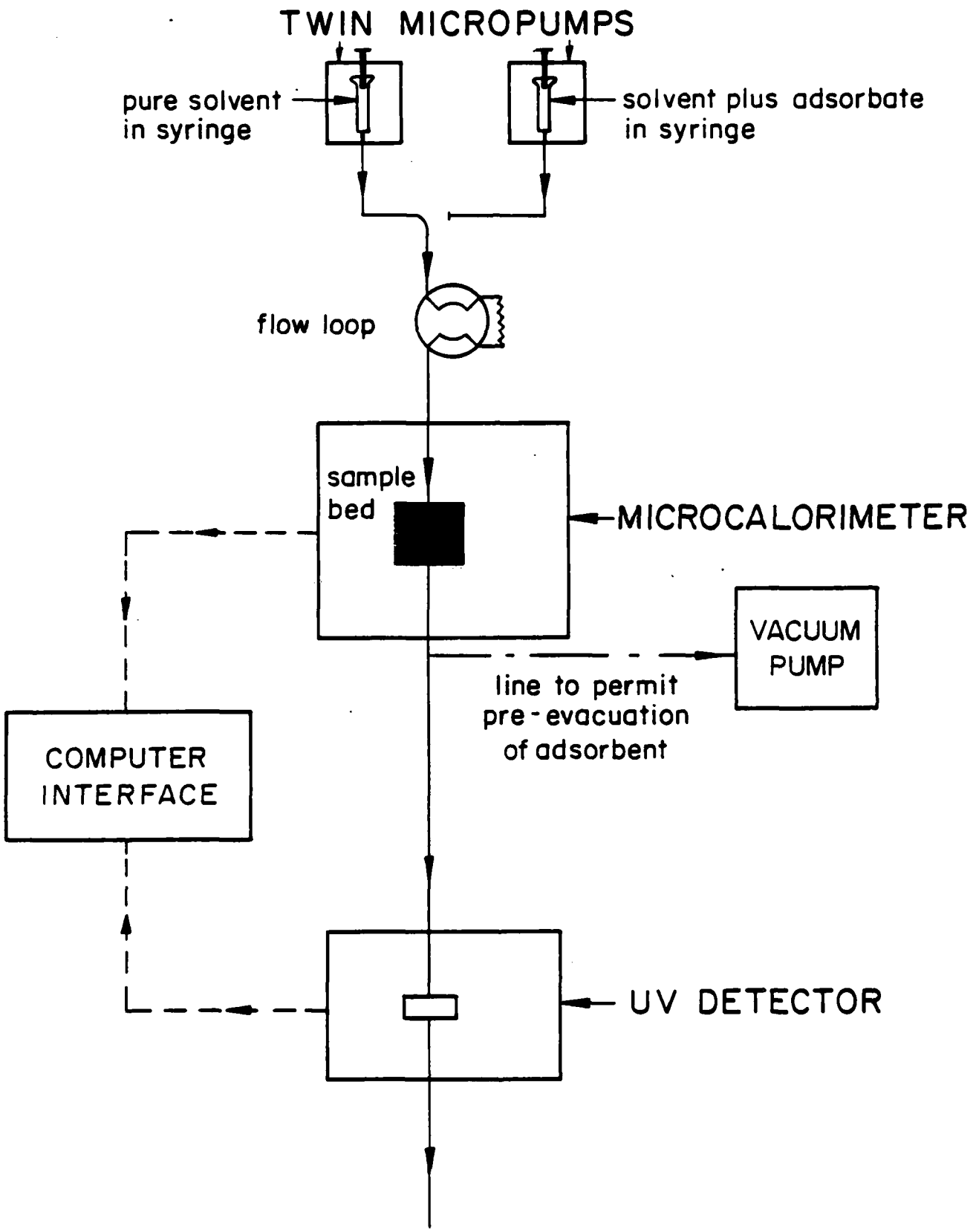

FLOW DIAGRAM

Figure 1. Block diagram for the microcalorimetric experimental arrangement.

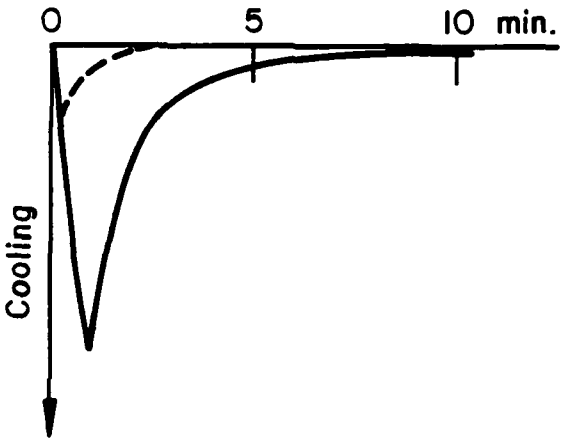

Figure 2. Evaporative cooling in the microcalorimeter bed during vacuum pumpdown, used as a measure of the removal of adsorbed water. Dashed line is for empty bed and solid line is for a bed of 150 mg of alpha ferric oxide.

levels in the bed can be obtained by pump-down through the evaporative cooling process, and even lower moisture levels can be obtained by pump-down to low Hastings gage readings.

Calibration of the heat-sensing system is done with a calibration coil of fine wire placed in the adsorption bed and attached to an outlet tube (supplied by the manufacturer). The calibration is done by passing known amounts of electrical energy through the coil in the packed bed while the solvent is being pumped through the bed at the desired rate.

Typical adsorption exotherms and UV-absorption plots are shown in Figures 3 and 4; these and all others in this paper were determined at 40°C. The UV-absorption plot compares the absorption of the pyridine solution passing through the bed of ferric oxide with the absorption of the same solution passing through an empty bed. The amount of pyridine adsorbed (in moles) is proportional to the area between the two curves in that time period.

Because of the need to relate the time-dependence of the exotherms and endotherms observed by the heat-sensors to the time-dependence of the concentration-sensor, a laboratory microcomputer became an essential part of the unit. We chose an MTU-130 from Microtechnology Unlimited (Raleigh, N.C.), and Douglas Eadline of this laboratory write the data-recording and display software in CODOS, the machine language of this computer. The data were recorded at two points per second for adsorption exotherms or desorption endotherms of about 1000 seconds' duration, and also for the UV calibration and absorption measurements; the data were displayed on the screen as stripchart data by software entitled STRIPCHART. After the experiments were completed, the data were analyzed with a light-pen operated program (DATAPENCIL-2, written in BASIC); this included base-line selection, integration, and "time-slicing" of both the thermal and UV data so that the time-dependence of molar heats of adsorption could be determined.

Adsorption Isotherms

The adsorption of pyridine onto the R-1299 alpha ferric oxide was studied in several hydrocarbon solvents and at several temperatures, using tightly sealed vials containing 10 ml of solution and 0.8 to 3.0 g of powder which were shaken in a water bath for three days to reach equilibrium. Supernatant solutions were diluted into a range where Beer's Law held for the UV absorption at 252 nm, using an Hitachi UV Spectrophotometer.

EXPERIMENTAL RESULTS AND DISCUSSION

Importance of Moisture Control in Adsorption on Ferric Oxides

Exploration of the importance of moisture content and development of procedures to control moisture content of the flow system, oxide and solutions was done largely with pyridine and with n-butanol solutions in cyclohexane. Butanol, like water, is both a base and an acid and it, too, is self-associated; it can adsorb on the acidic FeOH sites of ferric oxide and it can also

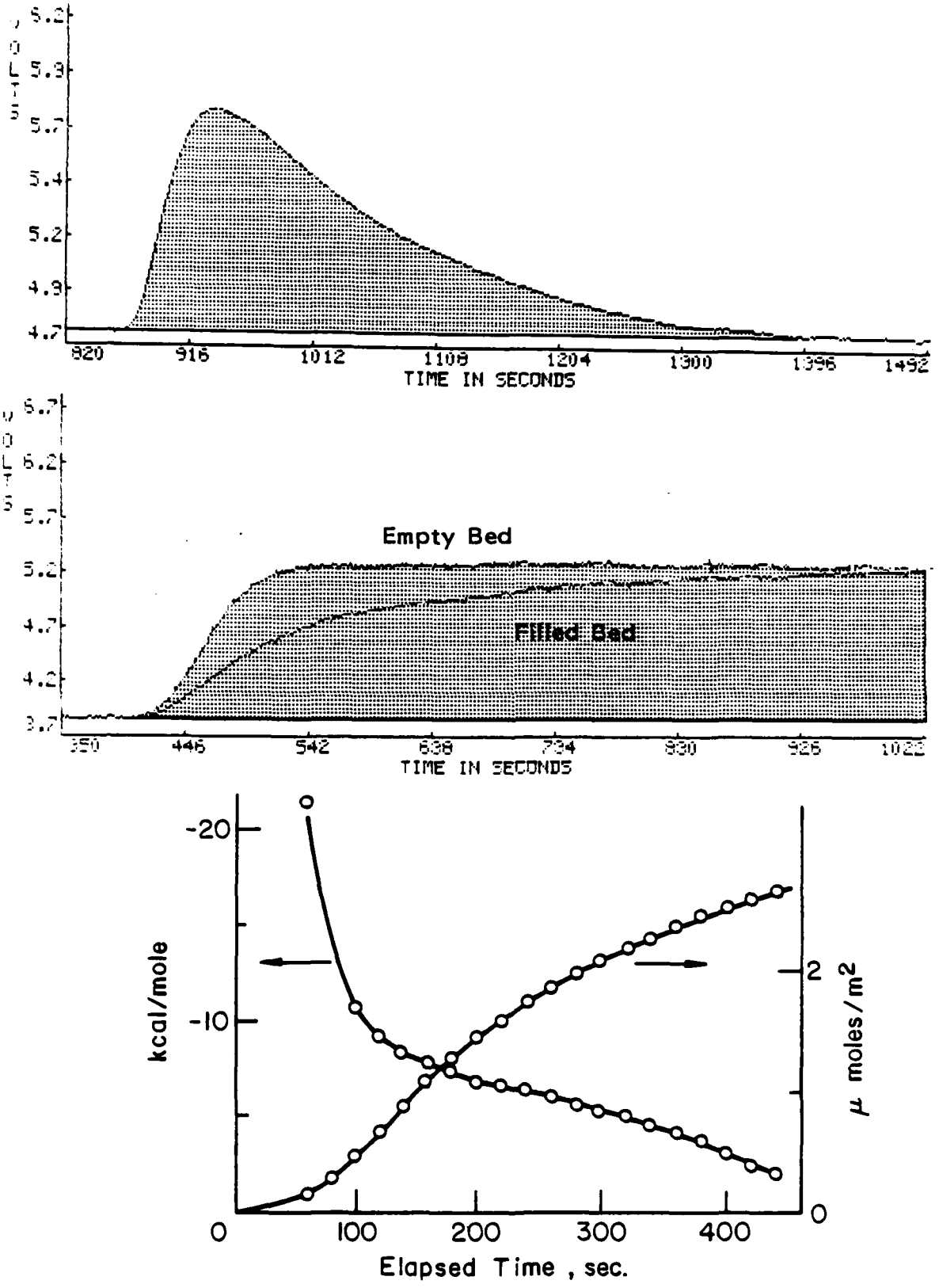

Figure 3. Typical flow calorimetric adsorption exotherm (top) and UV absorption plot (center) for a 25 mM solution of pyridine in cyclohexane flowing through a bed of 150 mg of alpha ferric oxide. Bottom: differential heats of adsorption calculated from the above data.

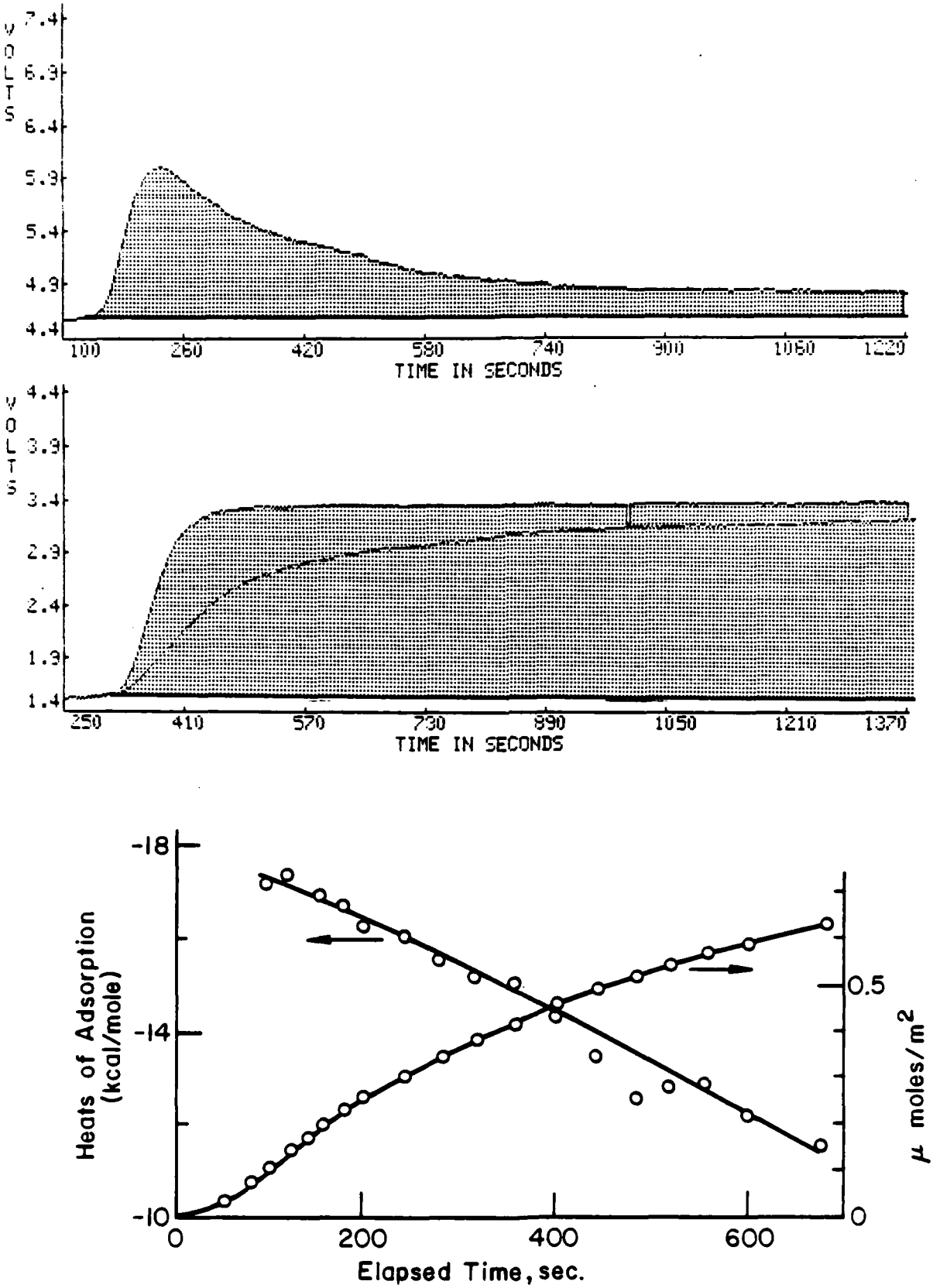

Figure 4. Flow calorimetric adsorption exotherm (top) and of the ultraviolet absorbtivity of a pyridine solution flowing from the adsorption bed (middle). Bottom: differential heats of adsorption calculated from above data.

adsorb onto adsorbed layers of water as well. Pyridine is much more basic than butanol and has little acidity or self-association. Pyridine adsorbs strongly onto acidic sites, but it can interact rather strongly with water, especially with adsorbed water which has been rendered more acidic by having its oxygens bonded to acidic sites. The Drago E and C constants for the acidity of water [3] show that its heat of mixing with pyridine is -5.0 kcal/mole. Thus, if all of the ferric oxide surface were water-covered, the observed heat of adsorption of pyridine should be close to the above value.

A series of heats of adsorption (in ergs/sq.cm.) were made with 0.2% solutions of n-butanol in n-heptane as a function of degrees of dryness, and the results are compared with published values. When the undried oxide was loaded into the adsorption bed in a slurry of undried heptane (having about 50 ppm of water), the heat of adsorption was high, 139 ergs/sq.cm., which compared well with the 146 ergs/sq.cm. determined with undried ferric oxide [8]. Drying the oxide by dry-loading with subsequent pumping-down of the bed dropped the measured heat to 114 ergs/sq.cm., a decrease similar to the 113 ergs/sq.cm. which Groszek[9] reported when his n-heptane was dried in a silca gel column. Partial drying of the n-heptane (to 20 ppm of water) and the pumping-off of moisture with a vacuum pump with liquid nitrogen trap reduced the heat of adsorption all the way to about 50 ergs/sq.cm. More heroic drying procedures led to much higher heats of adsorption; 206 and 198 ergs/sq.cm., much like those reported by Heal and McEwen [10] after overnight evacuation. These higher heats were obtained by better drying of the n-heptane (to 3 ppm and to 5 ppm), and by flowing this dry liquid through the bed for two hours after vacuum-drying of the oxide (with liquid nitrogen trap).

We conclude that reliable calorimetric results in agreement with the literature can be obtained at any chosen degree of dryness, but that low water contents of the liquids and of the adsorption bed are necessary to determine the real nature of the oxide. This conclusion may be illustrated with flow calorimetric heats of adsorption of pyridine on the R-1299 ferric oxide from 3 mM solutions in cyclohexane having a range of water contents (Table I).

Table I

Effect of Solvent Water Content on Heats of Adsorption onto R-1299 Ferric Oxide of Pyridine from 3 mM Solution in Cyclohexane

ppm Water	Contact Time	Micromoles/sq.m.	kcal/mole
4	120 min	1.42	-12.1
8	120	1.84	-6.5
16	120	1.71	-4.6

We chose the following procedure to insure reproducibly dry liquids and powder beds. It was found unnecessary to first dry the powder in a vacuum oven, for too much moisture was picked up during transfer through the air into the bed. The as-received powder was dry-loaded into the bed and evacuated at 40°C with vacuum pump and liquid nitrogen trap for 5-10 minutes (when the Hastings gage reached about 5 torr), and then the solvent, dried to the required degree of water-saturation (usually 10% or less), was pumped through the bed for two hours at a flow rate of 6 ml/hr. This procedure insured that the oxide bed and the solvent had a controlled degree of water saturation.

Heats of Adsorption of Pyridine on Ferric Oxides

Figure 3 shows a typical adsorption exotherm and ultraviolet absorption plot for a 25 mM solution of pyridine in cyclohexane containing 20 ppm of dissolved water as it flows through the 150 mg bed of ferric oxide in the flow microcalorimeter. At these higher pyridine concentrations, the adsorption is complete in about eight minutes, as evidenced by the return of the exotherm nearly to the base-line, and the close approach of the pyridine concentration to the calibration value. The bottom plot of Figure 3 shows the rate of adsorption and the incremental values of the heat of adsorption as a function of elapsed time, determined by time-slicing the integrated areas of the upper plots. About eight bed-volumes of solution flow through the bed during the exotherm and after the first hundred seconds most of the pyridine flowing through is unadsorbed; therefore, it is proposed that the distribution of heats of adsorption versus time is a good representation of the distribution of equilibrium heats of adsorption.

An adsorption exotherm and UV absorption plot for a more dilute pyridine solution, 3.2 mM in cyclohexane with 8 ppm of dissolved water, are shown in Figure 4. Even though this run extended twice as long as the run of Figure 3, only about 0.7 micromoles per square meter were adsorbed as compared to the 2.8 of Figure 3. This comparison illustrates the marked concentration-dependence of rates of adsorption. It should also be noticed that the exotherm of Figure 4 did not return as close to the base-line as in Figure 3, nor did the concentration of pyridine flowing from the bed return as close to the calibration value as in Figure 3. At first glance it appears that the exotherm has established a higher base-line, but the heats of adsorption calculated with a flat base-line are seen to decrease in the same manner as those of Figure 3.

In Figure 5 the heats of adsorption as a function of coverage are shown for the two runs of Figures 3 and 4. The 3.2 mM solution averages about -14 kcal/mole over the range 0-0.7 micromoles per square meter, whereas the 25 mM solution averages about -12 kcal/mole over the same range; this is attributed to their water contents (8 ppm vs. 20, respectively). The average heat of adsorption of pyridine from the 25 mM solution over the whole range (0-2.8 micromoles/m^2) is found to be -7.5 kcals/mole.

Similar runs have been made with a wide range of pyridine concentrations, shown in Table II. The water content of these solutions was 10-20 ppm. The decline of heats of adsorption with coverage results simply from the larger number of sites sensed by the higher pyridine concentrations, as illustrated in Figure 5 and discussed in the preceding paragraph.

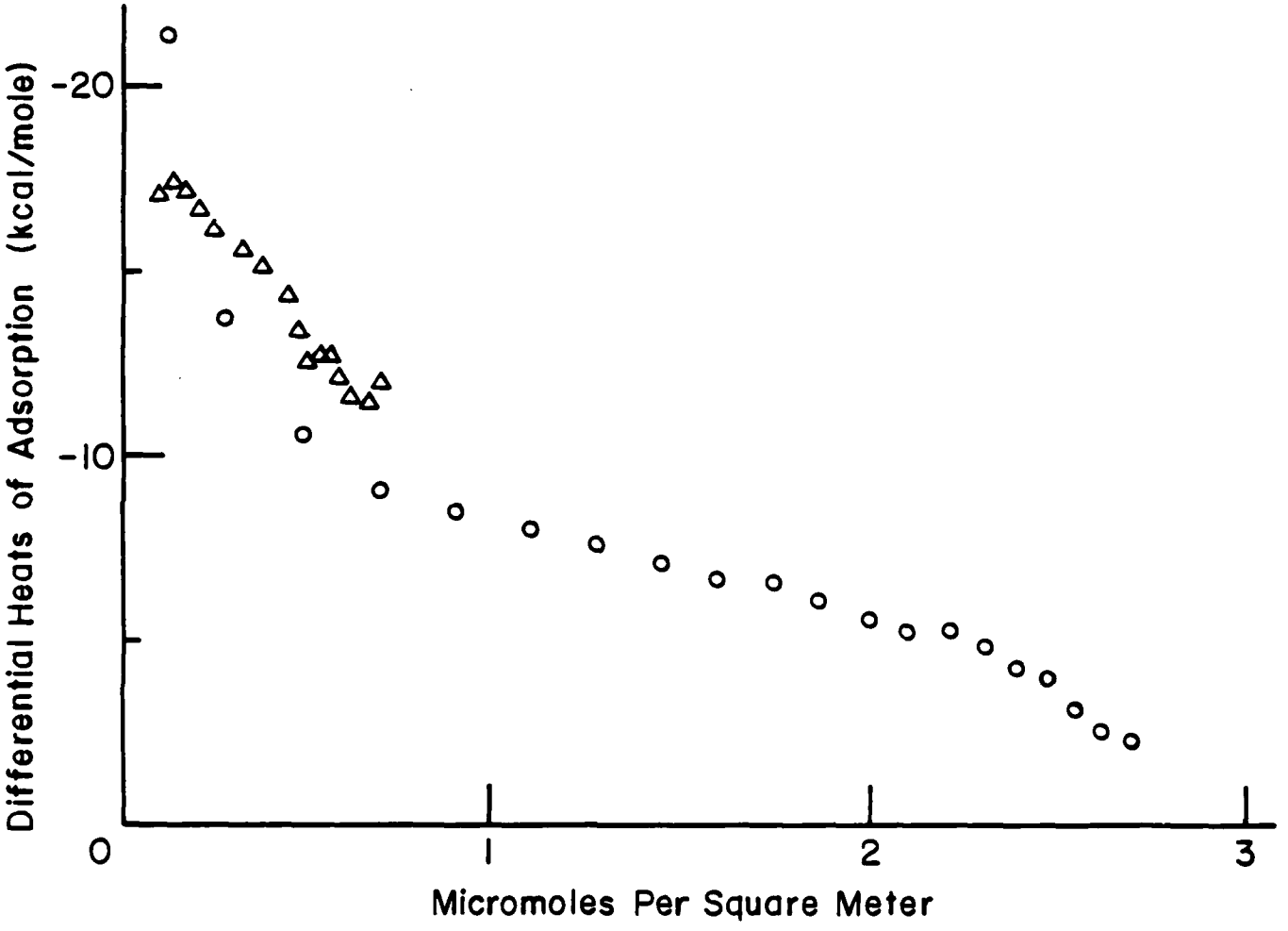

Figure 5. Comparison of differential heats of adsorption of pyridine adsorbing from a 3.2 mM solution in cyclohexene with 8 ppm water (Δ), and from a 25 mM solution with 18-20 ppm of water (O).

Table II

Total Amounts Adsorbed and Total Integral Heats of Adsorption of Pyridine onto R-1299 Alpha Ferric Oxide vs. Concentration of Pyridine in Cyclohexane

(20-30 min, 40°C, 10-20 ppm water)

Pyridine Conc. (mM/liter	Amount Adsorbed (micromoles/sq.m.)	Area per Molecule (sq. nm.)	Heats of Adsorption (kcals/mole)
3.6	1.42	1.17	-12.1
10.4	1.61	1.03	-12.0
10.4	1.73	0.96	-11.9
16.9	3.19	0.52	-7.0
23.5	3.02	0.55	-6.5
23.5	3.19	0.52	-6.8
29.5	3.69	0.45	-6.45
30.3	3.77	0.44	-5.95
35.0	4.15	0.40	-5.75

Adsorption of pyridine onto the same oxide and from the same solvent was determined at two temperatures (see the Langmuir plots of Figure 6) and by using the temperature-coefficient of the equilibrium constant K, determined from those isotherms, the heat of adsorption can be determined with the van't Hoff equation, as was done previously [11]. In these studies the pyridine concentration varied from 2 to 30 mM, and the amount of oxide equilibrated with each solution was chosen so that 30% to 60% of the pyridine was adsorbed. Consequently the vials contained such a high ratio of oxide surface to water content of the solvent (19 to 35 ppm) that even if all the water adsorbed onto the oxide, it could provide less than 10% of a monolayer, and could not affect the results significantly. The results obtained at 28 and 48°C (shown in Figure 6), predict a heat of adsorption of -7.2 kcal/mole. This heat should be compared to the integral heat at the same coverage, which would be about the mid-point of the concentration range shown in Table II, or -7.0 kcal/mole. This perfect agreement between calorimetric heats of adsorption by flow microcalorimetry and the heats of adsorption determined by the van't Hoff equation (using the temperature-coefficient of adsorption isotherms), is helpful in demonstrating the significance of these flow microcalorimetric results.

A gamma ferric oxide prepared at Lehigh by T. C. Huang [7] was also investigated for pyridine adsorption from cyclohexane. This oxide had been prepared by oxidation of a pure laboratory preparation of magnetite, and was then ball-milled, suspended and rinsed with conductivity water until the sol

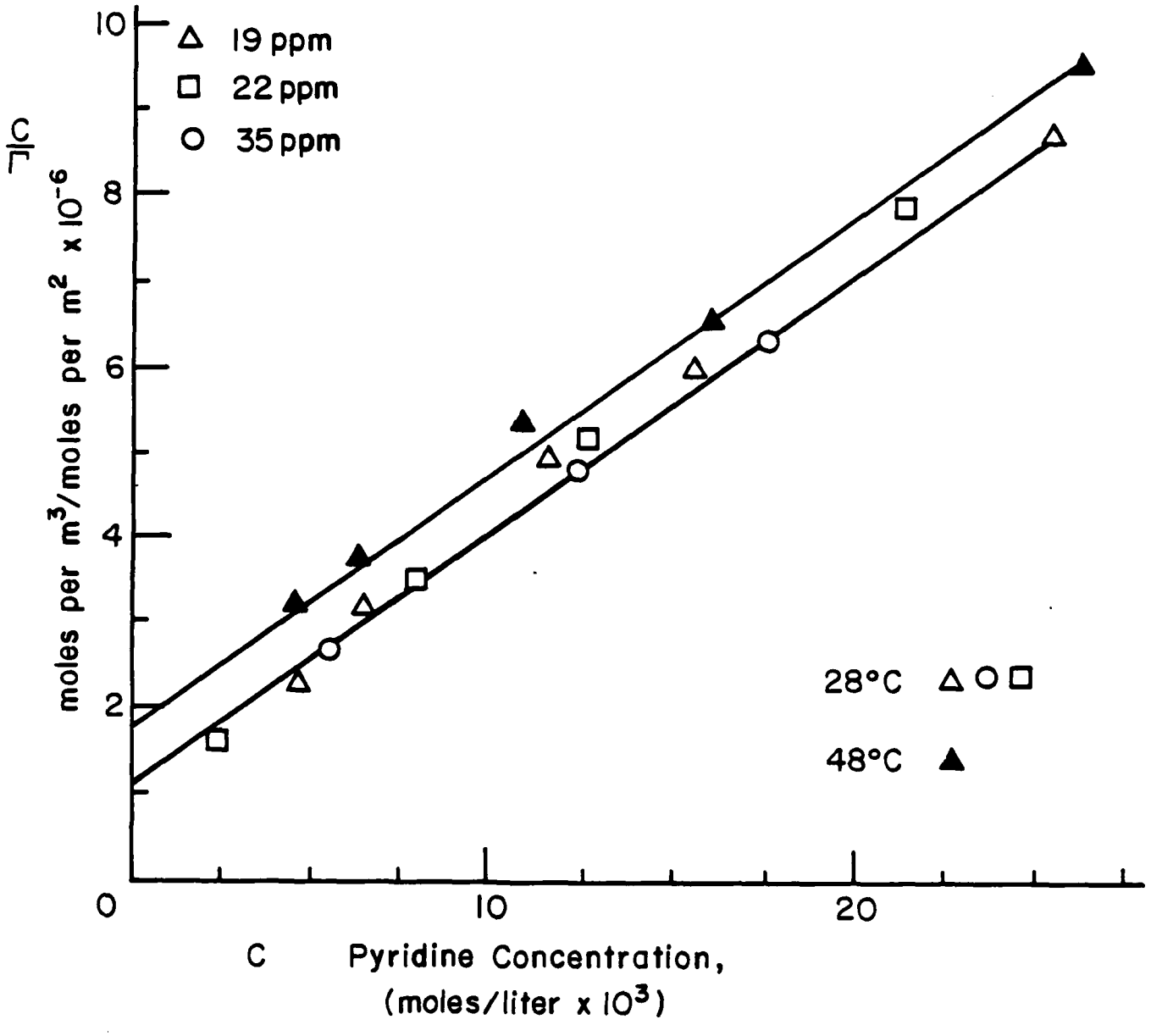

Figure 6. Langmuir adsorption isotherm plots for pyridine adsorption from cyclohexane onto alpha ferric oxide. The temperature-dependence of the vertical displacement of these lines is used to calculate heats of adsorption.

sol had a final conductance of 2.6 micro-mhos/cm. This sample had an excellent match of X-ray d-spacings to the literature, and it had a BET surface area of 68.9 sq.m./g., determined by argon adsorption. Table III shows the time-sliced heats of adsorption obtained on this oxide with flow microcalorimetry, using a 9.78 mM solution of pyridine in cyclohexane, and with the standard five-minute pumpdown of the bed in order to reach the same degree of dryness used in the alpha ferric oxide studies. This oxide had a much higher surface area than the alpha oxide, and the bed may therefore have had smaller pores; it is seen that the rate and amount of pyridine adsorbed was distinctly less than with the coarser 10 sq.m./g. alpha oxide. The heats of adsorption are seen also to be less at the same calculated average coverage, suggesting that with this highly porous sample there was more channeling and less uniform adsorption than with the coarser oxide.

Table III

Time-Sliced Heats of Adsorption of Pyridine
(9.8 mM in Cyclohexane) onto Gamma Iron Oxide

Time (sec)	Amount Adsorbed (micromoles/sq.m.)	Heat of Adsorption (kcal/mole)	
		Differential	Integral
60	0.010	-19.9	-19.9
120	0.065	-10.6	-11.9
180	0.127	-8.5	-10.2
240	0.184	-7.5	-9.4
300	0.232	-7.4	-9.0
730	0.499	-5.1	-6.9
1420	0.686	-4.0	-6.1

Determination of the Drago E and C Constants of Ferric Oxide

In previous studies with silica and titania [2,5], it was shown that basic adsorbates interact with the acidic surface sites much as they do with the acid sites of small molecules, and that heats of adsorption of bases onto acidic surfaces obey the Drago correlation of Eqn. (1). By measuring the heats of adsorption of these solids with bases of different C/E ratios, the E and C parameters of the acidic surface sites were determined: for silica, $C_A = 1.16 \pm 0.02$ and $E_A = 4.3 \pm 0.1$; and for titania, $C_A = 1.02 \pm 0.03$ and $E_A = 5.7 \pm 0.2$ $(\text{kcal/mole})^{\frac{1}{2}}$. These earlier heats of adsorption were determined by two different techniques, calorimetric and spectrometric. A Tronac

calorimeter was used with a stirred suspension of powder which was titrated with solutions of bases in neutral hydrocarbons to provide very accurate heat measurements; after the heat of adsorption was generated the concentration of residual base was determined by UV absorption. Heats of adsorption were also determined by the shift of carbonyl infrared absorption peaks upon adsorption of esters and ketones. Both methods gave identical E and C constants for silica.

In these flow microcalorimetric studies we used three bases of appreciably different C/E ratios so that C and E constants could be accurately determined. Pyridine, triethylamine and ethyl acetate were chosen as the test bases for microcalorimetric heats of adsorption studies on the R-1299 ferric oxide equilibrated with cyclohexane having 10-20 ppm of water. All three bases absorb in the UV region well enough to be monitored with the UV detector in the same manner as pyridine. Figure 7 compares the integral differential heats of adsorption of the three bases as a function of the surface concentration of sites neutralized. The integral heats were used because of their greater accuracy and because integral heats were used in the earlier studies with silica and titania.

The E and C constants for the acidic surface sites of the R-1299 alpha ferric oxide can be determined from the heats of adsorption of the three bases. We have chosen to use the integral heats of adsorption at 1.1 micromoles per square meter (-14.2, -10.0 and -6.5 kcal/mole for ethylamine, pyridine and ethyl acetate, respectively) and to determine the E and C parameters for these stronger acidic sites of ferric oxide by a graphical technique (Figure 8). This "E and C plot" is based on a rearrangement of Eqn. (1):

$$E_A = -\Delta Hads/E_B - C_A(C_B/E_B) \qquad (3)$$

As can be seen in Figure 8, the heat of adsorption of each base gives a straight line of slope C/E, and the intersection of lines gives the E and C constants for the acidic surface sites. The line for triethylamine is the steepest (C/E = 11.1), the line for ethyl acetate is the flattest (C/E = 1.78), while the pyridine line falls in between (C/E = 5.47). The average intersection of these three lines gives the Drago E and C parameters for the stronger FeOH sites of alpha ferric oxide:

$$C_A = 0.8 \pm 0.2 \text{ and } E_A = 4.5 \pm 1.1$$

As can be seen in Figure 7, these oxide have a wide distribution of heats of adsorption, so either lower or higher E and C constants could be obtained, depending at what surface coverage we choose for the comparison. The stronger acid sites of the plateau regions of Figure 7 are somewhat less acidic than either the SiOH or TiOH sites, but their C/E ratio (0.18) is rather like those of the TiOH sites (0.18), rather than the SiOH sites (0.27). The C/E ratio is used as a measure of "softness" or "hardness" of acids or bases. Softness is characteristic of high polarizability; soft acids include iodine (C/E = 1.00) and antimony pentachloride (C/E = 0.70). The hydrogen acids are much

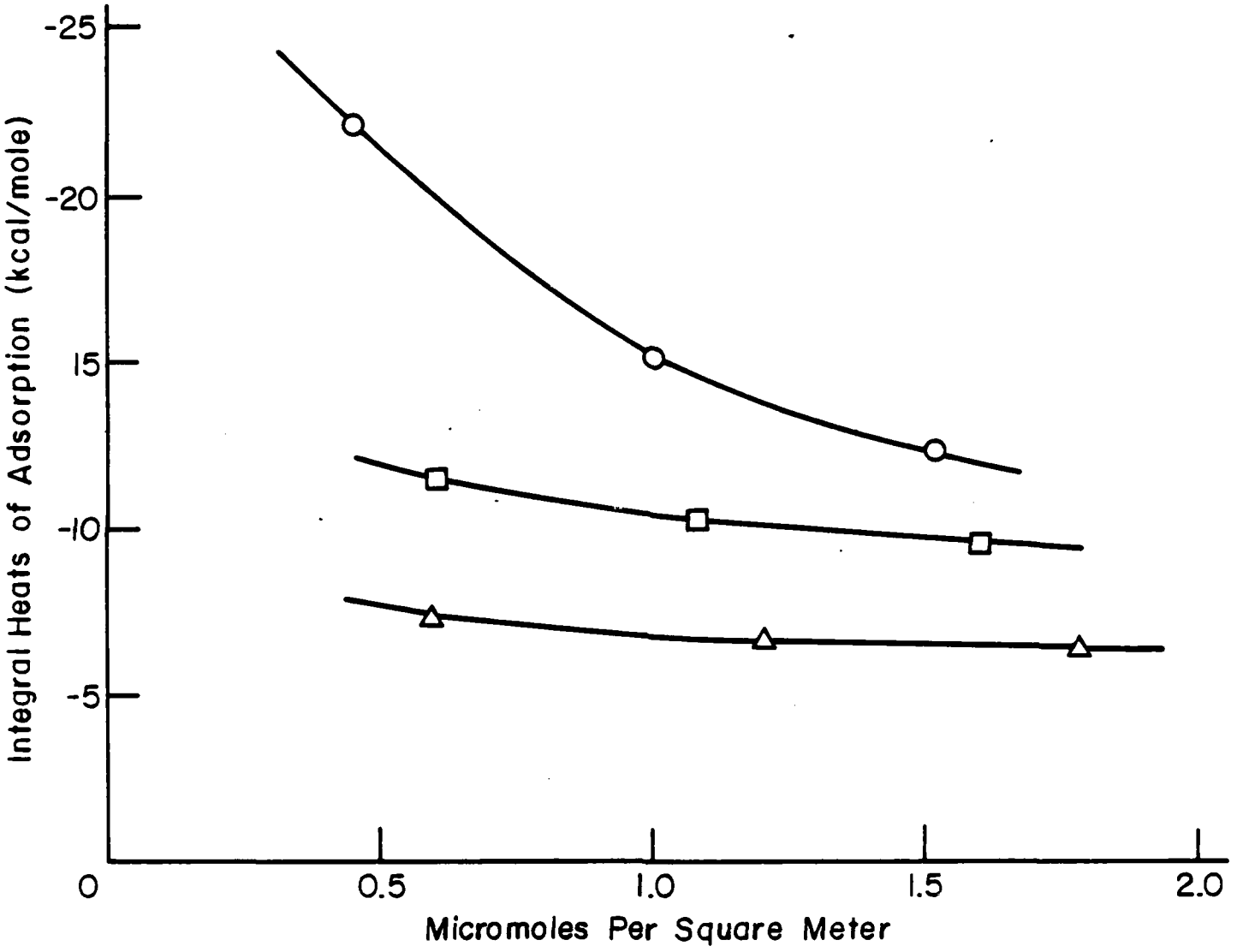

Figure 7. The distribution of the integral heats of adsorption of three bases on alpha ferric oxide, determined by "time-slicing" adsorption exotherms and the corresponding UV adsorption traces. Triethylamine (O), pyridine (□), and ethyl acetate (△). All concentrations 25 mM and water contents 13-20 ppm.

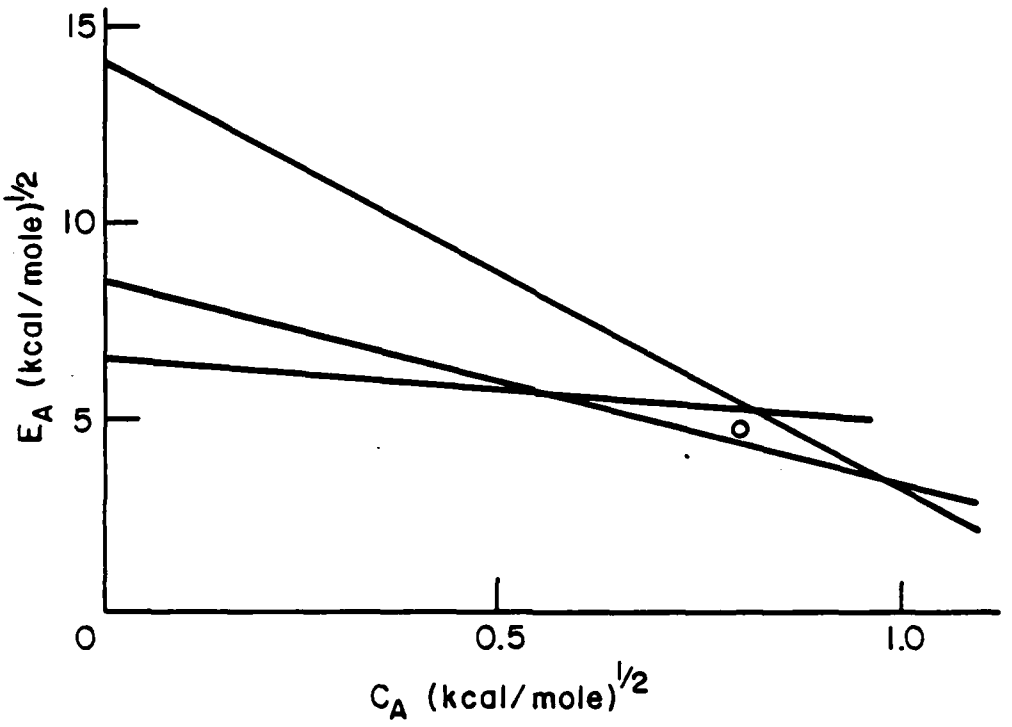

Figure 8. Graphical determination of the E and C parameters for the acidic FeOH sites of alpha ferric oxide, using the heats of adsorption of the plateaus of Figure 6, and the principle of Eqn. (3). The average intersection (O) predicts C = 0.73 and E = 4.6 for these FeOH sites.

less polarizable: examples are phenol (C/E = 0.10), butanol (0.15), and thiphenol (0.20). It is therefore reasonable that FeOH sites have a C/E ratio in this range, and not a higher value such as that estimated in our earlier work with magnetite powders [11].

Effect of Solvent on Heats of Adsorption

The adsorption of pyridine onto the R-1299 alpha ferric oxide was measured in four solvents: n-hexane, cyclohexane, decalin, and benzene. The Langmuir-type adsorption isotherms obtained with saturated solvents, shown in Figure 9, all have the same slope. That means the site area for adsorbed pyridine is not affected by the differences in solubility parameter or the differences in work of adhesion of these saturated solvents. The heats of adsorption of pyridine from these three saturated solvents were found identical by flow microcalorimetry (Table IV).

Table IV

Effect of Carrier Solvent on Heat of Adsorption of Pyridine onto R-1299 Alpha Ferric Oxide

Solvent	Water (ppm)	Pyridine (mM/liter)	Area/Molecule (sq. nm.)	Heat of Adsorption	
				millical/sq.m.	kcal/mole
Hexane	8	29.2	0.48	23.5	-6.8
	3	28.8	0.40	20.5	-5.5
Cyclohexane	6	29.5	0.45	23.8	-6.45
	3	30.3	0.44	22.5	-5.95
Decalin	1	30.5	0.45	24.7	-6.7
	4	29.8	0.42	20.7	-5.3

The case of benzene is quite different, however, for its pi-electrons provide sufficient basicity for it to compete against pyridine for the FeOH sites, and this results in weaker pyridine adsorption and in lower surface concentrations of adsorbed pyridine. The site area per pyridine molecule was 0.97 sq. nm. in benzene as compared to 0.40 sq. nm. in saturated hydrocarbons, and the integral heat of adsorption by flow microcalorimetry at this coverage was -6.4 kcal/mole in benzene versus -9.5 kcal/mole in cyclohexane. If we use the E and C constants for benzene [3], together with those determined for ferric oxide in this work, the heat of benzene adsorption is predicted to be -2.6 kcal/mole, in good agreement with the observed difference of -3.1 kcal/mole for the adsorption of pyridine from saturated hydrocarbon solvents versus adsorption from benzene.

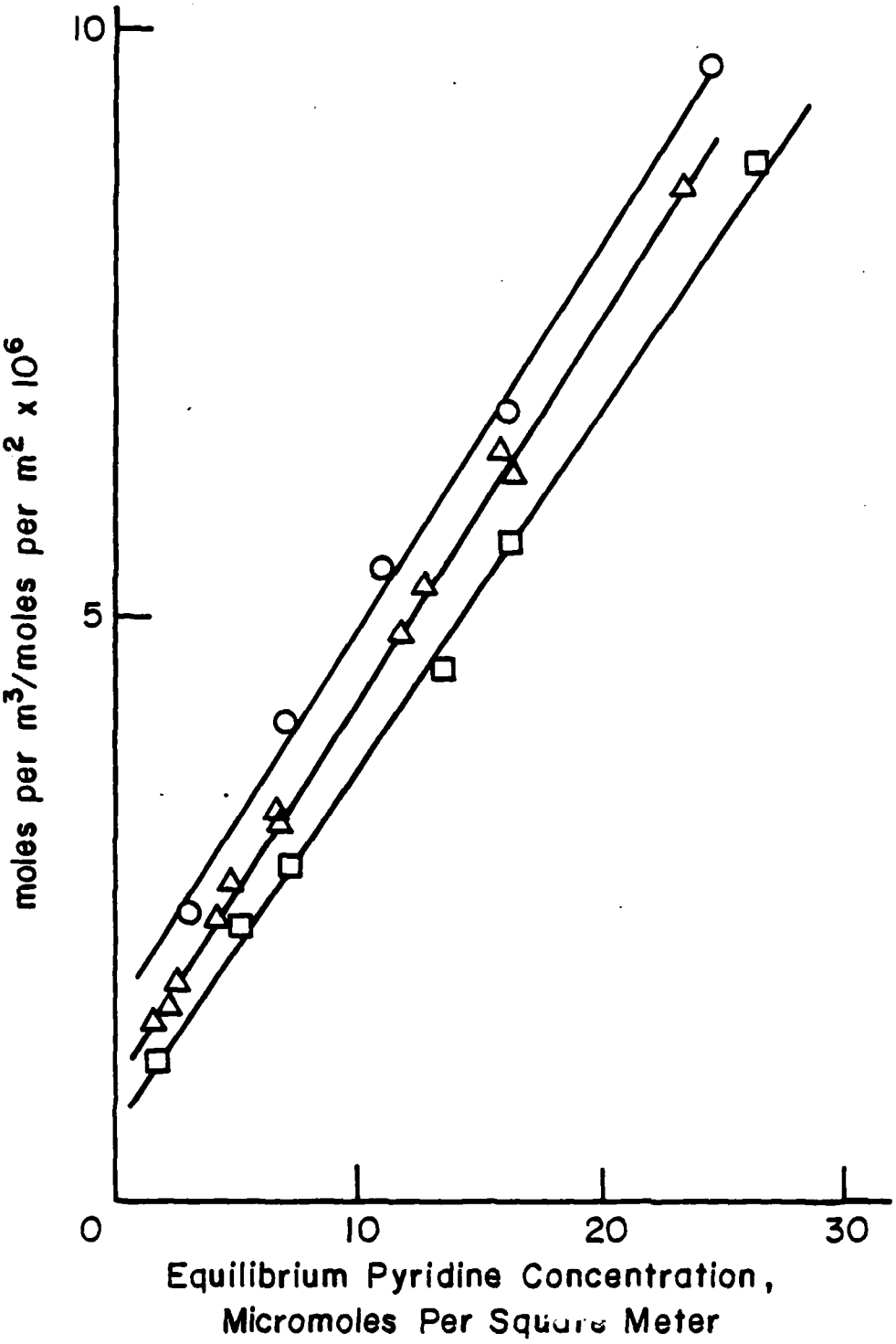

Figure 9. Langmuir plots for the adsorption of pyridine at 28°C onto alpha ferric oxide from hexane (○), from cyclohexane (△), and from decahydronaphthalene (□).

Adsorption of Polyvinylpyridine from Benzene onto Ferric Oxide

Flow microcalorimetry studies were made of the adsorption of a 90,000 MW polyvinylpyridine from benzene onto the R-1299 alpha ferric oxide. All of the previously described precautions for drying the solvent, the adsorbate and the adsorbent were followed rigorously. The bed contained the usual 150 mg of oxide and the concentration of polymer in the incoming stream of the flow calorimeter was 0.1%. The concentration of polymer in the outflowing stream was determined by UV absorption at 285 nm, where Beer's Law was found to hold.

The UV sensor indicated that the adsorption was rapid, and that saturation of the bed (9.36 micromoles of repeat units on 1.5 sq. m. of oxide surface) was reached in six minutes. However, the heat sensor showed evolution of heat for twenty-five minutes, for a total of 28 millicalories. Evidently the polymer molecules take some time to reach the configurations which maximize interaction with the surface.

After the polymer was completely equilibrated on the oxide surface, we probed the amount of bare surface by pumping through the bed a 30 mM solution of pyridine in benzene; 8.05 millicalories were evolved as 1.32 micromoles of pyridine were adsorbed. This amounted to a heat of adsorption of -6.1 kcal/mole, a little less than the -6.5 kcal/mole found on a bare surface. By using the previously determined surface concentration of pyridine adsorbed from benzene, the number of 0.40 sq. nm. acidic sites blocked by the polymer could be determined, and from this information we find that an average of 52% of the polymer repeat units were bonded to the surface, with a heat of adsorption per mole of repeat units of -5.7 kcal/mole. This slightly lower heat of adsorption for pyridine groups in the polymer as compared to ordinary pyridine (-6.4 kcal/mole) could result from steric limitations. The high percentage of repeat units bound to the surface is not too surprising when the energy of bonding per repeat unit is this strong (-9 kT).

CONCLUSIONS

1. The FeOH surface sites of ferric oxides are acidic and adsorb nitrogen and oxygen bases with appreciable heats of adsorption, which can be quantitatively correlated and predicted with the Drago E and C equation.

2. The measured heats of adsorption of test bases of different C/E ratios predict that the stronger acidic surface sites have the following Drago constants: $C_A = 0.8 \pm 0.2$, and $E_A = 4.5 \pm 1.1$ $(\text{kcal/mole})^{\frac{1}{2}}$. These constants are similar to those already measured for the SiOH sites of silica and the TiOH sites of titania, all of which are hard acid sites similar to, but about twice as strongly acidic as, alcohol groups.

3. Polyvinylpyridine adsorbed rapidly onto ferric oxide from a dilute solution in benzene, with 52% of the repeat units bonded to acid sites, and with a heat of adsorption of -9 kT per site.

4. Flow calorimetry with a UV solute-concentration detector downstream of the calorimeter bed can give accurate distributions of heats of adsorption.

5. Moisture levels of solvents, solutes and adsorbents strongly influence heats of adsorption. In the flow microcalorimeter, control of the moisture levels was attained by pumping down with a vacuum pump with liquid nitrogen trap while monitoring evaporative cooling and pressure of the bed. Karl Fischer analyses of water contents of solvents and solutions were necessary to achieve proper dryness.

6. A laboratory microcomputer to collect and correlate heat and concentration sensors was an important part of this project.

ACKNOWLEDGMENTS

We acknowledge with thanks George Salensky of Union Carbide for valuable suggestions and Prof. D. W. Dwight of Virginia Polytechnic Institute and State University for ESCA analyses of our oxides.

REFERENCES

[1] F. M. Fowkes, D. O. Tischler, J. A. Wolfe, L. A. Lannigan, C. M. Ademu-John, and M. J. Halliwell, J. Polymer Sci., Polymer Chem. Ed. 22, 547-66 (1984).

[2] F. M. Fowkes, Rubber Chemistry and Technology 57, 328-43 (1984).

[3] R. S. Drago, G. C. Vogel and T. E. Needham, J. Amer. Chem. Soc. 93, 6014 (1971).

[4] R. S. Drago, L. B. Parr, and C. S. Chamberlain, J. Amer. Chem. Soc. 99, 3203 (1977).

[5] F. M. Fowkes, D. C. McCarthy, and D. O. Tischler, J. Polymer Sci., Polymer Chem. Ed., accepted for 1985.

[6] A. Silberberg, Plenary Address, 58th National Colloid Symposium, Cleveland, Ohio, June 1984.

[7] J. W. Vanderhoff and T. C. Huang, Third Annual Report, ONR Agreement N00014-79-C-0731, December 1982, pp.229-38.

[8] T. Allen and R. M. Tatel, J. Appl. Chem. 20, 165 (1970).

[9] A. J. Groszek, ASLE Trans. 13, 278 (1970).

[10] G. R. Heal and I. J. McEwen, Powder Tech. 30, 243 (1981).

[11] F. M. Fowkes, C.-Y. Sun, and S. J. Joslin, in "Corrosion Control by Organic Coatings," H. Leidheiser, Jr., Ed., NACE: Houston, 1981, p.1.

Program #3

Characterization of Acid-Base Properties of the Hydrated Iron Oxide and Titanium Oxide on Metal Surfaces by XPS and AES

Principal Investigator: Gary W. Simmons
Prof. of Chemistry

Associate: Bruce Beard
(Ph.D. awarded)

INTRODUCTION

Metals exposed to ambient atmosphere are readily oxidized and in the presence of moisture the outer surface of the metal oxide is hydrated [1-3]. Bolger and Michaels [4] have proposed that polymer coatings bond to metal surfaces via hydrogen bonding of polar groups in the polymer with the hydroxyls present on the hydrated metal oxide surface. Fowkes [5,6] has shown that the strength of adhesive bonds between a polymer and a filler (an oxide such as silica) can be correlated with the relative acidic or basic strength of the polymer, filler and solvent. If the bonding of polymer coatings to metal surfaces is indeed by hydrogen bonding, it should be possible to predict not only the relative strengths of the bonding between different coatings and metal surfaces but also the stability of the coating in the presence of water at different values of pH.

The surface hydroxyl (-MOH) interaction with an organic acid (HXR) and an organic base (XR) can be depicted as follows

$$\text{ORGANIC ACID} \quad -\text{MOH} + \text{HXR} \rightleftharpoons -\text{MO}\cdots\overset{\text{H}}{\text{HXR}} \rightleftharpoons -\text{M}\overset{-}{\text{O}}\overset{+}{\text{H}}_2\text{XR} \qquad (1)$$

$$\text{ORGANIC BASE} \quad -\text{MOH} + \text{XR} \rightleftharpoons -\text{MOH}\cdots\text{XR} \rightleftharpoons -\text{M}\overset{-}{\text{O}}\overset{+}{\text{H}}\text{XR} \qquad (2)$$

In these reactions, X is an oxygen, sulfur or nitrogen atom. The bond energy increases as the equilibrium shifts to the right and the bond becomes more ionic. Maximum strength of the bond between an organic coating and metal surface would then be obtained when the surface hydroxyl acts as a strong base and the polar group as a strong acid or when the surface hydroxyl acts as a strong acid and the polar group as a strong base.

Water can displace or interrupt hydrogen bonds according to the following interactions

$$\text{-MO}\cdots\overset{\text{H}}{\text{HXR}} + 2\text{H}_2\text{O} \rightleftharpoons \text{-MO}\cdots\overset{\text{H}}{\text{HOH}} + \text{H}_2\text{O} \quad \text{HXR} \qquad (3)$$

$$\text{-MOH}\cdots\text{XR} + 2\text{H}_2\text{O} \rightleftharpoons \text{-MOH}\cdots\text{OH}_2 + \text{HOH}\cdots\text{XR} \qquad (4)$$

Poor adhesion of a polymer to a metal surface would be expected if the water, acting either as a base or as an acid, forms a stronger hydrogen bond with the surface hydroxyl or with the polar groups in the polymer than the hydrogen bond between the polar group and the surface hydroxyl.

The pH of water at the interface is also expected to interfere with the hydrogen bonding between the polar group in the polymer and the surface hydroxyl.

$$\text{MOH} + \overset{+\ \ \text{H}^+}{\text{HXR}} \rightleftharpoons \text{MO}\cdot\cdot\text{H}\cdot\cdot\text{XR} \overset{\text{OH}^-}{\rightleftharpoons} \text{MO}^- + \text{HOH} + \text{XR} \qquad (5)$$

$$\text{MOH}_2^+ + \overset{\text{H+}\quad\text{H}}{\text{HXR}} \rightleftharpoons \text{M-O}\cdot\cdot\text{H}\cdot\cdot\text{XR} \overset{\text{OH}^-}{\rightleftharpoons} \text{MOH} + \text{HOH} + \bar{\text{X}}\text{R} \qquad (6)$$

The range of pH over which the coating would be expected to be stable is a function of the effective pK_a of the surface hydroxyls and the pK_a of the polar groups in the polymer.

The acid/base properties of polar groups that are typically present in polymer coatings are relatively well known. Acid/base properties of metal oxides have also been studied extensively for oxides in the form of high surface area powders. Less well known, however, is the nature of the hydrated oxide surface on flat metal surfaces that are usually coated for corrosion protection. The goal of our research was to determine the number and acid/base strength of hydroxyls present on oxidized metal surfaces. Based on the results of this study it may be possible to predict the relative stabilities of different coatings on different metal surfaces in the presence of water as a function of pH.

BACKGROUND

We have proposed that the presence and concentration of surface hydroxyls on oxidized metal surfaces can be determined directly by X-ray photoelectron spectroscopy, and that the acid/base properties of these hydroxyls can be determined by following the exchange of K^+ with the hydrated surfaces as a function of pH. The following considerations of surface/solution equilibria are the basis on which the acid/base properties of hydrated oxide surfaces were determined. The hydrated metal oxide on iron for example, when exposed to aqueous solutions, would be expected to behave as a function of pH in the following manner

$$\text{Low pH} \qquad \text{-FeOH} + H^+ \rightleftharpoons \text{-FeOH}_2^+ \; ; \; K_1 = \frac{[\text{-FeOH}_2^+]}{[\text{-FeOH}][H^+]} \tag{7}$$

$$\text{High pH} \qquad \text{-FeOH} + OH^- \rightleftharpoons \text{-FeO}^- + H_2O \tag{8}$$

$$\text{or} \qquad \text{-FeOH} \rightleftharpoons \text{-FeO}^- + H^+ \; ; \; K_2 = \frac{[\text{-FeO}^-][H^+]}{[\text{-FeOH}]}$$

Note that $K_1 = K_a$ when the surface hdyroxyl is acting as a base and $K_2 = K_a$ when it is acting as an acid.

These equilibria have been established for metal oxide powders from measurements of electrophoretic mobility as a function of pH. The pH at which oxide particles do not move in either direction in an applied field is known as the isoelectric point and is a measure of surface acid/base properties. Although electrophoretic mobility measurements are not applicable for low surface area metal surfaces, the equilibria given above can be used to determine the acid/base character of the hydrated oxide on metal surfaces by following the adsorption of anions on the -FeOH_2^+ surface at low values of pH and adsorption of cations on the -FeO^- surface at high values of pH. The following example is considered for cation exchange with the hydrogen of the surface hydroxyl on hydrated iron oxide as a function of pH. Similar arguments apply for the adsorption of anions.

$$\text{-FeOH} \rightleftharpoons \text{-FeO}^- + H^+ \quad ; \quad K_2 = \frac{[\text{-FeO}^-][H^+]}{[\text{-FeOH}]} \tag{9}$$

$$-FeO^- + M^+ \rightleftharpoons -FeO^-M^+ \quad ; \quad K = \frac{[-FeO^-M^+]}{[-FeO^-][M^+]} \qquad (10)$$

At any value of pH the sum of the surface hdyroxyls, ionized hydroxyls and hydroxyls for which hydrogen on the hydroxyl has been exchanged with M^+ is equal to the total number of hydroxyls originally present on the surface, N_o (sites/m^2).

$$[-FeOH] + [-FeO^-] + [-FeO^-M^+] = N_o \text{ (sites/m}^2\text{)} \qquad (11)$$

In the presence of excess cations, the ionized surface hydroxyls are all assumed to be exchanged, $[-FeO^-M^+] >> [FeO^-]$.

$$N_o = [-FeOH] + [-FeO^-M^+] \qquad (12)$$

$$K_2 = \frac{[-FeO^-][H^+]}{[-FeOH]} = \frac{[-FeO^-M^+][H^+]}{[-FeOH]} \qquad (13)$$

For convenience, the fraction, θ, of the total available hyroxyls which have undergone exchange, i.e., coverage, is defined by the following:

$$\theta = \frac{[-FeO^-M^+]}{N_o} \qquad (14)$$

Using this definition of the fraction of exchange, θ, in Eqn. (12) and, substituting the result into Eqn. (13), gives the following result.

$$pH = pK_2 - \log \frac{\theta}{1 - \theta} \qquad (15)$$

In this equation, pH = -log $[H^+]$ and pK_2 = -log K_2. The pK_2 of the hydroxyls can thus be obtained by plotting, θ, as a function of pH. The pH at which this fraction equals 0.5 (i.e., $\theta = 0.5$) is the pK_2 of -FeOH. Similar experiments using anions would give the pK_1 of $FeOH_2^+$ for the equilibrium shown in Eqn. (7). AES and XPS were used to measure the coverage, θ, of K^+ after exposure of these metals to solutions containing K^+ at different values of pH.

EXPERIMENTAL

Titanium and iron surfaces were chosen for study not only because of their practical importance, but also because their acid/base properties were expected to be different owing to differences in charge/radius ration of the Ti^{+4} and Fe^{+3} ions present in the respective oxides. The iron and titanium used in these experiments were obtained from Metron, Inc., Allamunchy, N.J. The iron was 99.99+% pure and the titanium was high purity with iron at 0.2 weight percent as the major impurity. The rough cut iron and titanium metal surfaces were mechanically polished (both faces) to a final finish with 0.3 μm alumina grit. Once polished, the specimens were rinsed with distilled water and fried with 100% ethyl alcohol.

The substrates were hydrogen annealed then subsequently "wet" oxidized in a quartz glass tube furnace. The tube furnace was purged for 2 hours with flowing zero-grade argon. The temperature was then raised to 600°C and 8 to 12% H_2 was added to the argon flow. Iron wool was placed in the quartz tube between the gas source and the specimens to remove oxygen from the annealing gas. A charcoal/zeolite trap in the gas line was used to remove water vapour and hydrocarbons from the gases. The annealing process lasted one hour. The specimens were then cooled under the flowing H_2/Ar mixture. The H_2 was cut-off and the Ar flow (0.25 ℓ/min.) was diverted through a water bubbler containing high purity water. The iron wool was moved out of the heated zone and the specimens were then oxidized for 24 hours at 200°C in the saturated water vapor.

Potassium ion was chosen for the exchange experiments because it does not hydrolyze over wide range of pH and potassium has a relatively high sensitivity for AES and XPS analysis. Solutions with the desired pH were prepared by adjusting the pH of a stock solution of 0.03 M solution of KOH with HNO_3. Ultra pure KOH obtained from Alfa Products was used in these experiments. The major impurities were 30 ppm sodium and 0.3 ppm calcium. All glassware used in preparing the solutions was cleaned with a 50/50 mixture of concentrated HNO_3/H_2SO_4.

The water used to prepare the potassium ions solutions was found to be a major source of "organic" contamination in the initial experiments. To minimize the "organic" contaminants, distilled water was further distilled in a quartz glass still which was continuously being purged with zero grade nitrogen. Further reduction of "organics" was accomplished by UV oxidation using a Barnstead Organic Pure system.

Specimens were immersed in the potassium hydroxide solutions for 300 seconds which was long enough for complete ion exchange [8,9] and short enough for minimal dissolution of the surface oxide [10]. Absolute ethyl alcohol was used for rinsing the specimens after removal from the potassium hydroxide solutions. The acid strength of ethanol is believed to be too low to disturb the equilibrium concentration of the potassium on the specimen surfaces.

Six specimens were used in each experiment for each value of solution pH. Four of these speicmens were ion exchanged, while the other two were used as controls. One control, referred to as the "water blank", was immersed in 20 milliliters of the water used to prepare the potassium hydroxide solution. This specimen was then rinsed with ethanol. The other control specimen designated at the "tube blank" was taken directly from the tube furnace and exposed to the ambient atmosphere for a time equal to that of all other specimens. Surface analysis of these control specimens was used to determine possible contamination sources.

EXPERIMENTAL RESULTS

Typical XPS spectra taken of specimens after preparation of the hydrated oxide surfaces, after immersion in distilled water and after immersion in potassium containing solutions at pH are shown in Figures 1 and 2 for iron and titanium, respectively. These spectra show the expected oxygen and oxidized metal peaks and, for the specimens that were immersed in the potassium solution, the expected potassium peaks. In addition, carbon and sodium were found. Comparison of the spectra shows that the carbon peak intensity was lowest on the as-prepared specimens. The carbon peak intensity increased slightly after immersion in either distilled water or in the potassium-containing solutions. Sodium, on the other hand, was present on the as-prepared specimens, and the amount of sodium remained essentially constant after further treatments.

A typical high resolution carbon (1s) spectrum is shown in Figure 3 which has been resolved into three components. The most intense peak at 284.5 eV is attributed to carbon in $-CH_2-CH_2-CH_2-$ and the peaks at 285.9 eV and 288.2 eV are oxidized carbon. The carbon (1s) binding energies of different oxygenated carbon that may be present in the organic contamination are shown in Table I. Unequivocal identification of the specific organic compound(s) that is present on these specimens is not possible. The carbon spectrum, however, does indicate that the organic compound(s) contains polar groups. The polar groups can account for the propensity of the adsorption of organic contamination observed on the hydrated oxides of the iron and titanium specimens after exposure to the atmosphere and to the solutions used in this study.

Figures 4 and 5 show high resolution oxygen (1s) spectra for iron and titanium specimens, respectively. These spectra show at least three resolved peaks at 529.9 eV, 531.5 eV and 532.8 eV. The most intense peak at 529.9 eV is attributed to the oxygen in the metal oxide, the lower intensity peak at 531.5 eV is believed to be the oxygen in a surface hydroxyl, and the relatively small peak at 532.8 eV can be attributed to adsorbed molecular water and/or to the oxygen present in the organic contamination. These assignments for the oxygen (1s) components observed for the iron specimen are in agreement with those reported for studies of the oxidation of iron in water vapor [1,9]. A similar assignment can be made for the oxygen (1s) components found on the titanium specimen. The intensities of the hydroxyl and molecular water peaks were found to increase relative to the oxide peak as the angle between the analyzer and the surface normal was increased. This result is direct evidence that the hydroxyls and molecular water are present on the outermost part of the specimen surfaces.

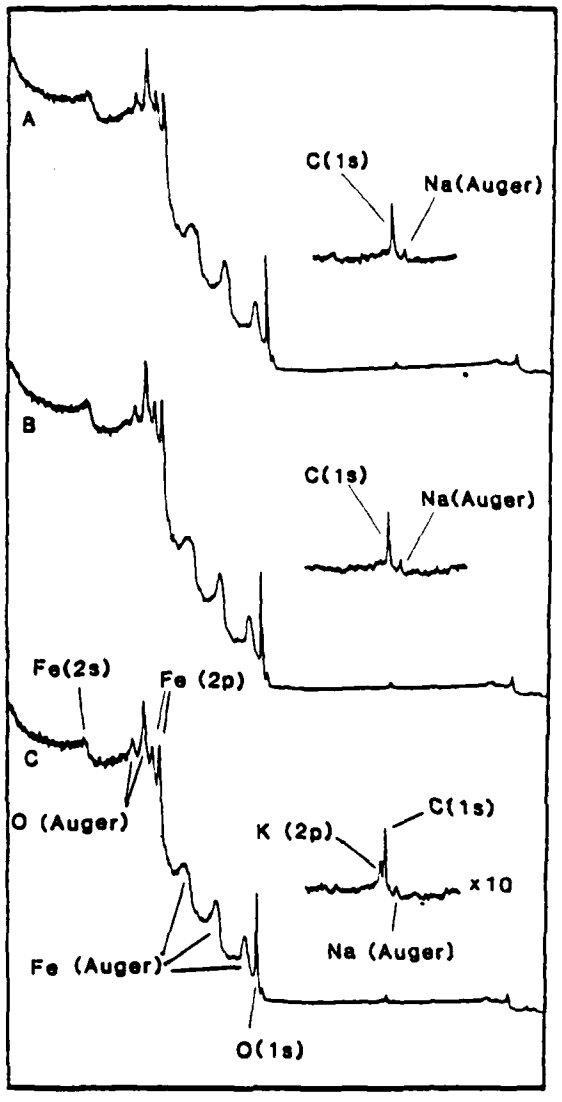

Figure 1. XPS survey scans of iron specimens: (a) after preparation, (b) after immersion in distilled water, (c) after potassium ion exchange.

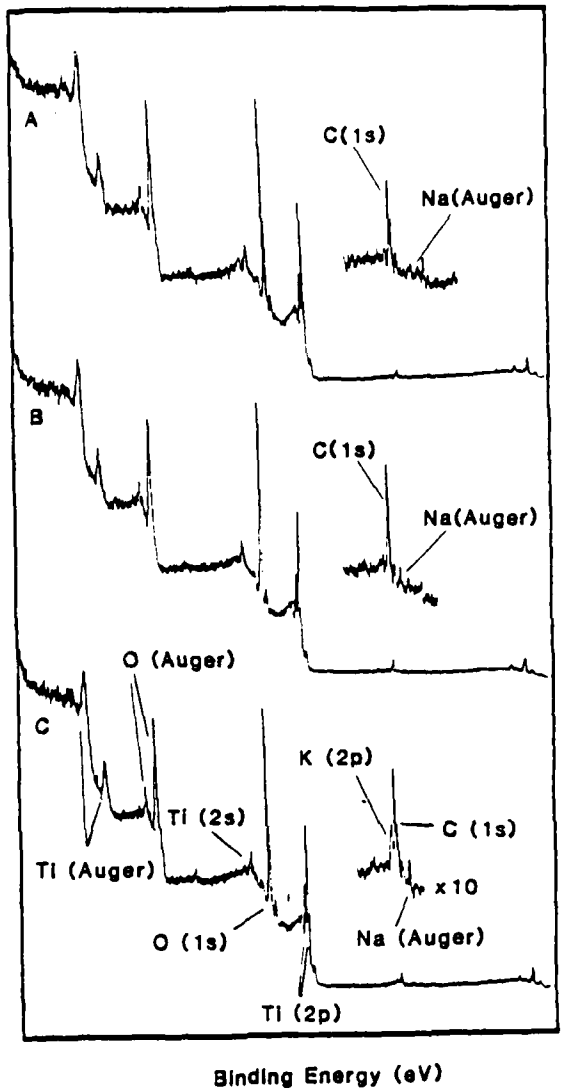

Figure 2. XPS survey scans of titanium specimens: (a) after preparation, (b) after immersion in distilled water, (c) after potassium ion exchange.

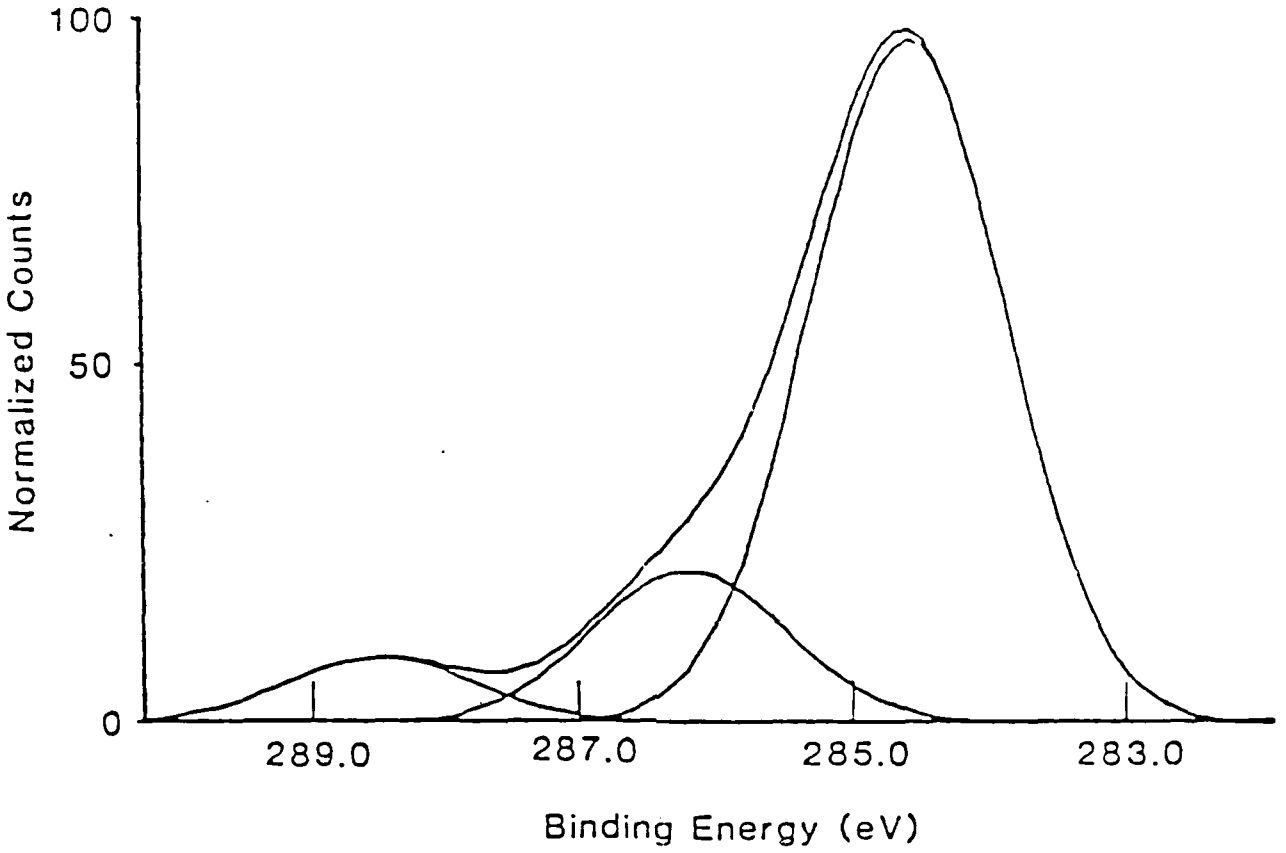

Figure 3. Typical C(1s) photoelectron spectrum of specimen surface.

Table I

Comparison of C(1s) Binding Energies of Carbon Contamination on Iron and Titanium Specimens C(1s) Binding Energies of Different Organic Functional Groups [11].

Experimental Binding Energy (eV)	Functional Group	Reported Binding Energy (eV) (86)
284.6	$-CH_2-$	284.6
Titanium 286.1 Iron 285.9	$-CH_2-OH$	286.2
	$-CH_2-O-CH_2-$	286.1
	$-\overset{O}{\overset{\|}{C}}-O-\overset{*}{C}H_2-$	286.2
Titanium 288.6 Iron 288.2	$>C=O$	287.5
	$-\overset{*}{\overset{O}{\overset{\|}{C}}}-O-CH_2-$	288.8
	$-\overset{O}{\overset{\|}{C}}-OH$	288.7

Binding Energies Referenced to ($-CH_2-$) Carbon(1s), 284.6 eV.

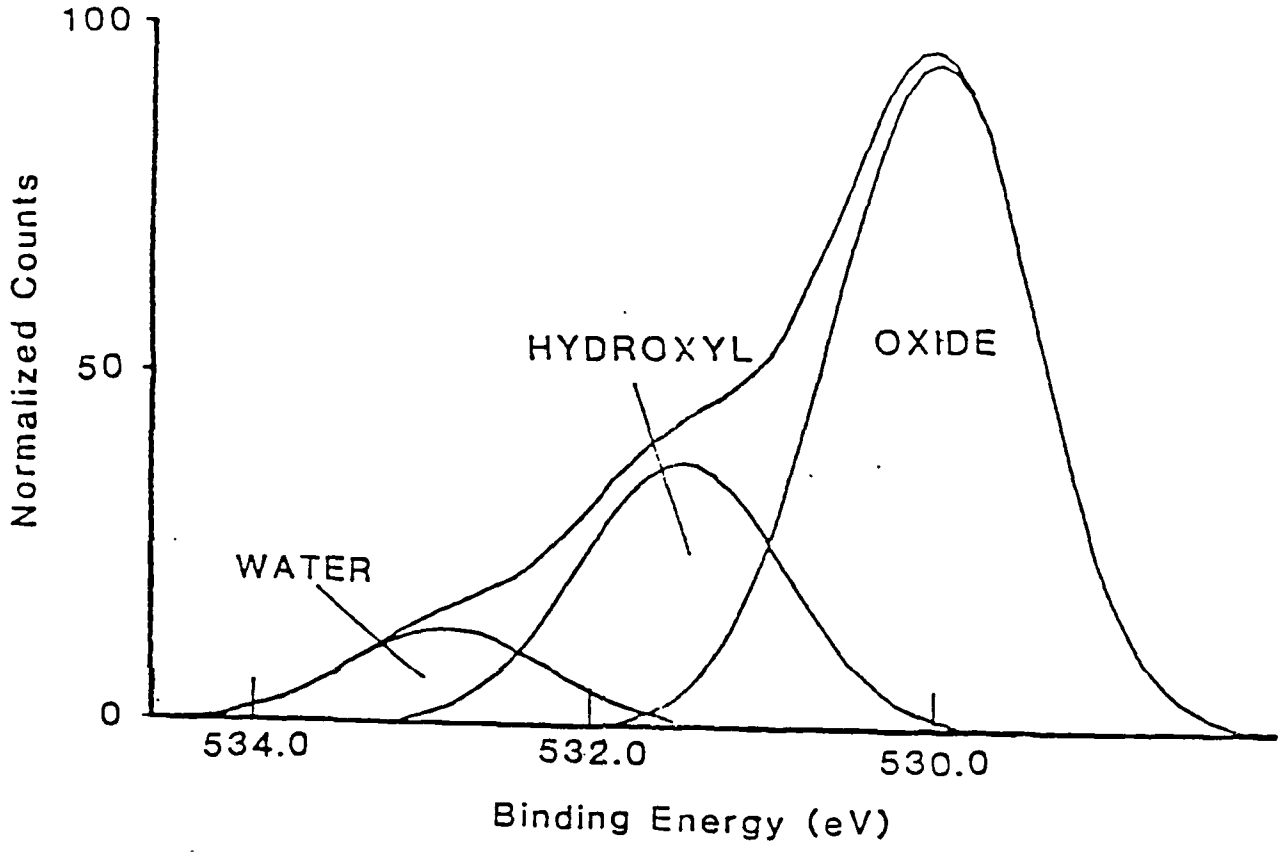

Figure 4. Curve resolved O(1s) photoelectron spectrum showing the oxide, hydroxy. and adsorbed water peaks on an iron specimen. Angle between analyzer and surface normal was 75 degrees.

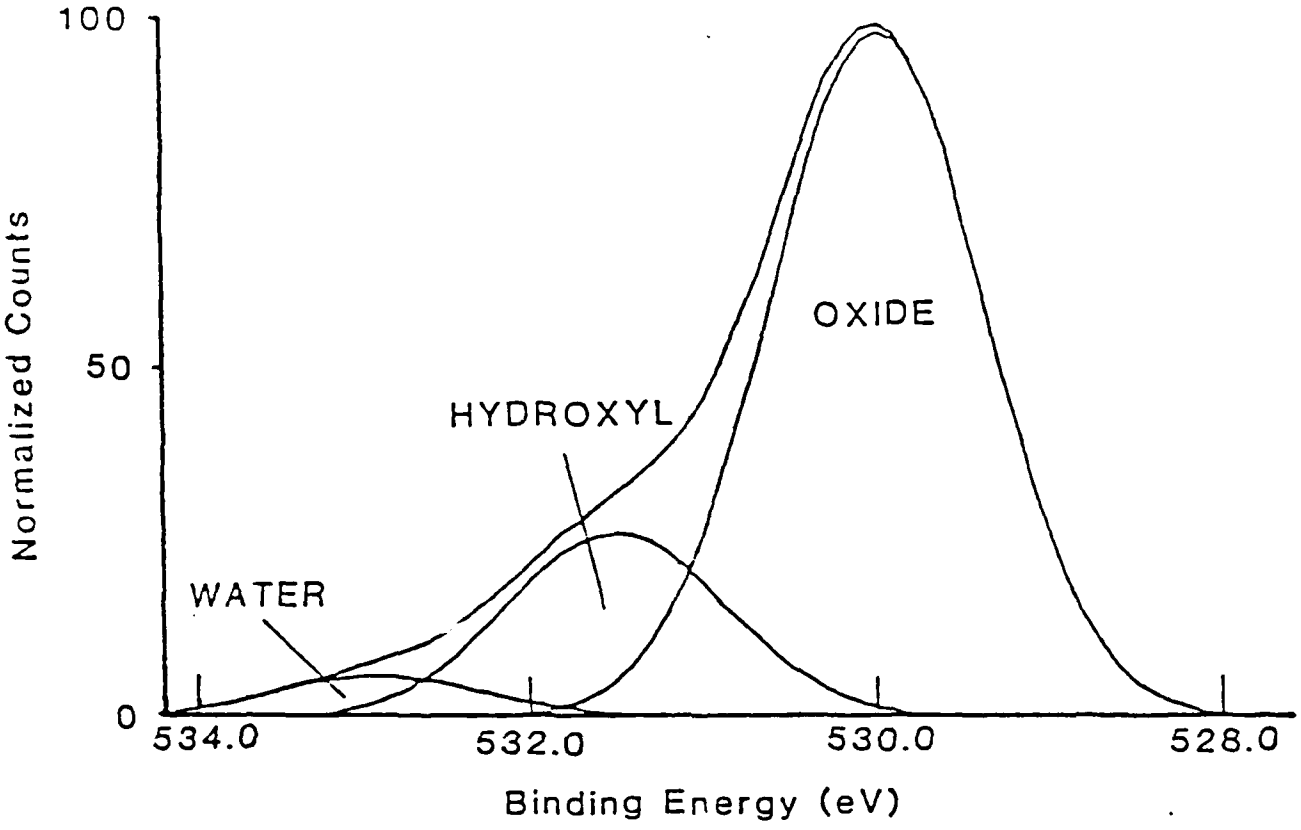

Figure 5. Curve resolved O(1s) photoelectron spectrum showing the oxide, hydroxy, and adsorbed water peaks on a titanium specimen. Angle between analyzer and surface normal was 75 degrees.

Estimates of the surface concentrations of hydroxyls were made on the basis of a method proposed by Dreiling [15]. The following analytical expression was used to make these estimates.

$$X_{OH} = \frac{I_{OH}[\exp(-Z/\lambda_O \cos\theta)]}{I_O[1-\exp(-Z\lambda_O \cos\theta)]} \cdot X_O Z \qquad (16)$$

In this expression, X_{OH} is the number of hydroxyls/nm^2, X_O is the number of oxygen/nm^3 in the bulk oxide, Z is the thickness of the hydroxyl layer, θ is the angle between the surface normal and the analyzer, λ_O is the mean escape depth for the oxygen (1s) photoelectrons, I_{OH} and I_O are the hydroxyl and oxide signal intensities, respectively. For both the titanium and iron specimens θ is 75°. A value for the mean escape depth of oxygen (1s) photoelectrons of λ_O= 1.1 nm was used for both specimens. The thickness of the hydroxyl layer was taken as 0.27 nm. For Fe_2O_3 the bulk density of oxygen is 59.3/nm^3, and for TiO the bulk density of oxygen is 63.7/nm^3. Using these values and the measured relative intensities of the oxygen (1s) photoelectron signals from the hydroxyl and oxide, the hydroxyl concentration of the iron specimen was found to be 2.6/nm^2 and for titanium specimens the concentration was 4.3/nm^2. These values are in reasonable agreement with those reported for high surface area oxides [16,17].

Since it was shown earlier that the organic compound(s) present on the specimens contained oxygen, the possible overlap of this organic oxygen with that of the hydroxyl and/or molecular water spectrum was considered. The binding energies of oxygen (1s) in several organic functional groups are summarized in Table II. It is apparent that the oxygen peak from the organic contamination does not overlap the oxygen peak from the hydroxyls. The oxygen (1s) binding energies in functional groups of organic compounds, however, are similar to the oxygen (1s) binding energy in molecular water.

A typical high resolution XPS spectrum of the potassium ($2p_{3/2}$, $2p_{1/2}$), carbon (1s) and sodium KLL_{23} Auger peak from a titanium specimen after immersion in potassium solutions at pH 11.0 is shown in Fig. 6. The integrated areas of the potassium photoelectron lines and the integrated area of the hydroxyl component of the oxygen spectrum were used in the determination of the fraction of the hydroxyls that had exchanged a hydrogen ion for a potassium ion as a function of pH.

The fraction of exchanged hydroxyls, also referred to as coverage, was estimated at each value of pH by the following relationships [15].

$$I_K = K_K X_K [1 - \exp(-Z/g\lambda_K)] \qquad (17)$$

$$I_{OH} = K_{OH} X_{OH} [1 - \exp(-Y/g\lambda_{OH})] \exp(-Z/g\lambda_O) \qquad (18)$$

Table II

Comparison of O(1s) Binding Energies from Iron and Titanium Surfaces with O(1s) Binding Energies in Oxides, Hydroxides, and Organic Functional Groups

Experimental O(1s) Binding Energy (eV) for Iron and Titanium surfaces		Reported Binding Energy (eV)		Ref.
Iron Surface	529.9	Fe_2O_3	530.0	12
	531.5	Fe-OH	531.4	12
	532.8	H_2O	532.0-534.0	1, 12, 13
		$-\overset{\overset{O}{\parallel}}{C}-O-CH_2-$	532.6* 534.0†	11
		$-\overset{\overset{O}{\parallel}}{C}-OH$	533.0* 533.9†	11
		$-CH_2-O-CH_2-$	533.2	11
		$>C=O$	533.2	11
		$-CH_2-OH$	533.2	11
Titanium Surface				
	529.7	TiO_2	530.2	18
	531.5			
	532.3	H_2O	532.0-534.0	13

Binding Energies Referenced to ($-CH_2-$) Carbon(1s), 284.6 eV.

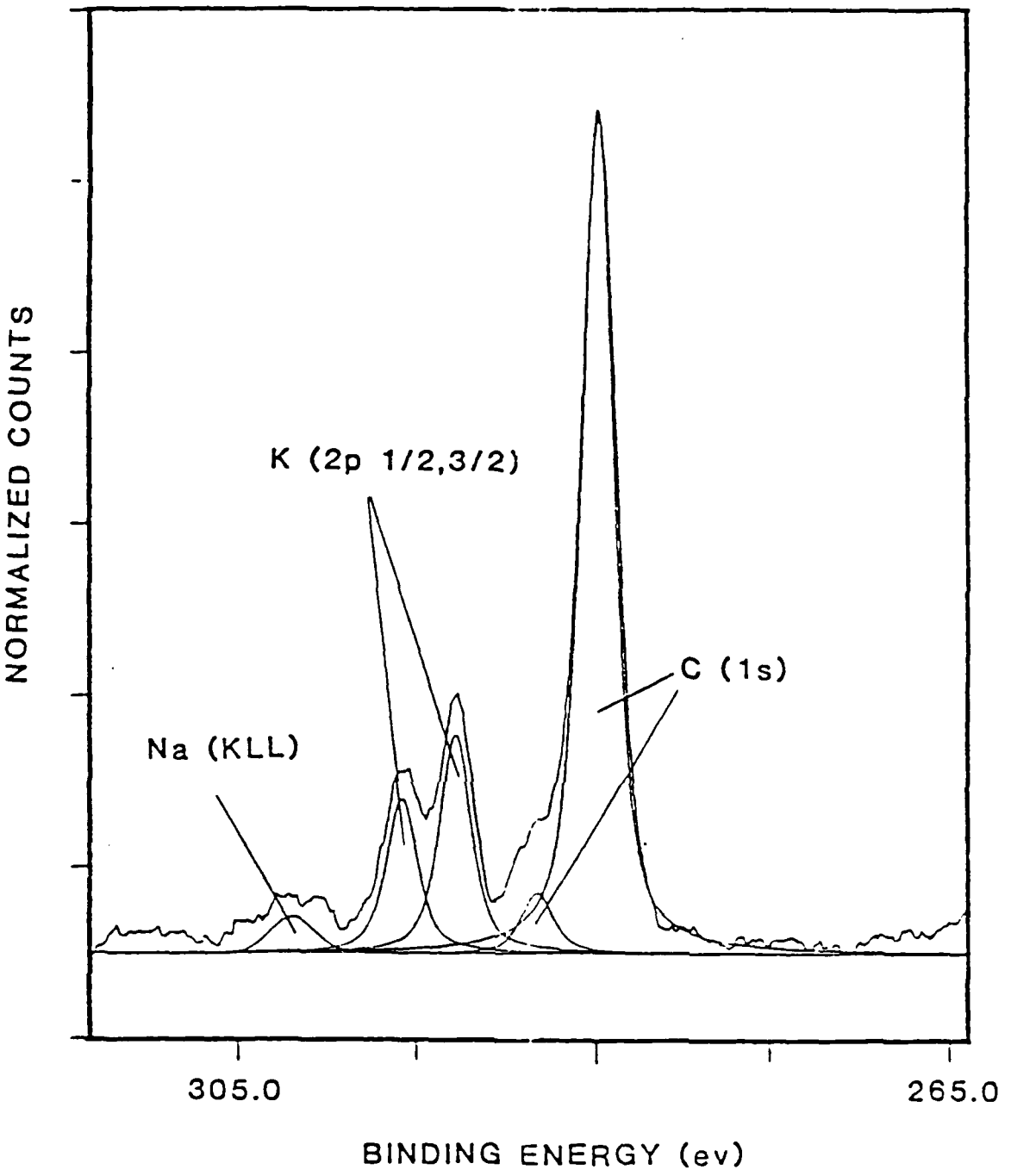

Figure 6. Curve resolved photoelectron spectrum of potassium on an iron surface following exposure to a potassium-containing solution.

In these equations $K_i = K\sigma_i g X_i/E$ for the ith component. The parameter K is characteristic of the instrument, σ is the photoelectron crossection, g is an instrument parameter that is a function of the angle between the surface normal and the entrance to the analyzer (g = 0.75 in this case), λ is the mean escape depth of the photoelectron, E is the kinetic energy of the photoelectron, Z is the thickness of the potassium ion layer and Y is the thickness of the hydroxyl layer. The following values were used in estimating coverage: λ_O = 1.1nm, λ_K = 1.2nm; $\sigma(O1s)$ = 2.85, $\sigma(K2p_{3/2})$ = 2.67; Z = 0.266 nm, Y = 0.27 nm; E = 960.7 eV, E = 721 eV. On the basis of the values of these parameters, the relationship between coverage and the ratio of the hydroxyl and potassium peaks was found to be as follows.

$$\theta = X_K/X_{OH} = (1.1)(I_K/I_{OH}) \qquad (19)$$

For iron specimens, Fig. 7, the coverage, θ, increased as a function of pH as expected for pH values up to 11.7. Above pH = 11.7, however, an unexpected drop in coverage was observed. The region of pH where the increase in coverage versus pH is most rapid was used to estimate the pK_2 for the hydrated iron oxide on iron. Figure 7 shows that the slope has the highest value at about pH 11.5 which corresponds to a pK_2 of 11.5. Because of the decrease in coverage at high values of pH, a saturation coverage was not observed. If it is assumed that the highest coverage obtained, $\theta \sim 0.45$, is close to the saturation value, then it is apparent that either some of the hydroxyls are not available for exchange or do not undergo exchange over the pH range shown in Fig. 7.

The coverage increased as a function of pH for the titanium specimens and appeared to reach a saturation value above pH 10.8, Fig. 8. This saturation value, as was found for iron, indicated that only about one half of the hydroxyls were exchanged. A decrease in coverage at high pH comparable to that found with iron, however, was not found for titanium. The pH at which the rate of change in coverage is the highest gave an estimated value for pK_2 = 10.0 for the hydrated oxide on titanium. The lower pK_2 value for titanium compared to that for iron is consistent with the larger charge radius ratio of Ti^{+4} in titanium oxide compared to that for Fe^{+3} in iron oxide.

DISCUSSION

High resolution oxygen (1s) spectra of iron and titanium surfaces indicated the presence of hydroxyls which could be clearly distinguished from oxygen in organic contamination. The hydroxyl concentration on the oxides of titanium and iron was found to be on the order of 2-4 hydroxyls/nm^2. The coverage versus pH results presented in Figs. 7 and 8 show that the iron and titanium surfaces behave as acids. Some scatter in the data, however, was observed. Furthermore, deviation in ideal behavior was seen for iron at high pH. The varying amounts of sodium and carbon contamination were considered as possible causes for the scatter in the data. No correlations were found, however, between coverage and either the total carbon signal or the sodium signal. The organic contamination, on the other hand, may have been bound to the surface by interaction between the organic polar group(s) and the surface

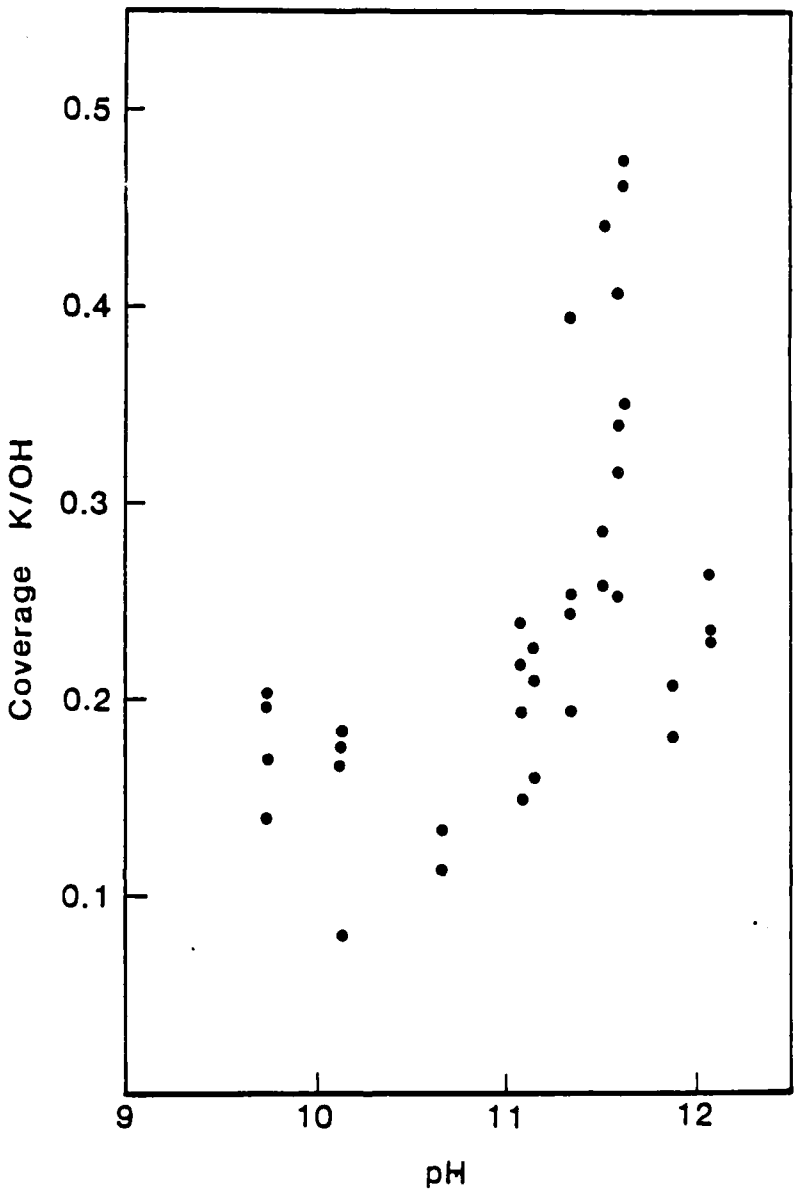

Figure 7. Potassium coverage as a function of pH for iron.

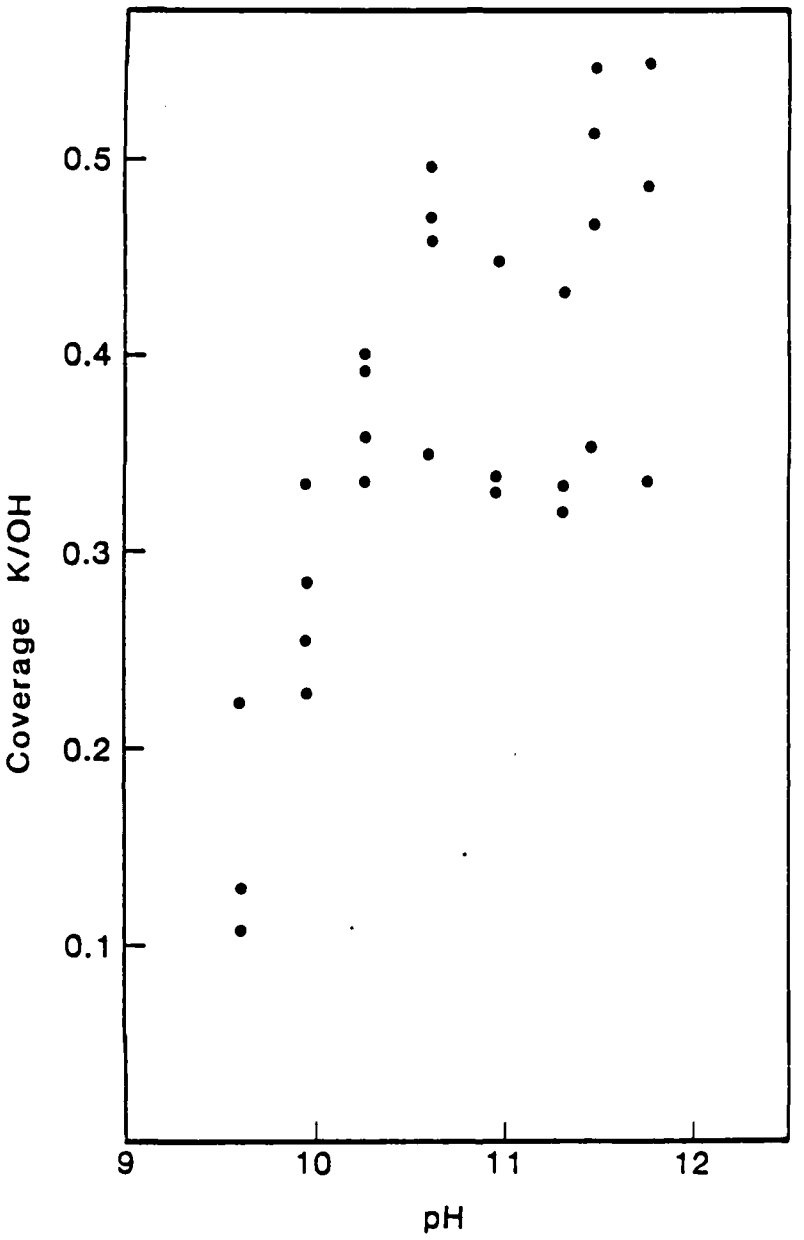

Figure 8. Potassium coverage as a function of pH for titanium.

hydroxyl. The number of surface hydroxyls tied up by the organic contamination would be expected to be a function of the intensity of the peaks from the polar group component at 288.6 eV in the carbon (1s) spectrum. No correlation, however, was found between coverage and the 288.6 eV carbon (1s) peak intensity.

It is possible that in solutions at high pH, the organic contamination is displaced according to the following reaction.

$$-FeOH_2^+OC(CH_2)_nCH_3 + OH^- \rightleftharpoons -FeOH + OC(CH_2)_nCH_3 + H_2O \quad (20)$$

Consequently, the surface hydroxyls could have undergone exchange with potassium even for specimens contaminated with organics. The carbon found on the specimen surfaces may have resulted from recontamination by organic compounds during subsequent rinsing and exposure to air. The possible role of sodium contamination during the exchange, on the other hand, is not clear. The decrease in potassium coverage for pH > 11.7 for the iron specimens may be attributed to instability of iron oxide at this pH [20].

Our studies have not yet included the anion exchange reactions at low pH that would provide a pK_1 value for $-MOH_2^+$. The uptake of phosphate ion by oxide films on mild steel, however, has been reported by Thomas [21]. The adsorption of phosphate on this oxide surface was followed using radioactive phosphorus doped phosphate over a pH range of 7-13, and the results are reproduced in Fig. 9. The highest phosphate uptake was estimated to be on the order of a monolayer for pH values lower than 7. Above pH 7 the phosphate adsorption decreased with increasing pH. One half of the maximum uptake occurred at pH 8.5, suggesting that the pK_1 for $-FeOH_2^+$ has a value of 8.5. On the basis of Thomas's results and the results of our study, the acid/base properties of the hydrated oxide on iron can be summarized as follows.

$$-FeOH_2^+ \rightleftharpoons -FeOH + H^+ \qquad pK = 8.5 \quad (21)$$

$$-FeOH \rightleftharpoons -FeO^- + H^+ \qquad pK = 11.5 \quad (22)$$

We are not aware, however, of any anion exchange studies for hydrated oxide on titanium surfaces. From our study of cation exchange, we propose the following acid/base properties for titanium surfaces.

$$-TiOH_2^+ \rightleftharpoons -TiOH + H^+ \qquad pK = \text{not available} \quad (23)$$

$$-TiOH \rightleftharpoons -TiO^- + H^+ \qquad pK = 10.0 \quad (24)$$

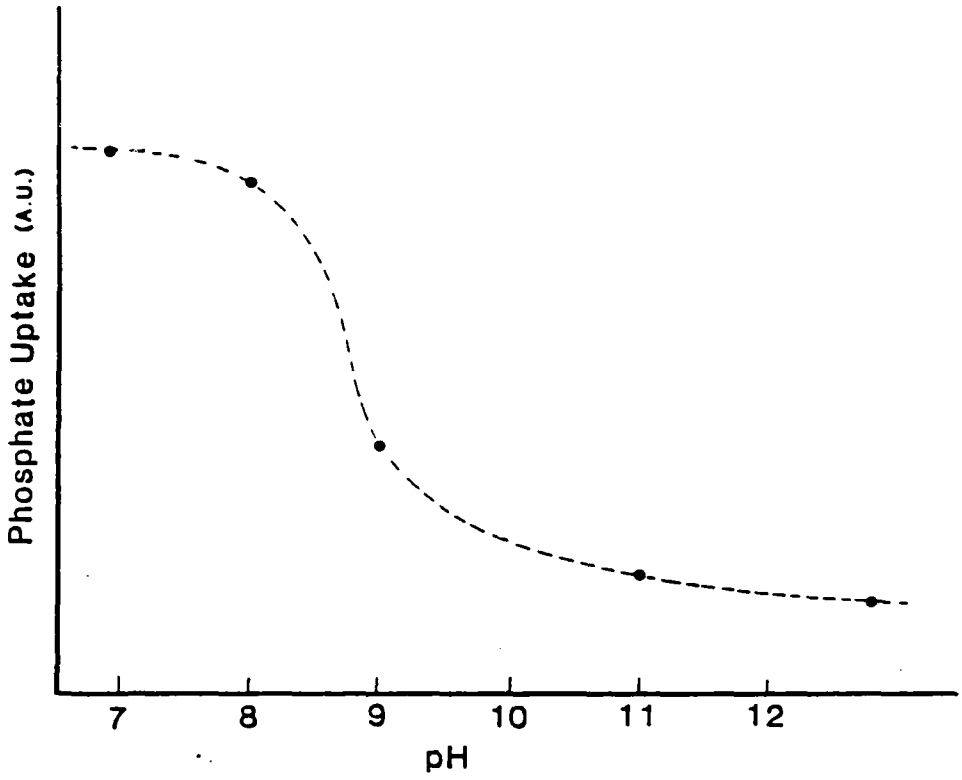

Figure 9. Adsorption of phosphate on mild steel surface as a function of pH. After Thomas [21].

The more acidic nature of titanium compared to iron is consistent with the higher charge/radius ratio of Ti^{+4} compared to Fe^{+3} in the respective metal oxide [7].

Bolger and Michaels [4] and Noller et al. [22] have proposed that the $pK_{1,2}$ of the surface and the pK_a of polar groups in organic coatings can be used to predict the strength of the hydrogen bonding between surface and coating. For example, the interaction between an organic acid and a hydrated metal surface can be considered for organic acids as follows.

$$-MOH + H^+ \rightleftharpoons -MOH_2^+ \qquad K_2 = 10^{-pK_1} \qquad (25)$$

$$RCOOH \rightleftharpoons RCOO^- + H^+ \qquad K_a = 10^{pK_a} \qquad (26)$$

The equilibrium constant for the interaction between the coating and surface can then be found.

$$-MOH + RCOOH \rightleftharpoons -MOH_2^+OOR^- \qquad K = 10^{pK_a}/10^{pK_2} \qquad (27)$$

The standard free energy of the coating/surface interaction is then a function of this equilibrium constant.

$$\Delta G^o = -RT \ln [K_a/K_1] \qquad (28)$$

The relative strength of the bonding between the surface and coating is thus a function of the difference between the surface pK_1 and organic polar group pK_a values.

$$\Delta G^o = f(pK_a - pK_1) \qquad (29)$$

On the basis of the equilibria shown above, the coating would be expected to be stable in solutions over the pH range $pK_1 > pH > pK_a$. Similar arguments are applicable for interactions between the hydrated metal surfaces and organic bases.

$$-MOH \rightleftharpoons -MO^- + H^+ \qquad K_2 = 10^{pK_2} \qquad (30)$$

$$RCH_2NH_2 + H^+ \rightleftharpoons RCH_2NH_3^+ \qquad K_a = 10^{-pK_a} \qquad (31)$$

The more acidic nature of titanium compared to iron is consistent with the higher charge/radius ratio of Ti^{+4} compared to Fe^{+3} in the respective metal oxide [7].

Bolger and Michaels [4] and Noller et al. [22] have proposed that the $pK_{1,2}$ of the surface and the pK_a of polar groups in organic coatings can be used to predict the strength of the hydrogen bonding between surface and coating. For example, the interaction between an organic acid and a hydrated metal surface can be considered for organic acids as follows.

$$-MOH + H^+ \rightleftharpoons -MOH_2^+ \qquad 1/K_1 \qquad (25)$$

$$RCOOH \rightleftharpoons RCO\bar{O} + H^+ \qquad K_a \qquad (26)$$

The equilibrium constant for the interaction between the coating and surface can then be found.

$$-MOH + RCOOH \rightleftharpoons -M\overset{+}{O}H_2\bar{O}OR \qquad K = K_a/K_1 \qquad (27)$$

The standard free energy of the coating/surface interaction is then a function of this equilibrium constant.

$$\Delta G^o = -RT \ln [K_a/K_1] \qquad (28)$$

The relative strength of the bonding between the surface and coating is thus a function of the difference between the surface pK_1 and organic polar group pK_a values.

$$\Delta G^o = f(pK_a - pK_1) \qquad (29)$$

On the basis of the equilibria shown above, the coating would be expected to be stable in solutions over the pH range $pK_1 > pH > pK_a$. Similar arguments are applicable for interactions between the hydrated metal surfaces and organic bases.

$$-MOH \rightleftharpoons -M\bar{O} + H^+ \qquad K_2 \qquad (30)$$

$$RCH_2NH_2 + H^+ \rightleftharpoons RCH_2\overset{+}{N}H_3 \qquad 1/K_a \qquad (31)$$

The relative strength of the interaction, in this case, is a function of the difference between the surface pK_2 and the organic polar group pK_a value.

$$\Delta G^{\circ} = f(pK_2 - pK_a) \qquad (32)$$

Interactions of this type would be expected to be stable over the pH range $pK_2 < pH < pH_a$.

The reactions between hydrated metal oxide surface and the polar groups in organic coatings are represented by equations (1) and (2) given earlier. According to reaction (1) when the organic polar group is a strong acid the surface may behave as a base. The more negative the value of $(pK_2 - pK_a)$ the greater the equilibrium is shifted to the right resulting in a stronger bond between the organic coating and the metal substrate. On the other hand, when the organic polar group is a strong base the surface may behave as an acid. With increasingly negative values of $(pK_a - pK_1)$, the equilibrium shown in equation (2) is shifted more to the right, forming a stronger bond between the surface and coating.

The pK values for a number of organic acids and bases are listed in Table III along with calculated values of $(pK_2 - pK_a)$ and $(pK_a - pK_1)$ for iron. On the basis of the $pK_1 = 8.5$ derived from Thomas's study and the $pK_2 = 11.5$ from our studies of iron, it is possible to predict which organic functional groups are likely to form strong hydrogen bonds with iron surfaces. For organic acids, strong bonds are favored when the organic acid pK_a is less than pK_1. Thus, for example, stronger surface bonding would be expected for carboxylic acids than that for phenols. Organic bases that would form strong surface bonds should have pK_a greater than 11.5. Since there are not many organic bases with pK_a higher than this value, basic functional groups in organic coatings would not be expected to contribute to strong hydrogen bonding with the surface of iron.

Since the pK_1 of titanium has not been determined, predictions of relative bond strengths only between titanium surfaces and organic bases is considered in Table IV. The hydrated oxide on titanium was found to be more acidic ($pK_2 = 10.0$) than for the oxide on iron ($pK_2 = 11.5$). Consequently, organic bases should interact more strongly with titanium than with iron. Addition of base functionality to organic coatings should, therefore, be effective in promoting bonding to titanium surfaces.

The interactions between metal surfaces and organic coatings are undoubtedly more complex than the simple model presented in this paper. The experimental approach and the results that were obtained have shown, however, that surface hydroxyls are present on hydrated metal oxide surfaces and that these hydroxyls exhibit acid/base properties. The predictions of the relative strengths and stabilities of the interactions between organic coatings and metal surfaces on the basis of relative pK values need to be evaluated experimentally.

Table III

Estimates of the Relative Bond Strengths Between Organic Polar Groups and Hydrated Iron Oxide Surfaces. The Bond Strength Increases With Decreasing Δ.

Organic Compound	pK_a	Iron Surface $pK = 8.5$ $\Delta = (pK_a - pK_1)$	Iron Surface $pK = 11.5$ $\Delta = (pK_2 - pK_a)$
Ethylamine	11.0	2.5	0.5
Triethylamine	10.8	2.3	0.7
Phenol	9.9	1.4	1.6
Benzylamine	9.3	0.8	2.2
Pyridine	5.7	-2.8	5.8
Acetic Acid	4.8	-3.7	6.7
Benzoic Acid	4.2	-4.3	7.3
Trichloracetic Acid	0.7	-7.8	10.8

Table IV

Estimates of the Relative Bond Strenths Between Organic Polar Groups and Hydrated Titanium Oxide Surfaces.

Organic Compound	pK	Titanium Surface pK = 10.0 $\Delta = (pK_2 - pK_a)$
Ethylamine	11.0	-1.0
Triethylamine	10.8	-0.8
Phenol	9.9	-0.1
Benzylamine	9.3	0.7
Pyridine	5.7	4.3
Acetic Acid	4.8	5.2
Benzoic Acid	4.2	5.8
Trichloroacetic Acid	0.7	9.3

REFERENCES

[1] M. W. Roberts and R. P. Wood, J. Elect. Spect. Rel. Phen. 11, 431, (1977).

[2] J. Kruger and H. T. Yolken, Corrosion 20, 29 (1964).

[3] "Thermodynamics of Wetting of Solids", W. H. Wade and N. Hackerman, Adv. Chem. Ser. #43, c. 1964, p. 222.

[4] "Molecular Structure and Electrostatic Interface at Polymer-Solid Interfaces", J. C. Bolger and A. S. Michaels, from Interface Conversion, P. Weiss and D. Cheever, eds., Elsevier Publishing Co. (1969).

[5] "Donor-Acceptor Interactions at Interface", F. W. Fowkes in Adhesion and Adsorption of Polymers, Part A., Leing Huang Lee, ed., Plenum Press, c 1980, p. 43.

[6] "Pigment-Matrix Interactions", F. W. Fowkes in Proceedings of Corrosion Control by Coatings Conference, Lehigh University, November 13-15, 1978.

[7] G. A. Parks, Chem. Rev. 65, 177 (1965).

[8] Adsorption of Inorganics at Solid-Liquid Interfaces, M. A. Anderson, and A. J. Rubin, eds., Ann Arbor Science, Ann Arbon, Mich. (1981).

[9] J. J. Morgan and W. Stumm, J. Coll. Int. Sci. 19, 347 (1964).

[10] F. Dumont and A. Watillon, Disc. Fara. Soc. 52, 352 (1971).

[11] D. T. Clark and A. Dilks, J. Poly. Sci., Poly. Chem. 17, 957 (1979).

[12] K. Asami and K. Hasimoto, Corro. Sci. 17(7), 559 (1977).

[13] A. G. Akimov, Soviet Electrochem. 15, 1301 (1980).

[14] N. S. McIntyre and D. G. Zetaruk, Anal. Chem. 49, 1521 (1977).

[15] M. J. Dreiling, Surface Sci. 71, 231 (1978).

[16] E. McCafferty and A. C. Zettlemoyer, Dis. Faraday Soc. 52, 239 (1971).

[17] G. D. Parfitt, Prog. Surf. Mem. Sci. 11, 181 (1976).

[18] N. R. Armstrong and R. K. Quinn, Surf. Sci 67, 451 (1977).

[19] J. H. Scofield, J. Elect. Spec. Rel. Phen. 8, 129 (1976).

[20] Atlas of Electrochemical Equilibria in Aqueous Solution, M. Pourbaix, National Assoc. of Corrosion Engineers (1974).

[21] J. G. N. Thomas, Br. Corro. J. 5, 41 (1970).

[22] H. Noller, B. Mayerbock, and G. Zundel, Surf. Sci. 33, 82 (1972).

Program #4

Surface Modification by Abrasive Blasting

Principal Investigator: Henry Leidheiser, Jr.
Prof. of Chemistry

Associate: H. E. G. Rommal
Graduate Student

INTRODUCTION

Abrasive blasting is a common method of preparing a metal surface for subsequent coating. The performance of the coated surface in corrosive environments depends on many factors, including the adhesion of the coating and the activity of the metal/coating interface. These properties are affected by the preparation of the metal surface, and can be influenced by the choice of abrasive blasting parameters.

Impingement of abrasive particles can change the nature of a metal surface in three ways. First, and most obviously, the roughness or surface profile can be changed. Second, abrasion can introduce residual stresses in the surface of the metal by plastic deformation [1], and these stresses can alter the corrosion behavior [2]. Finally, the chemistry of the metal substrate can be altered by removal of surface layers or by deposition of abrasive-borne material. Surface preparation by abrasive blasting usually involves removing most or all of any rust or scale layers, but can also be used to deposit a desirable component on the surface, as in the case of zinc-coated abrasives on steel [3].

A recent study [4] has revealed the fascinating observation that the cathodic delamination performance of an epoxy coating is significantly better if applied to steel that has been abrasively blasted with alumina as compared to panels blasted with steel grit. The mechanism(s) responsible for this improvement have not been conclusively identified, but it is presumed [5] that some of the alumina is incorporated in the surface iron oxide on an atomic scale, thereby altering the electrochemical activity

of the oxide with respect to the oxygen reduction or anodic dissolution reactions.

The purpose of this study is to find abrasive blasting techniques which give markedly different corrosion and/or coatings performance when used on steel, and to attempt to identify the mechanism(s) responsible for the changes. Samples used consisted of steel panels blasted with a variety of abrasives, and also some steel panels coated with various metals and blasted with glass beads to simulate blasting with a coated abrasive.

EXPERIMENTAL

Abrasive blasting was performed with a Hunter Associates Model 63E blast gun operating at 100 psi air inlet pressure and an impingement angle of 90° to the sample surface. Substrates used were disks punched from Q-panel type QD panels of SAE 1010 plain carbon steel. Disks were degreased in acetone and rinsed in methanol before subsequent surface preparations.

It was desired to blast some panels with abrasives coated with different metals, but coating a large quantity of particles with any given metal is a very difficult task. Instead, different metals were evaporated onto polished steel disks and then blasted with glass beads. Evaporated film thicknesses were on the order of 300 Å.

Oxides of different metals were also used as abrasives, but due to the softness and low density of many of these oxides it was necessary to mix 50% glass beads by volume with the oxides in some cases. All these sample types were tested in the as-blasted condition.

The final sample type was prepared using glass geads which were soaked in aqueous solutions of corrosion inhibitors, sodium benzoate or sodium acetate and allowed to dry. After blasting, disks were thoroughly washed with methanol to remove any loosely adherent benzoate or acetate. Plain steel disks abraded with 180 grit silicon carbide paper were also used as a reference. Table I lists sample types prepared.

Electrochemical studies were made using the polarization resistance technique, as it permits rapid corrosion rate determination with only small deviations from the corrosion potential. The polarization resistance can be represented by [6]:

$$R_p = \frac{\beta_A \beta_C}{2.3\, i_{corr}(\beta_A + \beta_C)}$$

where R_p is the polarization resistance in ohms·cm^2, β_A and β_C are the anodic and cathodic Tafel constants, and i_{corr} is the corrosion current density in A/cm^2. To avoid errors in determination of β_A and β_C, i_{corr} values were not calculated. However, since

Table I

List of Sample Types

Substrate	Abrasive Type	Abrasive Size (Mesh)
Plain Steel	Silicon Carbide Paper	180
Plain Steel	Alumina	60
Plain Steel	Steel Grit	80
Plain Steel	Glass Beads	80
Plain Steel	Cu_2O + Glass Beads	~600
Plain Steel	Cr_2O_3 + Glass Beads	~600
Steel + Al Evap.	Glass Beads	80
Steel + Cu Evap.	Glass Beads	80
Steel + Cr Evap.	Glass Beads	80
Steel + Ni Evap	Glass Beads	80
Steel + Ti Evap.	Glass Beads	80
Steel + Co Evap	Glass Beads	80
Steel + Fe Evap.	Glass Beads	80
Steel + Sn Evap.	Glass Beads	80
Steel + Zn Evap.	Glass Beads	80
Steel + Au Evap.	Glass Beads	80
Plain Steel	Glass Beads + Sodium Benzoate	80
Plain Steel	Glass Beads + Sodium Acetate	80

$$R_p \propto \frac{1}{i_{corr}}$$

higher values of R_p indicate lower corrosion rates, and R_p values are a valid comparison.

Electrolytes used were 0.1M borate aqueous solutions of pH = 8.5 with three different concentrations of sodium chloride: Zero, 0.005M, and 3 wt.% (0.51M). In addition, plain distilled water and aqueous 0.1M sodium sulfate, pH 6.4, were used.

Polarization resistance measurements were performed using a PAR Model 350 corrosion measurement console at a scan rate of 0.1 mV/sec. High solution resistance values for the distilled water were measured using a PAR Model 356 IR compensation module, and the data were adjusted for that solution. All tests were carried out at 25°C and solutions were neither stirred nor deaerated.

Sample surfaces were characterized in several ways. Surface roughness values were calculated using data from a Taylor-Hobson Surtronic 3 profilometer, and used to calculate surface areas for the data at the end of the results section. Most of the R_p data are not corrected for surface area, and a value of 1.0 cm^2 (the geometric area) is assumed in these cases. For these tests, values of R_p will be given only in ohms rather than ohms·cm^2 to avoid confusion. As will be shown, the assumption of equal surface area is not valid, but the values obtained with the profilometer are equally questionable. A section on surface area analysis appears later in this report. Surface geometry was qualitatively characterized by scanning electron microscopy.

Elemental analysis was performed using energy dispersive X-ray microanalysis and Auger electron spectroscopy.

RESULTS

Electrochemical Measurements

Figure 1 shows the behavior of E_{corr} and R_p vs. time for four sample types in pH 8.5, 0.1M borate solution, a highly passivating medium. Sample types are plain steel abraded as follows: 180 grit SiC paper, 60 mesh alumina blasted, 80 mesh steel grit blasted, and 80 mesh glass bead blasted. The steel grit blasted samples showed the most noble E_{corr} while the 180 grit abraded disks had the most negative. However, both of these samples had similar R_p values when not corrected for surface area. Polarization resistance values were lowest for alumina blasted samples. All specimens showed increasing E_{corr} and R_p with time, typical of the highly passivating borate solution.

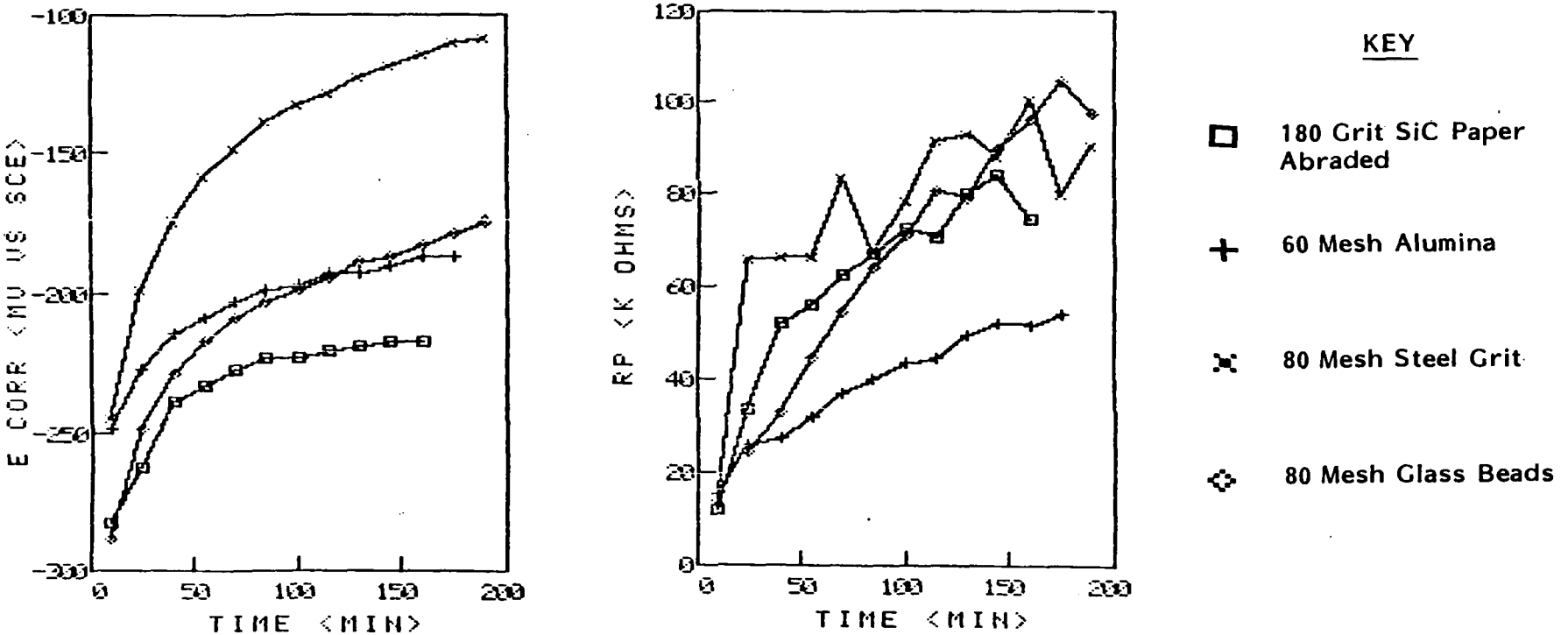

Figure 1. Plots of E_{corr} and R_p vs. time for different surface preparations on steel in 0.1M borate solution, pH = 8.5.

Similar plots for the samples blasted with Cu_2O and Cr_2O_3/glass bead blends and the 180 grit SiC paper abraded disks appear in Figure 2. Here, both blasted samples have significantly more noble E_{corr} values, with the Cu_2O/glass samples approaching 0.0 volts vs. SCE. R_p values are also remarkably high for the oxide blasted samples, indicating extremely low corrosion rates.

Figure 3 gives behaviors for all the evaporated metal/glass bead blasted disks which were tested in the 0.1M borate. E_{corr} was significantly raised for samples with evaporated films of Cu, while films of Ni, Ti, Co, and Fe lowered E_{corr} somewhat. Samples having pre-blasting films of Al and Cr had potentials much like that of the plain glass bead blasted disks, which also appear in this figure. All metal films, except Al, reduced R_p when compared with glass bead-only blasting, with Ni having the largest effect.

The performance of the inhibitor-coated glass bead blasted samples compared with plain glass bead blasted disks in borate is shown in Figure 4. E_{corr} for the samples blasted with sodium benzoate coated glass beads was more noble, while for those blasted with sodium acetate coated beads E_{corr} was more negative, when compared with blasting with uncoated beads. However, both inhibitors yielded improved performance, especially the sodium benzoate, which increased R_p by up to a factor of five. The improvement with sodium acetate was marginal.

The addition of 3 wt.% NaCl to the 0.1M borate solution increases its aggressiveness markedly.

Figure 5 depicts the performance of the same samples as in Figure 1 in the borate with 3% NaCl. Ignoring differences in surface area, plain steel abraded with SiC paper had the highest R_p, while the alumina blasted disks had the lowest. The most noble E_{corr} values were for the SiC abraded and steel grit blasted samples, while alumina blasting yielded the lowest E_{corr}.

Disks blasted with Cu_2O and Cr_2O_3/glass bead mixtures are compared to SiC abraded steel in Figure 6. In the solution with 3% NaCl, large differences in E_{corr} resulted from these three samples. Cu_2O blasting caused the most noble E_{corr} while Cr_2O_3 blasting led to the most negative. R_p values have a similar trend, where Cu_2O blasted disks had the highest values.

Three of the evaporated metal/glass bead blasted sample types were tested in this aggressive solution. Figure 7 depicts the behavior of samples with pre-blasting films of Al, Cu, and Cr along with that of plain glass bead blasting. As was the case for the borate-only solution (Figure 3), the Cu and Cr reduced R_p, Al increased R_p slightly, and Cu gave a more noble E_{corr}. For all samples in this solution, E_{corr} showed a steady decline with time while R_p remained virtually constant (except Cu_2O blasted).

The same three series of sample types tested in borate-3% NaCl were also tested in distilled water. Figure 8 contains data for SiC paper abraded, and alumina, steel grit, and glass bead blasted steel in distilled

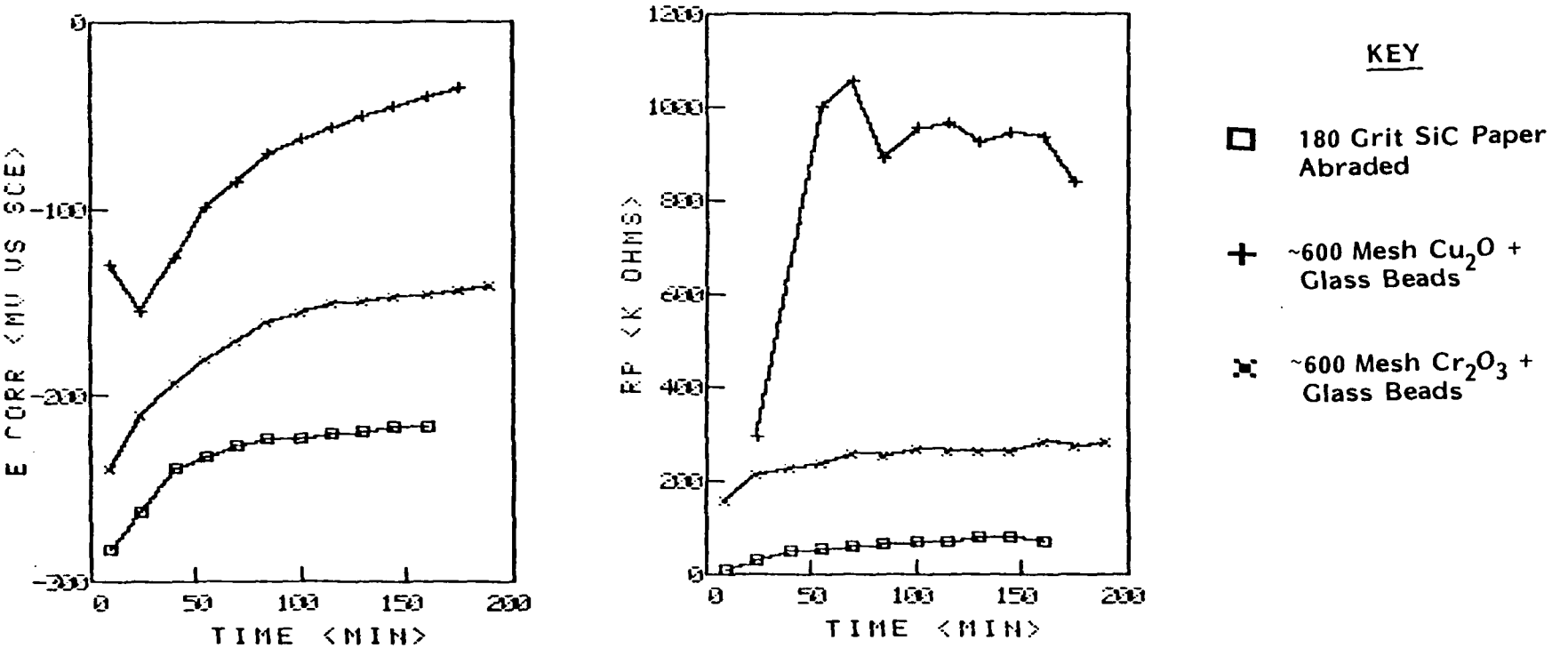

Figure 2. Plots of E_{corr} and R_p vs. time for different surface preparations on steel in 0.1M borate solution, pH = 8.5.

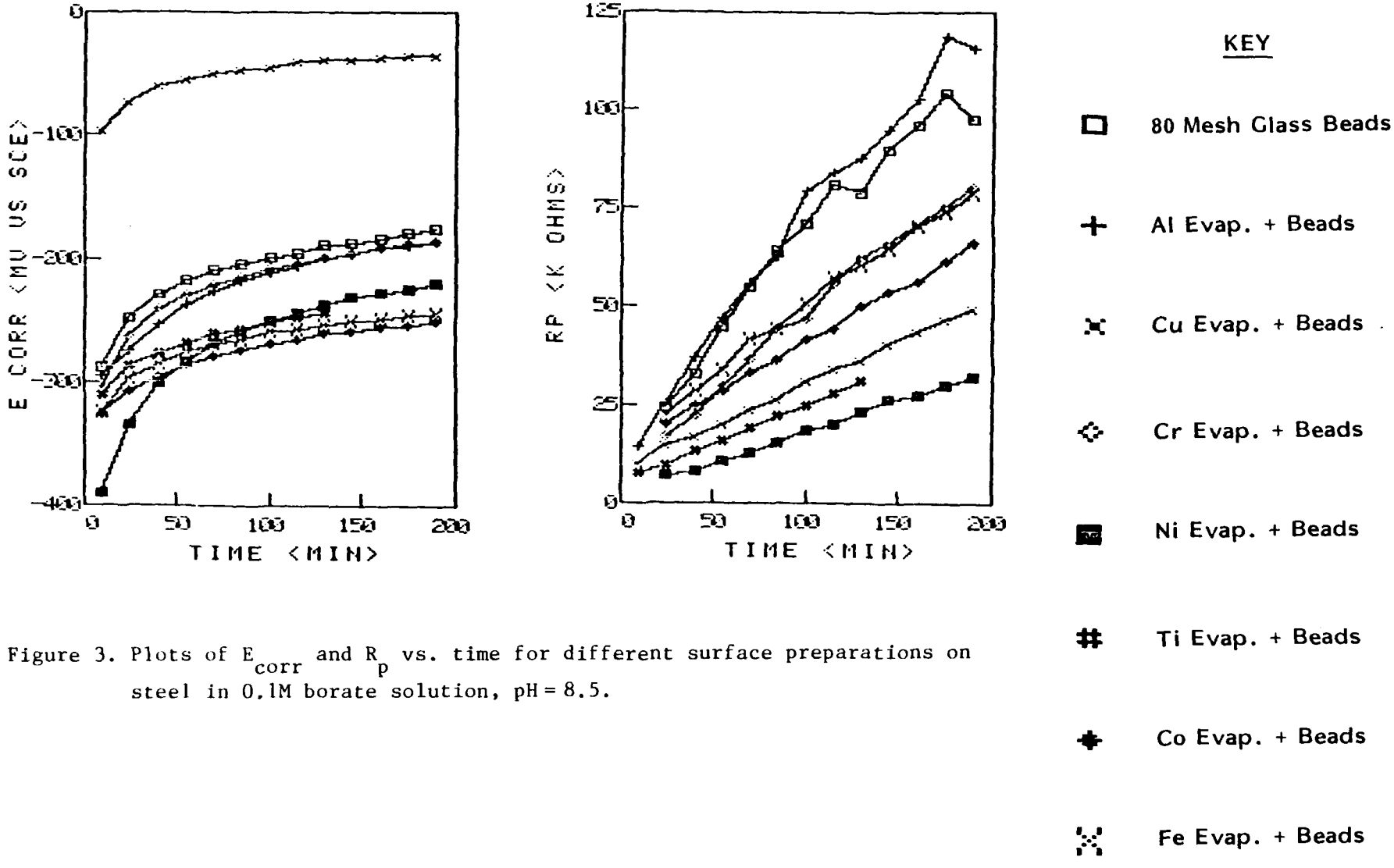

Figure 3. Plots of E_{corr} and R_p vs. time for different surface preparations on steel in 0.1M borate solution, pH = 8.5.

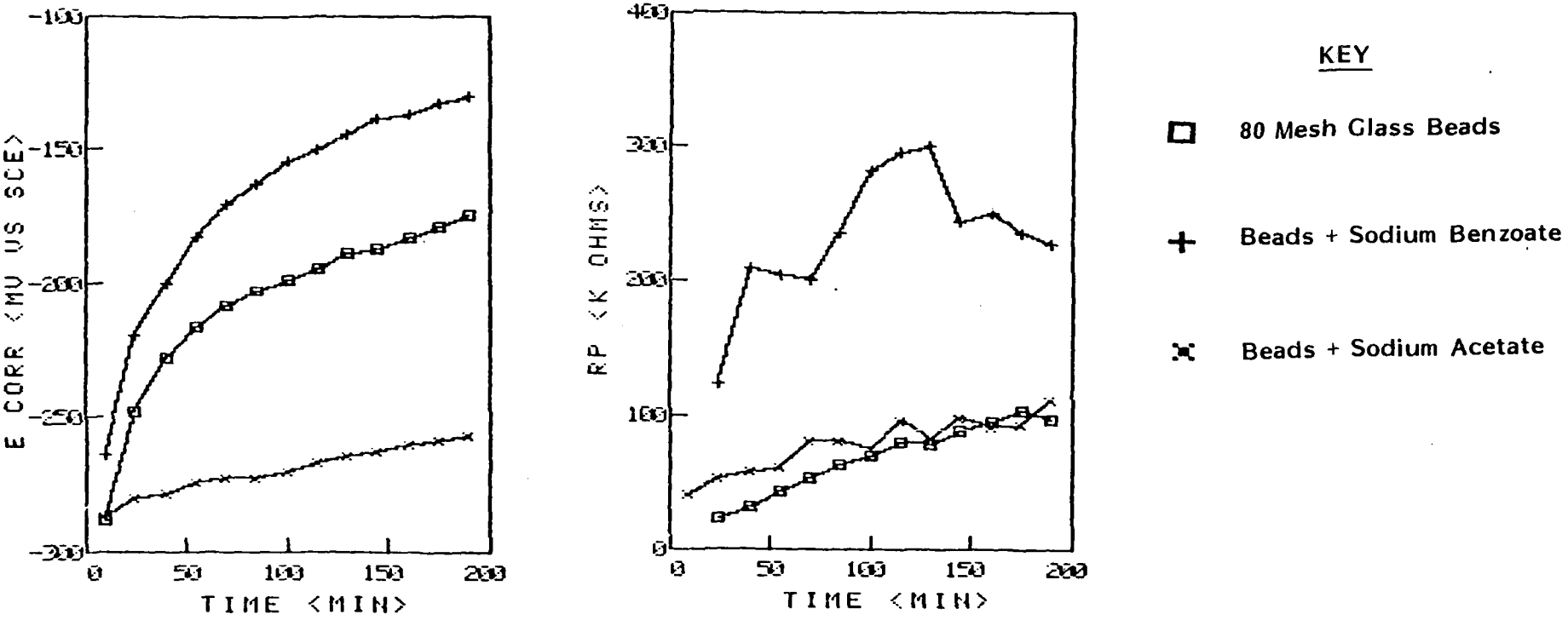

Figure 4. Plots of E_{corr} and R_p vs. time for different surface preparations on steel in 0.1M borate solution, pH 8.5.

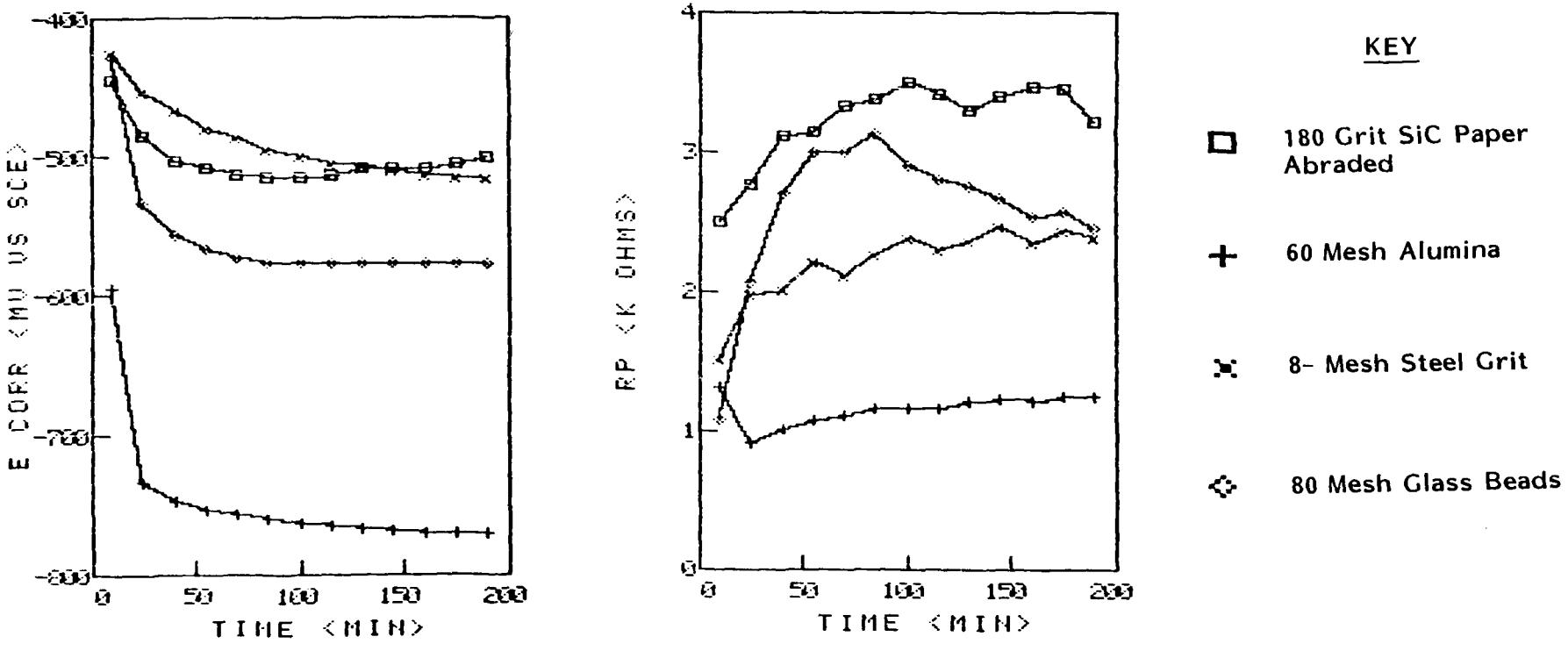

Figure 5. Plots of E_{corr} and R_p vs. time for different surface preparations on steel in 0.1M borate, 3% NaCl solution, pH 8.5.

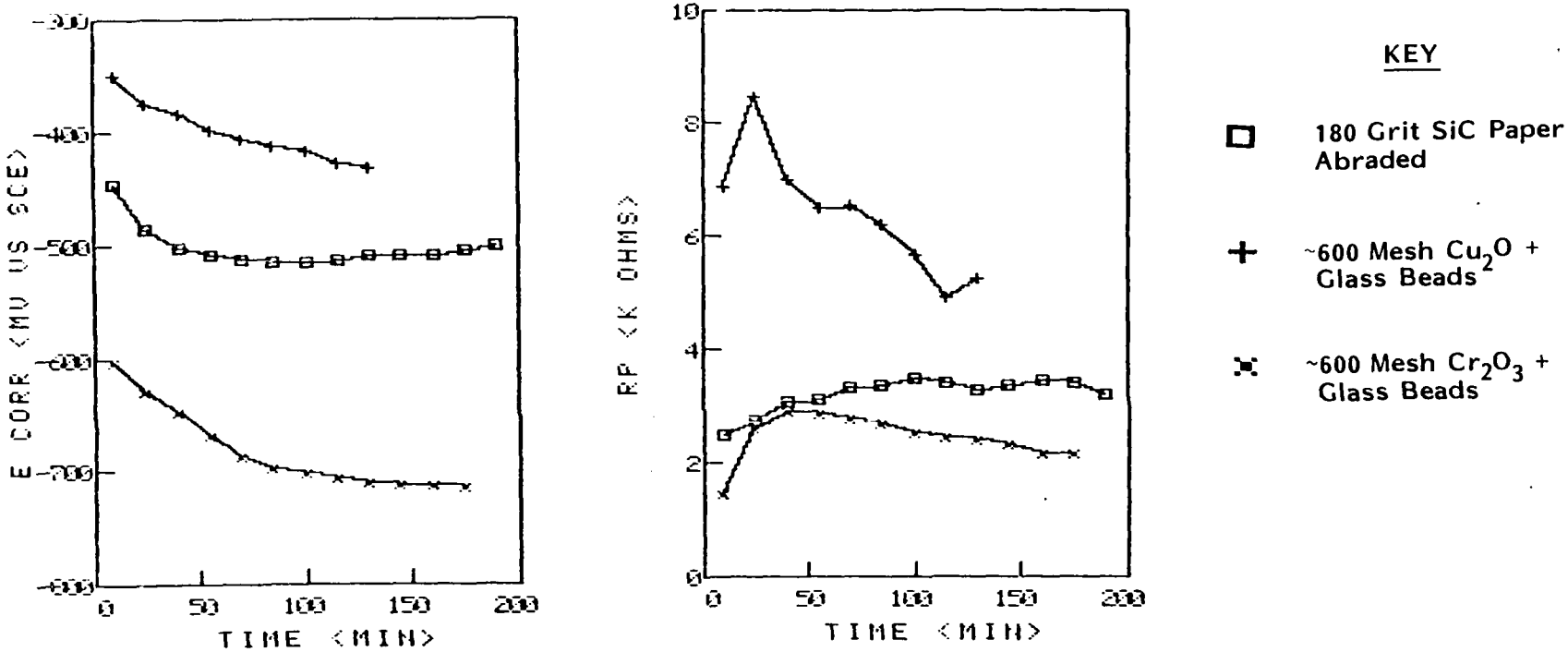

Figure 6. Plots of E_{corr} and R_p vs. time for different surface preparations on steel in 0.1M borate, 3% NaCl solution, pH = 8.5.

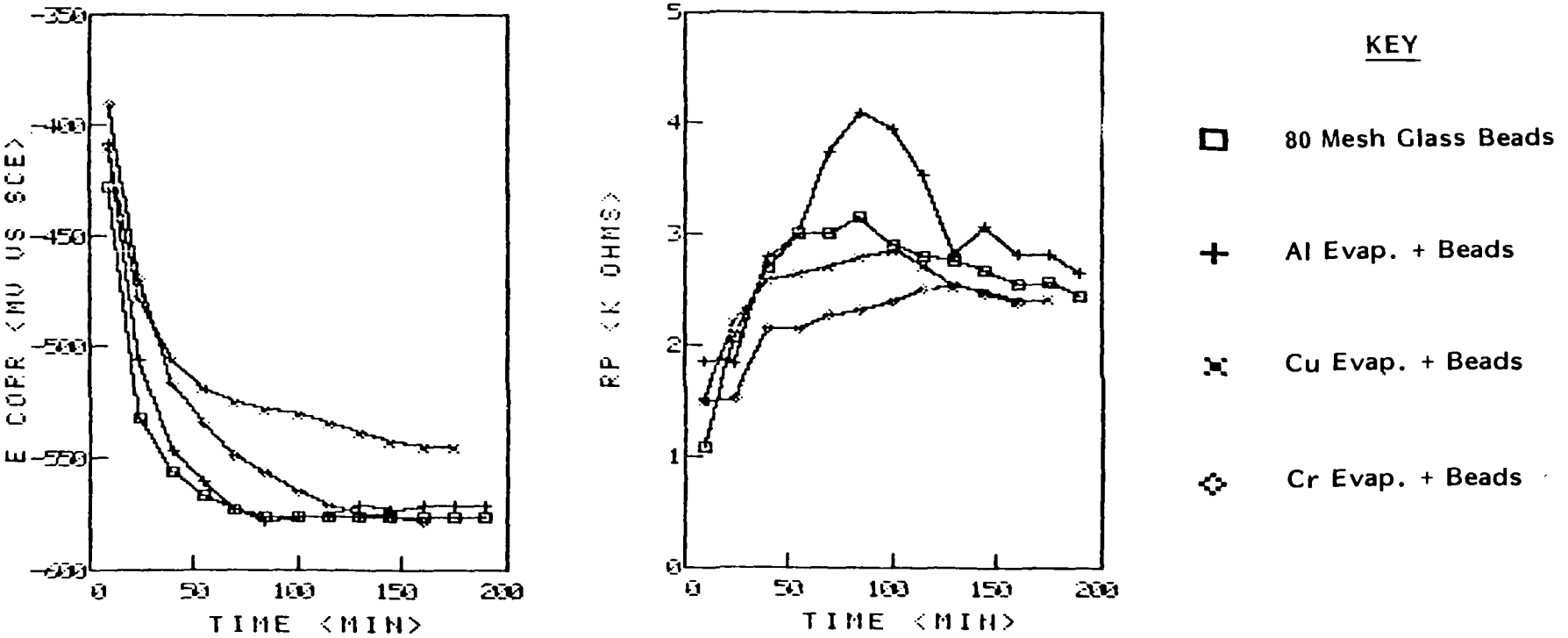

Figure 7. Plots of E_{corr} and R_p vs. time for different surface preparations on steel in 0.1M borate, 3% NaCl solution, pH = 8.5.

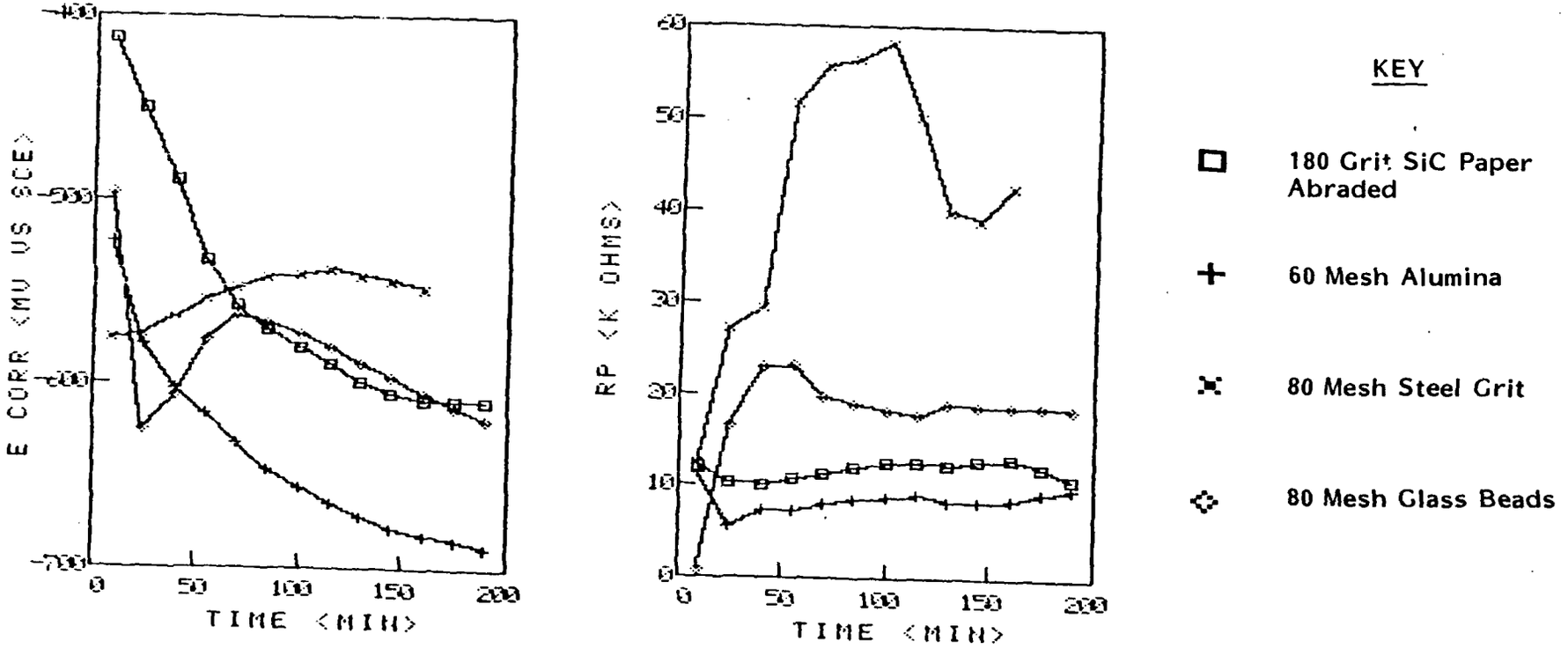

Figure 8. Plots of E_{corr} and R_p vs. time for different surface preparations on steel in distilled water.

H_2O. Once again, if surface area is not considered, alumina blasting results in the lowest R_p values. Also in this case, blasting with steel grit gave the most improvement in R_p. E_{corr} values followed the trend with steel grit blasting yielding the most noble value and alumina the most negative.

The relative performance of Cu_2O and Cr_2O_3/glass bead blasting to plain abraded steel in distilled water is very similar to their behavior in borate-3%NaCl. Cu_2O blasting resulted in the most noble E_{corr} and the highest R_p, while Cr_2O_3 led to the lowest R_p, as seen in Figure 9.

The commonly detrimental effect of the metal films on steel prior to glass bead blasting holds for distilled water, as shown in Figure 10. Glass beads alone gave the highest R_p while films of Cu and Cr gave the lowest. However, the Cu films no longer result in a more noble E_{corr}, but both Cu and Cr reduced E_{corr} somewhat.

In the two remaining solutions, 0.1M borate-0.05M NaCl and 0.1M sodium sulfate, only the two series of glass bead-type samples have been tested. Disks having pre-blasting evaporated films of Cu, Ni, Ti, Co, and Fe were used in both solutions, while films of Sn, Zn, and Au have also been tested in the borate-0.05M NaCl solution. In addition, the two inhibitor-coated beads, as well as plain glass beads, were used to prepare samples for both solutions.

Figure 11 shows the behavior of the metal film/glass bead samples in the borate-0.05M NaCl. Notable increases in R_p were observed for films of Co, Fe, and Zn with Zn being the highest. E_{corr} for the Co and Fe film samples was more noble than the rest while all film samples showed a higher E_{corr} than glass beads alone.

The effect of the inhibitors is much less noticeable in the borate-0.05M NaCl solution. R_p values were similar for all three sample types, as shown in Figure 12, with sodium benzoate having an initially higher R_p value which decayed with time. The differences in E_{corr} are more striking, with the benzoate yielding a much more noble value, and sodium acetate the lowest.

For the sulfate solution, the pre-blasting metal films had much less effect on R_p values. Figure 13 shows that only Co produced a measureable increase. A range of values of E_{corr} were observed. However, with all metals yielding a more noble E_{corr}, Cu yielded the highest value.

Finally, the inhibitor coating of glass beads provided no improvement of R_p in the sulfate solution. E_{corr} was also lowered by both inhibitors as shown in Figure 14.

Surface Morphology and Chemical Analysis

Disks which had been blasted with 60 mesh alumina, 80 mesh steel grit or 80 mesh glass beads were examined by scanning electron microscopy (SEM). Figure 15 shows micrographs of the three sample types. The surfaces of the alumina and steel grit blasted samples were very rough and angular while the

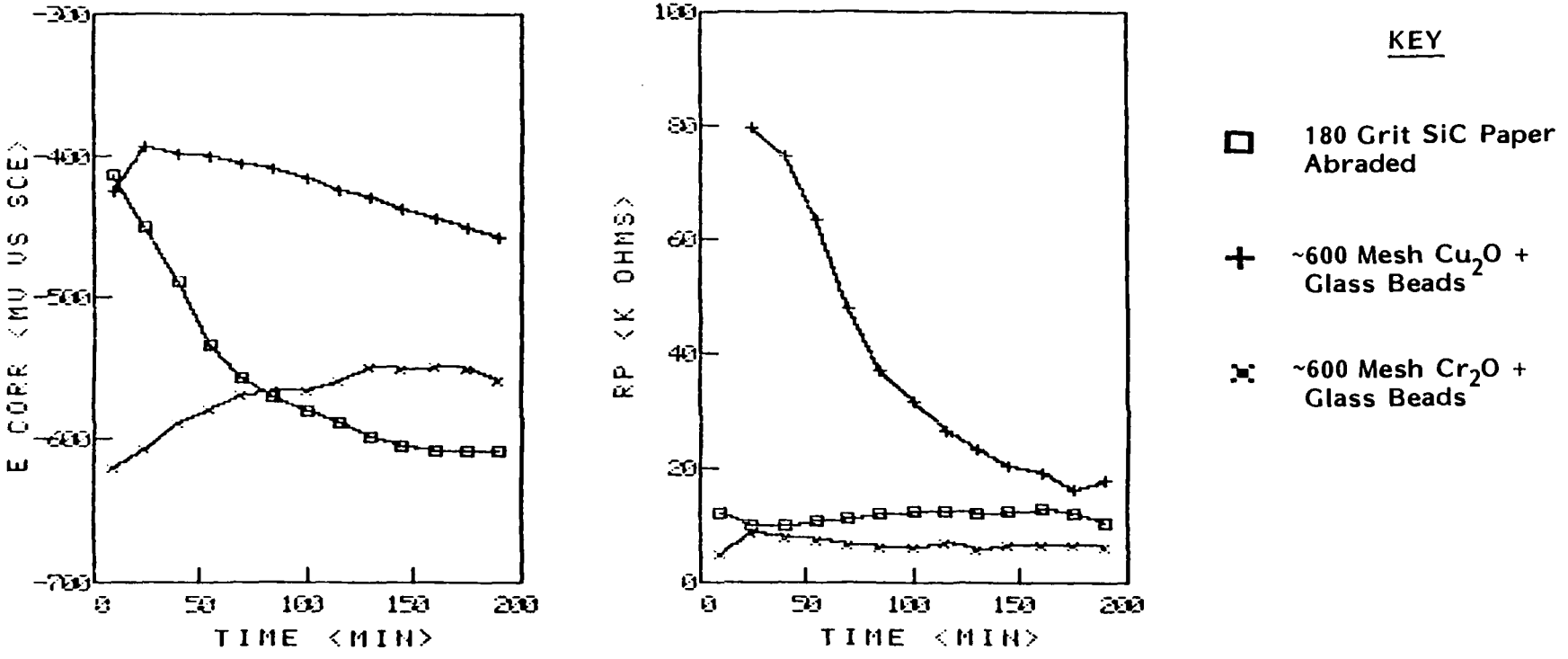

Figure 9. Plots of E_{corr} and R_p vs. time for different surface preparations on steel in distilled water.

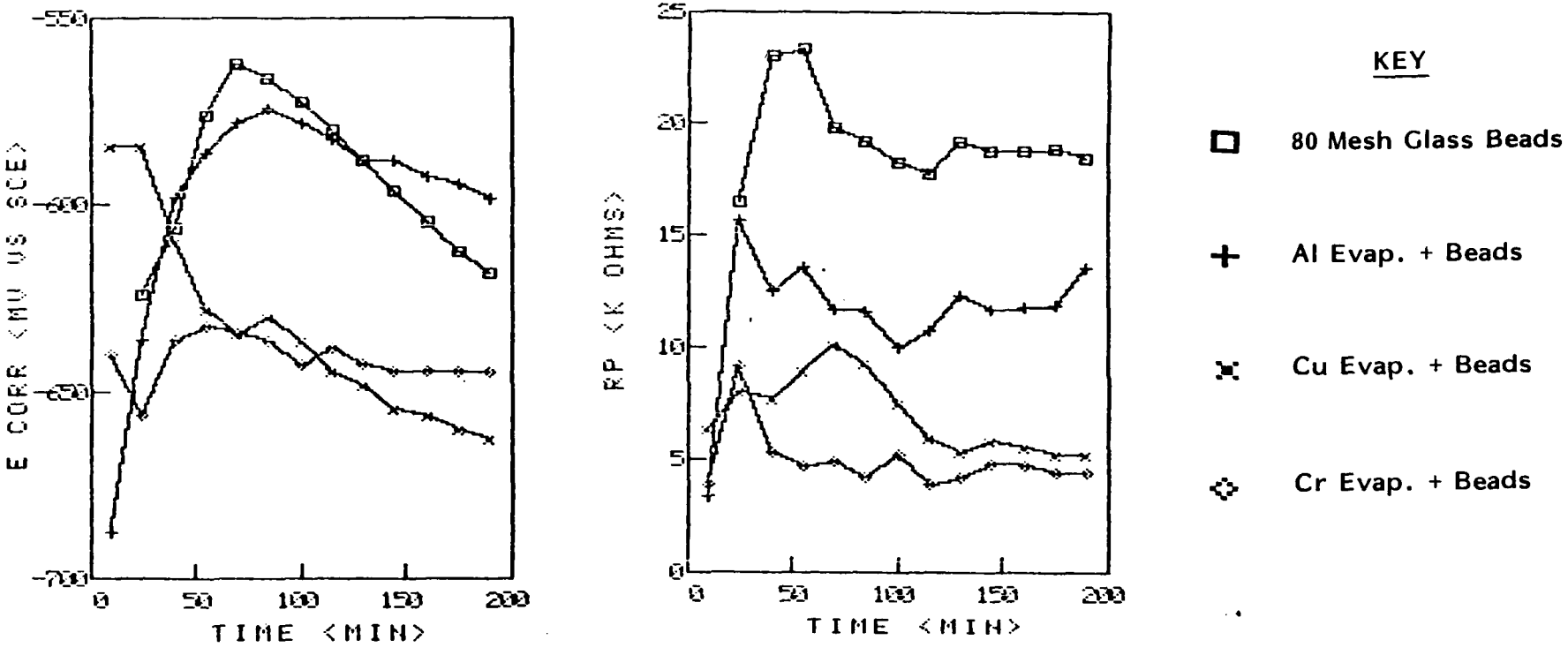

Figure 10. Plots of E_{corr} and R_p vs. time for different surface preparations on steel in distilled water.

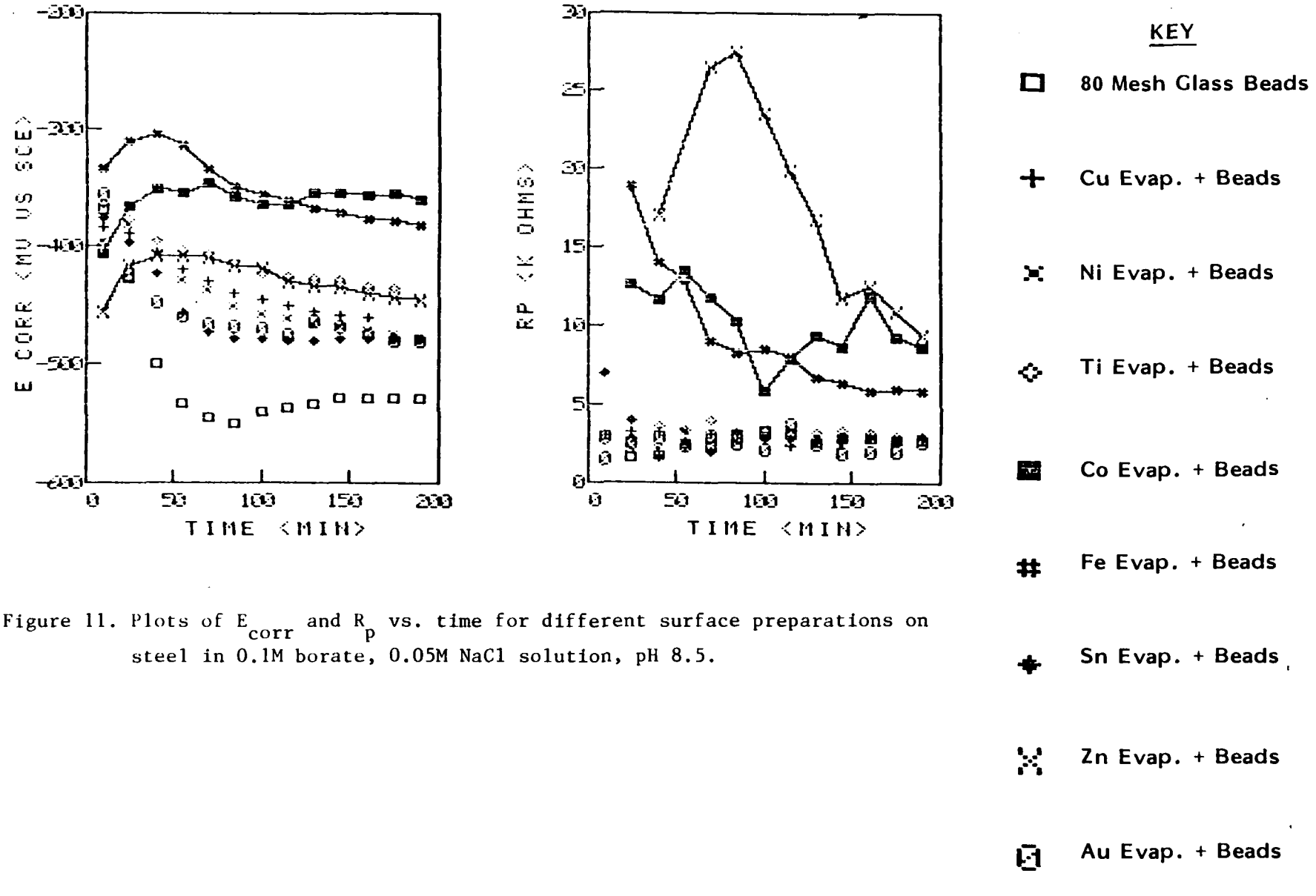

Figure 11. Plots of E_{corr} and R_p vs. time for different surface preparations on steel in 0.1M borate, 0.05M NaCl solution, pH 8.5.

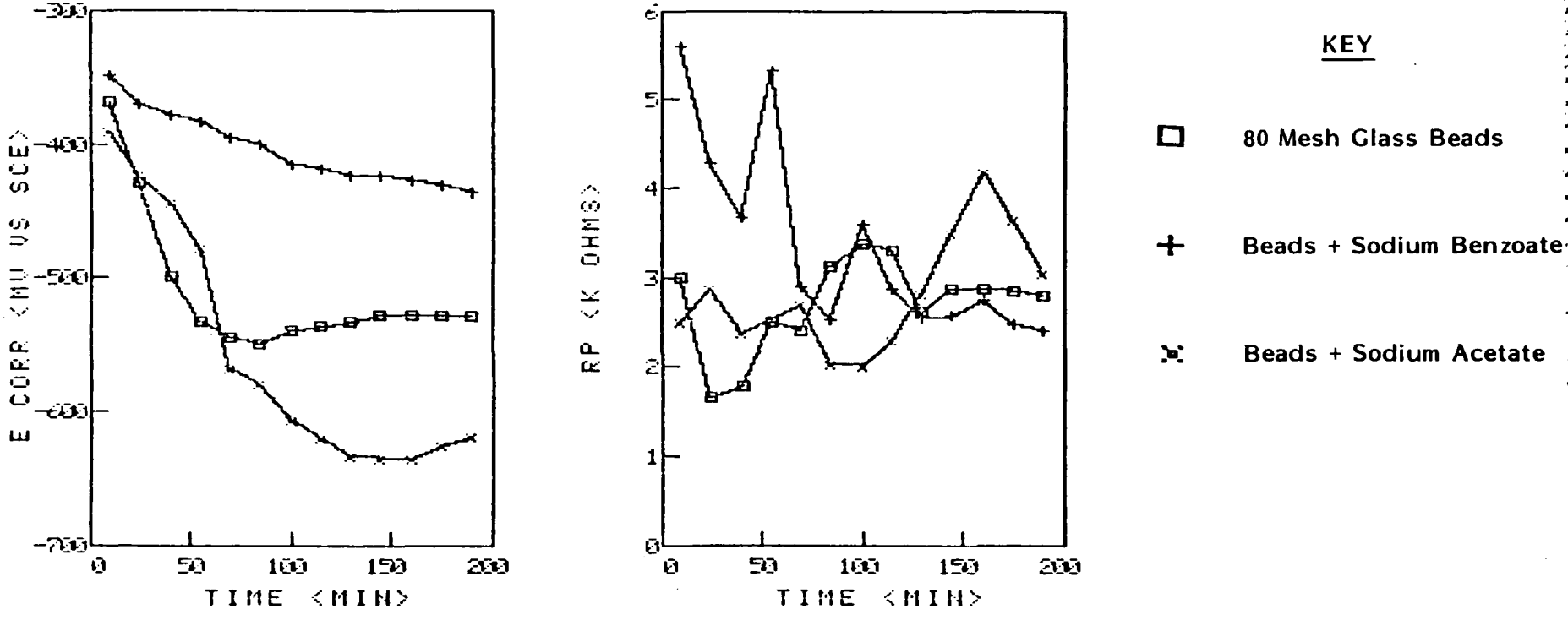

Figure 12. Plots of E_{corr} and R_p vs. time for different surface preparations on steel in 0.1M borate, 0.05M NaCl solution, pH 8.5.

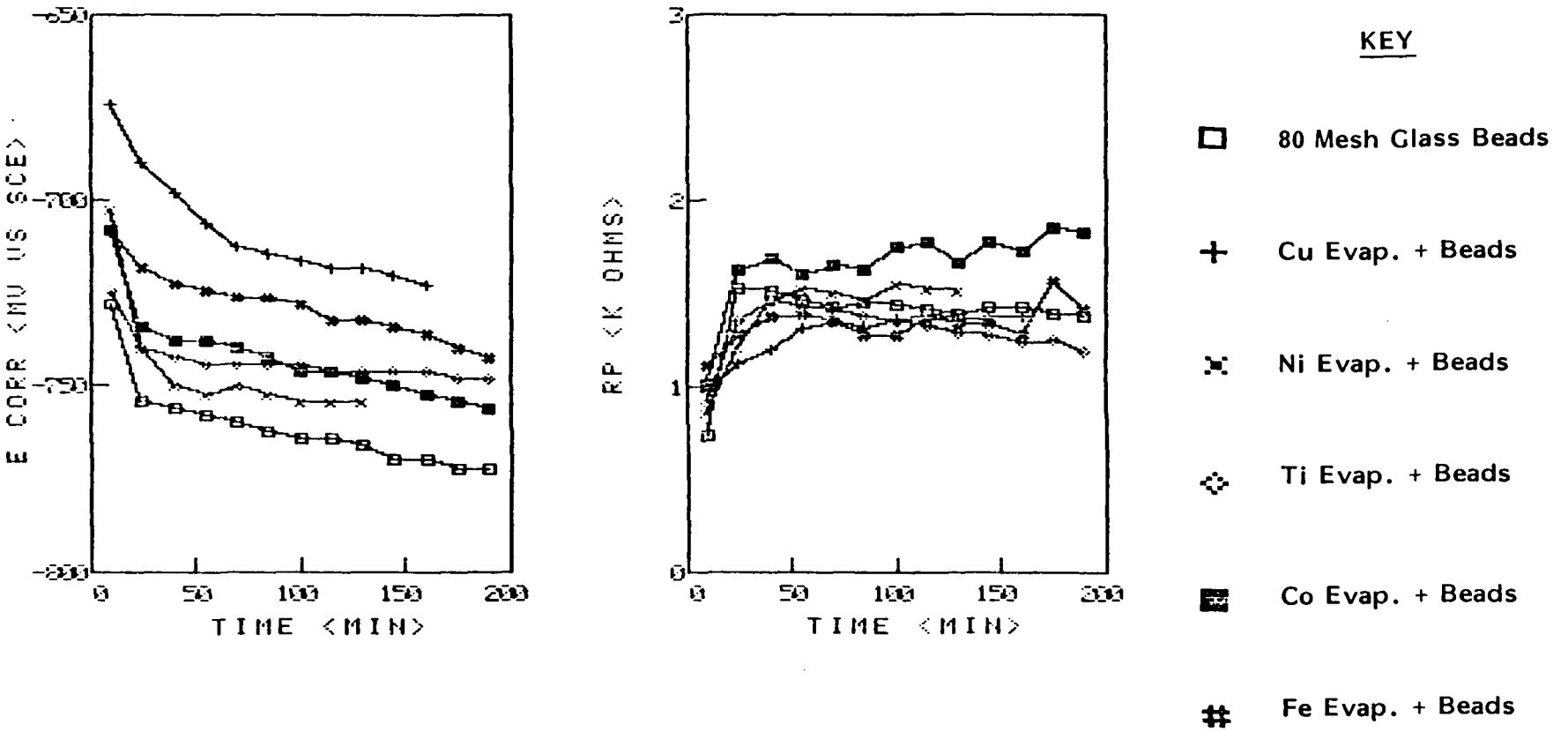

Figure 13. Plots of E_{corr} and R_p vs. time for different surface preparations on steel in 0.1M sodium sulfate solution, pH 6.4.

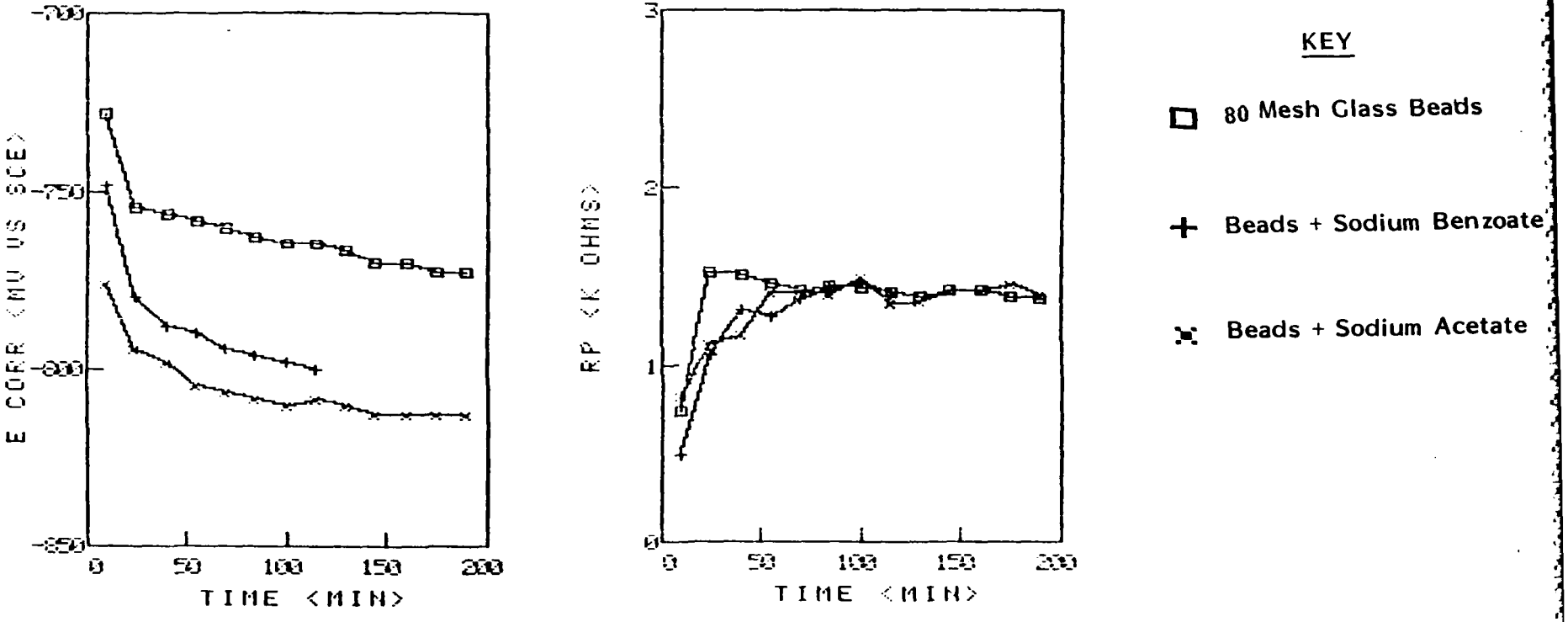

Figure 14. Plots of E_{corr} and R_p vs. time for different surface preparations on steel in 0.1M sodium sulfate solution, pH = 6.4.

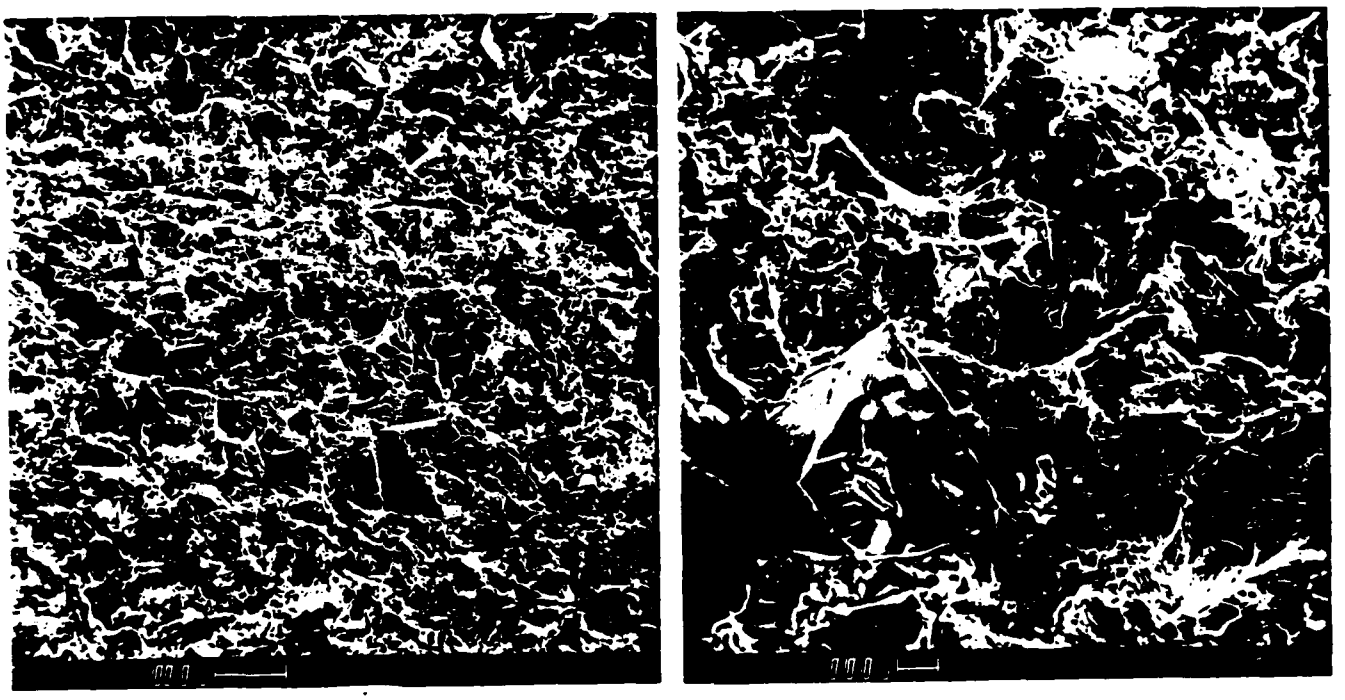

60 MESH ALUMINA

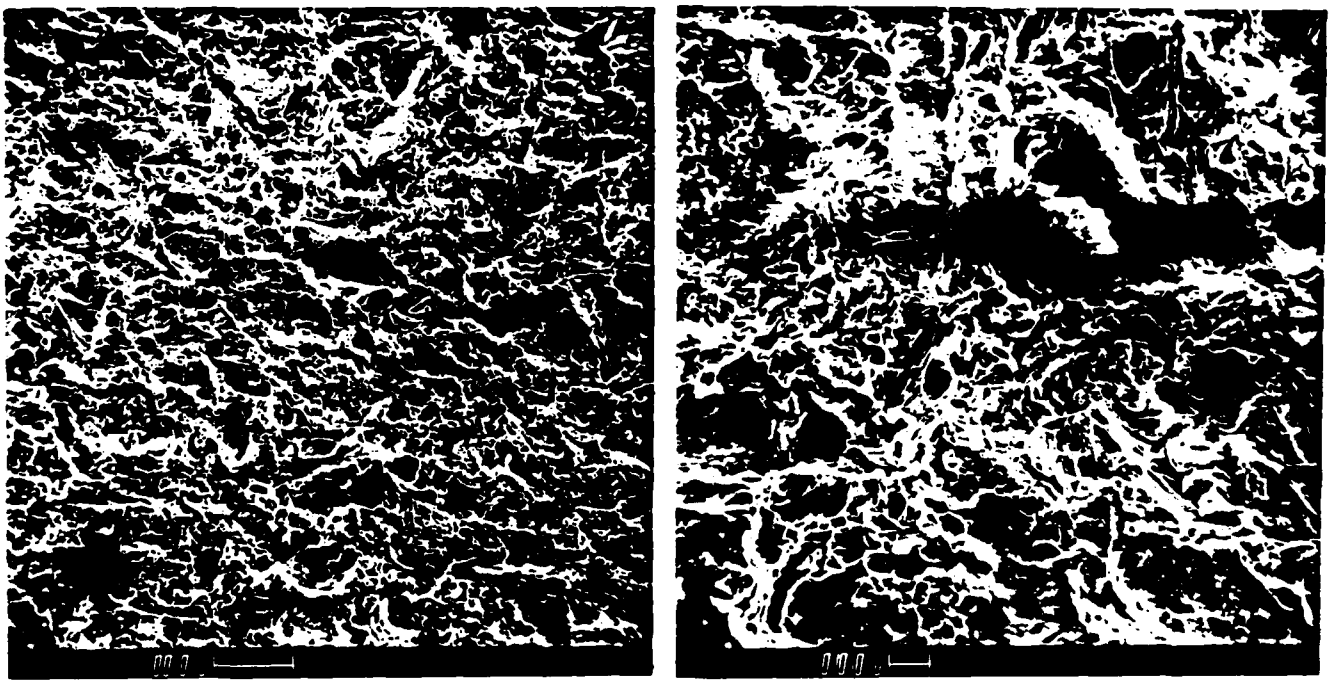

80 MESH STEEL GRIT

Figure 15. Scanning electron micrographs of steel surfaces after different abrasive blasting. (Continued on following page.)

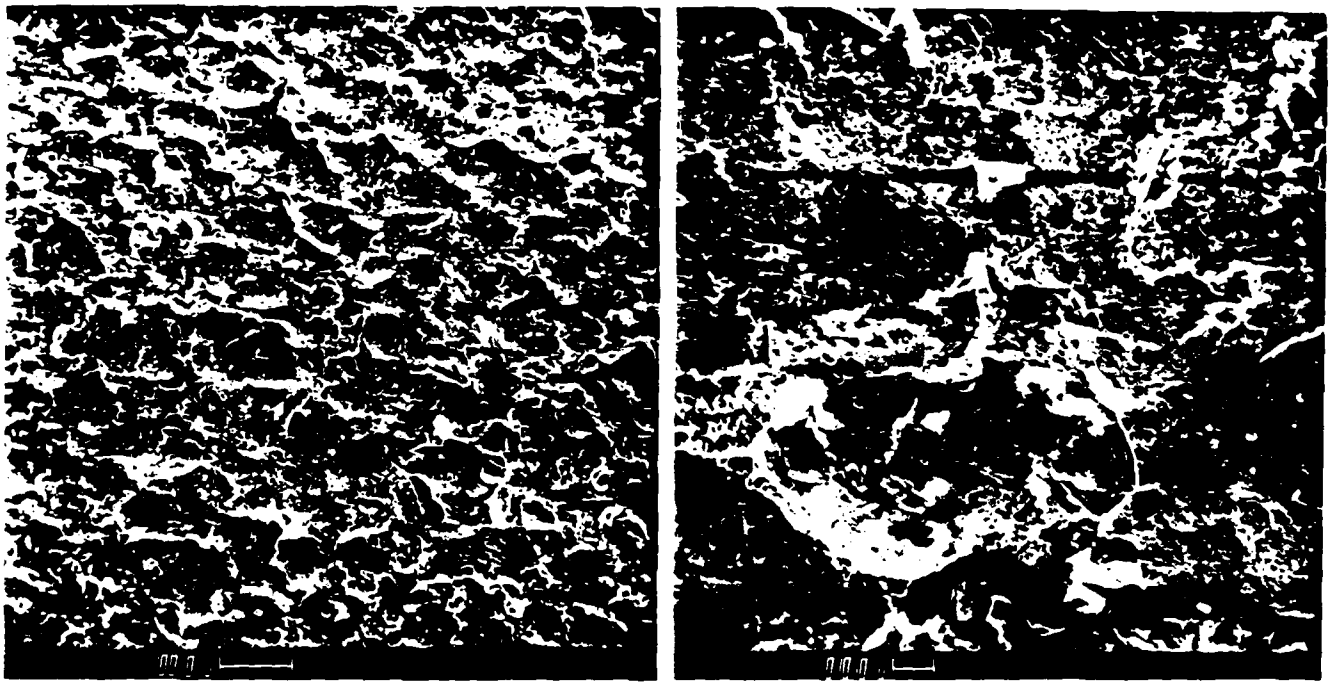

80 MESH GLASS BEADS

Figure 15. (Cont'd.)

smoother glass bead blasted surface had a peened appearance. Embedded fragments of all three particle types are visible, especially in the higher magnification photos.

Energy dispersive X-ray spectrometry (EDS) was used to identify elements present in several sample types. Aluminum was easily detectable in the alumina blasted samples, as were significant quantities of silicon, sodium and calcium in the glass bead blasted disks. Copper and chromium were likewise found in the case of the specimens blasted with their oxides. No traces of the metal film elements were found by EDS on the blasted surfaces.

Auger electron spectroscopy (AES) revealed the presence of the Al, Si, Na, Ca, Cu, and Cr mentioned above, in addition to some elements from the metal films. Very small quantities of Al, Cu, Cr, Ni, and Co were found on their respective evaporated film/glass bead blasted samples. However, no traces of Ti, Sn, Zn, or Au could be detected for their sample types. Since the substrate was steel, presence of iron peaks in EDS or AES spectra gives no information about the steel grit blasted or Fe film/glass bead blasted samples.

SURFACE AREA DETERMINATION

The profilometer method used in this study for the determination of sample surface areas was the same as that used in a previous study [5]. The profilometer output gives a value of R_A or "roughness average." R_A is simply the average deviation of the diamond stylus as it traverses the sample from a mathematically constructed center line. It is truly a measure of average asperity height. It is, however, not a good measure of surface roughness as it relates to surface area.

Figure 16 depicts hypothetical surface profiles for two different samples. Note that both profiles are modeled as triangle waves with equal amplitude but different frequencies. Both curves have equal R_A values since the average deviation from the center line is simply half the peak amplitude. The relative areas of the two surfaces would be quite different, however, and the area ratio would be given by the ratio of the two curve lengths. For the curves shown, this ratio is 1.22:1 for the dashed curve: the solid curve. Hence a 22% error is introduced simply by using R_A values, and it is easy to imagine errors of much greater magnitude on real surfaces. In addition, the diamond stylus is fairly large—10 μm tip radius—and would miss any surface changes of lesser magnitude. Clearly the fine detail of surface profile plays an important role in the determination of the electrochemically relevant area.

In order for any electrochemical measurement involving the corrosion current density to be meaningful, the surface roughness must be known. To date the profilometer method gives the best estimate. Though its values are probably not very accurate, they have been used to modify the pertinent R_p data. Table II lists R_A values and estimated surface areas for all sample types on the basis of 1 cm^2 geometric area, where

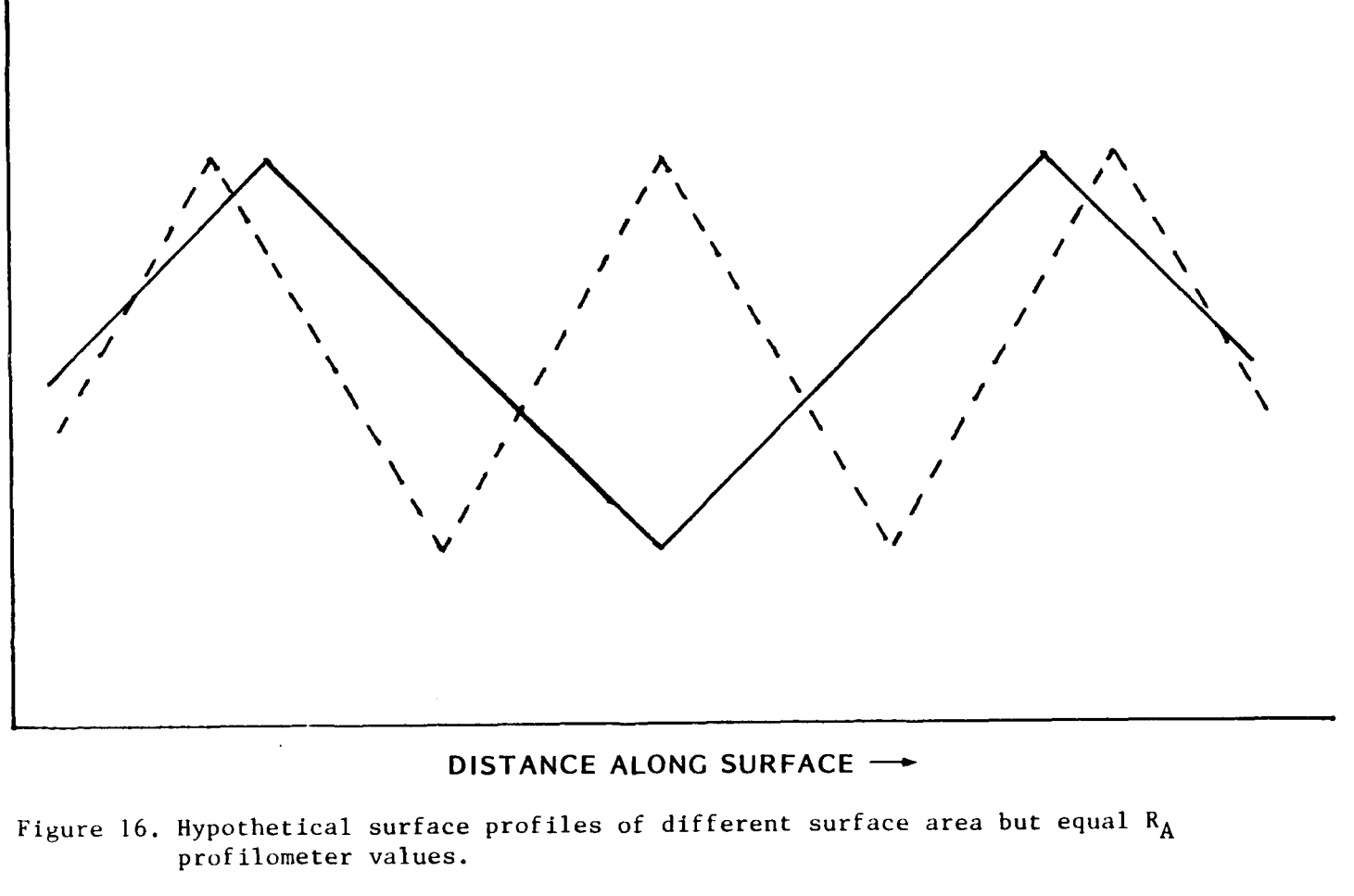

Figure 16. Hypothetical surface profiles of different surface area but equal R_A profilometer values.

AD-A151 238 CORROSION CONTROL THROUGH A BETTER UNDERSTANDING OF THE METALLIC SUBSTRAT..(U) LEHIGH UNIV BETHLEHEM PA CENTER FOR SURFACE AND COATINGS RESE.. E M ALLEN ET AL. 2/3

UNCLASSIFIED 13 DEC 84 N00014-79-C-0731 F/G 11/3 NL

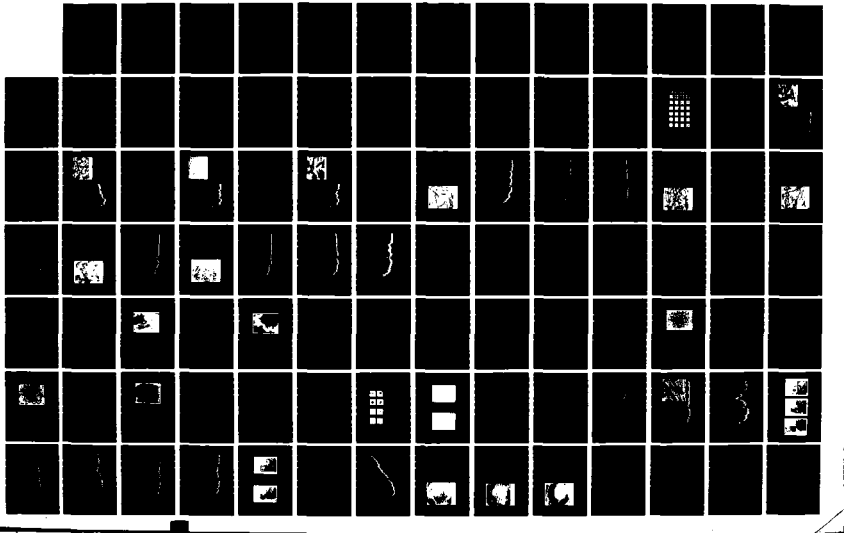

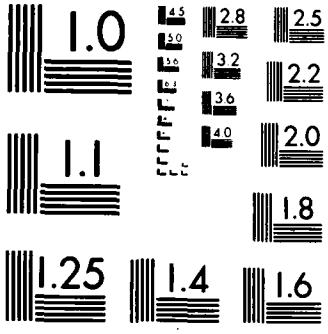

MICROCOPY RESOLUTION TEST CHART
NATIONAL BUREAU OF STANDARDS-1963 A

$$\text{Surface Area} = \frac{R_A \text{ Value for Sample}}{R_A \text{ Value for Standard}} \times 1.0 \text{ cm}^2 \quad .$$

The standard for a smooth surface used was a steel disk polished with 0.05 μm alumina.

Figures 17-19 show the R_p data from Figures 1, 2, 5, 6, 8, and 9, corrected for surface area using these values. Clearly, the relative ranking of samples changes dramatically in most cases. In Figure 17a (see also Fig. 1), all three blasted samples show an improved R_p value, with steel grit being far the best. Similar results are obtained for Figure 18a as compared to Figure 5. Lesser changes are noted in the other graphs.

Table II

Roughness Values and Surface Area Estimates
by Profilometer Measurements

Steel Surface Preparation	R_A (μm)	Surface Area (cm^2)
Polished	0.046	1.0 (STD)
180 Grit SiC Abraded	0.390	8.5
60 Mesh Alumina Blasted	2.790	61
80 Mesh Steel Grit Blasted	3.262	71
80 Mesh Glass Bead Blasted (with & without metal films)	1.818	40
Cu_2O + 600 Mesh Glass Bead Blasted	0.350	7.6
Cr_2O_3 + 600 Mesh Glass Bead Blasted	0.570	12

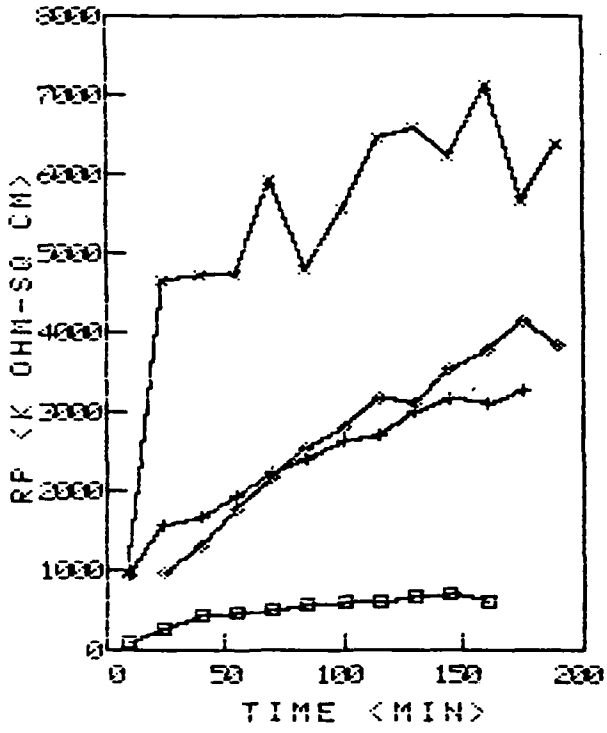

(a)

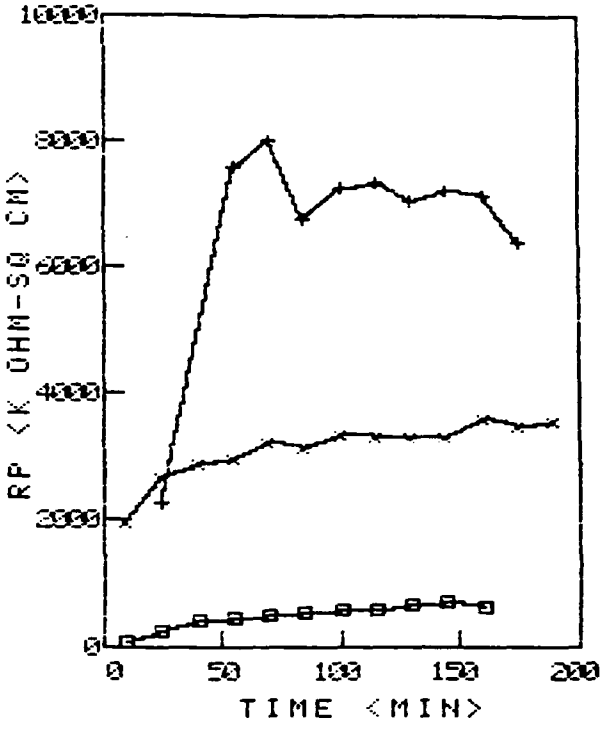

(b)

KEY

□ 180 Grit SiC Paper Abraded

\+ 60 Mesh Alumina

⋇ 80 Mesh Steel Grit

◇ 80 Mesh Glass Beads

KEY

□ 180 Grit SiC Paper Abraded

\+ ~600 Mesh Cu_2O + Glass Beads

⋇ ~600 Mesh Cr_2O_3 + Glass Beads

Figure 17. Plots of R_p adjusted for surface preparations on steel in 0.1M borate solution, pH = 8.5. See Figures 1 and 2 for comparison.

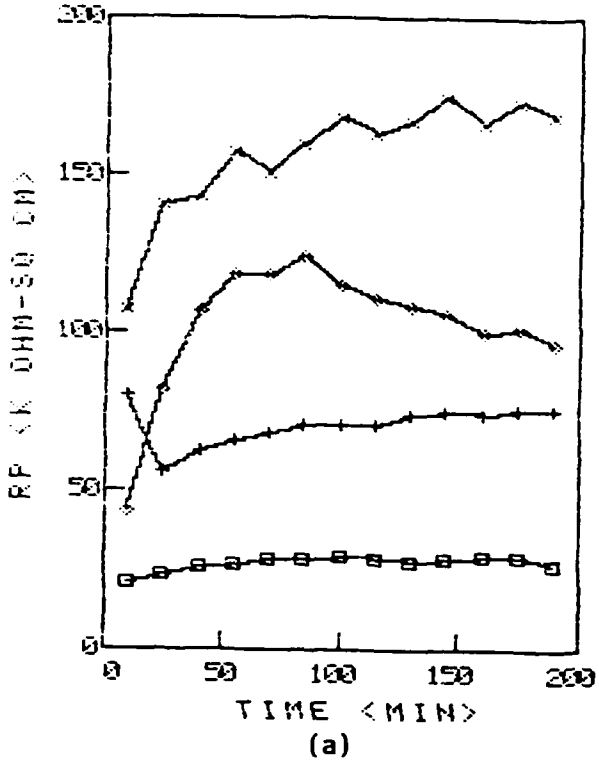

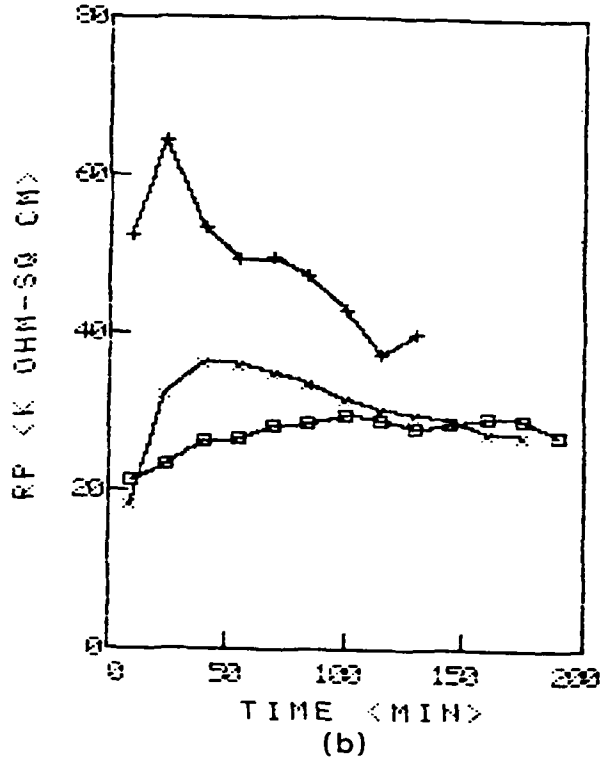

KEY

- 180 Grit SiC Paper Abraded
- 60 Mesh Alumina
- 80 Mesh Steel Grit
- 80 Mesh Glass Beads

KEY

- 180 Grit SiC Paper Abraded
- ~600 Mesh Cu_2O + Glass Beads
- ~600 Mesh Cr_2O_3 + Glass Beads

Figure 18. Plots of R_p adjusted for surface preparations on steel in 0.1M borate, 3% NaCl solution, pH = 8.5. See Figures 5 and 6 for comparison.

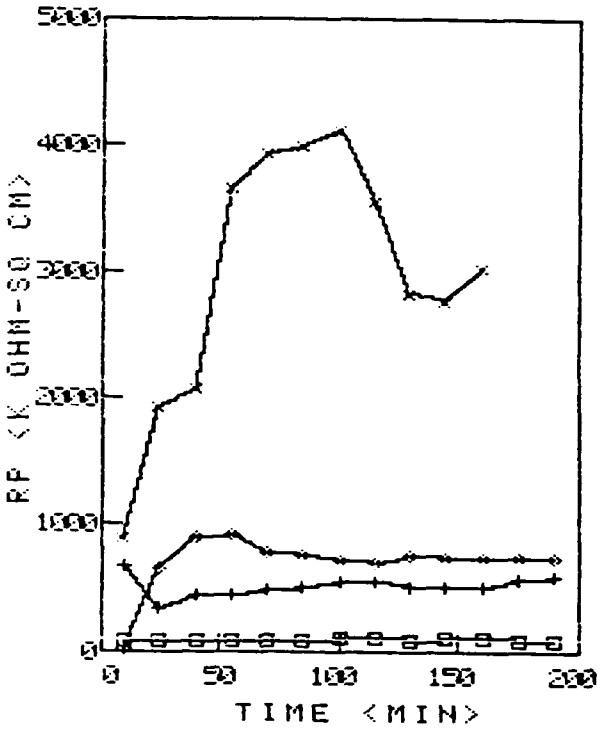

(a)

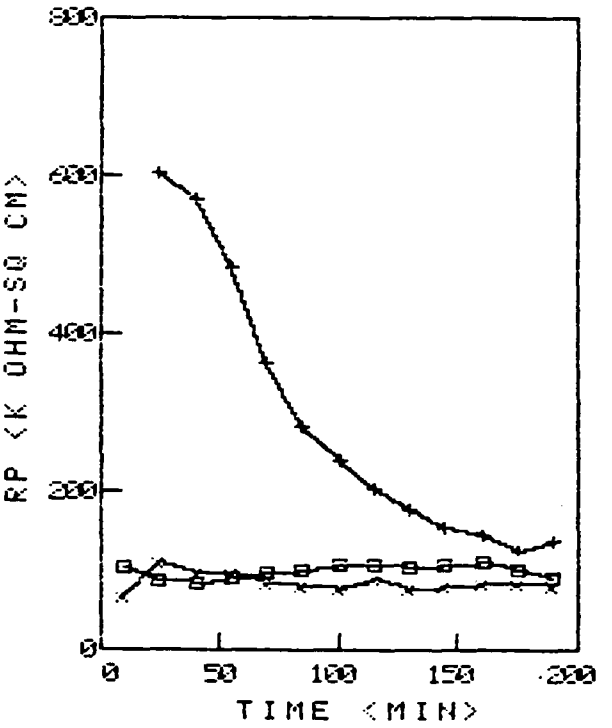

(b)

KEY

- 180 Grit SiC Paper Abraded
- 60 Mesh Alumina
- 80 Mesh Steel Grit
- 80 Mesh Glass Beads

KEY

- 180 Grit SiC Paper Abraded
- ~600 Mesh Cu_2O + Glass Beads
- ~600 Mesh Cr_2O_3 + Glass Beads

Figure 19. Plots of R_p adjusted for surface preparations on steel in 0.1M borate solution, pH = 8.5. See Figures 8 and 9 for comparison.

DISCUSSION

It is clear that using different values of roughness to correct polarization resistance data, or any other data related to corrosion currents, can alter the apparent electrode behavior considerably. Thus it is essential to use correct values for surface area. Data from the profilometer probably adjust R_p values in the right direction, but not the right magnitude from sample to sample. Another method of roughness determination must be found before the real magnitude of the polarization resistance values can be calculated. In this study to date, values adjusted with profilometer data are the best estimates and will be used in further discussion.

Figure 20 shows schematic Evans diagrams (potential vs. log current density) of a corroding system in which the activity of the sample for the anodic (Fig. 20a) or cathodic (Fig. 20b) half-cell reactions changes. In both cases, a decrease in i_{corr}, corresponding to increasing R_p, is shown in the change from state 1 to state 2. However, in Figure 20a, as the corrosion rate decreases, E_{corr} increases, while the reverse is true for Figure 20b. Thus a knowledge of the correlation between changes in R_p with changes in E_{corr} upon surface modification indicates which half-cell reaction is more greatly influenced. This treatment involves the assumption that the anodic and cathodic Tafel slopes do not vary considerably with surface treatment.

For neutral to alkaline aerated solutions such as those used in this study, the predominant reduction reaction is oxygen reduction,

$$O_2 + 2H_2O + 4e^- \longrightarrow 4OH^- \quad ,$$

while the anodic reaction is metal dissolution and/or oxide formation. A closer examination of each sample/electrolyte group leads to the following deductions.

Referring to Figure 17a for R_p and Figure 1 for E_{corr}, all three blasting treatments increased both R_p and E_{corr}. This indicates that it is primarily the anodic reaction which undergoes the most reduction in activity for alumina, steel grit, and glass bead blasting when exposed to 0.1M borate solution.

The same can be said for Cu_2O and Cr_2O_3 abrasives, as shown by Figures 17b and 2. It was noted, however, that samples blasted with those materials were coated with a substantial film of loosely adhering oxide which would serve to act as an insulating coating. Increases in R_p and E_{corr} for these samples indicate little about the nature of the steel surface, and steel prepared in this way would have little usefulness as a corrosion resistant surface or a substrate for coatings. For this reason, results pertaining to these samples will not be discussed further.

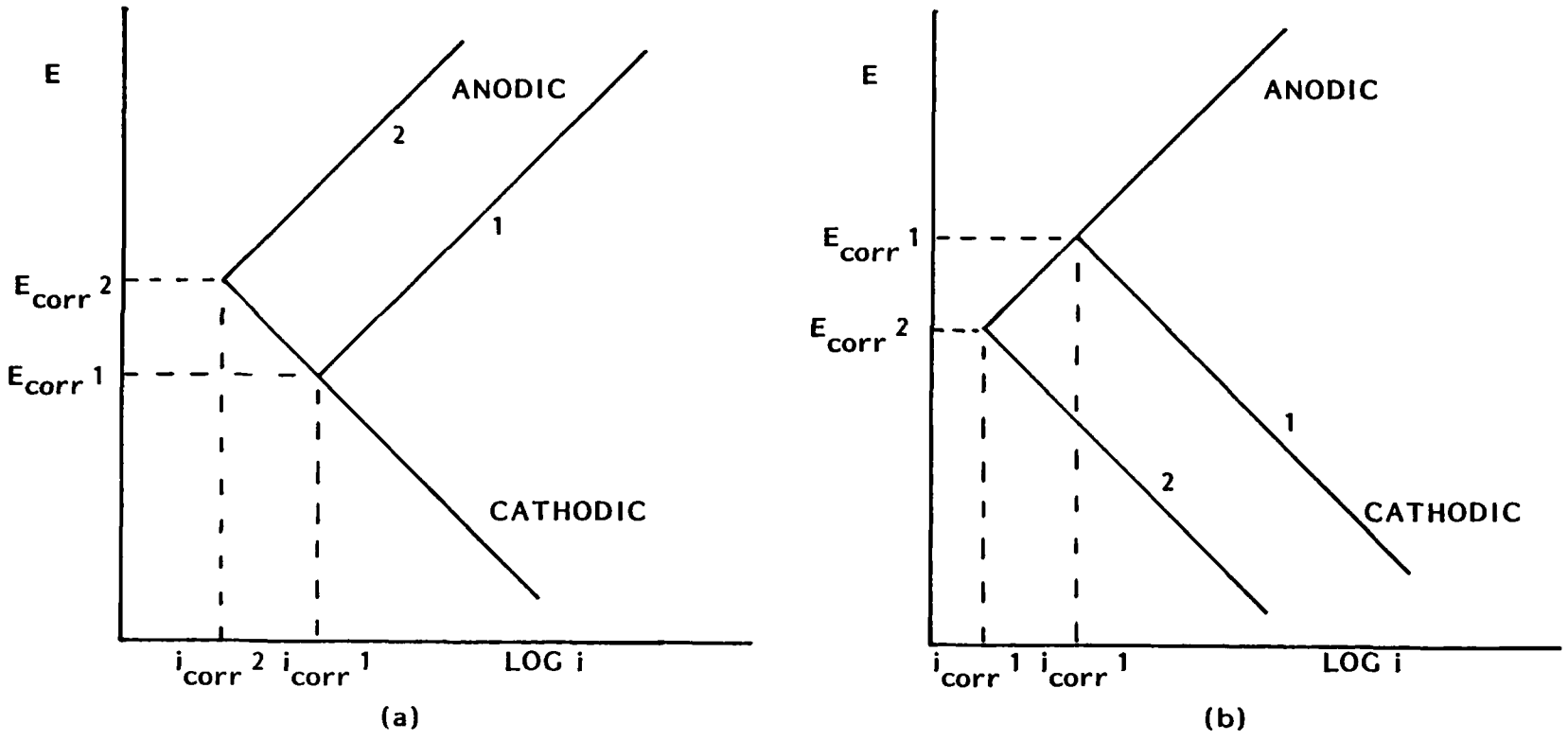

Figure 20. Schematic Evans diagrams of possible E_{corr} changes with reductions in i_{corr}.

Following this pattern of analysis through the rest of the data, nine examples of simple abrasive blasting yielding an increase in R_p compared to SiC abraded steel can be found, while an additional six instances of metal film deposition or inhibitor soaking cause an improvement relative to glass bead blasting alone. These results are consensed into Table III.

It is interesting to note that since the abrasives were identical for the disks with evaporated metal films, the surface areas and stress states should be equal. Hence, any changes in electrochemical behavior were for purely chemical reasons. Also, in some cases for films of Ti, Sn, Zn, and Au, the values of R_p and/or E_{corr} changed even though no traces of these elements could be found by Auger electron spectroscopy. This result suggests that small chemical changes in the surface can lead to large changes in corrosion behavior.

It should be stressed that no large table of all samples in each solution ranked from best to worst can be constructed without first obtaining reliable surface area measurements. In addition, the analysis by comparing R_p and E_{corr} variations involves many simplifying assumptions which are not necessarily entirely obeyed. Further electrochemical characterization is needed to substantiate these speculations.

Perhaps most important of all, it is necessary to separate the effects of each of the three components of surface modification by abrasive blasting (roughening, residual stresses, chemical changes) before a complete understanding of any one abrasive/substrate/electrolyte combination can be realized.

CONCLUSIONS AND SUGGESTIONS FOR FURTHER WORK

Abrasive blasting as a surface preparation technique causes complex changes in corrosion behavior. These changes are brought on by one or more of: variations in surface profile, alterations in the stress state of the surface, and chemical changes of oxides or other surface species.

Characterization of electrochemical behavior requires a knowledge of real surface area. This quantity is quite elusive, and is worthy of further attention. Techniques which measure adsorption or surface capacitance are possible candidates. Once this is accomplished, more definite comparisons can be made between abrasive blasting techniques.

Using surface area data obtained to date, steel grit blasting of steel yields a greater increase in polarization resistance than either alumina or glass bead blasting. This conclusion depends on the accuracy of area measurements.

In general, abrasively blasted steel surfaces have a higher corrosion resistance than plain steel surfaces. Also, some preliminary work with abrasives coated with chemical inhibitors shows promise.

Table III

List of R_p Improvements and Assumed Reaction Changes

Surface Treatment	R_p Higher Relative to	Direction of E_{corr} Change	Reaction with Reduced Activity
	0.1M Borate, pH 8.5		
Alumina	Abraded	+	Anodic
Steel Grit	Abraded	+	Anodic
Glass Beads	Abraded	+	Anodic
Beads + Benzoate	Glass Beads	+	Anodic
Beads + Acetate	Glass Beads	-	Cathodic
	0.1M Borate, 3% NaCl, pH 8.5		
Alumina	Abraded	-	Cathodic
Steel Grit	Abraded	0	Both
Glass Beads	Abraded	-	Cathodic
	0.1M Borate, 0.05M NaCl, pH 8.5		
Co Evap. + Beads	Glass Beads	+	Anodic
Fe Evap. + Beads	Glass Beads	+	Anodic
Zn Evap. + Beads	Glass Beads	+	Anodic
	0.1M Sodium Sulfate, pH 6.4		
Co Evap. + Beads	Glass Beads	+	Anodic
	Distilled Water		
Alumina	Abraded	-	Cathodic
Steel Grit	Abraded	+	Anodic
Glass Beads	Abraded	0	Both

Very small changes in surface chemistry— even those below the detection limit of Auger electron spectroscopy—can have noticeable effects on the corrosion behavior of abrasively blasted steel. More detailed surface chemical analysis will be carried out, including X-ray photoelectron spectroscopy. Surface residual stresses will be determined for each sample type by X-ray diffraction methods. Also, samples will be tested after stress relief.

REFERENCES

[1] G. E. Dieter, Mechanical Metallurgy, Second Edition, McGraw-Hill Book Co., New York (1976).

[2] W. J. Tomlinson and K. P. Smith, Corrosion 39, 432 (1983).

[3] P. J. Robinson, Materials Performance 23(2), 31 (1984).

[4] H. Leidheiser, Jr., S. Music, and J. F. McIntyre, Corrosion Science 24, 197 (1984).

[5] J. F. McIntyre and H. Leidheiser, Jr., in "Corrosion Control through a Better Understanding of the Metallic Substrate/Organic Coating/Interface," Fourth Annual Report, Office of Naval Research, Washington, DC (1983), p.39.

[6] M. Stearn and A. L. Geary, J. Electrochem. Soc. 104, 56 (1957).

Program #5

Surface Modification of Iron by Anodization and Titanation

Principal Investigator: Richard D. Granata
Research Scientist

ABSTRACT

Previously completed work suggested pursuing sulfate or nitrate media for anodic treatment of iron substrates for the purpose of modifying the protective oxide layers. A sulfate medium has been developed which permits anodic passivation in the presence of ferrous ion. Various ratios of aluminum-ferrous ion additions have been tested with the sulfate medium. Polarization resistance measurements and cathodic polarization curves have been determined using specimens prepared from these media with an anodization treatment. Results have shown that a 1:2 ratio of aluminum to ferrous ion in the anodizing medium may yield lower corrosion rates due to decreased oxygen reduction rates. Another means of modifying the iron substrate has been investigated in which a titanium chelate compound was reacted with the iron surface to produce a titanized surface layer. The titanized iron surfaces yielded higher corrosion potentials and polarization resistance values in buffered borate solution than did non-titanized surfaces. Cathodic polarization curves suggest that the titanated steel surface is more stable towards reductive dissolution than non-titanated steel. Anodic polarization curves suggest that the titanated steel surface was more easily passivated than non-titanated steel. Auger surface analysis showed that the titanizing technique incorporated 10% titanium versus iron in the surface oxide layer. The titanizing technique appears to be a viable means of modifying steel surfaces.

INTRODUCTION

The importance of the oxygen reaction in atmospheric corrosion is well known [1]. The reaction,

$$O_2 + 2H_2O + 4e^- = 4OH^- ,$$

is also firmly established as a fundamental process in coatings failure on metal substrates in cathodic delamination studies [2-8]. It has been proposed that the corrosion rate of a zinc substrate can be decreased by control of the cathodic reaction [9]. It was further shown that such control was possible through use of Co(II) or Ni(II) salts to decrease the rate of the oxygen reduction reaction [10]. It has also been shown that the cathodic reaction on zinc can be inhibited by cathodic treatment of a chromated surface [11]. The cathodic reaction on iron and steel can also be inhibited by anodic treatment of the steel surface in a solution containing an appropriate organic compound [13]. Mechanisms of corrosion inhibition pertaining to organic coatings have been reviewed [14] and control of the oxygen reduction reaction on the interfacial oxide was emphasi Specifically, control of the electronic properties of the oxide at the ir face, particularly with regard to the catalytic inactivity towards the cathodic reaction, has been proposed [8].

The studies and areas of research cited above were, in part, the basis for the current program work. The work has included a literature survey [15] which is summarized below in terms of the program's objectives:

1. Understanding of the passive layer on iron has progressed to semiconductor models and there is increased use of semiconductor techniques for studies of passive iron layers.

2. The semiconductor properties of oxide-covered metal substrates and modified electrode surfaces are being more intensely studied with the major emphasis on catalysis of oxygen reduction for applications in the energy industry.

3. Chemical modification of electrode surfaces is a powerful technique for tailoring special purpose electrochemical surfaces, especially with respect to catalysis of the oxygen reduction reaction. Inhibition of the oxygen reduction reaction has not been specifically studied.

4. The study of oxygen reduction reactions on the surfaces of bulk materials without surface modification is being pursued more aggressively and the prognosis is for moderate success in the design of materials with desired properties.

The results obtained and reported previously in this research program using an anodizing technique on an iron substrate have shown modest inhibition of the oxygen reduction reaction. An alternate means of modifying oxide-covered metal surfaces using chemical modification of an iron substrate with a titanium

chelate compound is being investigated for comparison purposes. The results of this study are reported herein.

The studies and results discussed above were the basis for this study of the oxygen reduction reaction kinetics on electrode surfaces modified using chemical techniques [16]. The objective was development of a better understanding such that a substrate/interface/coating system may be designed with knowledge of chemical modification effects and compared to anodic electrochemical modification effects. Comparisons are made which are applicable to enhanced coating system performance.

The titanizing technique was adapted from chemical methods for surface modification [16]. In this technique, the iron surface was treated with a reactive titanium compound to produce a modified surface layer containing titanium. The titanium compounds considered for surface modification reactions generally undergo hydrolysis to form more stable products. In the presence of water, the hydrolysis may continue to formation of titanium dioxide or hydrous titanium dioxide as the final product. A variety of titanium compounds is commercially available, including alkyl, alkoxy, and chelate compounds. For the initial studies with titanizing, titanium acetylacetonate was selected for its moderately slow hydrolysis rate, permitting better reaction control than for the rapidly hydrolyzing alkyl and alkoxy compounds. The formula for the titanium acetylacetonate used for this study is given by:

$$Ti(OC_3H_7)_2[OC(CH_3):CHCOCH_3]_2$$

The initial reaction between the iron surface and titanium acetylacetonate is given below in schematic form:

$$Ti(OR)_4 + FeOOH = (OR)_3TiOFeO + ROH$$

The remaining reactive sites of the titanium compound may react with additional iron hydroxyl groups or with water to form a mixed oxide containing titanium and iron ($TiFe_xO_y$). Depending upon the extent of reaction, organic groups may be made to remain as substituents of the titanium/iron mixed oxide.

EXPERIMENTAL METHODS

Two methods for modifying iron surfaces were used in this investigation. The anodization technique was a continuation of work reported previously [12]. The titanizing technique has been developed during the current report period.

Anodization Technique and Evaluation

The anodization technique was adapted from that described by Leidheiser and Konno [13]. The technique consisted of abrading the substrate, SAE 1010 steel,

with 240 grit silicon carbide paper, rinsing with water, a final rinse with methanol, and allowing the specimen to dry in a desiccator. The specimen was abraded with 600 grit silicon carbide paper just prior to immersion in the anodizing medium and subjected to anodic polarization to produce a passive oxide film. The anodic polarization was conducted in either a glass battery jar fitted with reference, counter electrodes, and a mechanical stirrer, or a standard electrochemical cell (Princeton Applied Research Corp. Model K47) with a magnetic stirrer. All potentials are reported versus the saturated calomel electrode (SCE). A Princeton Applied Research Corp. Model 350 Corrosion Measurement Console or Model 173/376 potentiostat was used for the application of the anodic potential. The treatment solutions are given along with the results in a later section of this report. The anodization treatment was a two-step anodization process consisting of polarization at 0.8 v for 10 minutes followed by polarization at 1.0 v for 10 minutes. These treatments were selected with the intent of growing passive oxide films into which dopants (impurities) were incorporated. The specimens were immediately evaluated for corrosion resistance with the polarization resistance technique using an EG&G Princeton Applied Research Corp. Model 350 Corrosion Measurement Console with a Model K47 electrochemical cell containing a pH 8.5 borate solution. The polarization resistance measurement was conducted on a smaller surface area (1 cm^2) than the anodized area (2 cm^2) such that edge effects (untreated areas) were avoided. The polarization potential range was -0.025 to +0.025 v versus the corrosion potential with a scan rate of 0.1 mv/sec. Immediately after completion of the polarization resistance measurement, a cathodic polarization curve was obtained in the same electrolyte at a scan rate of 1 mv/sec from the corrosion potential to -1.5 v.

Titanizing Technique and Evaluation

The titanizing procedure for ferrous substrate consisted of abrading a specimen of SAE 1010 steel with 120 grit silicon carbide paper, rinsing with distilled water, rinsing with methanol and drying in a Freon stream. The specimen was dipped in a solution of 1:5 Dupont Tyzor® AA (titanium acetylacetonate) in ethyl acetate until a uniform film was obtained upon removal from the solution. The solvent was removed by blow-drying in a Freon stream. The specimen was heated on a hotplate at 100-150°C for 15-60 minutes. After cooling for 5 minutes, the specimen was mounted in a holder, inserted in an EG&G Model K47 electrochemical cell and electrochemical tests were begun. Blank specimens were prepared and tested in a similar manner without exposure to titanium acetylacetonate to permit direct comparison of electrochemical data.

Electrochemical testing consisted of consecutive polarization resistance measurements for several hours followed by cathodic and then anodic polarization curve determinations. Additional polarization resistance measurements were made after polarization curve determinations for most specimens. The electrochemical testing was performed with an EG&G Princeton Applied Research Model 350 Corrosion Measurement Console. The test electrolyte was borate buffer solution prepared by dissolving 38 g sodium borate decahydrate and 17 g boric acid in water to make 1000 ml of solution and yielded a pH of 8.4. The polarization resistance measurements were obtained repetitively every 15 or 60 minutes using a -0.006 to +0.002 volt range versus the corrosion potential. The cathodic and anodic polarization curves were determined at a scan rate of 1 mv/sec from the corrosion potential to -1.2 and + 1.2 volts, respectively.

Surface analysis of the titanized surface was made with Auger electron spectroscopy. The specimens subjected to the titanizing and electrochemical techniques were analyzed.

RESULTS AND DISCUSSION

A summary of the results obtained for anodized specimens is given in Table I. These data represent some of the more favorable results obtained with this technique. Many additional trials were attempted, but problems were experienced with the solution chemistry (pH/solubility) or the anodization did not yield a passivated surface during treatment. The results obtained for the polarization resistance experiments were small differences in R_p values relative to the many orders of magnitude observable with this technique. Also, the R_p values did not reveal a response to the presence of aluminum ion in the anodizing medium. Since the relationship of R_p to the electrochemical activity of the specimen depends partly upon the values of the Tafel constants, there may be no direct relationship of R_p to anodization in the presence of aluminum. The data given for the cathodic Tafel constant indicate a dependence on aluminum. For small differences in R_p values, the cathodic Tafel behavior can have a significant influence on electrochemical activity. The corrosion currents, I_c, determined from the cathodic Tafel slope and the corrosion potential, are lower by a factor of 2 or 3 for the samples anodized in the presence of aluminum. Figure 1 shows cathodic polarization curves obtained for specimens anodized without Fe or Al present, with Fe present and with Fe and Al present (Media A, B and C, respectively, Table I). The curve for A shows transitions from cathodic to anodic currents indicating less stable oxide layers than the other specimens. The curve for B shows more stable oxide layers, but higher hydrogen reduction currents at the more negative potentials. The curve for C shows stable oxide layers, low hydrogen reduction currents and modified cathodic activity in the vicinity of the corrosion potential for the specimen anodized in the presence of aluminum.

Table I

Treatment Media and Electrochemical Data for Anodized Specimens

Medium	R_p (kohm-cm^2)	CTC (v/dec)	I_c (μA/cm^2)
(A): 1M Na_2SO_4, 0.001M H_2SO_4	120	0.135	0.51
(B): (A) plus 0.1M $FeSO_4$	91	0.136	0.52
(C): (B) plus 0.05M $AlK(SO_4)_2$	90	0.108	0.16
(D): " " "	87	0.127	0.29
(E): (B) plus 0.075M $AlK(SO_4)_2$	130	0.109	0.16

CTC - Cathodic Tafel constant

I_c - Corrosion current determined from cathodic Tafel slope and corrosion potential.

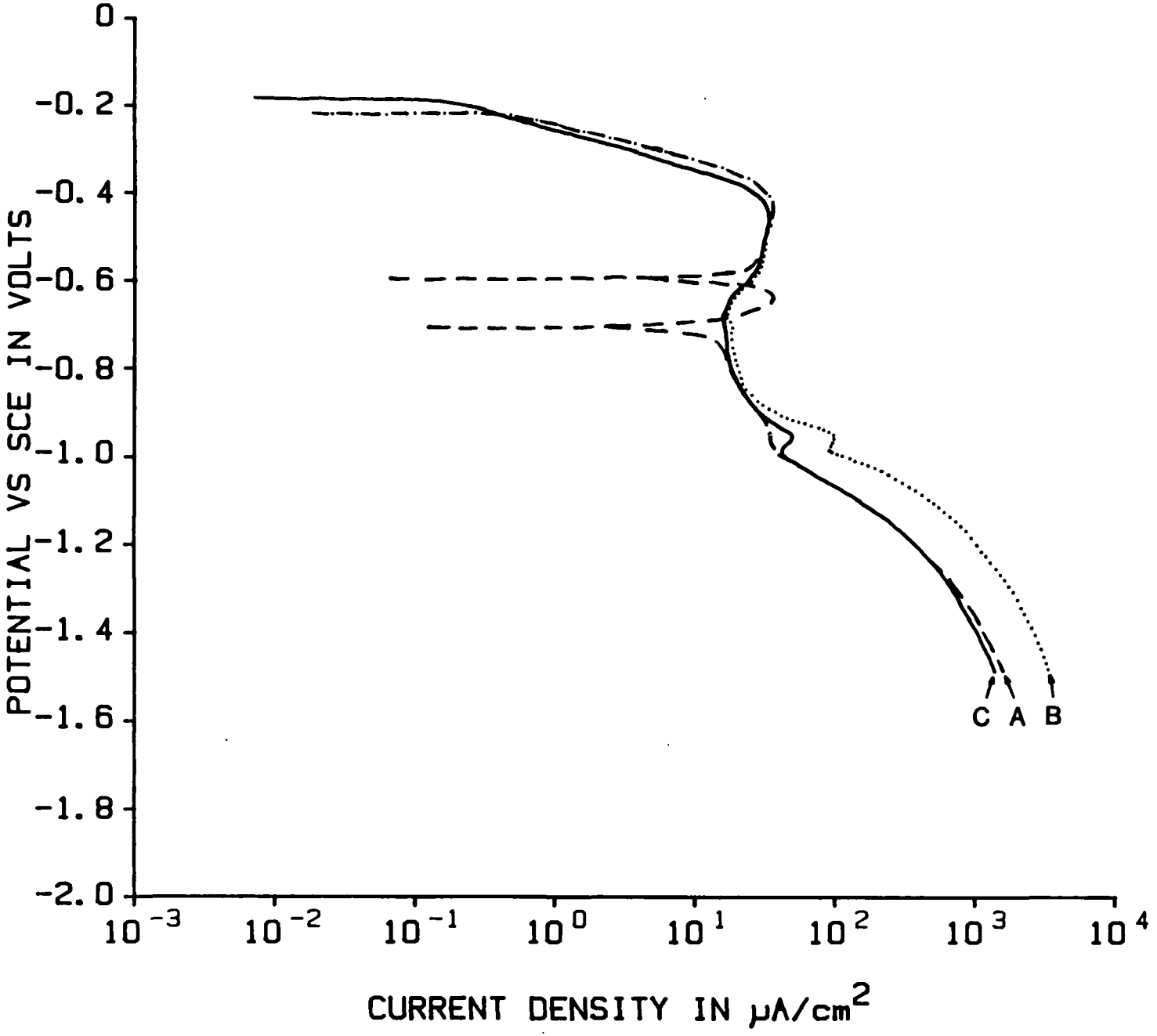

Figure 1. Cathodic polarization curves for anodized steel in borate buffer (pH 8.5) solution. Steel anodized without Fe or Al in media denoted by dashed line (A), anodized with Fe only, dotted line (B), and with Fe and Al, solid line (C).

Figure 2 shows the polarization resistance values versus time for blank (non-titanized) and titanized specimens. The R_p values for the titanized specimen show a more rapid increase versus time than for the blank specimen. After immersion for 8 hours, the titanized specimen yielded an R_p value 4 times greater than that for the blank specimen. Figure 3 compares the cathodic polarization curves for blank and titanized specimens. The titanized specimen gave more positive corrosion potential values, a lower cathodic Tafel constant and more stable currents at -0.6 volt versus SCE than did the blank specimen. These characteristics are indicative of a more stable and corrosion protective surface layer for the titanized specimen versus the blank. Figure 4 compares the anodic polarization curves for blank and titanized specimens. The anodic curves are similar. However, the curve for the titanized specimen shows a smaller anodic peak at -0.6 volt suggesting a more readily passivated surface versus the blank specimen. Note that the anodic curves were obtained after cathodic polarization, which treatment leaves the specimens in an active state before commencement of the anodic curves.

Results obtained for Auger electron spectroscopic surface analysis of a titanized specimen are shown in Figure 5. The spectrum is that expected for a steel specimen subjected to electrochemical treatment in borate solution. The main distinguishing feature of the spectrum is the presence of a relatively small peak due to titanium. The titanium peak indicates that titanium has been incorporated in the surface oxides of the steel substrate and is present in a sufficiently stable form to resist dissolution upon application of electrochemical treatments. An estimate of the ratio of titanium versus iron in the surface oxide layers is 10%. The specimen was analyzed at several different point locations on the surface and yielded similar spectra indicating a uniform incorporation of the titanium in the steel surface layers.

REFERENCES

[1] J. C. Scully, "The Fundamentals of Corrosion," 2nd Edition, Pergamon Press, Ltd., New York, 1975.

[2] H. Leidheiser, Jr., M. W. Kendig, Corrosion 32, 69 (1976).

[3] M. W. Kendig, H. Leidheiser, Jr., J. Electrochem. Soc. 123, 982 (1976).

[4] H. Leidheiser, Jr., M. W. Kendig, Ind. Eng. Chem. Prod. Res. Dev. 17, 54 (1978).

[5] H. Leidheiser, Jr., Croat. Chem. Acta 53, 197 (1980).

[6] H. Leidheiser, Jr., W. Wang, J. Coatings Technol. 53, No. 672, 77 (1981).

[7] R. A. Iezzi, H. Leidheiser, Jr., Corrosion 37, 28 (1981).

[8] H. Leidheiser, Jr., Ind. Eng. Chem. Prod. Res. Dev. 20, 547 (1981).

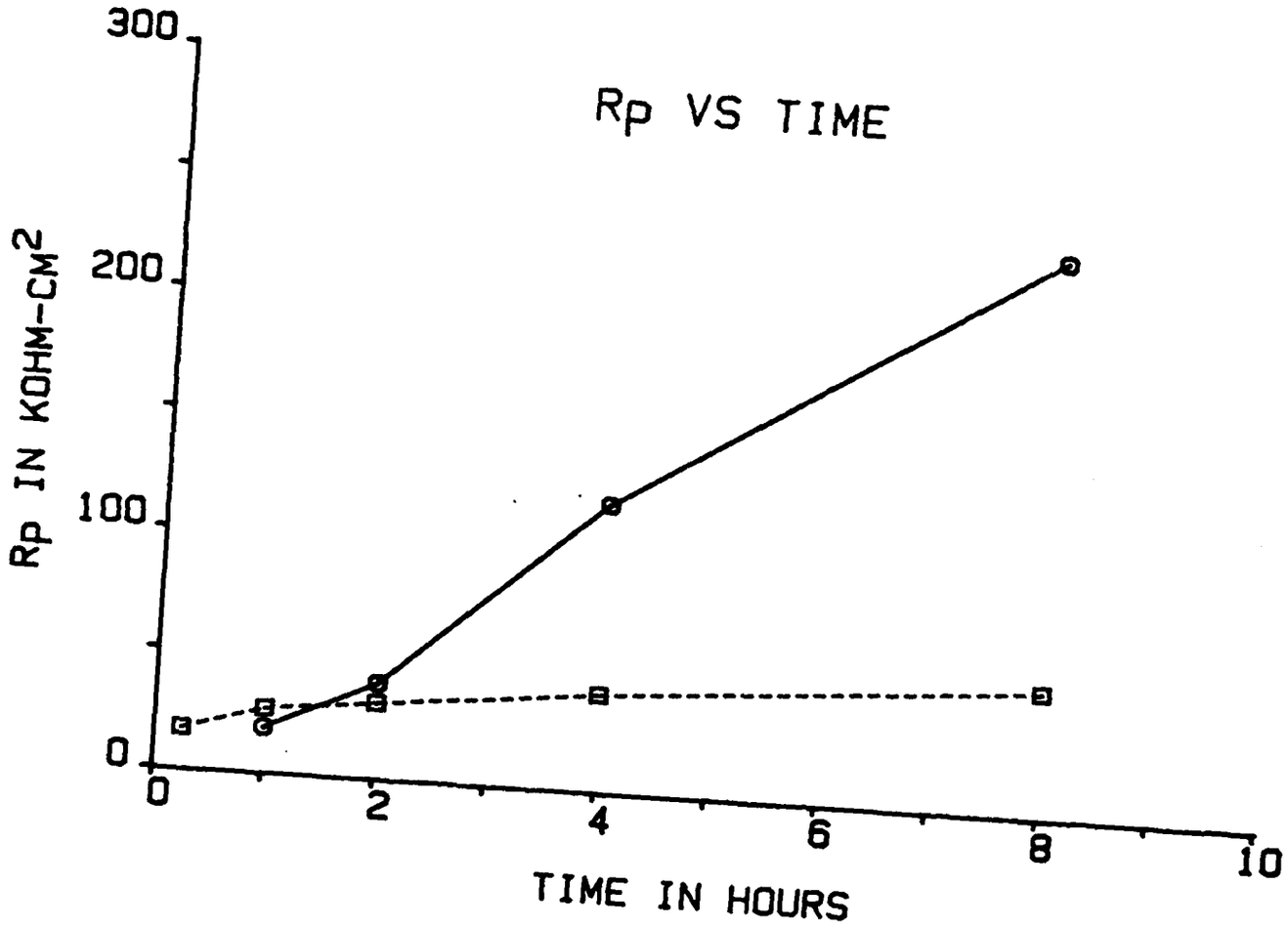

Figure 2. Comparison of polarization resistance versus time data for titanized steel (solid line) and non-titanized steel (dashed line).

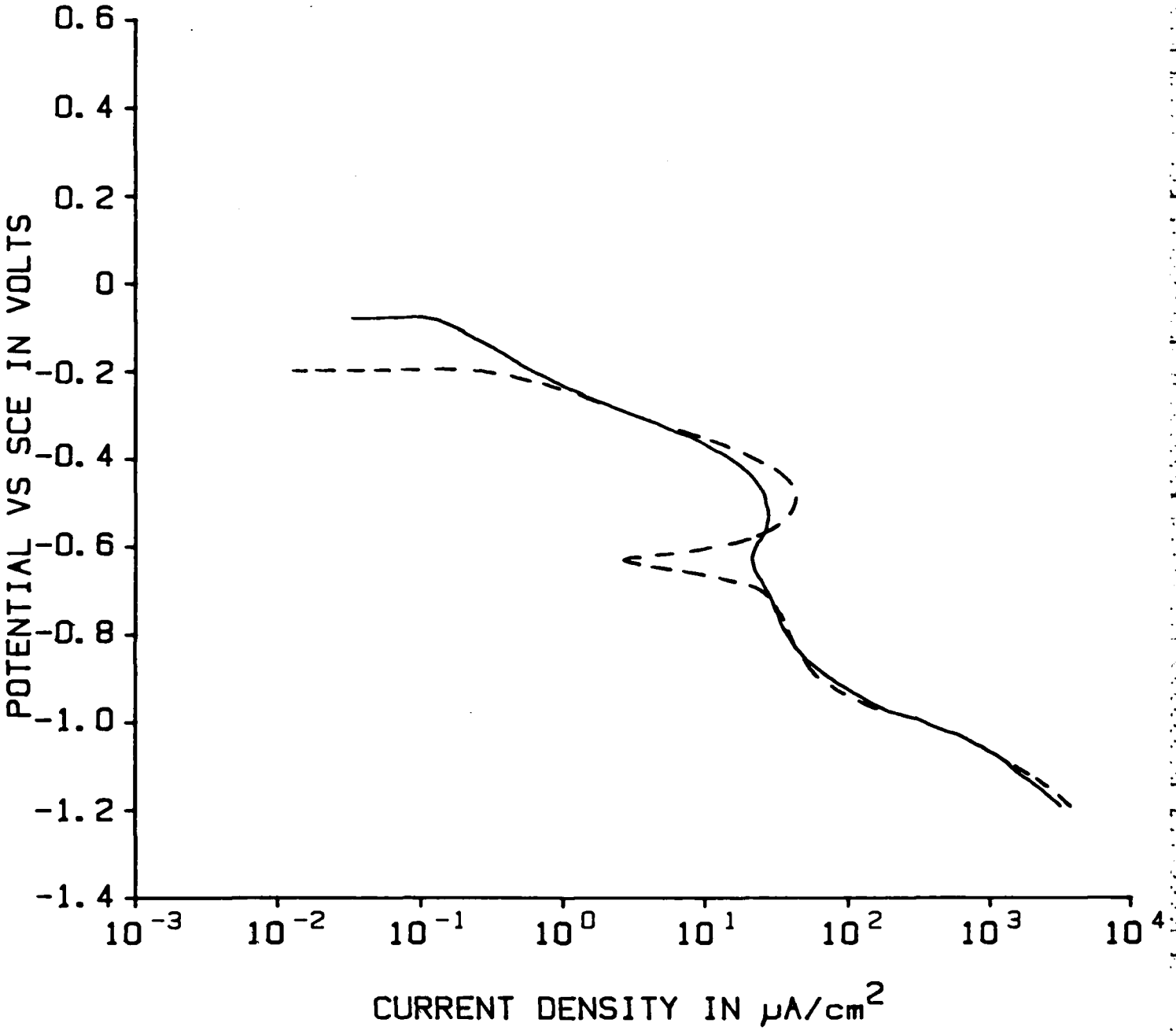

Figure 3. Comparison of cathodic polarization curves for titanized steel (solid line) and non-titanized steel (dashed line).

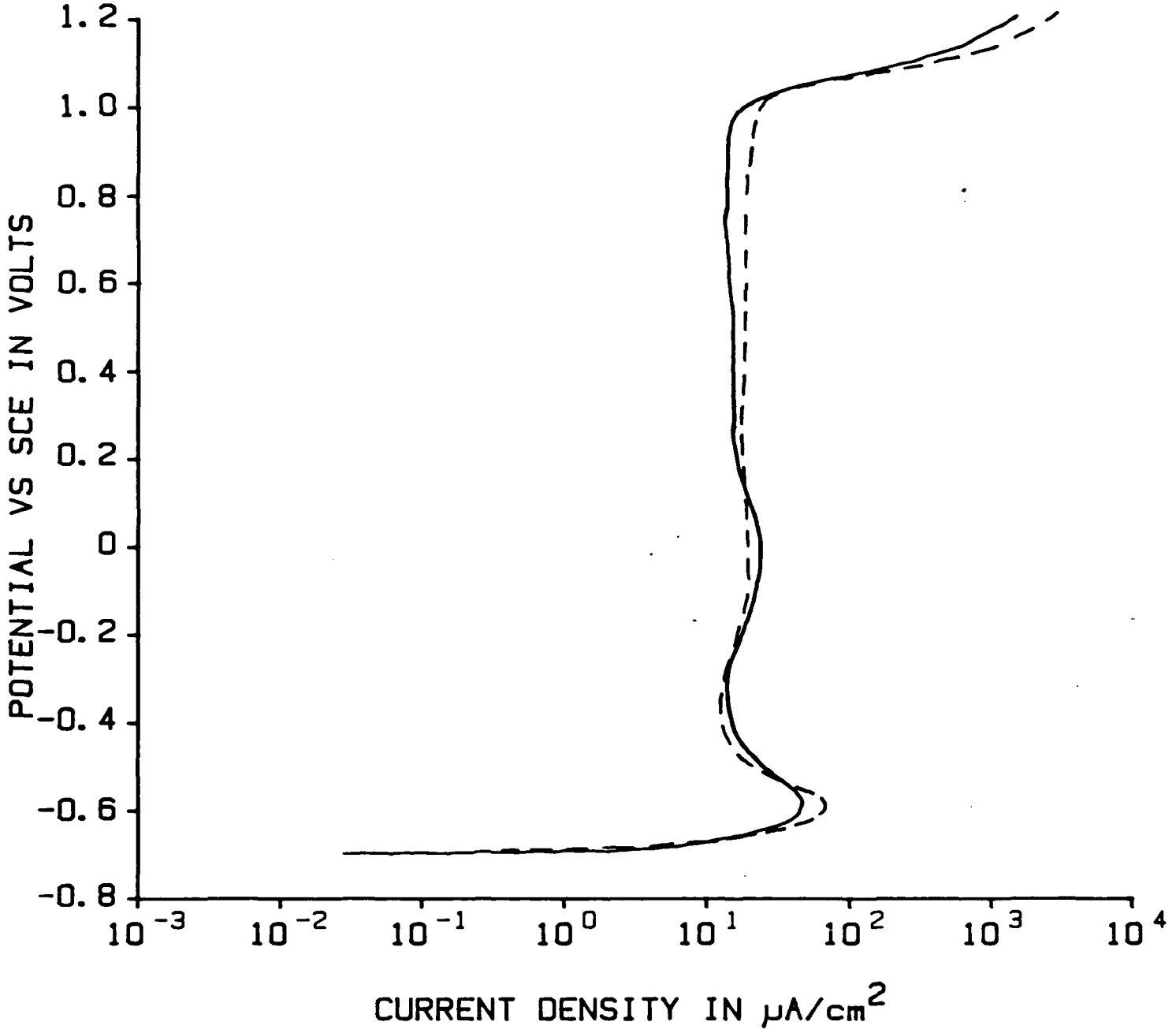

Figure 4. Comparison of anodic polarization curves for titanized steel (solid line) and non-titanized steel (dashed line).

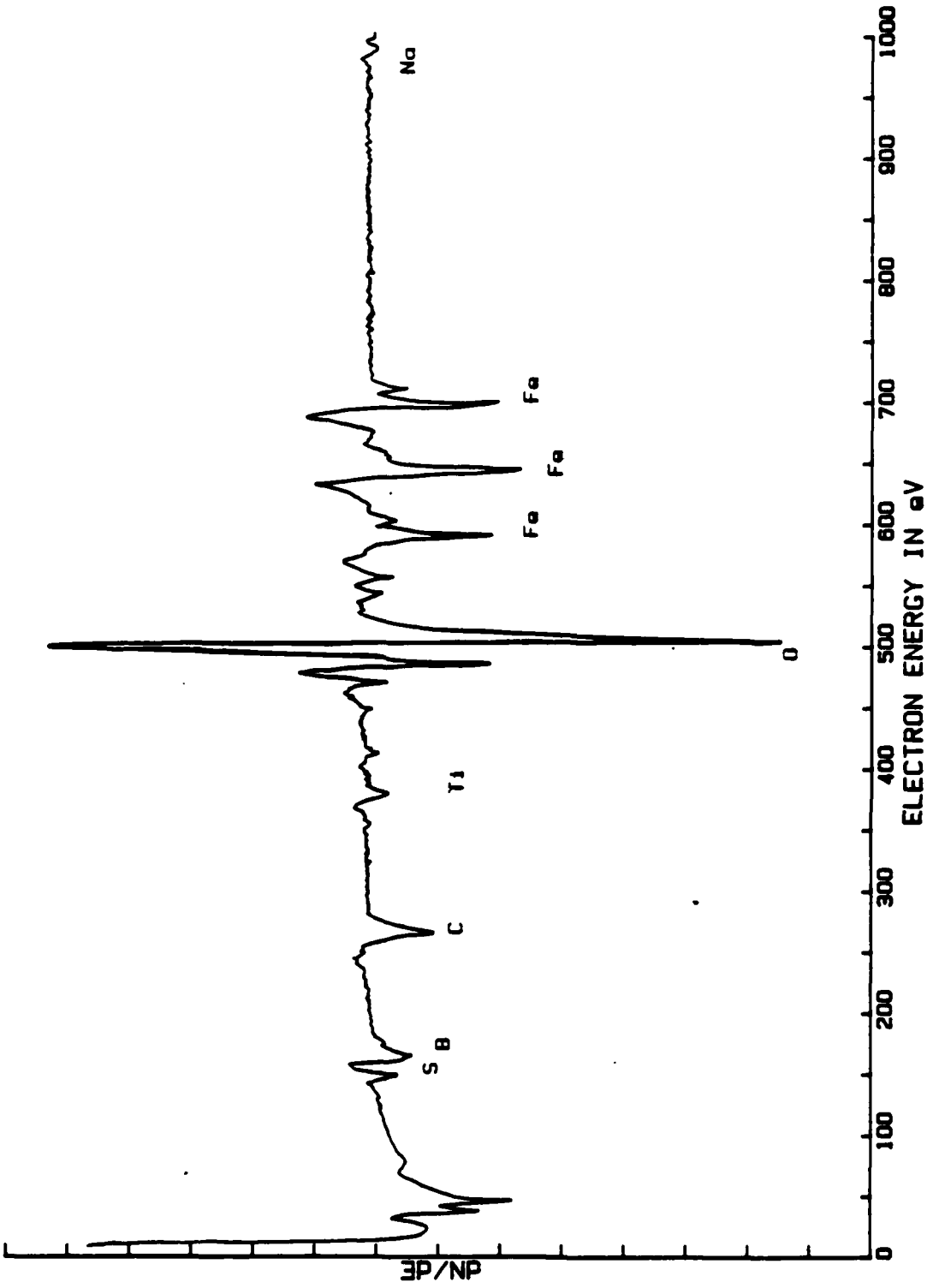

Figure 5. Auger electron spectrum of titanized steel specimen analyzed after electrochemical measurements in borate medium.

[9] H. Leidheiser, Jr., I. Suzuki, Corrosion 36, 601 (1980).

[10] H. Leidheiser, Jr., I. Suzuki, J. Electrochem. Soc. 128, 242 (1981).

[11] H. Leidheiser, Jr., Y. Momose, R. D. Granata, Corrosion 38, 178 (1982).

[12] R. D. Granata, "Inhibition Methods for Semiconducting Protective Oxides on Mild Steel," Paper No. 124, National Association of Corrosion Engineers, Corrosion '84 Conference, 1984.

[13] H. Leidheiser, Jr., H. Konno, J. Electrochem. Soc. 130, 747 (1983).

[14] H. Leidheiser, Jr., J. Coatings Technol. 53, No. 678, 29 (1981).

[15] Annual Report, this project, 1983.

[16] R. W. Murray, Acc. Chem. Res. 13(5), 135 (1980).

[17] "Mössbauer Spectroscopic Study of the Corrosion Inhibition of Zinc by Cobalt Ions," H. Leidheiser, Jr., G. W. Simmons, S. Nagy, and S. Music', J. Electrochem. Soc. 129, 1658-62 (1982).

[18] "Technical Note: Inhibition of the Cathodic Reaction on Zinc in Aerated 3% NaCl Solution," H. Leidheiser, Jr., Y. Momose, R. D. Granata, Corrosion 38, 178-79 (1982).

Program #6

The Effect of Cations on the Dissolution in Alkaline Environments of Zinc Phosphate Conversion Coatings on Steel

Principal Investigator: Henry Leidheiser, Jr.
Prof. of Chemistry

Associate: André Sommer
Graduate Student

INTRODUCTION

The cathodic reaction which takes place at the delaminating front during cathodic delamination generates hydroxyl ions. To maintain charge balance in this region, cations must migrate to the reaction zone through the polymer coating or laterally along the polymer/substrate interface from the defect. Leidheiser and Wang [1] have demonstrated that the cathodic delamination rate of organic films from metal substrates is greatly dependent on the cation of the electrolyte solution. Experiments conducted with Li, Na, K and Cs show that the rate of delamination increases linearly with the diffusion coefficient of the cation. The delamination rate was greatest for cesium and decreased on going to lithium. Studies summarized elsewhere in this report involve cathodic delamination of organic coatings from phosphated steel substrates. In order to understand this phenomenon better, it is essential to determine the effects of cations on the dissolution of phosphate conversion coatings in alkaline environments.

EXPERIMENTAL RESULTS

Zinc phosphated steel samples were exposed to 0.1M hydroxide solutions of lithium, sodium, potassium and cesium at ten-minute intervals for 1 hour. After exposure, the solution volumes were analyzed for zinc ion and phosphate ion by atomic absorption spectrophotometry and colorimetric spectrophotometric techniques, respectively. The phosphated steel samples exposed for 1 hour

were dried and analyzed by scanning electron microscopy, energy dispersive spectroscopy and Raman spectroscopy. The physical appearance of the phosphated steel samples after exposure at each 10-minute interval and samples exposed for four days are exhibited in Figure 1. The experimental results of the solution analysis are presented as plots of ion concentration in solution (micromoles/liter) vs. exposure time in minutes. These relations are shown in Figures 2, 4, 6 and 8 for samples exposed to LiOH, NaOH, KOH and CsOH, respectively. The SEM, EDS and Raman results are given in Figures 3, 5, 7 and 9.

A comparison of the dissolution curves for each hydroxide solution reveals three major differences. First, the amount of phosphate ion removed from the conversion coating is greatest for sodium followed by potassium, cesium and lithium. Second, the zinc ion concentration in solution becomes constant after 30 minutes of exposure in NaOH and KOH. Third, a greater amount of phosphate ion is released from the surface compared to zinc ion except in the case of samples exposed to LiOH. Samples exposed to CsOH initially show the same amount of zinc and phosphate ions being released with the amount of phosphate ion in solution increasing as the experiment continues.

The SEM micrographs for the samples exposed to NaOH and KOH show the formation of a precipitate on the phosphate coating surface while the micrographs of the samples exposed to LiOH and CsOH are characteristic of a normal zinc phosphate coating. The EDS spectra of the latter two samples were also typical of a normal zinc phosphate coating. However, the EDS spectra of the samples exposed to NaOH and KOH exhibited a marked decrease in the amount of phosphorus in the phosphate coating. The EDS spectra of all the samples show approximaely the same amount of zinc remaining in the coating. The Raman spectra for each of the samples are characteristic of normal zinc phosphate coatings except in the case of the sample exposed to NaOH solution. The Raman spectrum for this sample exhibits a decrease in the signal-to-noise ratio and an increasing background on going to higher wavenumber shift.

Energy dispersive spectroscopy at best is a semiquantitative technique, but the trends shown for the different samples are consistent with the wet chemical analysis and physical appearance of the samples. The precipitates formed on the samples treated with NaOH and KOH are probably a form of zinc oxide and/or zinc hydroxide (zincate). Formation of zincate as a precipitate accounts for the constant zinc ion concentration in solution and the relative amount of zinc shown in the EDS spectra. The decrease in the amount of phosphorus in the EDS spectra for the NaOH and KOH treated samples agrees with the increase in the phosphate ion concentration in solution. The observation that more zinc ion is released to solution than phosphate ion for the sample treated with LiOH may be due to the fact that LiOH is the weakest of all the alkali metal hydroxides [2]. Another possible explanation for this behavior is that Li_3PO_4 is being formed as a precipitate; however, the SEM micrograph shows no sign of precipitate formation. Lithium phosphate is much more insoluble than other alkali metal phosphates [3]. To gain more information about this behavior and to answer the question of why sodium hydroxide dissolves a greater amount of zinc phosphate, zinc phosphated steel samples were exposed to the different hydroxides for a period of four days. The phosphated steel samples were then dried and analyzed as before.

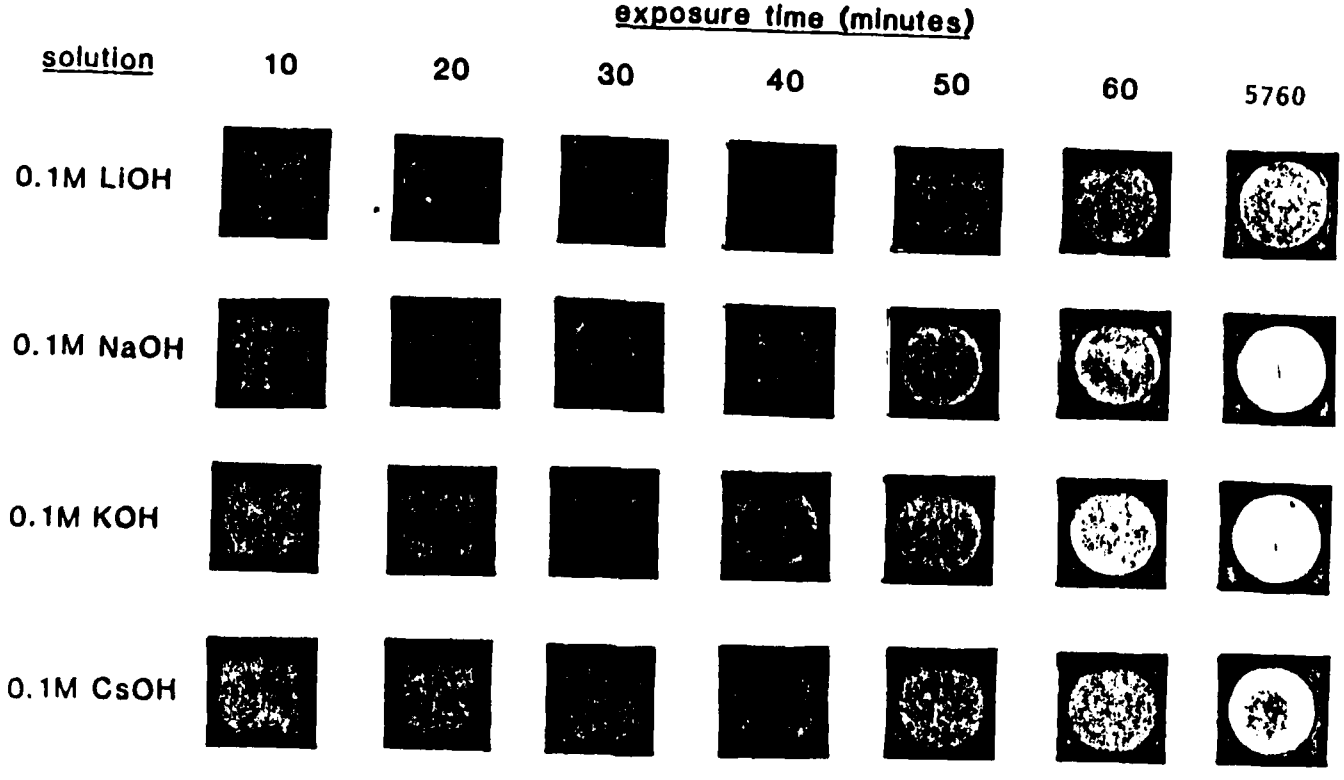

Figure 1. The appearance of phosphated steel samples after exposure for various times to 0.1M alkali hydroxides at room temperature.

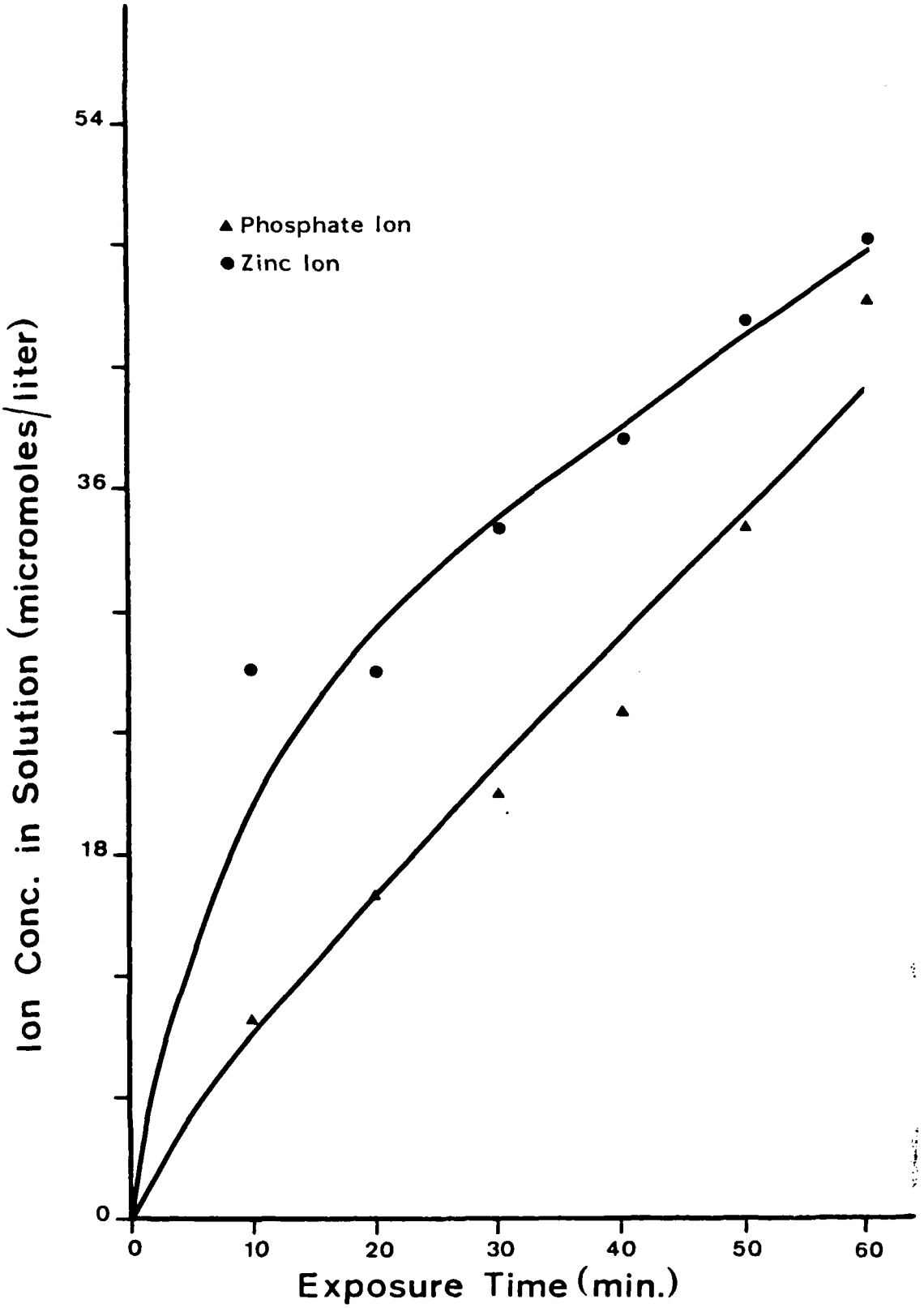

Figure 2. The amount of zinc and phosphate in solution after exposure of a phosphated steel to 0.1M LiOH.

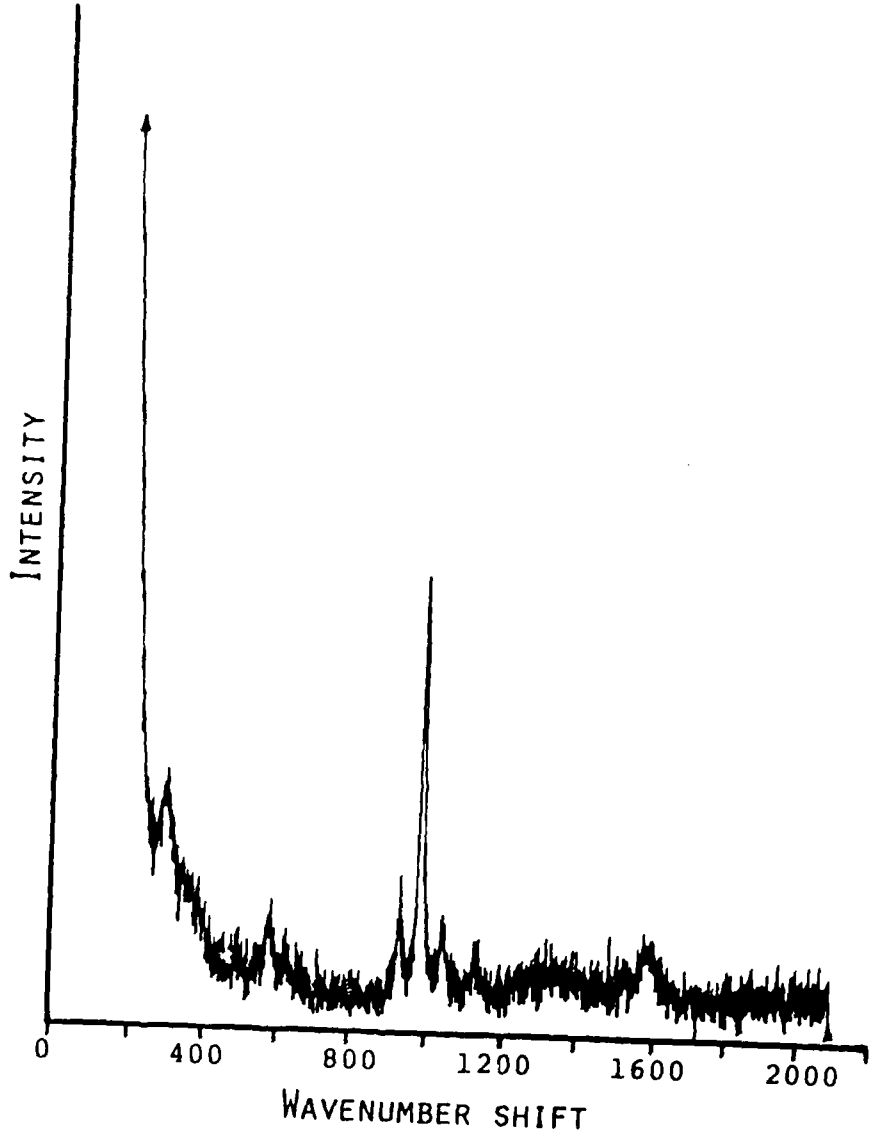

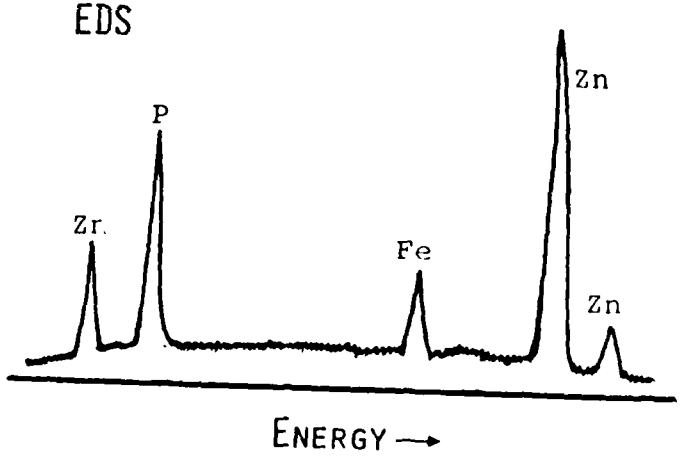

Figure 3. The Raman spectrum, EDS spectrum and scanning microscope view of phosphated steel exposed to 0.1M LiOH for 1 hour.

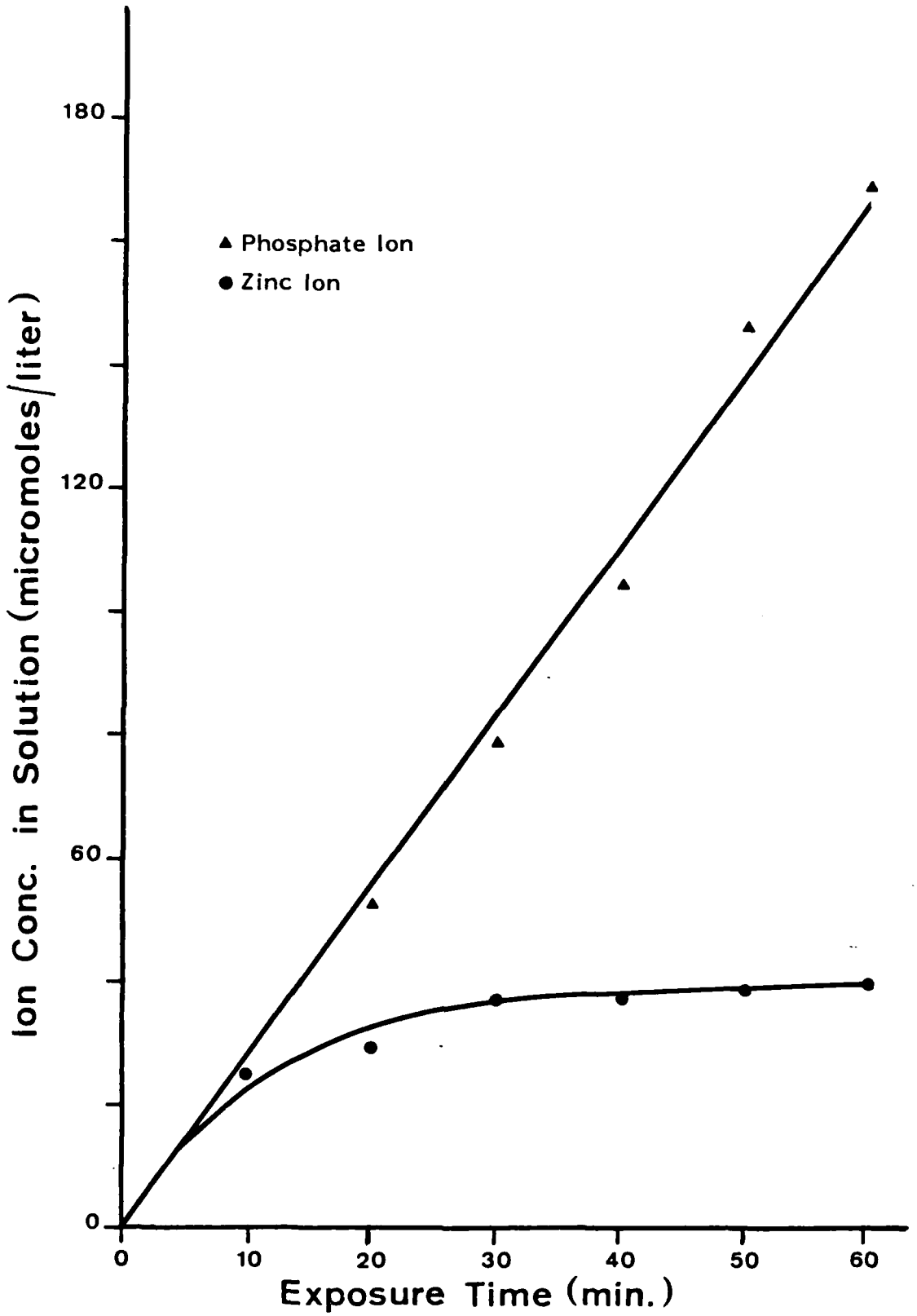

Figure 4. The amount of zinc and phosphate in solution after exposure to a phosphated steel to 0.1M NaOH.

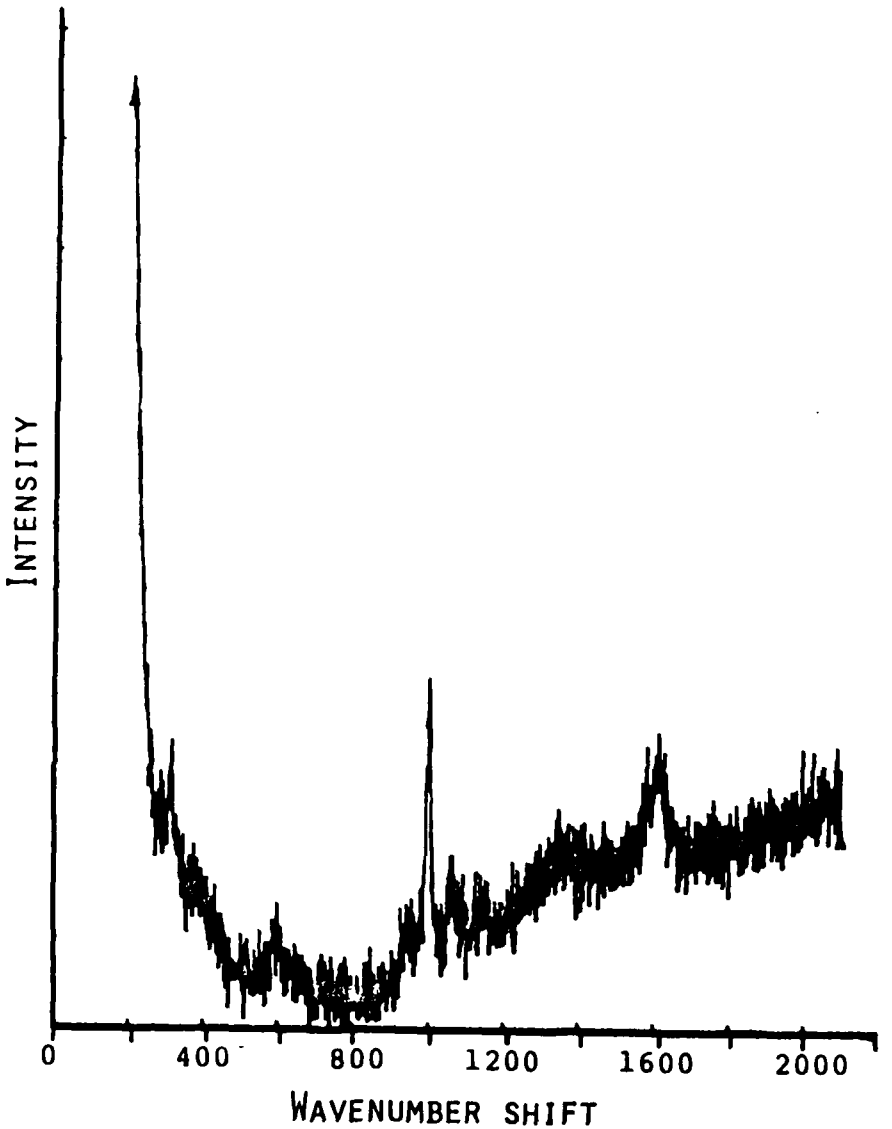

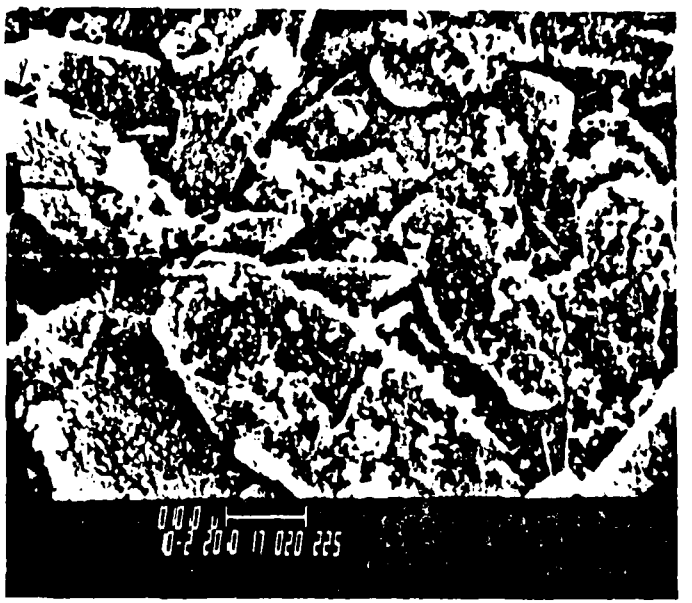

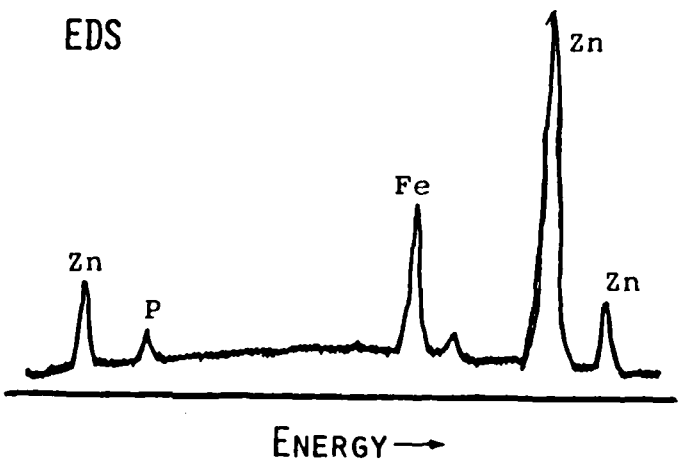

Figure 5. The Raman spectrum, EDS spectrum and scanning microscope view of phosphated steel exposed to 0.1M NaOH for 1 hour.

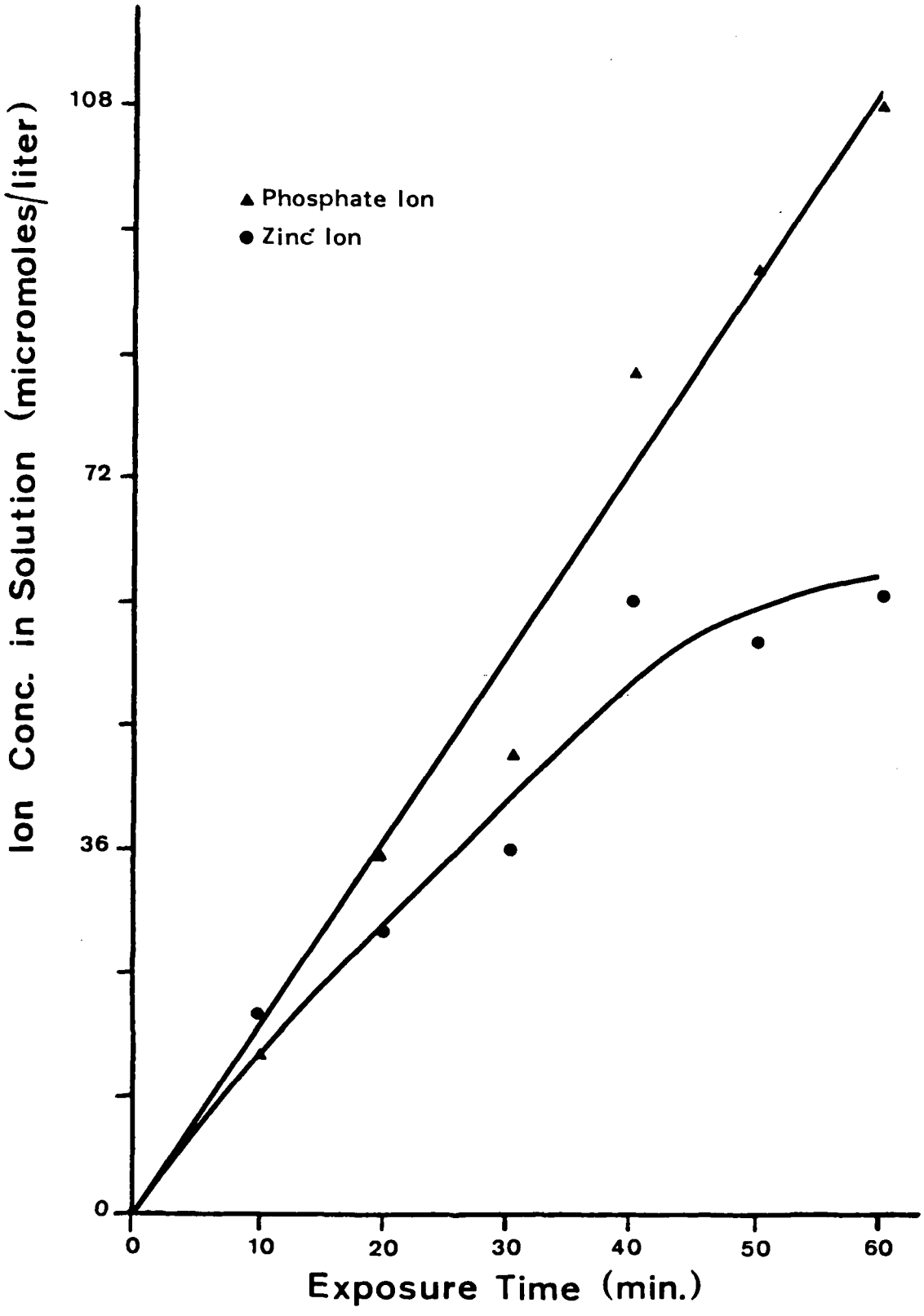

Figure 6. The amount of zinc and phosphate in solution after exposure of a phosphated steel to 0.1M KOH.

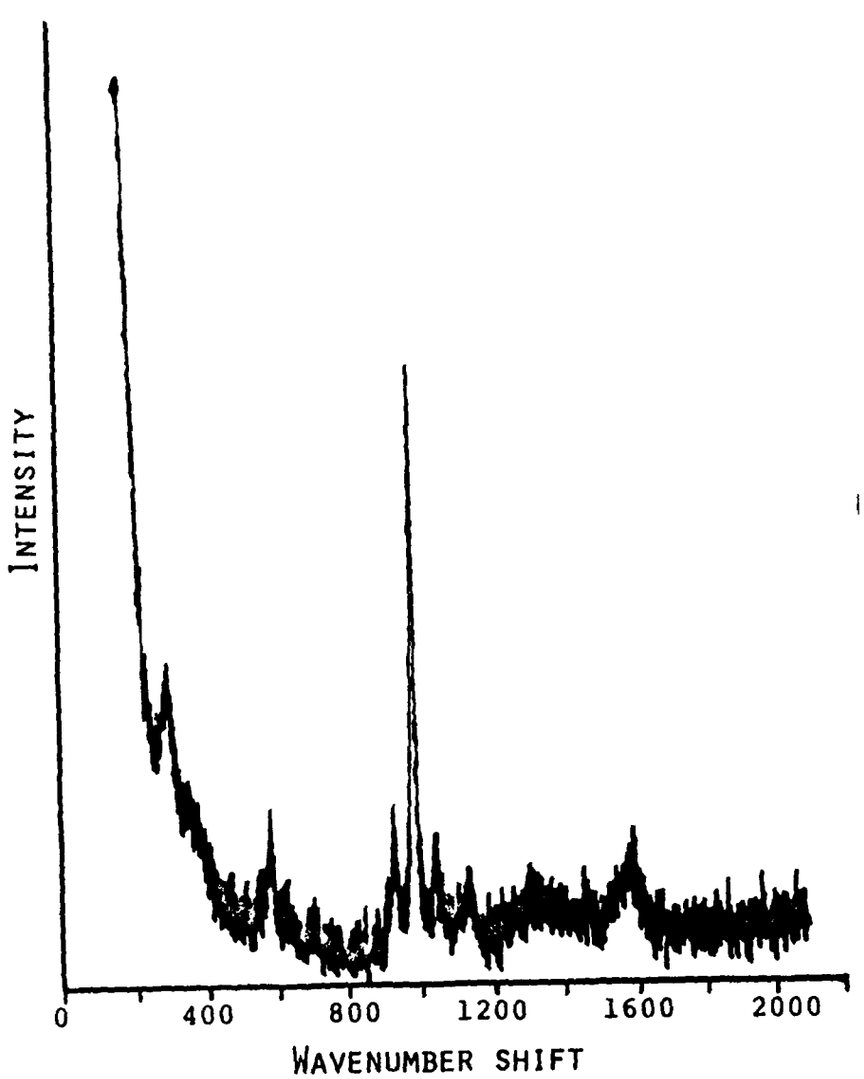

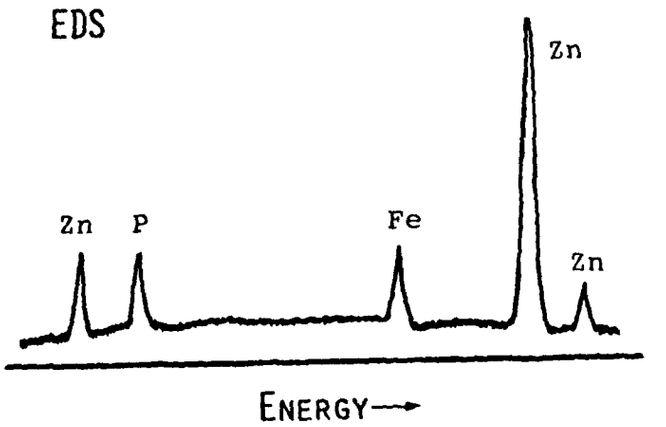

Figure 7. The Raman spectrum, EDS spectrum and scanning microscope view of phosphated steel exposed to 0.1M KOH for 1 hour.

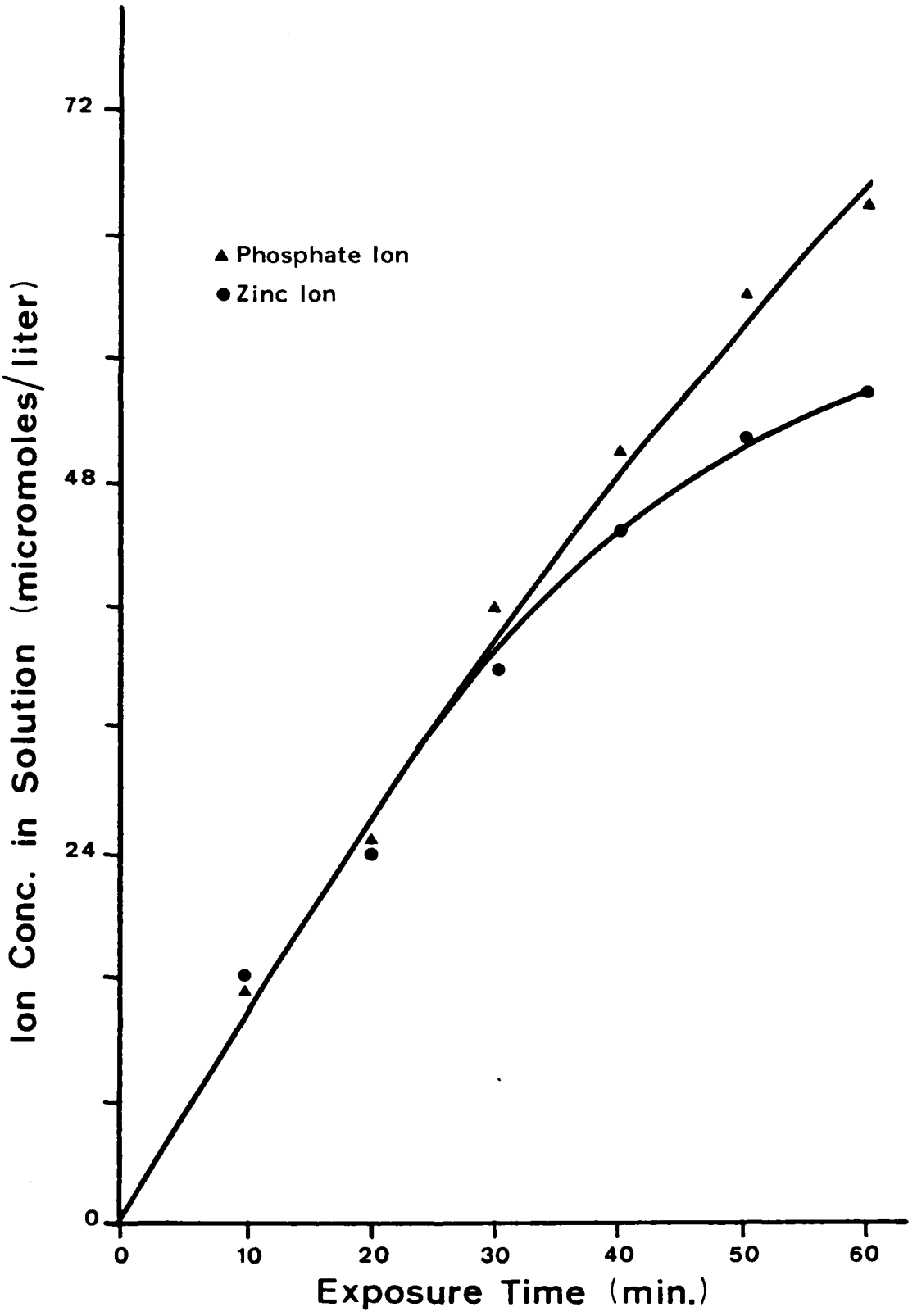

Figure 8. The amount of zinc and phosphate in solution after exposure of a phosphated steel to 0.1M CsOH.

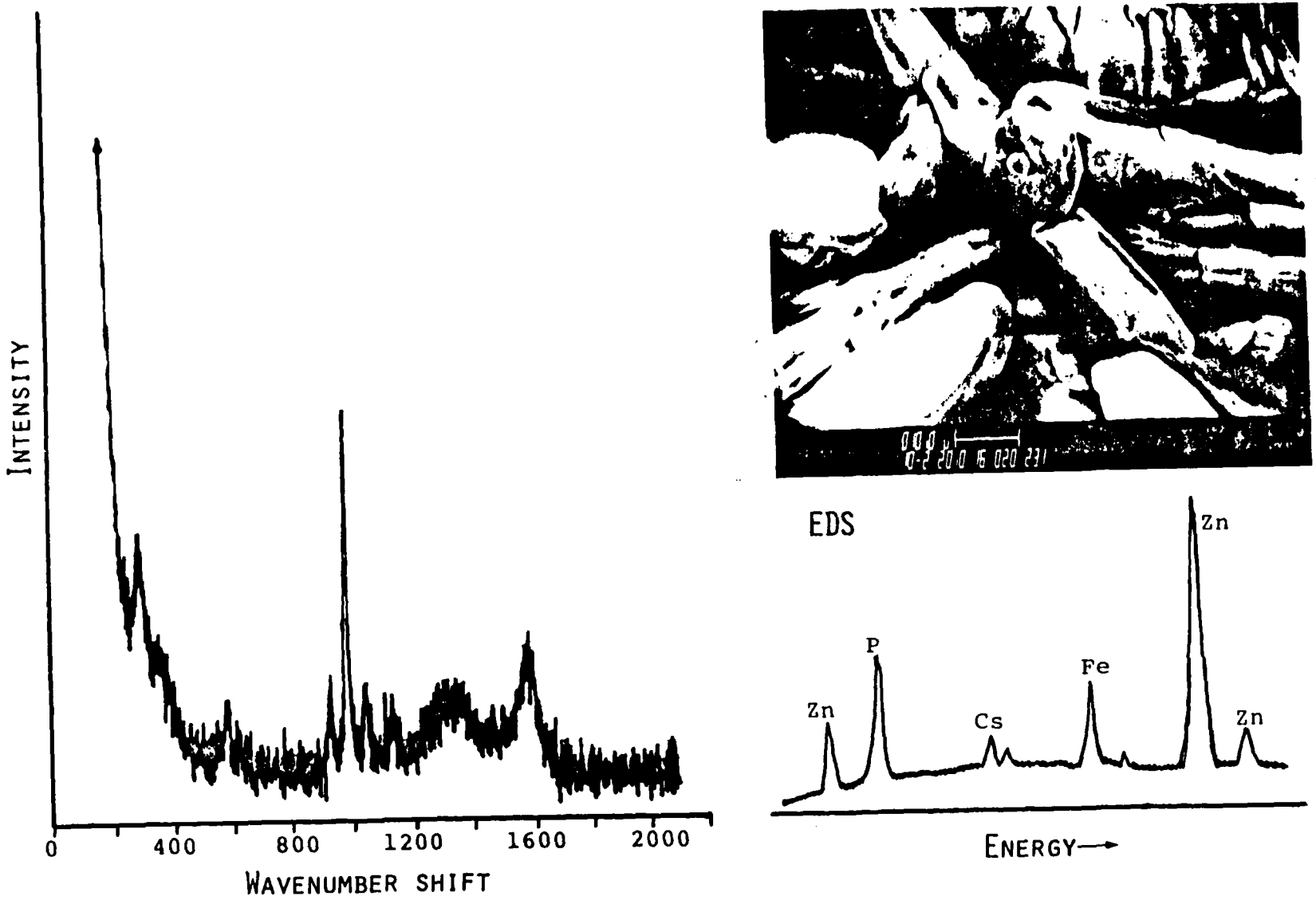

Figure 9. The Raman spectrum, EDS spectrum and scanning microscope view of phosphated steel exposed to 0.1M CsOH for 1 hour.

The SEM micrograph and EDS spectrum for the sample exposed to lithium hydroxide are shown in Figure 10. Both the micrograph and the EDS spectrum are characteristic of a normal phosphate although the micrograph does show signs of precipitate formation on the coating. Three different phases were detected in the coating on examination by optical microscopy. The Raman spectra for each of these phases are illustrated in Figures 11-13. Figure 11 shows the Raman spectrum recorded for a brownish-yellow phase which looked like a normal phosphate crystal. The band located around 950 cm^{-1} shift is indicative of a phosphate different from zinc phosphate. The position of the band is characteristic of an iron phosphate known as vivianite [$Fe_3(PO_4)_2 \cdot 8H_2O$]. The broad band located at 650 cm^{-1} shift may arise from Fe_3O_4 in the coating. Figure 12 shows the spectrum obtained from raised white crystallites in the coating. This phase may be a transition from normal zinc phosphate to the iron phosphate detected in the previous spectrum as judged from the fact that the 995 cm^{-1} shift band is present along with the bands associated with vivianite (iron phosphate). A third phase characterized by round clear crystallites gave the Raman spectrum shown in Figure 13. Based on the location of the band at 367 cm^{-1} shift and the elements present in the coating, the only reasonable structure that could account for this spectrum is a zincate of iron with the possible formula, $Fe_2(ZnO_2)_3$.

The samples exposed to sodium and potassium hydroxide for four days were very similar to those samples exposed for 1 hour. SEM micrographs and EDS spectra shown in Figures 14 and 16 indicate the presence of a heavy precipitate on a coating which is largely devoid of phosphorus. The Raman spectra in Figures 15 and 17 recorded for these samples are characteristic of zinc oxide associated with a small amount of hydrozincite. Zinc oxide gives rise to the band at 435 cm^{-1} shift and zinc carbonate gives rise to the broad band in the 1100 cm^{-1} shift region. One phase was detected for the sodium-treated sample, while two phases were detected for the potassium-treated sample. The second phase in the latter sample is shown in the SEM micrograph of Figure 18 as cubic crystllites. The EDS spectrum was recorded in a point mode and indicated the presence of K, P, Fe, and Zn. Two bands were detected in the Raman spectrum (Figure 19) of these crystallites and were located at 528 cm^{-1} shift and 976 cm^{-1} shift. The band located at 976 cm^{-1} shift is typical of a phosphate-type structure. The band located at 528 cm^{-1} may possibly be due to a zincate structure (i.e., K_2ZnO_2). Since the crystal is a single phase it may be a mixed phosphate of zinc and potassium.

The SEM micrograph and EDS spectrum of the sample treated with CsOH are shown in Figure 20. The micrograph shows the formation of crystallites which grow as needles on the phosphate coating. EDS spectroscopy indicated the presence of a large amount of cesium and zinc associated with small amounts of iron and phosphorus. Four different phases were identified using optical microscopy. The Raman spectra of each of these phases are shown in Figures 21-24. The spectrum shown in Figure 21 was recorded on raised brown crystals in the coating and is almost identical to the spectrum of the brown phases occurring in the LiOH-treated sample. The band located at 950 cm^{-1} shift can be assigned to the phosphate structure known as vivianite and the band located at 650 cm^{-1} shift may be accounted for by Fe_3O_4. Small transparent crystals gave rise to the Raman spectrum shown in Figure 22. The band located at 1063 cm^{-1} shift is indicative of a carbonate vibration and can be assigned to hydrozincite $2ZnCO_3 \cdot 3Zn(OH)_2$. The Raman spectrum shown in Figure 23 was recorded

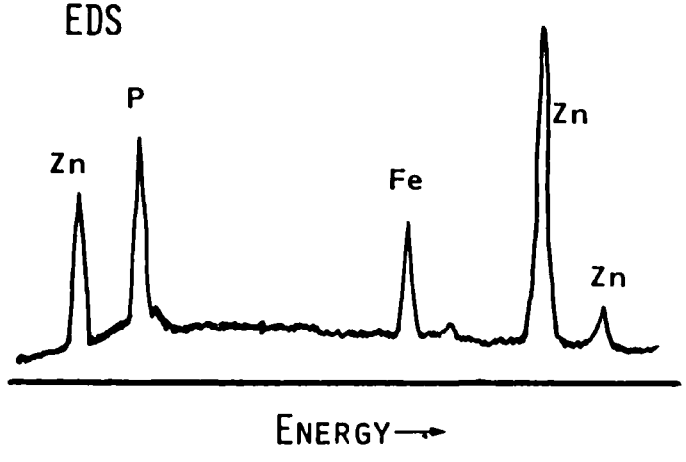

Figure 10. SEM micrograph and EDS spectrum of zinc phosphated steel exposed to 0.1M LiOH solution for four days.

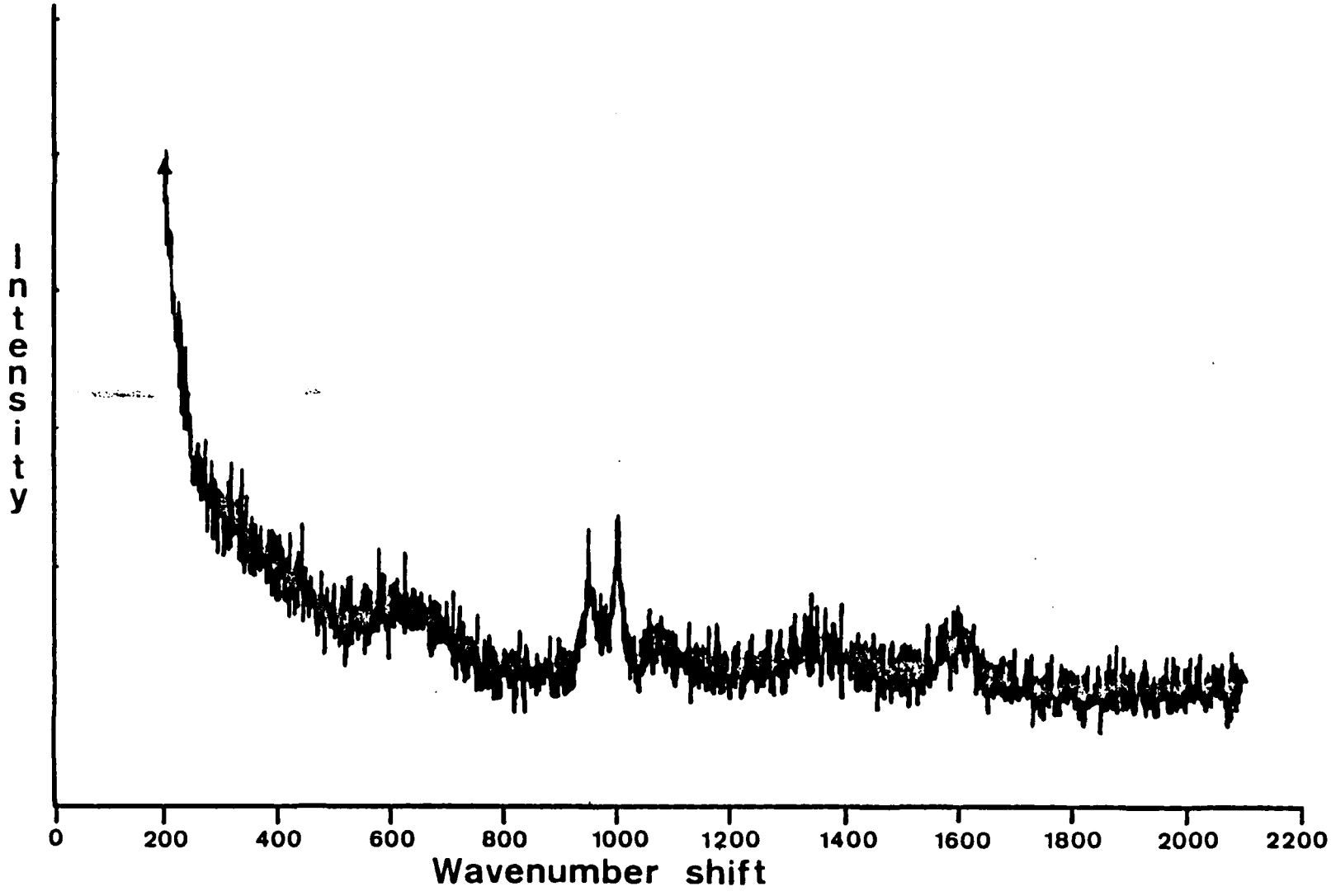

Figure 11. Raman spectrum obtained from zinc phosphated steel exposed to 0.1M LiOH solution for four days.

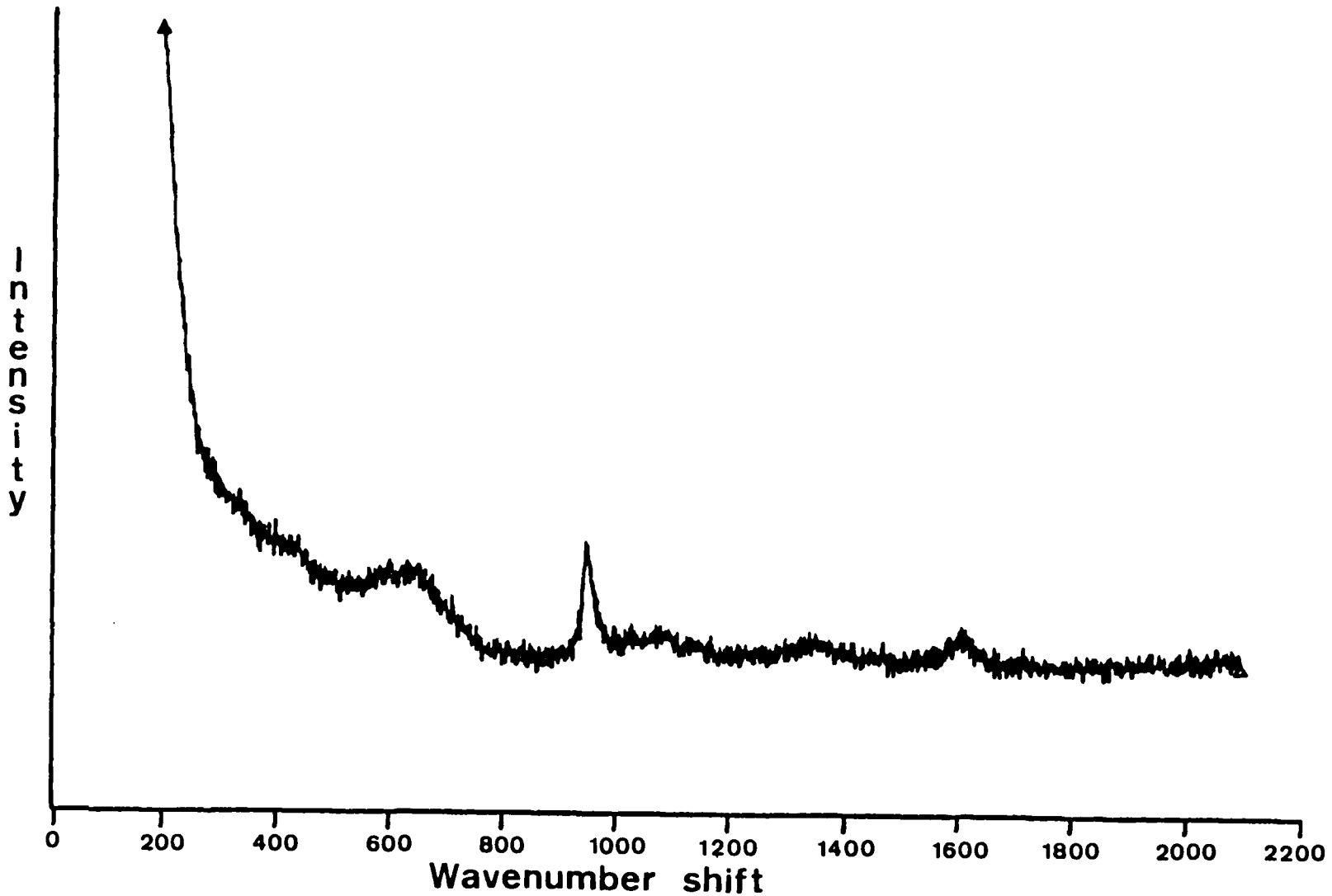

Figure 12. Raman spectrum obtained from zinc phosphated steel exposed to 0.1M LiOH solution for four days.

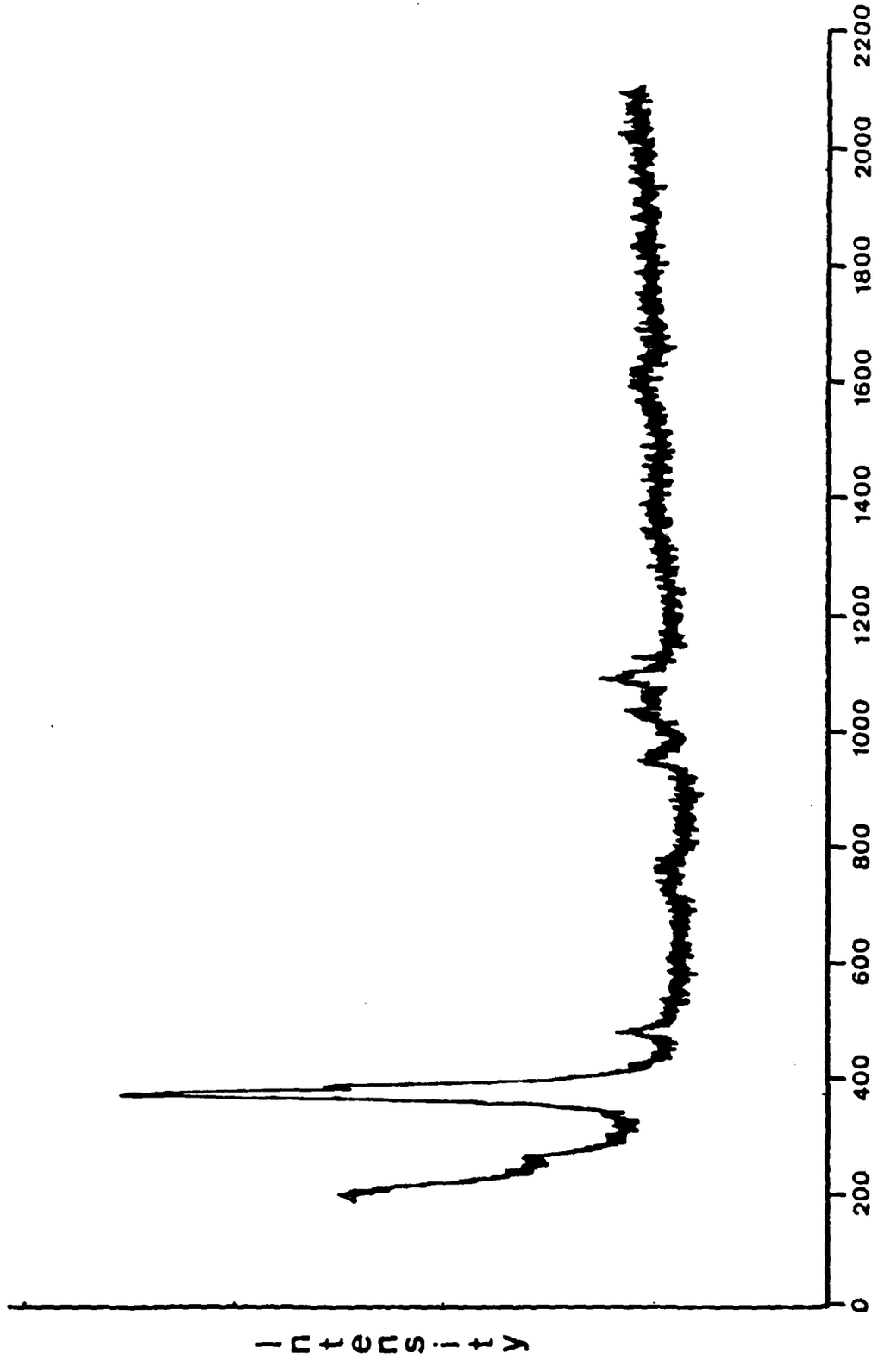

Figure 13. Raman spectrum obtained from zinc phosphated steel exposed to 0.1M LiOH solution for four days.

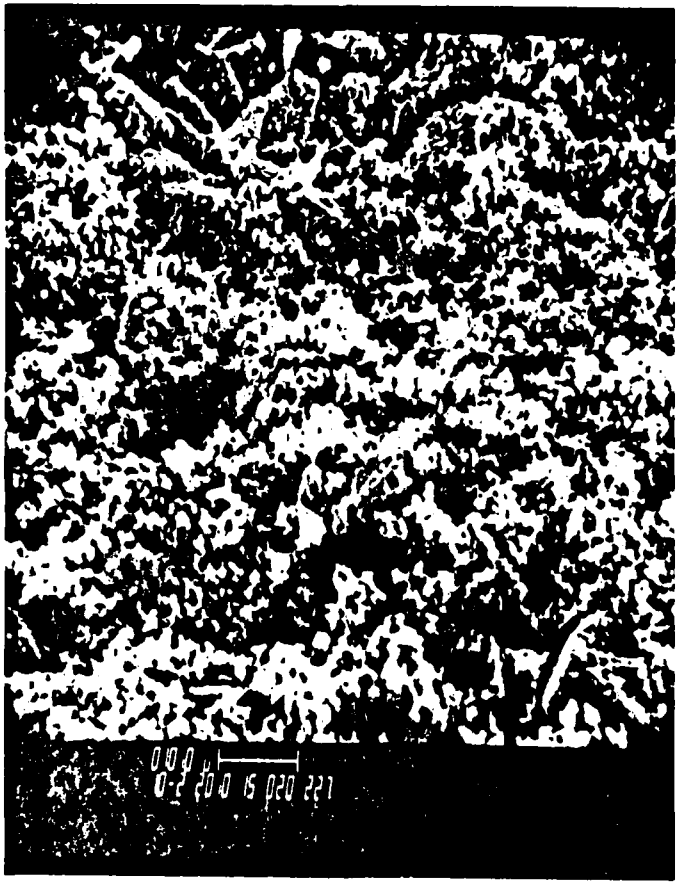

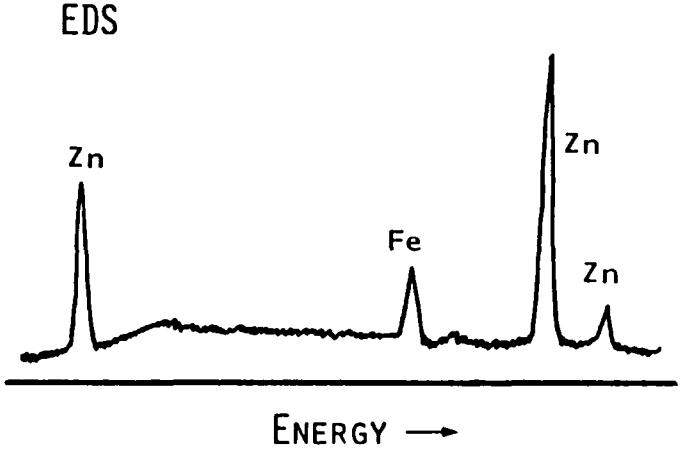

Figure 14. SEM micrograph and EDS spectrum of zinc phosphated steel exposed to 0.1M NaOH solution for four days.

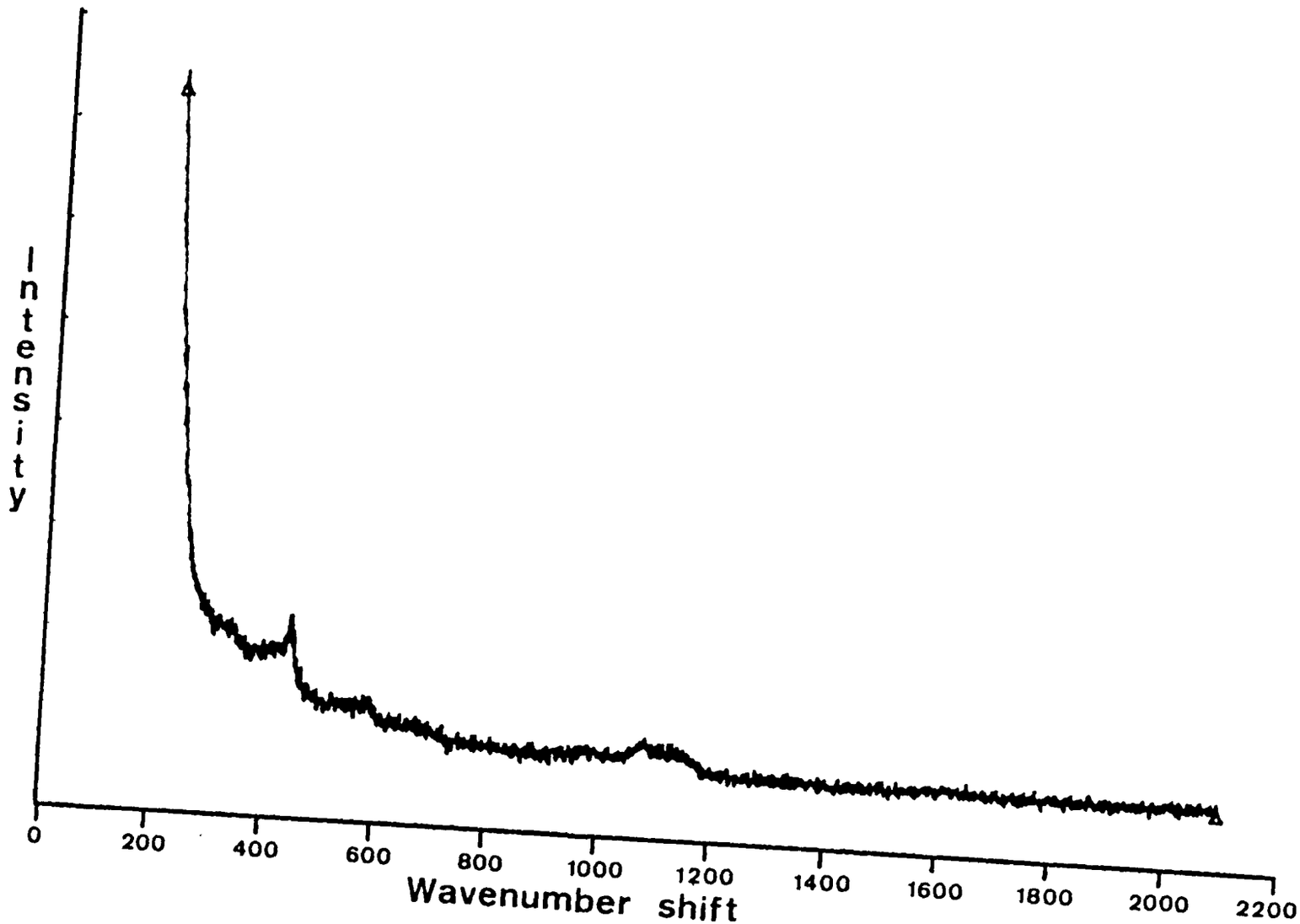

Figure 15. Raman spectrum obtained from zinc phosphated steel exposed to 0.1M NaOH solution for four days.

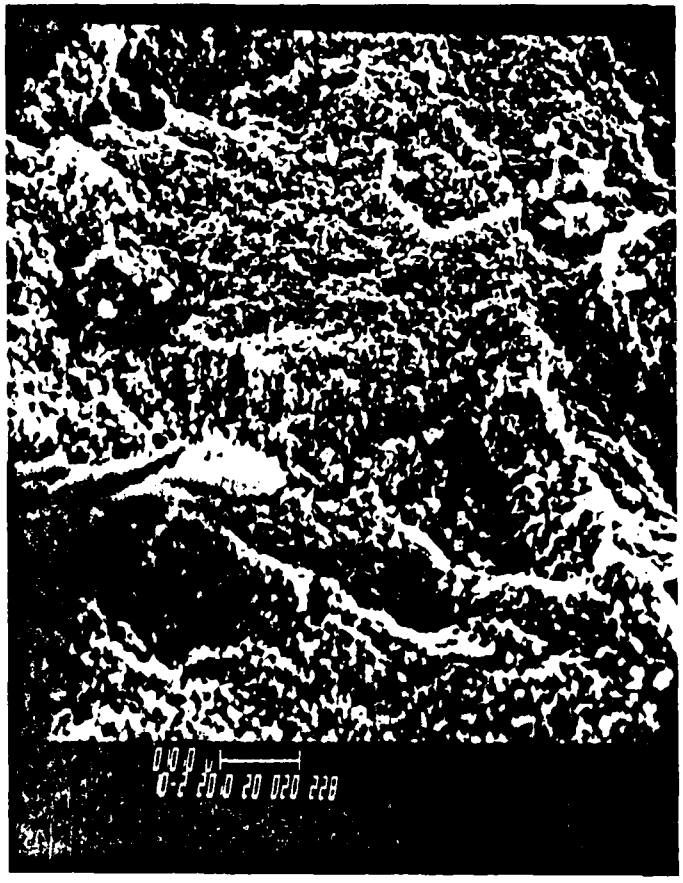

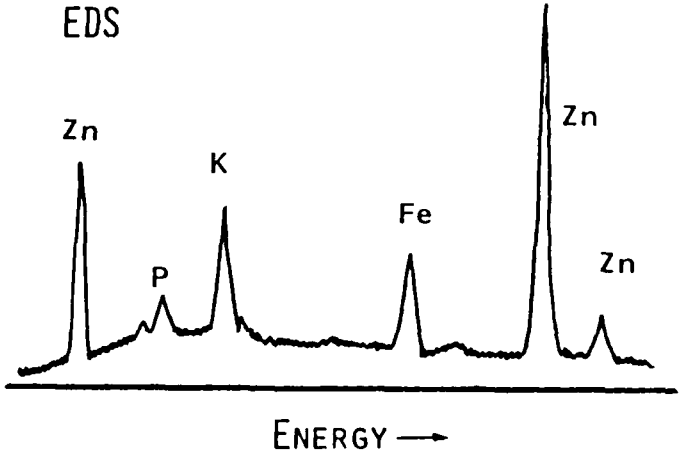

Figure 16. SEM micrograph and EDS spectrum of zinc phosphated steel exposed to 0.1M KOH solution for four days.

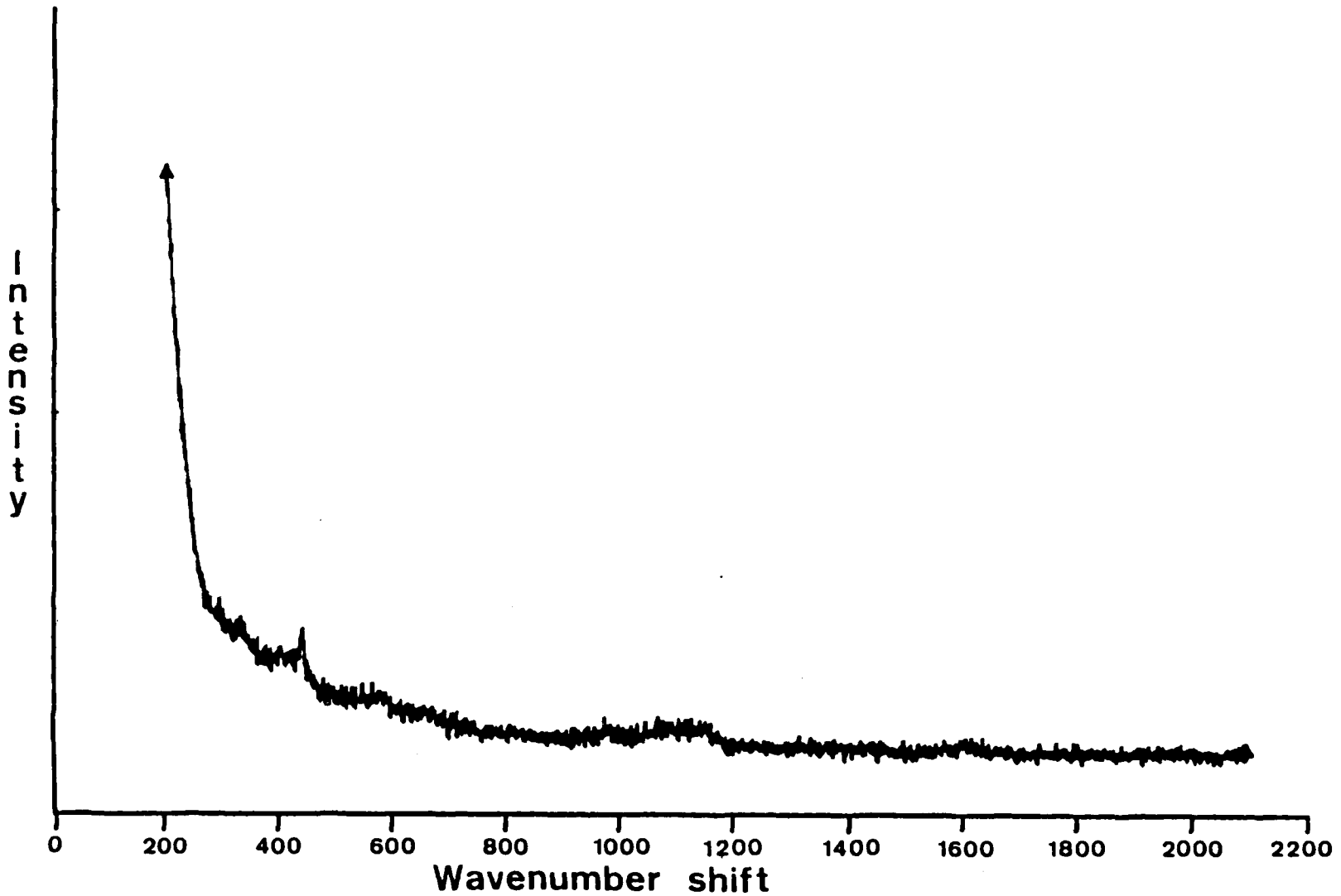

Figure 17. Raman spectrum obtained from zinc phosphated steel exposed to 0.1M KOH solution for four days.

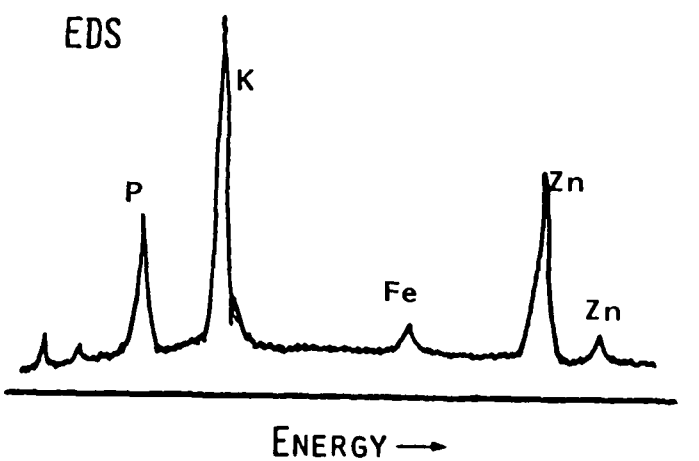

Figure 18. SEM micrograph and EDS spectrum of cubic crystallites in zinc phosphated steel after exposure to 0.1M KOH solution for four days.

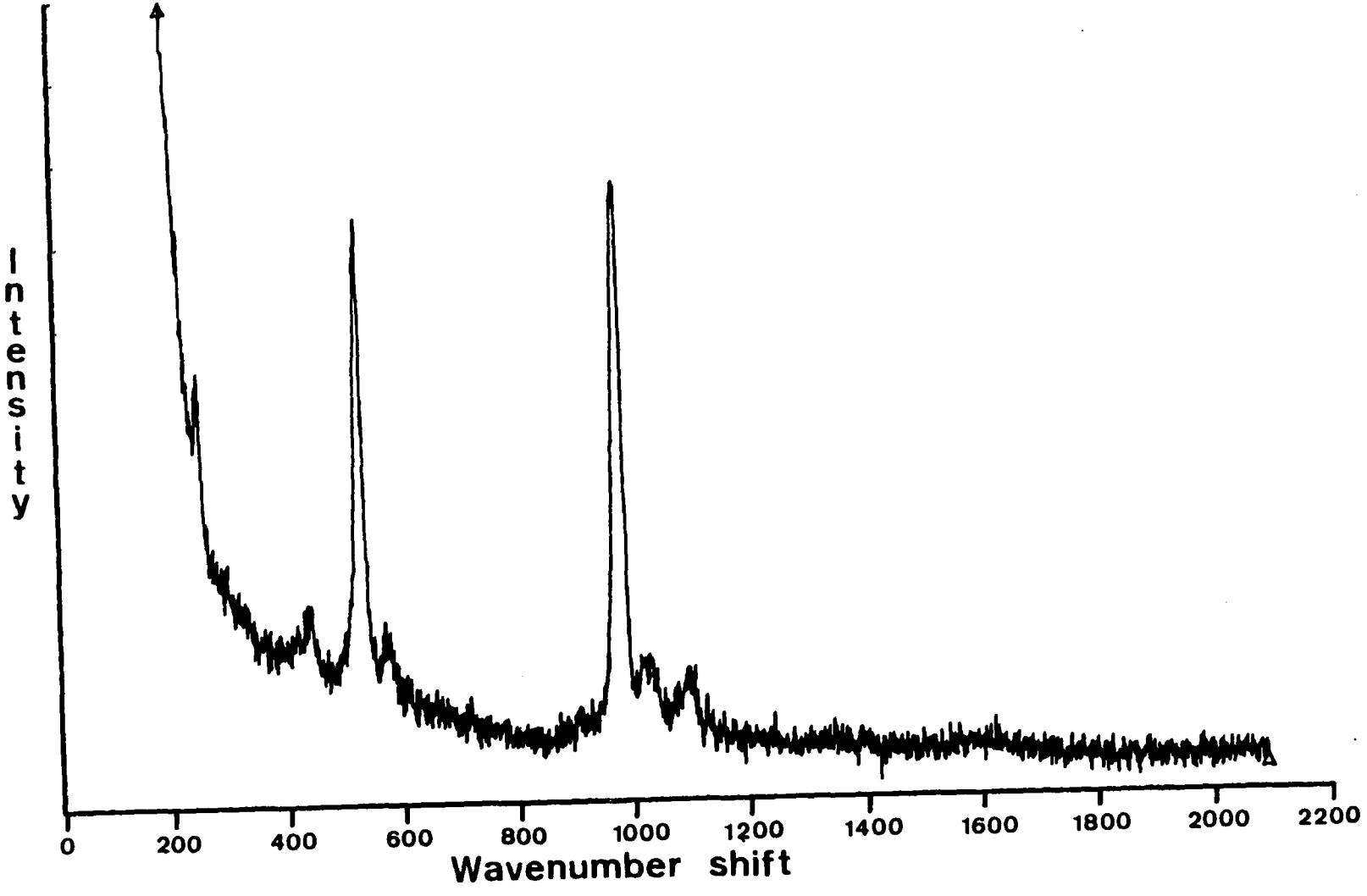

Figure 19. Raman spectrum of cubic phase shown in Figure 18.

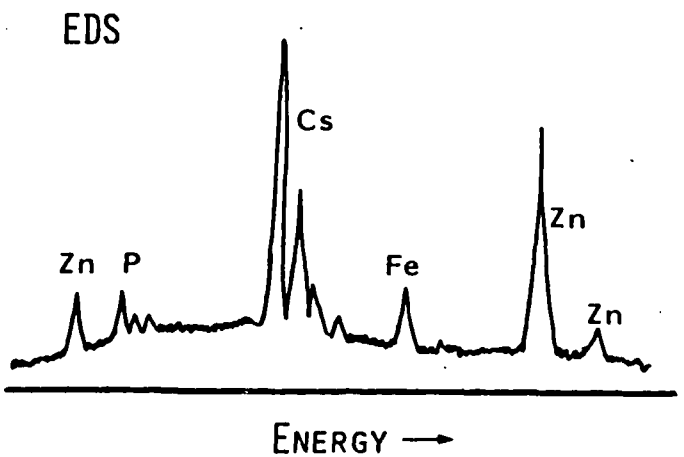

Figure 20. SEM micrograph and EDS spectrum of zinc phosphated steel exposed to 0.1M CsOH solution for four days.

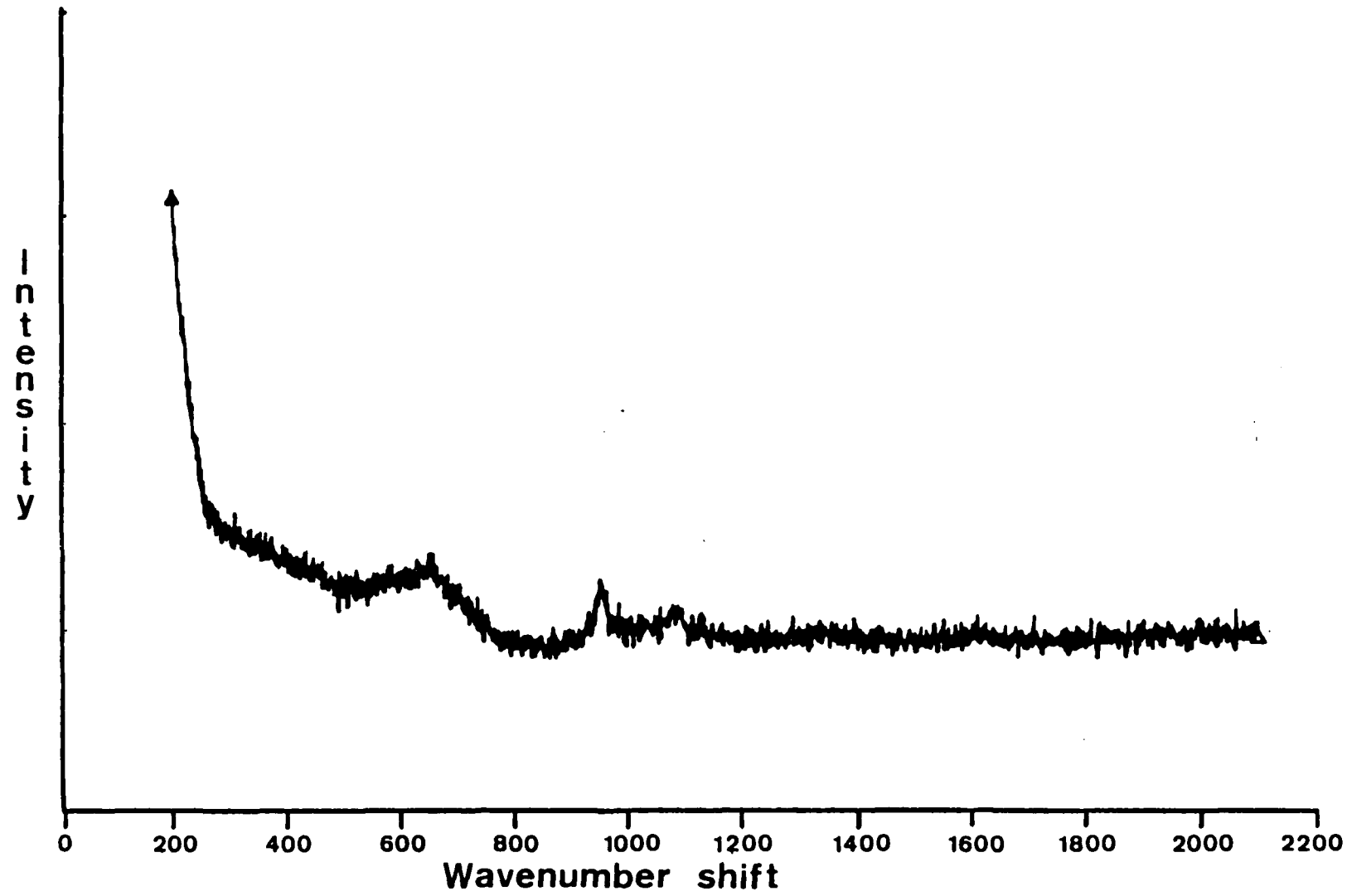

Figure 21. Raman spectrum obtained from zinc phosphated steel exposed to 0.1M CsOH solution for four days.

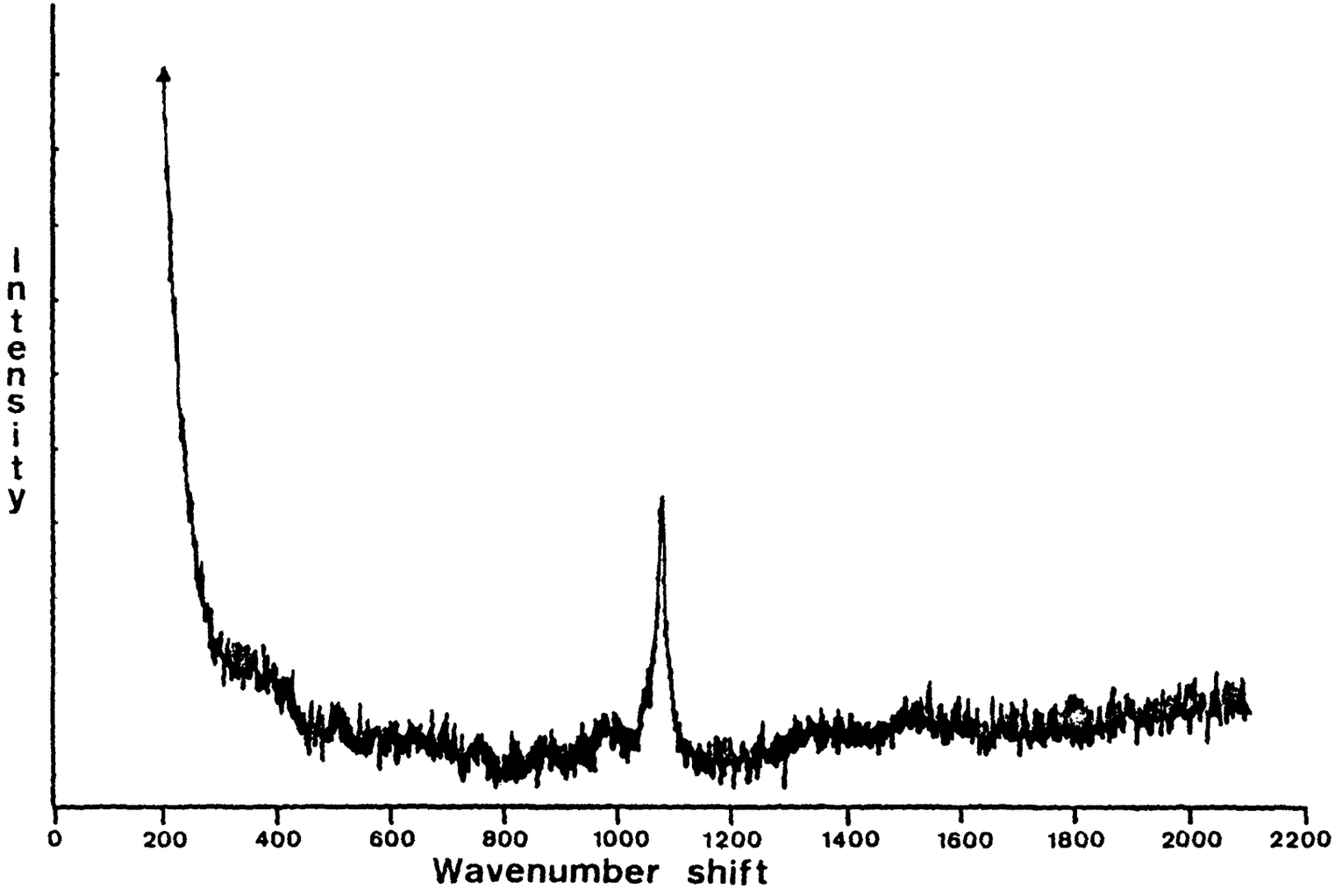

Figure 22. Raman spectrum obtained from zinc phosphated steel exposed to 0.1M CsOH solution for four days.

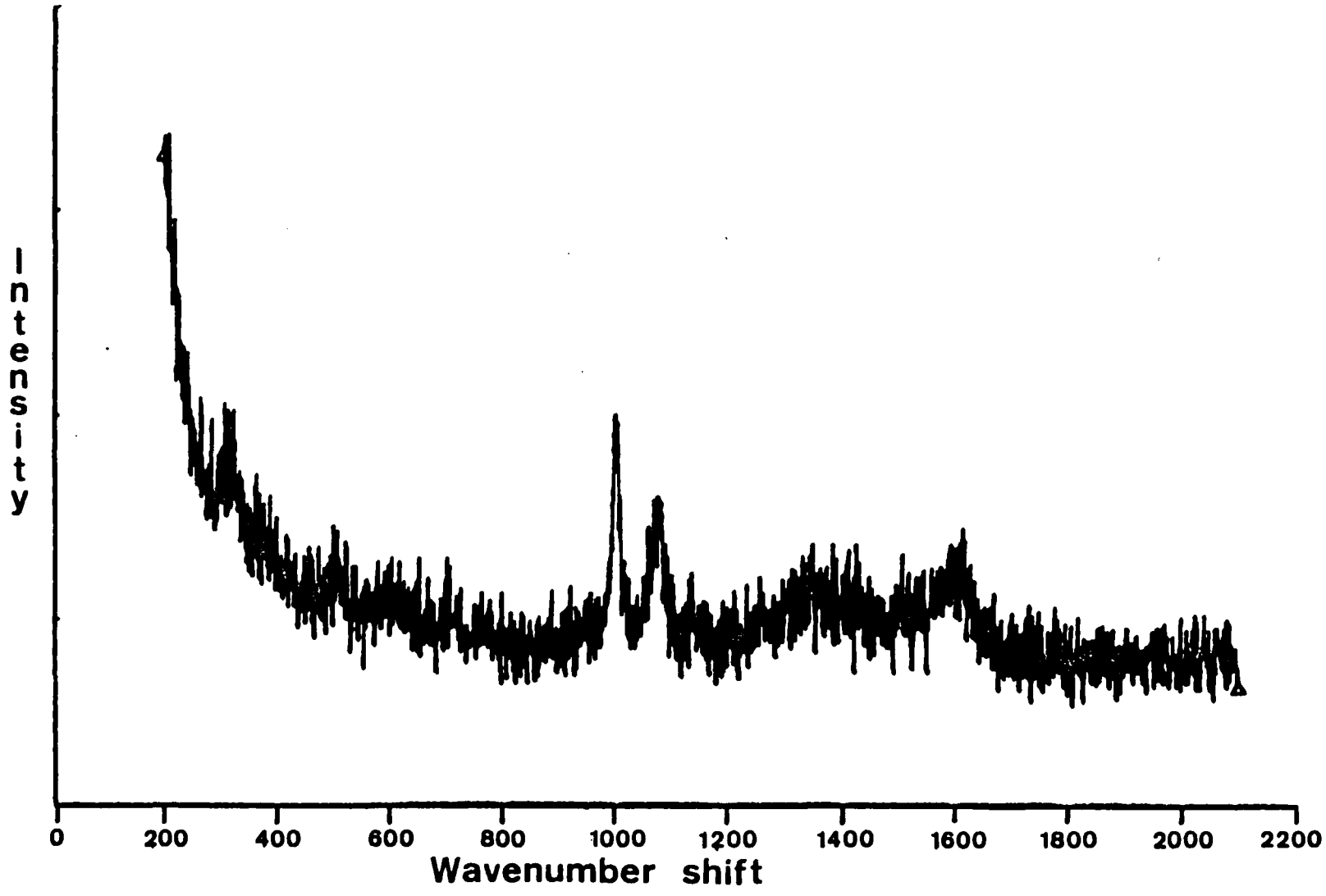

Figure 23. Raman spectrum obtained from zinc phosphated steel exposed to 0.1M CsOH solution for four days.

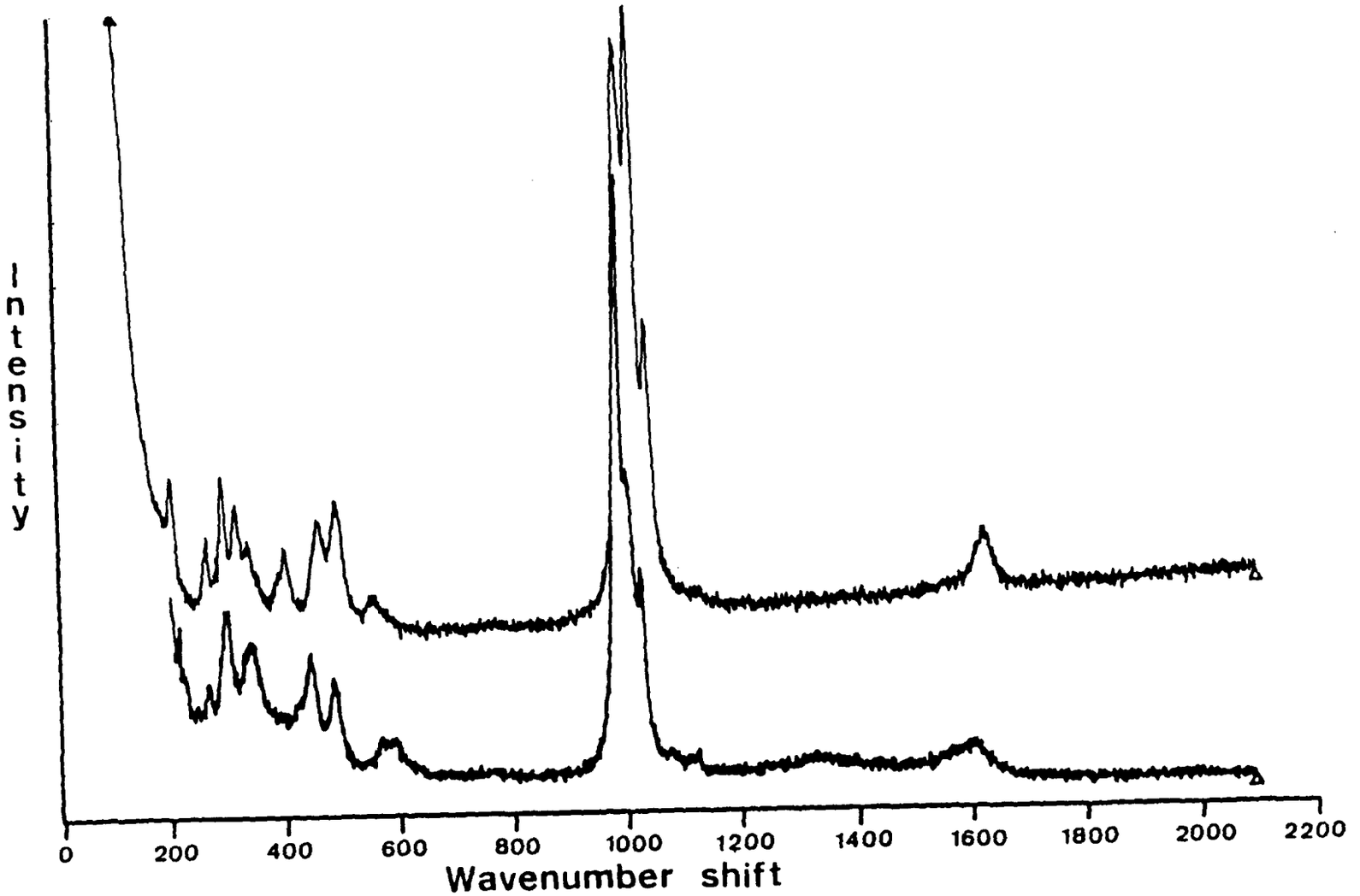

Figure 24. Raman spectrum obtained from zinc phosphated steel exposed to 0.1M CsOH solution for four days.

on the remaining normal phosphate crystals. Bands located at 995 cm^{-1} shift and 1063 cm^{-1} shift are characteristic of normal zinc phosphate tetrahydrate (hopeite) and hydrozincite, respectively. Small square crystallites in the coating produced the Raman spectrum shown in Figure 24. These crystallites were identified as iron phosphate ($FePO_4 \cdot 2H_2O$) from the bands located around 1000 cm^{-1} shift and those bands occurring in the low wavenumber shift region.

To summarize, the samples exposed to the different hydroxide solutions showed the greatest rate of dissolution for phosphated steel exposed to NaOH followed by KOH, CsOH and LiOH. Phosphate ion was selectively removed from the coating in each case except for LiOH. The samples exposed for four days indicated that the types of corrosion products varied as the cation of the alkali solution was changed. Samples treated with NaOH were found to have formed a zincate type film on the phosphate coating surface. The KOH treated samples also formed a zincate on the surface along with a modified phosphate of potassium and zinc. Vivianite $Fe_3(PO_4)_2 \cdot 8H_2O$ was found to have formed for samples treated with LiOH and CsOH. The samples treated with LiOH were also found to contain an iron zincate and small amounts of hydrozincite. Other corrosion products found in the samples treated with CsOH included hydrozincite and iron phosphate of the form $FePO_4 \cdot 2H_2O$.

CONCLUSIONS

The results of the long term exposure of zinc phosphated steel to alkaline environments with different cations show that the chemistry of the phosphate dissolution is greatly affected by changing the cation of the exposure solution. Sodium hydroxide probably dissolves the zinc phosphate coating to greater extent because the ions, once in solution, remain there. In contrast, the other ions form precipitates as evidenced by the different number of molecularly distinct phases in the phosphate coating after exposure. The sample exposed to potassium hydroxide formed two distinct phases that were identified. The samples exposed to lithium and cesium hydroxides formed three and four distinct phases, respectively. The effect of the cations on the dissolution of zinc phosphate could not be explained on the basis of the physical properties of the alkali metals (i.e., hydrated radii, ionic mobilities).

REFERENCES

[1] H. Leidheiser, Jr., and W. Wang, "Corrosion Control by Organic Coatings," H. Leidheiser, Jr., Editor, NACE, Houston, Texas, p.70 (1981).

[2] A. F. Trotman-Dickenson, Editor, "Comprehensive Inorganic Chemistry," Pergamon Press, Oxford, Vol. 1, p.352 (1973).

[3] Ibid., Vol. 2, p.490 (1973).

Program #7

Parallel DC Resistance Measurements on Thin Film Substrates as a Technique for Studying the Metal/Coating Interface

Principal Investigator: Jack F. McIntyre
Research Associate

Associate: Henry Leidheiser, Jr.
Prof. of Chemistry

ABSTRACT

A variation of a four-point probe method was used to study the change in the parallel DC resistance of thin iron and nickel metal films covered with an organic coating and exposed to water and NaCl. Optical observations of the initiation and propagation of corrosion from the substrate side were correlated with changes in the metal film resistance. AC impedance data were obtained for several of the test samples and those results were compared to results obtained using the DC resistance technique. The DC parallel resistance was successfully used to detect the effects of water after migration to the coating/metal interface. The AC impedance measurements and the DC parallel resistance measurements provide complementary information. The former provides information about the electrical properties of the coating and the latter provides information about the electrical properties of the metal substrate.

INTRODUCTION

Organic coatings as applied to metals act as physical barriers to protect metal structures from the environment. The failure modes of a coated metal can be a result of many differnnt types of interfacial attack. Test methods have been developed to assist in the selection and testing of prospective coating systems based on the expected mode of failure. An effective technique

must be able to detect the initiation of interfacial breakdown; however, the many inherent difficulties associated with predicting these changes often prevent reliable and accurate assessment of a coating's useful lifetime.

Among the many techniques available to test the suitability of a coating is a group of methods that rely on visual assessments which, in most cases, require long exposure times. These methods include: salt spray exposure, atmospheric exposure, and exposure to high humidity. On the other hand, electrical and electrochemical techniques, designed to provide quantitative data and information in short times to predict the protective capacity of a coating, have been used with moderate success. The use of AC impedance to study the degradation of coated metals has been made popular by Touhsaent and Leidheiser (1972), Piens and Verbist (1981), Epelboin et al. (1981), Scantlebury and Sussex (1981), Callow and Scantlebury (1981a), (1981b), and (1981c), Strivens and Taylor (1982), Mansfeld et al. (1982), and Hubrecht et al. (1984). The DC resistance of polymer films has been investigated by Bacon et al. (1948), Wormwell and Brasher (1950), Rothwell (1969), Mayne and Scantlebury (1970), and Mayne and Mills (1975). An electrical technique is described herein which provides information about the early stages of underfilm attack and which complements the AC impedance and DC film resistance measurements.

A variation of a four-point probe method was used in this study to follow the change in the parallel DC resistance of coated thin metal films on glass substrates during exposure to aqueous solutions. Optical observations of the initiation and propagation of corrosion from the glass side were correlated with changes in the metal film resistance. In addition, AC impedance data were obtained for several samples and those results were compared to results obtained using the DC resistance technique.

The object of this research was to determine whether the parallel DC resistance technique could detect the presence and consequences of water at the coating/metal interface before visible corrosion could be detected. Results reported herein will be limited to demonstrating the effectiveness of the method. A later paper will describe the application to the method to studies of cathodic delamination.

EXPERIMENTAL

Samples

Sample preparation involved the vapor deposition of pure iron or nickel onto clean glass slides. Metals of 99.99% purity in the form of wires were obtained from Alpha Products. A Denton Vapor Deposition Instrument, model DV-520, was used to deposit the metal of interest at approximately $10^{-5} - 10^{-6}$ torr, using resistive heating. The thin metal films were typically of the order of 400 Å in thickness. Subsequently, four lead wires, #32-7/40, were attached to the metal film using low resistance contact cement obtained from the Ernest Fullam Co.

Coatings

Polymeric materials were applied to the metal films using a spin-coater. Polybutadiene coatings were cured at 195°C for 30 minutes in an air-forced oven. Commercial alkyd primer and commercial alkyd systems were cured at room temperature for seven days. Coaing thicknesses ranged from approximately 9 μm to 17 μm. All samples were stored in desiccators prior to testing, at which time samples were mounted in polyethylene cells and sealed with a commercial silicone caulking.

DC Resistance

The basic experimental setup can be seen in Figure 1 for the measurement of the parallel DC resistance of the thin metal films. A DC current is applied to the coated metal film using a variable DC source. A Keithley electrometer, model 600A, is used to measure the potential drop across the test area and a Beckman, Tech 300, multimeter is used to measure the applied current. Ohm's law is then used to calculate the metal film resistance.

AC Impedance

A Princeton Applied Research, model 368, AC Impedance system, interfaced to an Apple IIe computer was used to make all AC measurements. A block diagram of the instrumentation can be seen in Figure 2. High frequency measurements, typically 1-20 kHz, are obtained using the lock-in amplifier, M-5260, which uses analog electronics to measure the amplitude of an AC signal, given a particular phase characteristic and frequency. The total cell response signal at a given frequency is sent to the lock-in amplifier where it is resolved into its real and imaginary components. This information is then transmitted by the lock-in system to the computer for digitization, manipulation and display. Low-frequency measurements, .01-2.0 Hz, are obtained in the Fast Fourier Transform (FFT) mode using a 10 mV amplitude pulse-excitation comprised of the low frequencies of interest. The pulse is applied to the test sample via the potentiostat, M173, and interface module, M276; the interface also functions as the response measurement device. The complex response is obtained and an inverse FFT operation is performed on this waveform to resolve it into discrete frequency data. Data collected using the lock-in amplifier and the FFT application can be displayed individually or the data can be merged and displayed collectively over the entire sampling window.

RESULTS AND DISCUSSION

Results typical of samples which exhibited no deterioration or interfacial attack and those which showed signs of significant corrosion or adhesion loss can be seen in Figure 3. Here a plot is made of change in resistance, ΔR, that is, the initial resistance, R_o, minus the resistance at time t, R_t, versus the time of exposure. Depicted in this graph are results obtained for

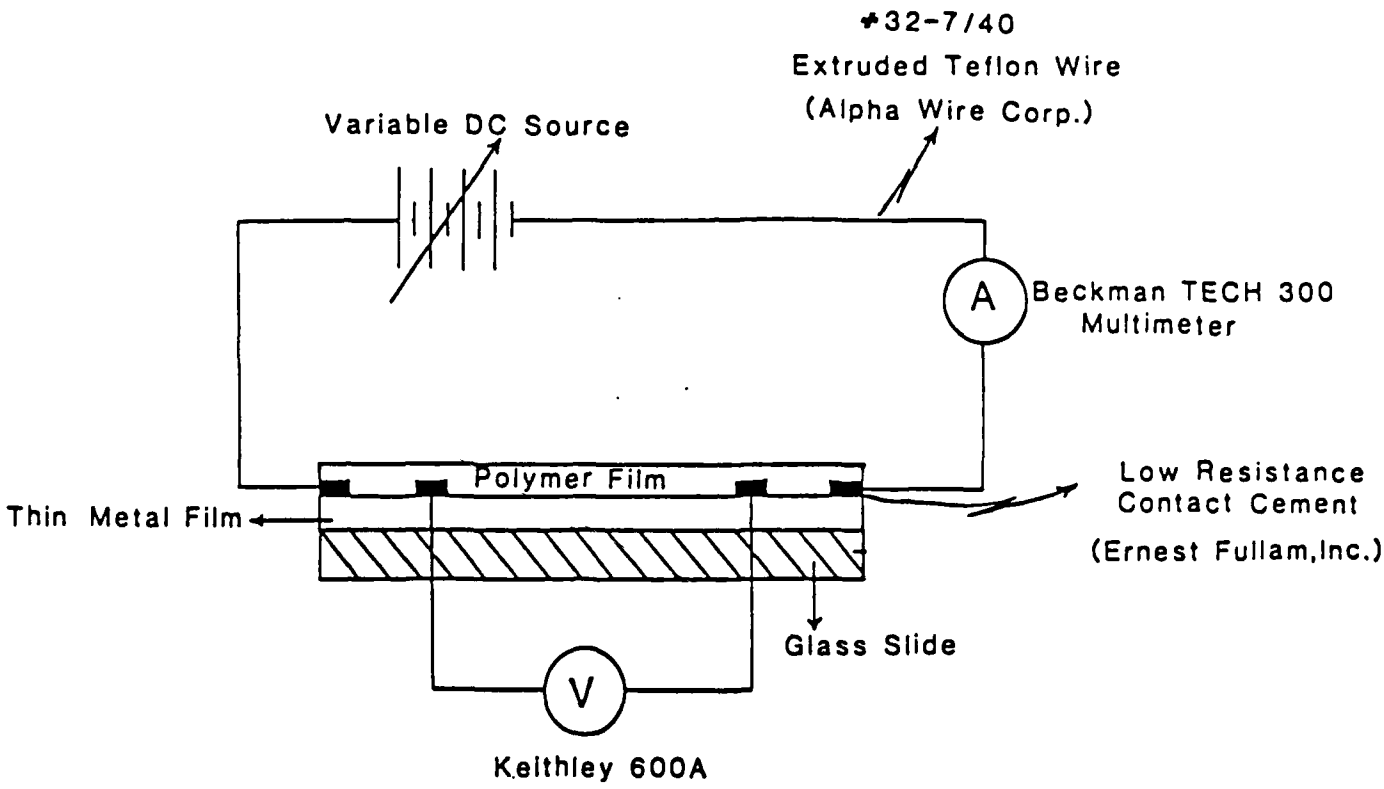

Figure 1. Experimental setup for measurement of the parallel DC resistance of coated thin metal films.

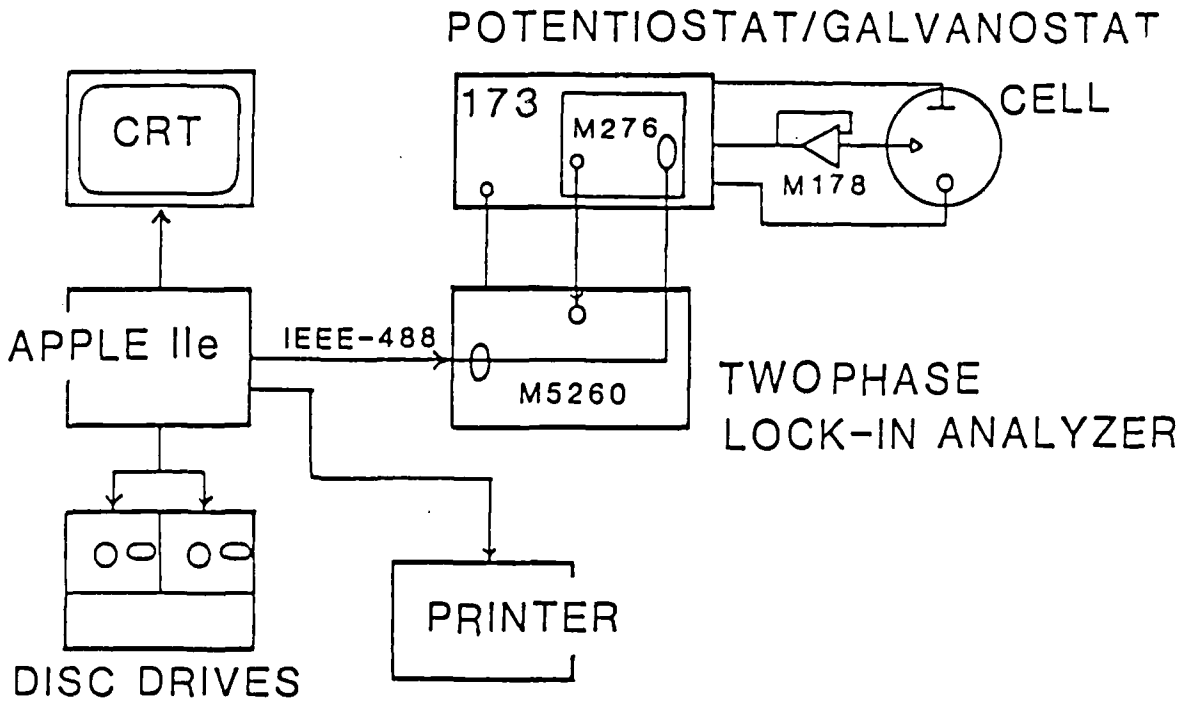

Figure 2. Block diagram of the AC impedance measurement system.

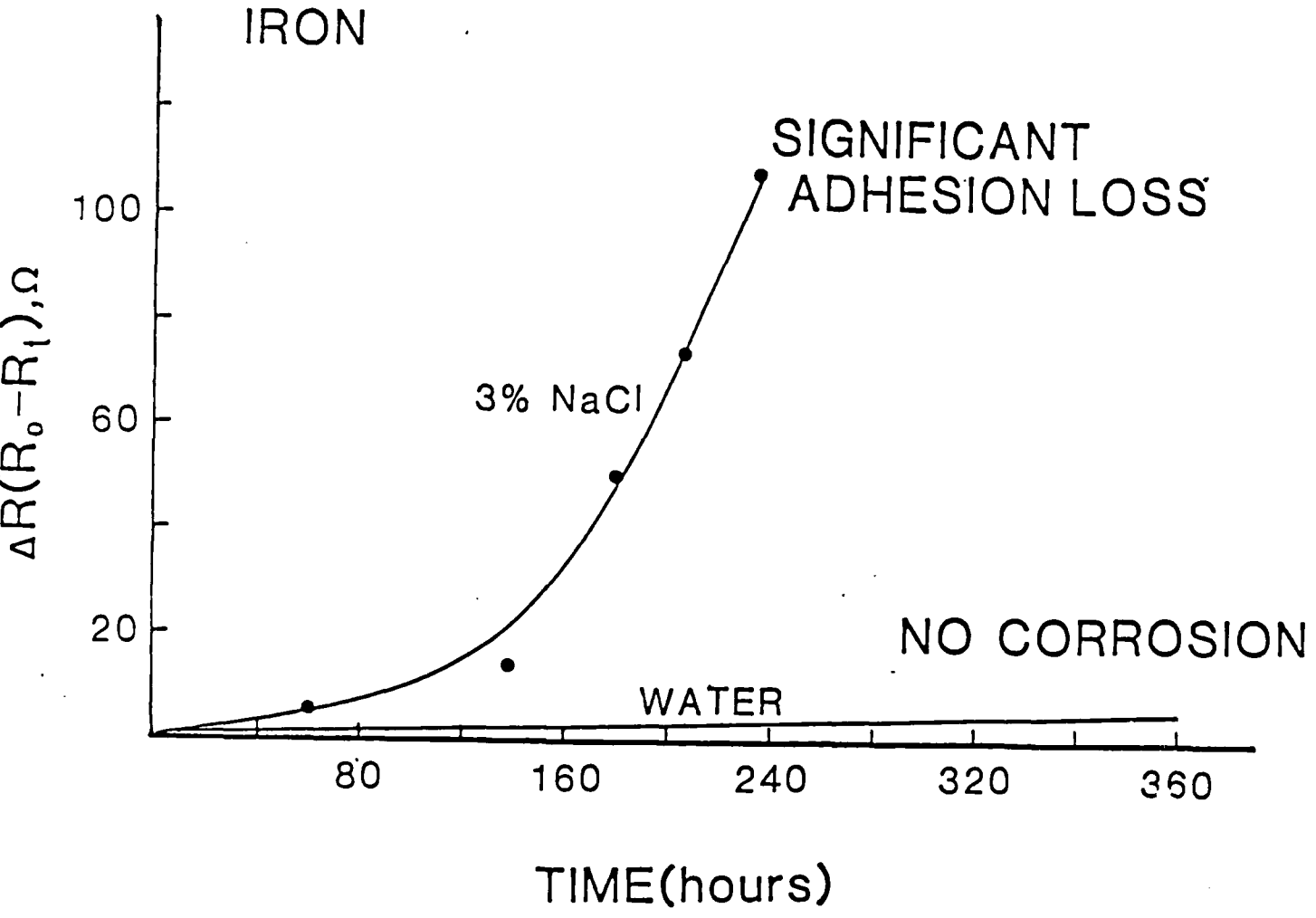

Figure 3. Plot of change in parallel DC resistance against time of exposure to water or 3% NaCl for two iron samples with 10 μm thick polybutadiene coatings.

an iron film coated with a commercial primer exposed to 3% NaCl and water. For the sample exposed to water, the change in DC resistance remained small during the test period and this behavior was characteristic for intact coating systems. However, a large change in resistance was obtained for systems which exhibited significant underfilm attack; this behavior was obtained for the sample exposed to 3% NaCl. A photograph of this sample at 240 hrs, Figure 4, revealed that, indeed, significant corrosion had occurred over much of the specimen. Dark areas are regions of corrosion while light areas are unaffected regions of iron film.

An intentional defect was introduced into the coating of an iron-polybutadiene system and the coated metal was exposed to 3% NaCl. Results for this sample can be seen in Figure 5. A defect placed in a coating represents real situations where protective coatings are injured accidently. As a consequence, large changes in the DC resistance were obtained and the appearance of visible corrosion occurred in less than 40 hrs as indicated by the asterisk in the lower left of the graph. Generally, samples with large defects exhibited significant increases in DC resistance in shorter times than samples with no apparent defects. A photograph for this iron-polybutadiene system obtained at 350 hours, in an area removed from the defect, revealed interfacial attack similar to filiform corrosion, Figure 6. This corrosion pattern was typical for iron-polybutadiene systems.

A comparison between two iron-polybutadiene samples prepared at the same time under identical conditions and exposed to 3% NaCl can be seen in Figure 7. Again, the sample with the intentionally placed defect gave larger changes in the DC resistance. The important result shown here is that DC resistance began to increase prior to the identification of visible corrosion at 120 hours for the defect-free sample. Correspondingly, a small change in resistance was recorded for the defect sample at times before noticeable corrosion occurred, generally in areas adjacent to the defect.

The results already presented indicate that the measurement of the parallel DC resistance of coated thin metal films can be used to monitor changes at the interface. Next, it was decided to determine whether this technique could be used to observe differences among various aqueous environments. Results obtained for iron-alkyd and iron-polybutadiene systems can be seen in Figures 8 and 9. Both systems were exposed to water and 3% NaCl. Samples within each system were prepared together under identical conditions. Initially for both systems the DC resistance change was larger for the sample exposed to water; however, at later times, 190 hrs (Figure 8) and 240 hours (Figure 9), the NaCl environment began to exacerbate the corrosion process. These results support the idea that water uptake by coatings may be very rapid and show that water uptake is more rapid from pure water than from a salt solution. Results by others, most notably Brasher and Nurse (1959) and Kinsella and Mayne (1969) suggest that due to osmotic effects, water penetrates a coating more slowly in salt solutions and water uptake is generally faster in low concentration salt solutions. Our results suggest that water uptake is the precursor to coating failure and other ions found in the environment exert their influences at later times.

In addition to making DC resistance measurements, AC impedance data were obtained to determine if the two techniques would indicate changes at the

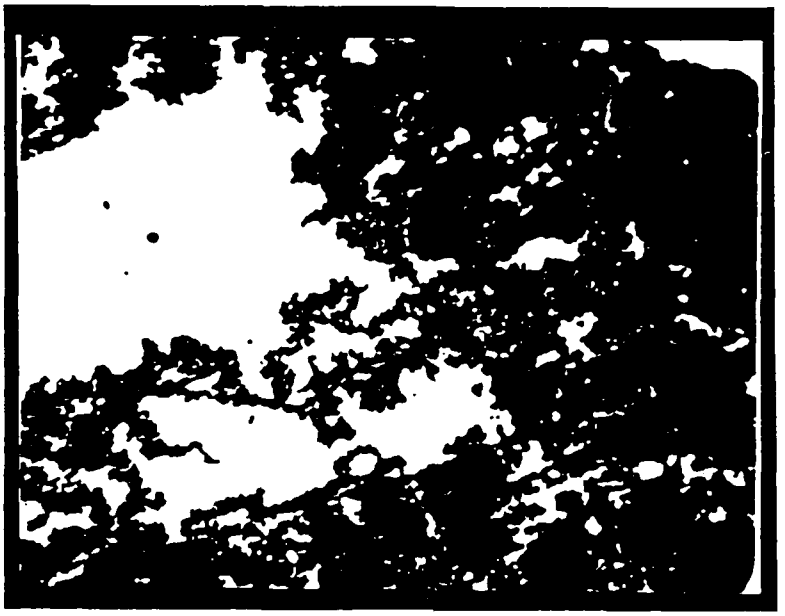

Figure 4. Photograph (10X) of an iron sample coated with a commercial primer and exposed to 3% NaCl for 240 hours.

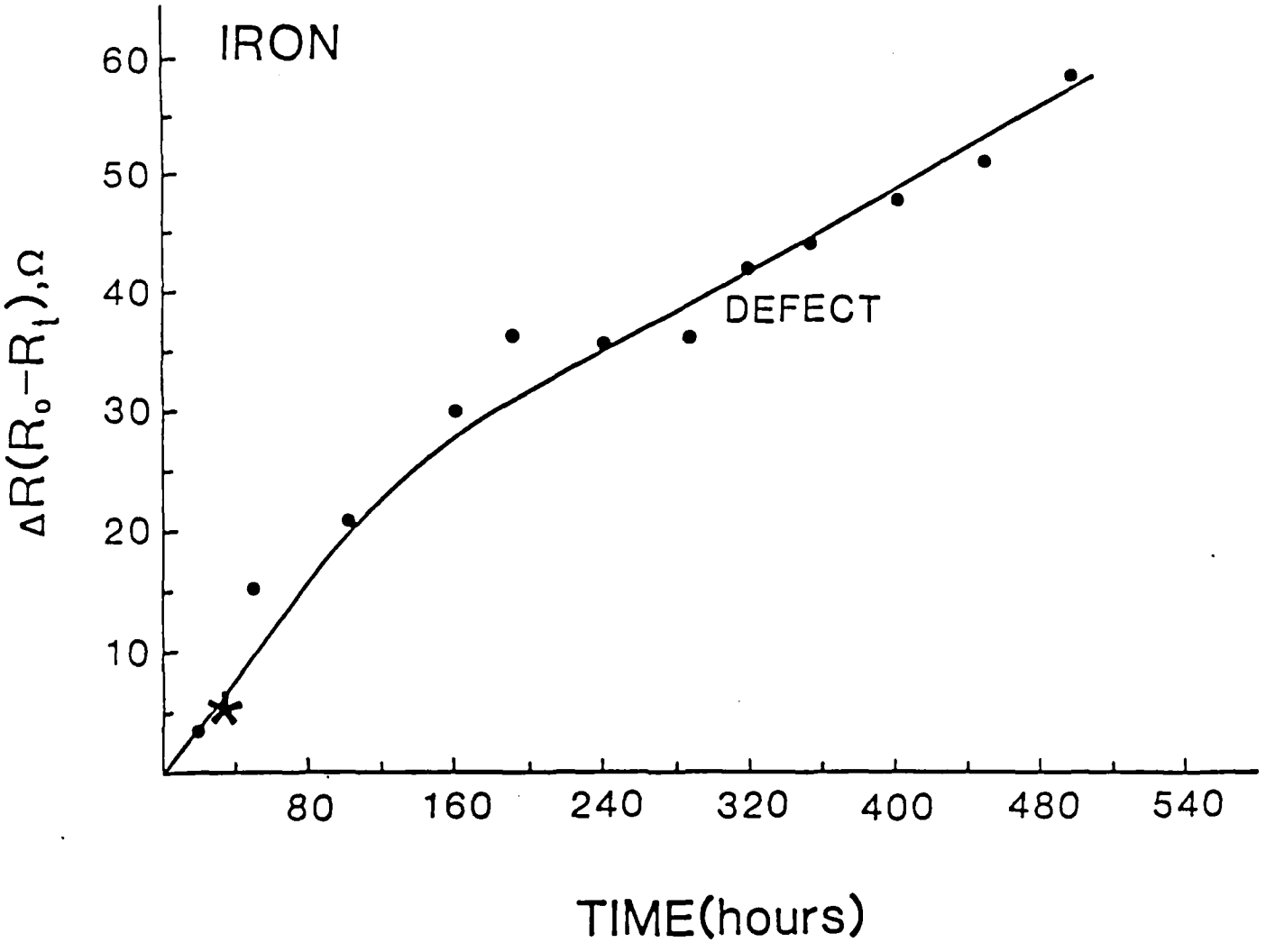

Figure 5. Plot of change in parallel DC resistance against time of exposure to 3% NaCl for a 15 μm polybutadiene-coated-iron sample with an intentionally placed defect in the coating. Asterisk indicates time at which visible corrosion was first noted.

Figure 6. Photograph (10X) of a polybutadiene-coated-iron sample exposed to 3% NaCl for 350 hours. Interfacial attack is similar to that of filiform corrosion.

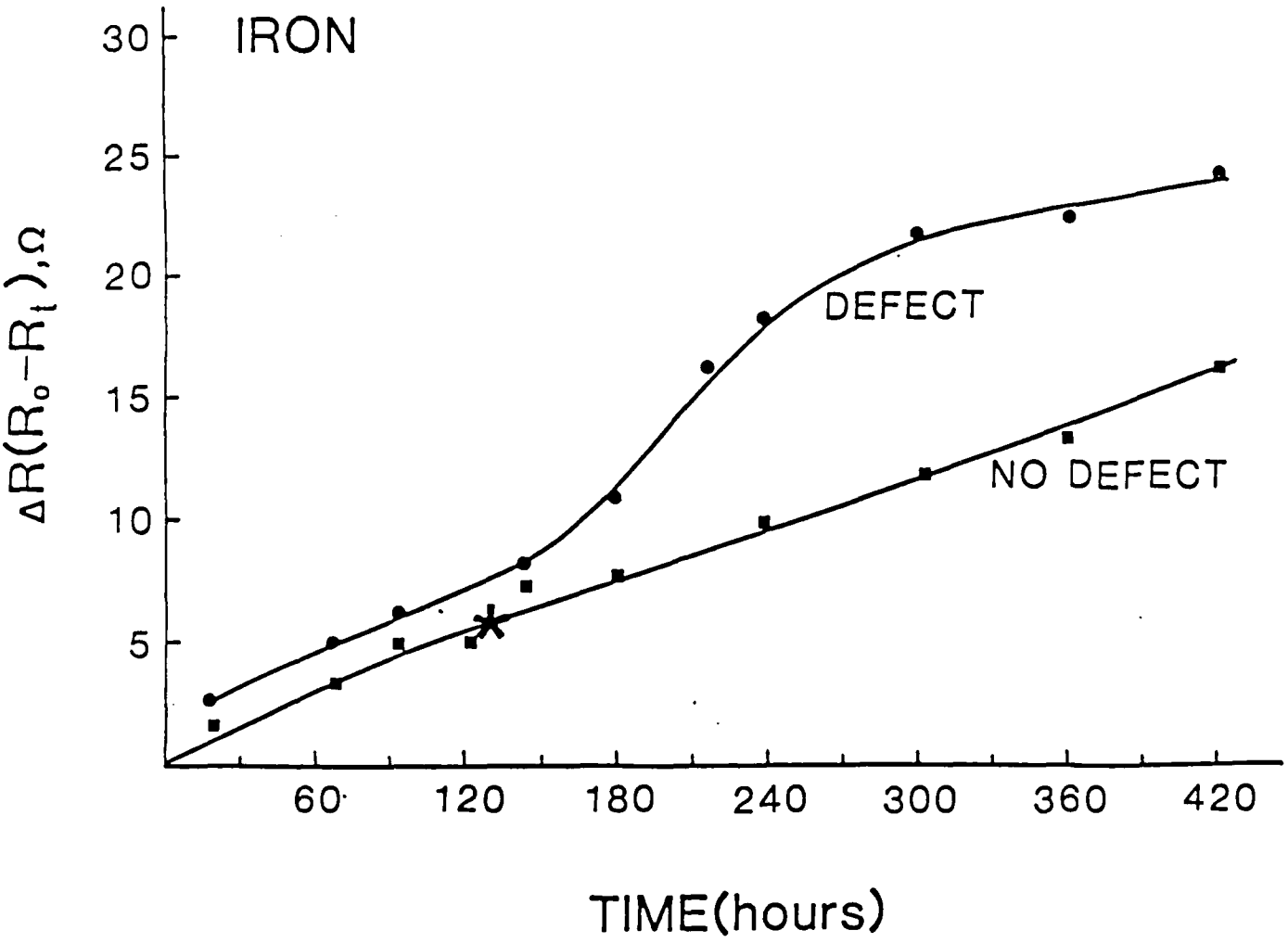

Figure 7. Plot of change in parallel DC resistance against time of exposure to 3% NaCl for defect-free and defect iron samples with 15 μm thick polybutadiene coatings. Asterisk indicates time at which visible corrosion was first noted.

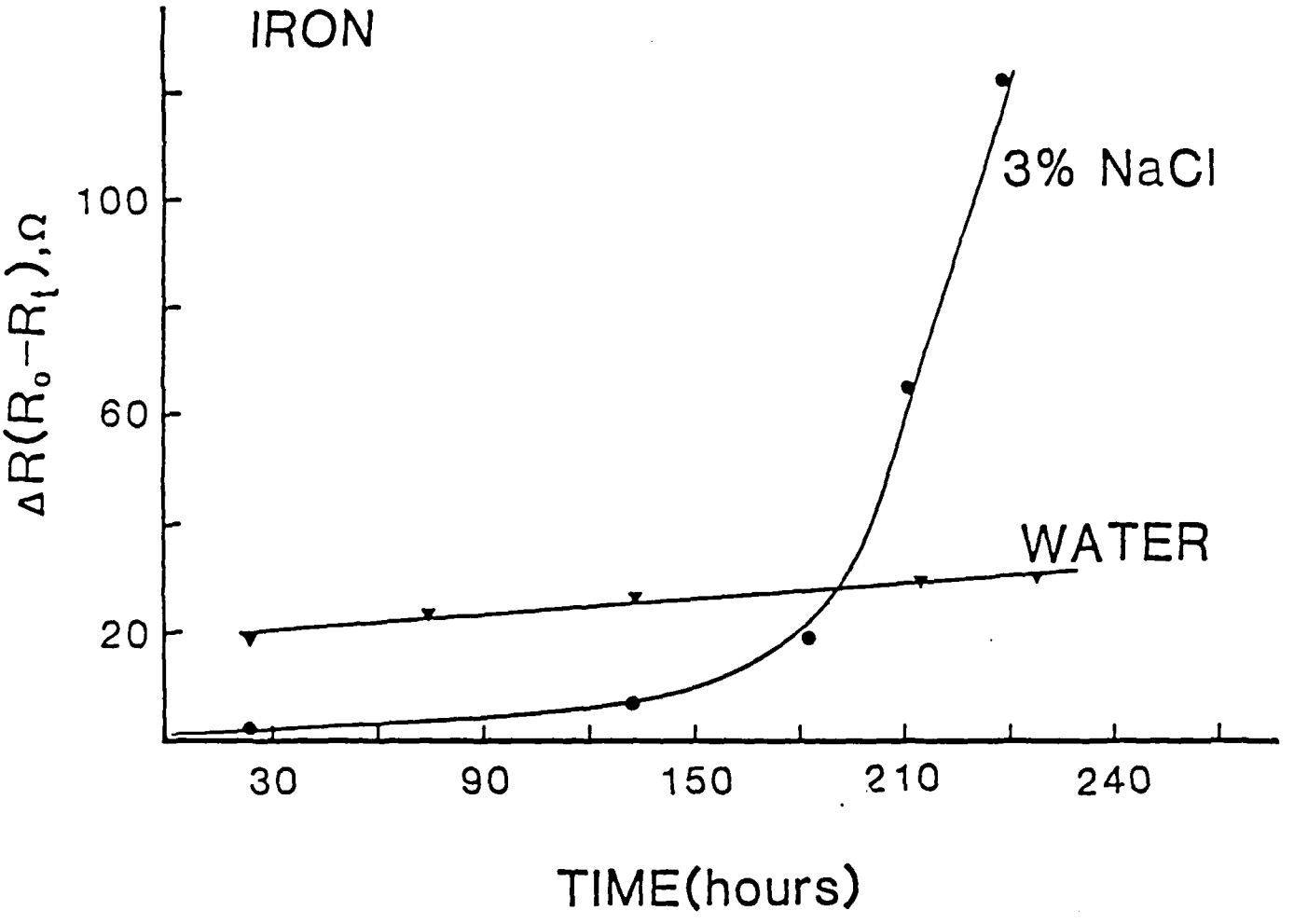

Figure 8. Plot of change in parallel DC resistance against time of exposure to water or 3% NaCl for two iron samples with 10 μm thick alkyd topcoat coatings.

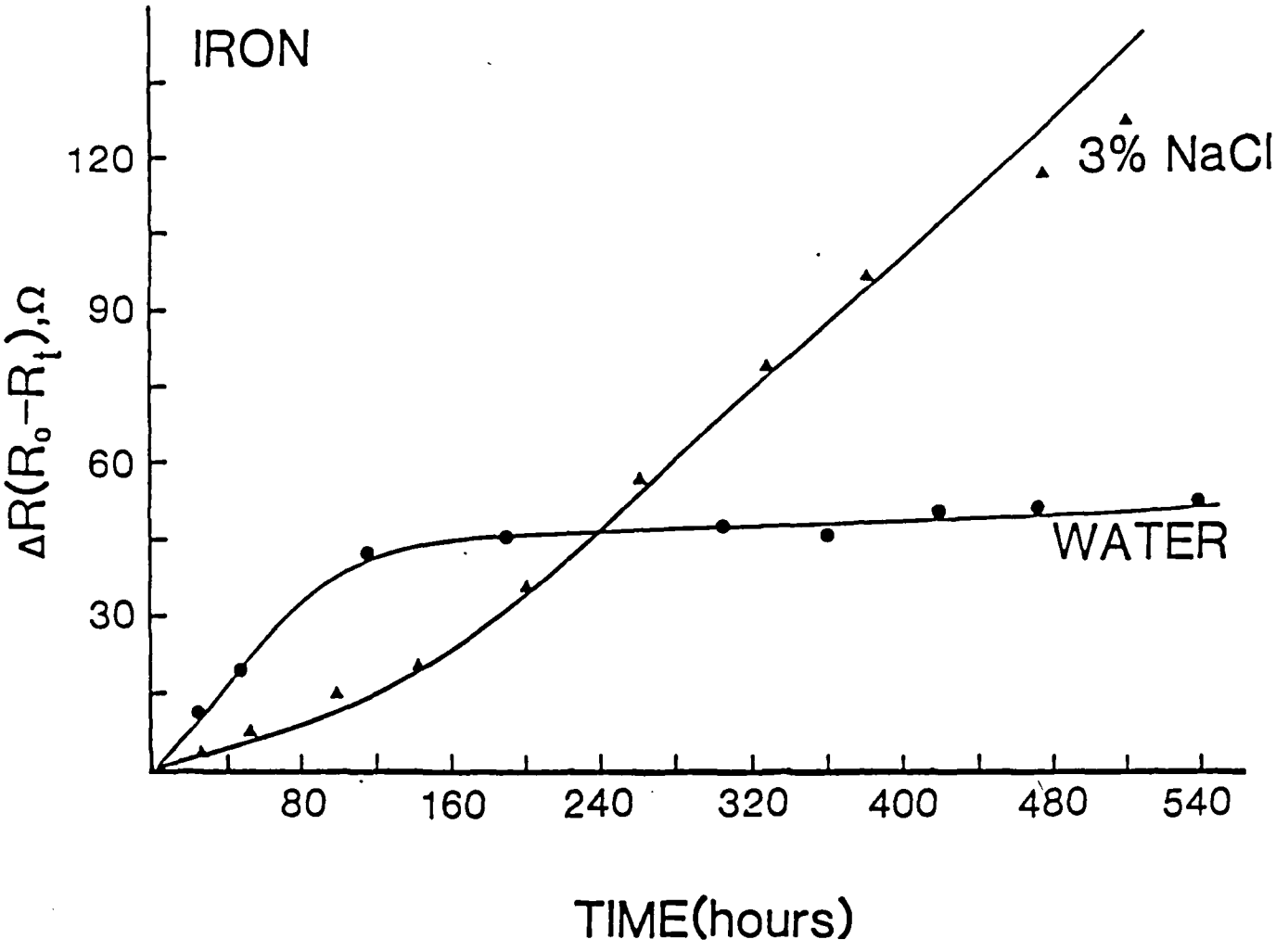

Figure 9. Plot of change in parallel DC resistance against time of exposure to water or 3% NaCl for two iron samples with 15 μm thick polybutadiene coatings.

interface within the same period of time. For a nickel-polybutadiene system after 420 hrs exposure to 3% NaCl pH = 11.4, a Bode plot, Figure 10, indicates that nearly pure capacitive behavior was obtained with a slope approaching -1. This result suggested that the coating was intact and affording adequate protection to the underlying metal. However, the parallel DC resistance results indicated otherwise. A plot of the change in DC resistance and capacitance is presented in Figure 11. These results revealed a significant increase in the DC resistance but a correspondingly small change in the capacitance. Generally it is accepted that an organic coating will pick up water and the capacitance of the coating will increase with time. Work by Wormwell and Brasher (1950), O'Brien (1966), and Leidheiser and Kendig (1976) have shown that indeed the capacitance of a coating increases with increasing time of exposure to aqueous environments. The AC impedance results suggested that the coating had not deteriorated and that the coating retained its high resistance. A photograph, Figure 12, of this nickel-polybutadiene sample at 420 hours revealed that some attack had occurred and, in addition, the presence of interference fringes implied a wet adhesion loss. Poor adhesion was indeed observed when an adhesive tape was applied to the coating and complete "pull-off" occurred.

A nickel-polybutadiene system exposed to 3% NaCl pH = 6.6, as seen in the Bode plot in Figure 13, exhibited capacitive behavior at high frequencies, which did not change with time, and resistance behavior at low frequencies. Presumably this system was behaving as an equivalent parallel capacitor and resistor, where the resistive component represented the ionic resistance of the coating. For this system, the ionic resistance was seen to decrease with time, an indication that more conductive pathways were developing through the coating. A plot of the change in parallel DC resistance versus time, as seen in Figure 14, indicated that the substrate had been attacked. This attack was confirmed by the appearance of the interface as shown in Figure 15. Also, as observed previously, a subsequent adhesive tape test indicated significant adhesion loss.

An example of a system for which the AC impedance and the parallel DC resistance data coincided and predicted that underfilm attack had not occurred was obtained for an iron-polybutadiene system exposed to 3% NaCL pH = 6.6. A Bode plot for this system, Figure 16, gave results similar to that obtained for the nickel-polybutadiene system exposed to the same environment, Figure 13. At high frequencies, capacitive behavior was obtained and resistive behavior representative of the coating's ionic resistance was obtained at low frequencies. As observed earlier for the nickel-polybutadiene systems, no information suggestive of interfacial attack could be extracted from the AC impedance data, except that the conductivity of the coating had increased with time and which may or may not be sufficient to support corrosion currents. Results obtained from parallel DC resistance measurements showed that little increase in the resistance had occurred during the 900 hours of the test, indicating that the substrate retained its integrity. The appearance of this sample, Figure 17, supported the experimental data, i.e., no interfacial attack. The photograph was typical of systems which exhibited little or no change in the DC resistance and should be compared to the photographs obtained for those systems which revealed significant underfilm attack or loss of adhesion.

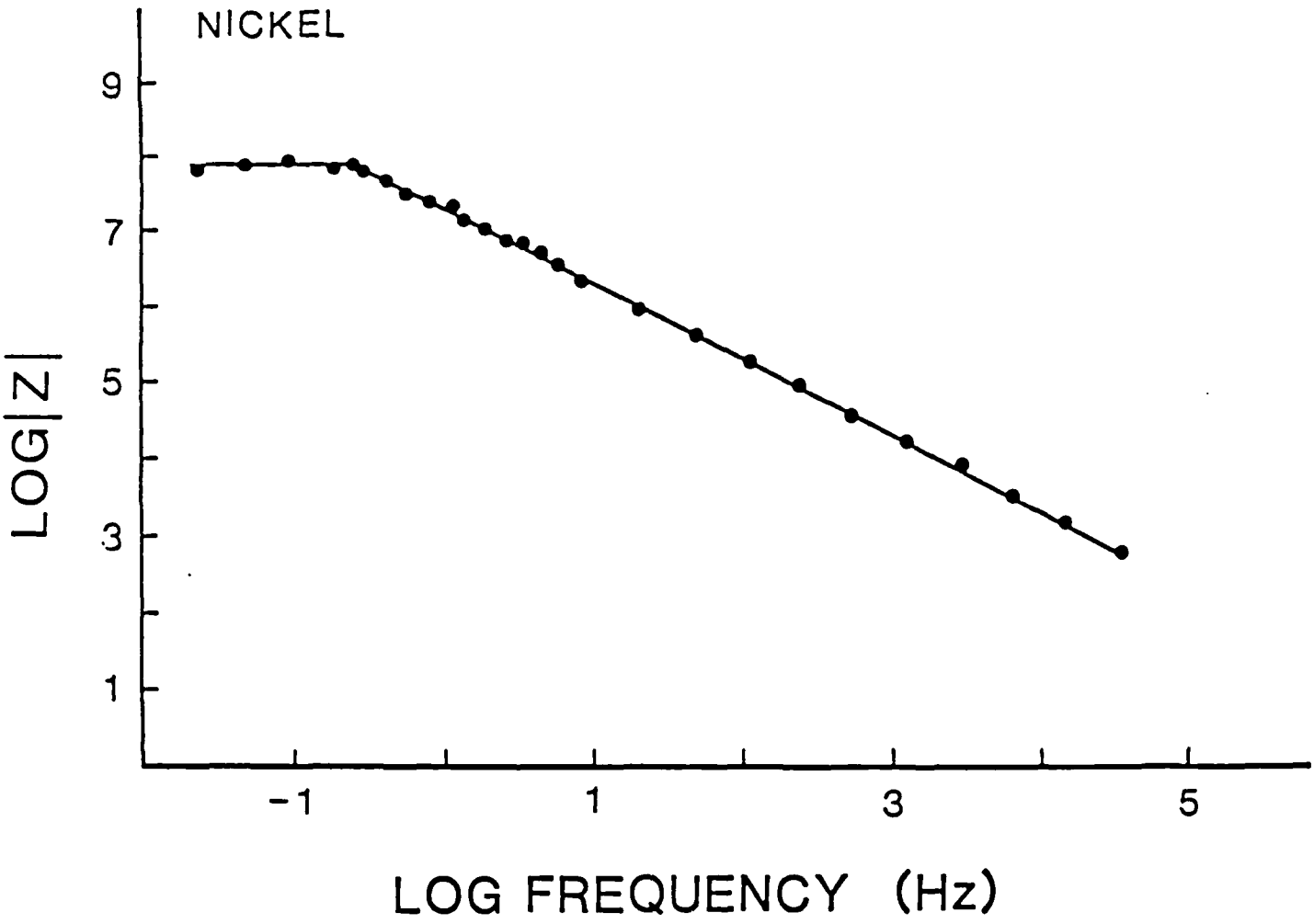

Figure 10. Bode plot for a 12.5 μm polybutadiene coated nickel sample exposed to 3% NaCl at pH = 11.4 for 420 hours. A slope of -1 was obtained at frequencies above about 0.4 Hz.

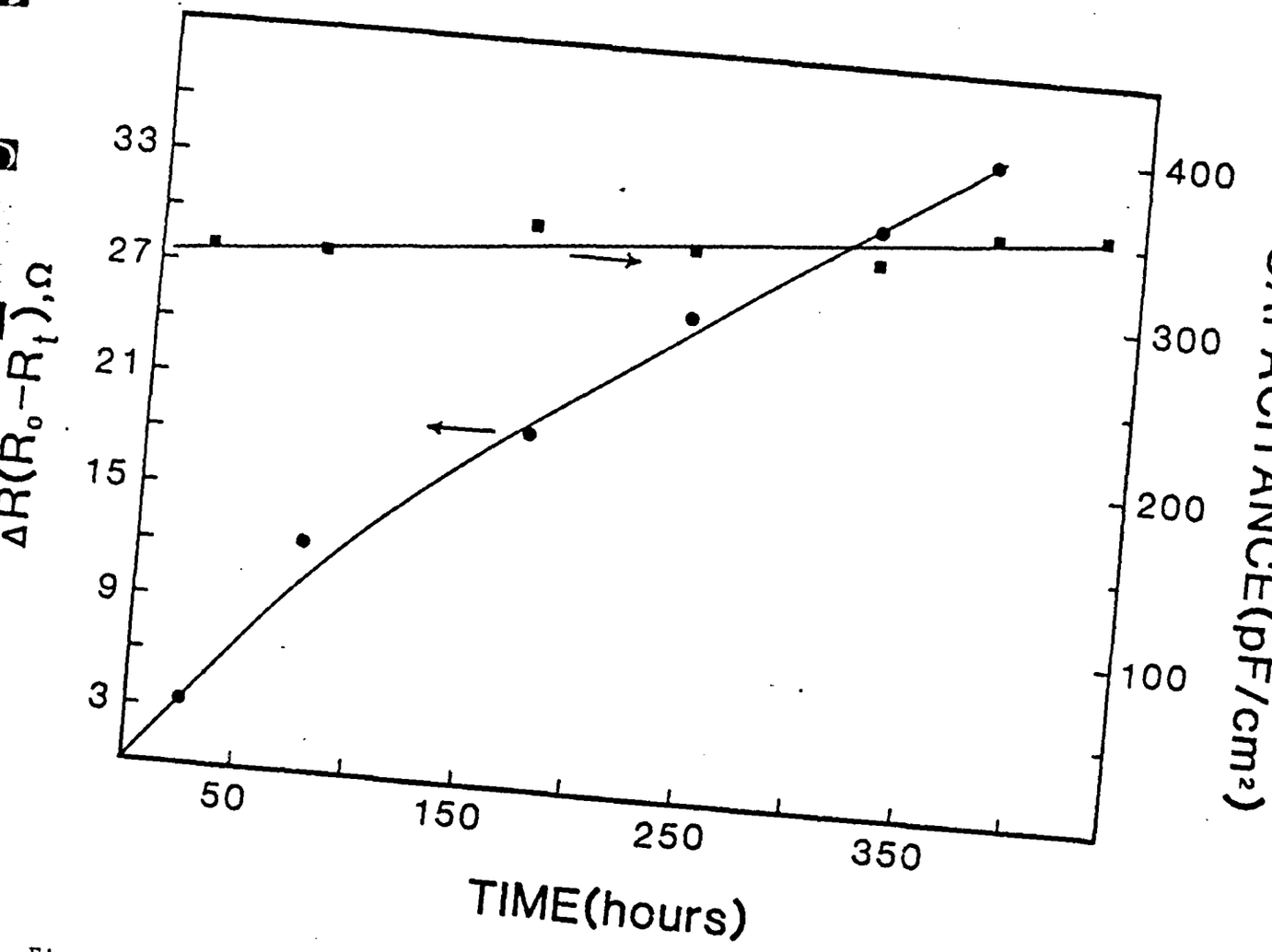

Figure 11. A plot of the change in DC resistance and AC capacitance against time of exposure to 3% NaCl at pH 11.4. Sample same as depicted in Figure 10.

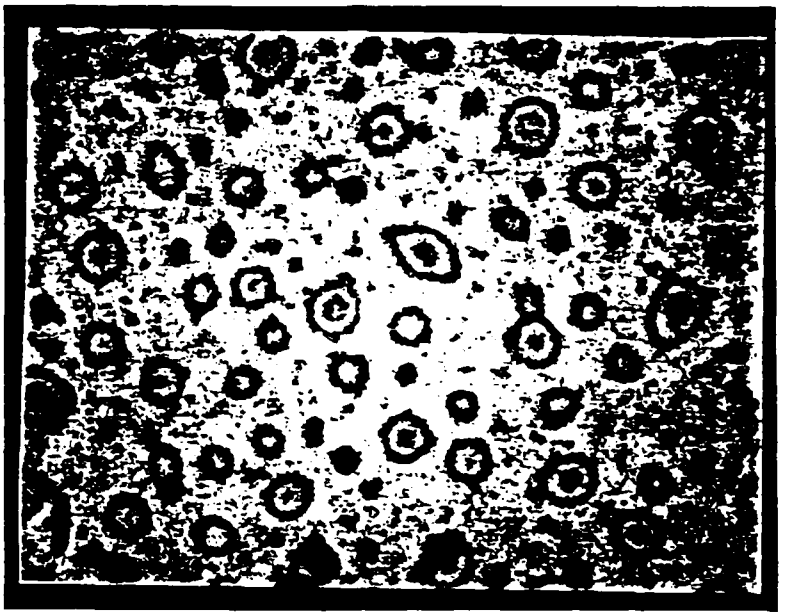

Figure 12. Aggregation of water at the metal/coating interface of a polybutadiene-coated-nickel sample exposed to 3% NaCl at pH = 14 for 420 hours (10X).

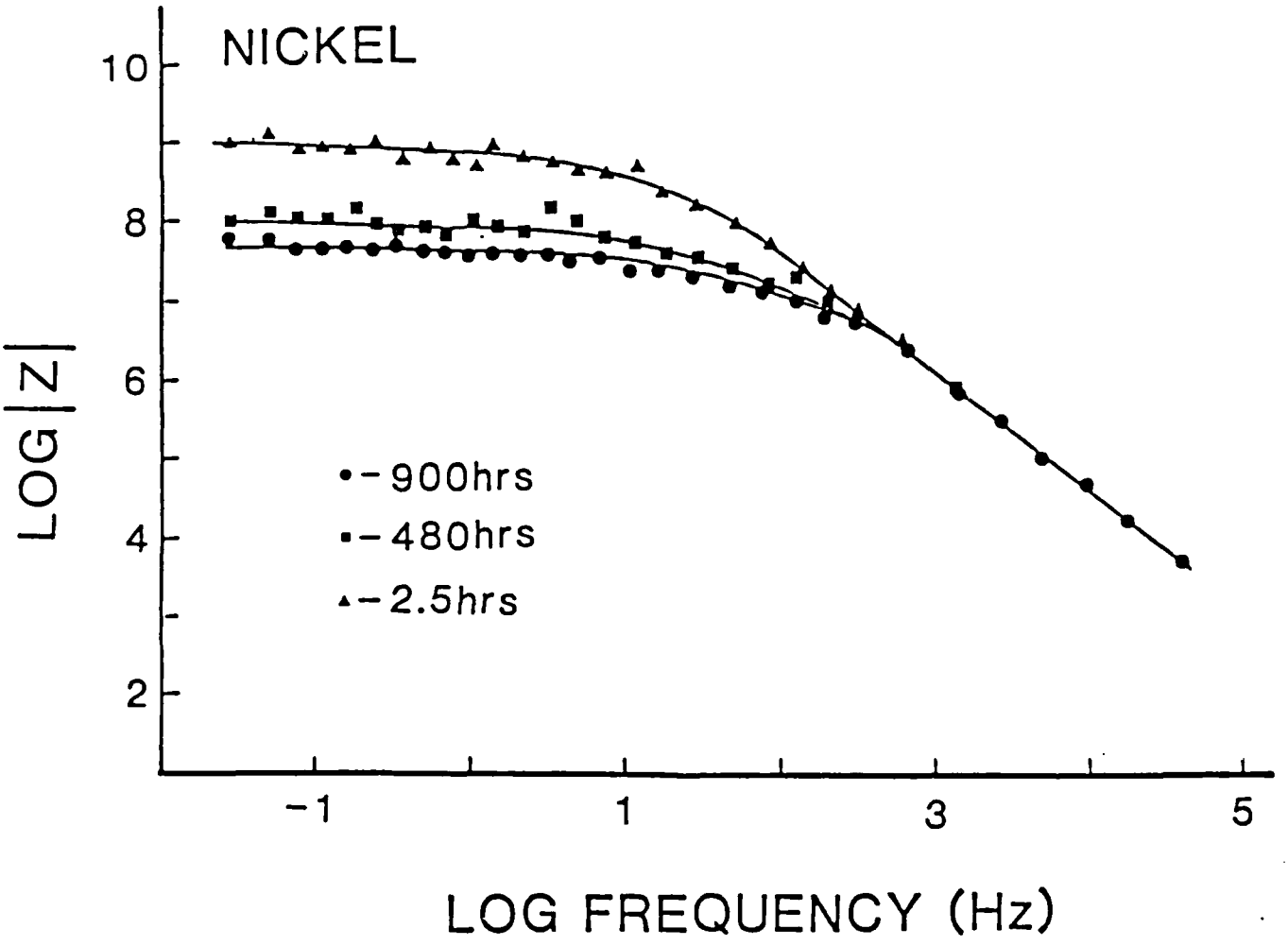

Figure 13. Bode plot for a 15 μm polybutadiene-coated-nickel sample exposed to 3% NaCl for different times. A slope of -1 was obtained at high frequencies.

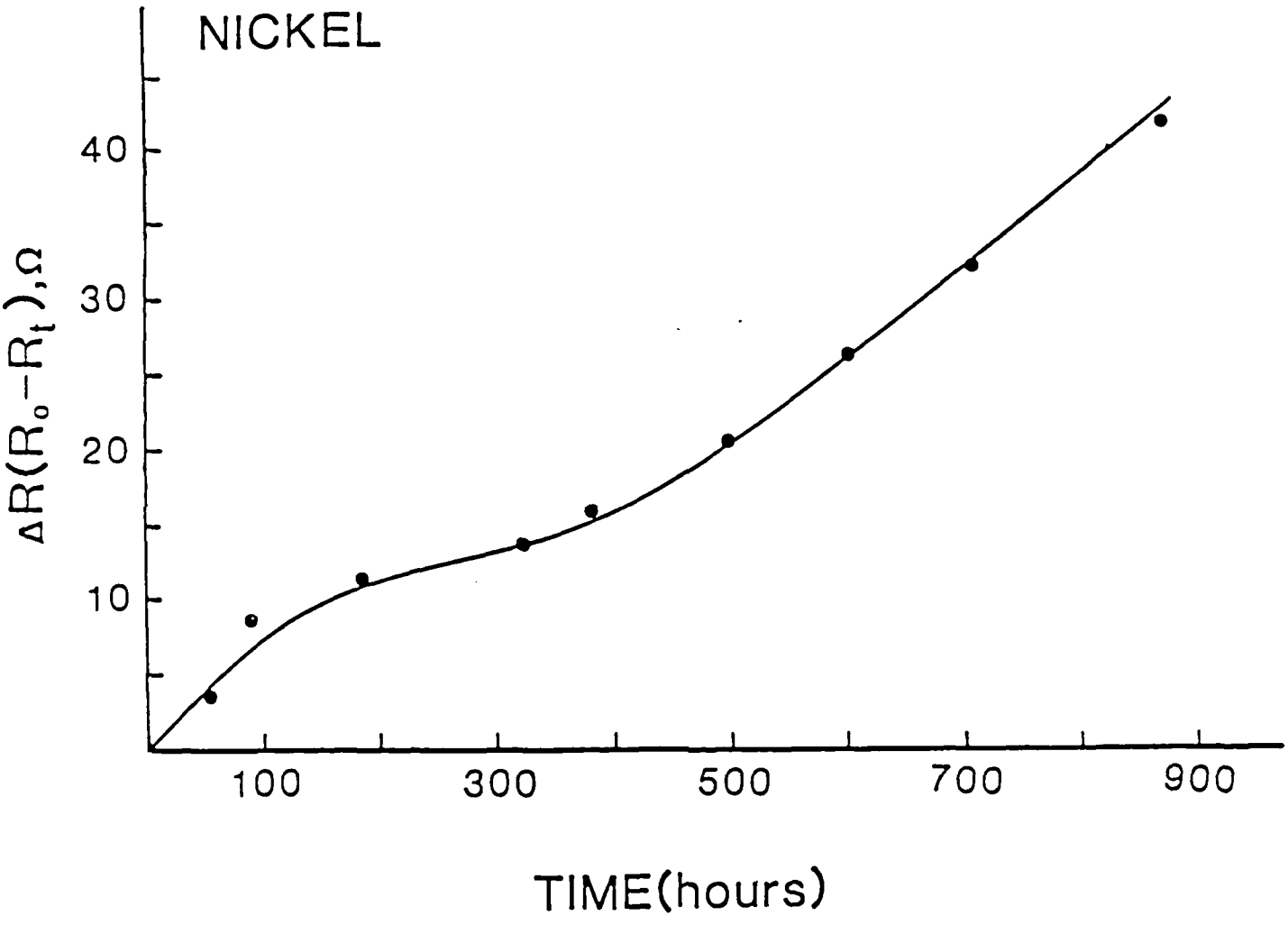

Figure 14. Plot of change in parallel DC resistance against time of exposure to 3% NaCl for a 15 μm polybutadiene-coated-nickel sample.

Figure 15. Aggregation of water at the coating/metal interface of a polybutadiene-coated-nickel sample exposed to 3% NaCl for 900 hours (10X).

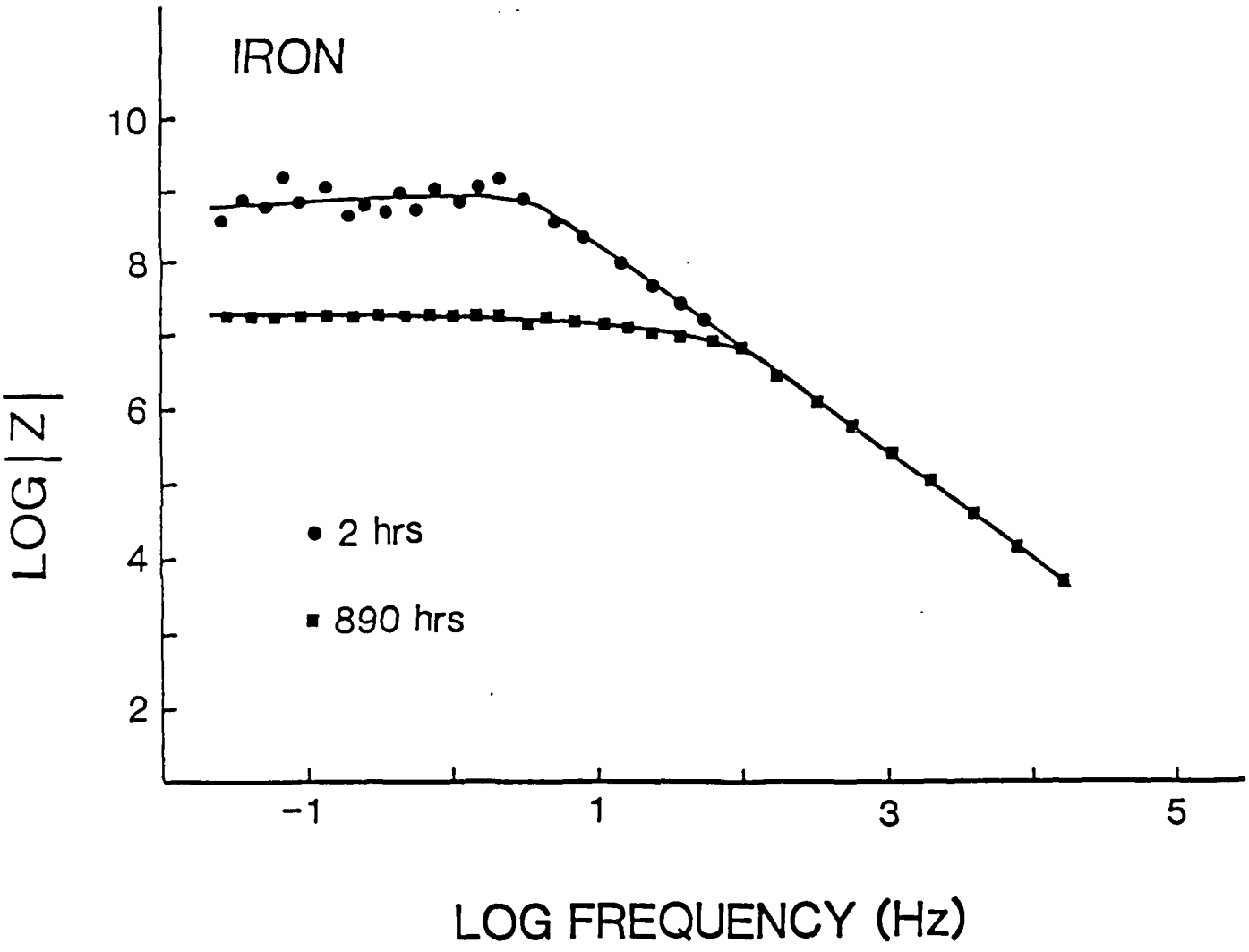

Figure 16. Bode plot for a 15 μm polybutadiene-coated-iron sample exposed to 3% NaCl for various times. A slope of -1 was obtained at high frequencies.

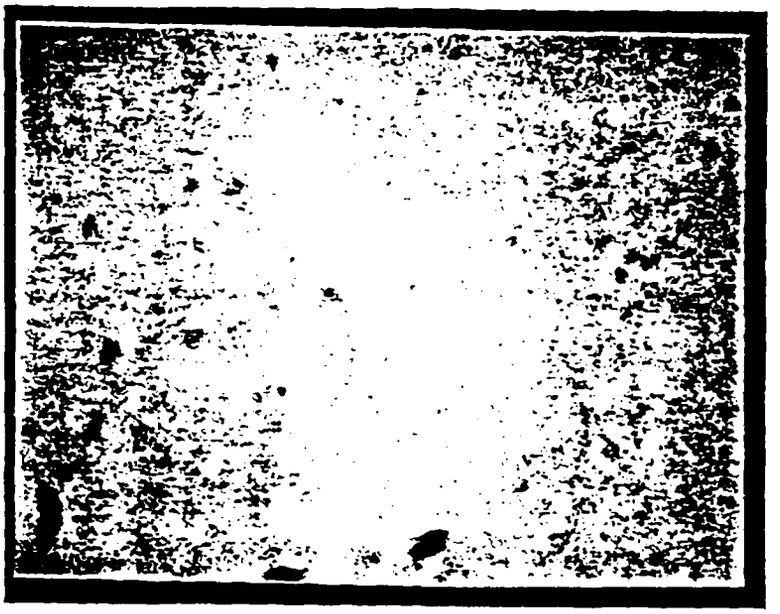

Figure 17. Appearance of a polybutadiene-coated-iron sample exposed to 3% NaCl for over 890 hours (10X).

CONCLUSIONS

The parallel DC resistance technique can be used to detect the ingress of water to the interface of coated metals and together with AC impedance techniques can adequately determine the protective characteristics of an organic coating, particularly in the case of thin polymeric films. A note of caution is in order when interpreting results obtained using AC impedance techniques, that is, the high impedance of an organic coating can, in many cases, dominate the system's response and obscure the information related to interfacial processes and often lead to erroneous conclusions with regard to the effectiveness of the protective coating. Discussions by Piens and Verbist (1981) on their work using AC impedance to study the deterioration of coated metals, warn of the difficulties encountered when attempting to interpret AC impedance data. Only when the impedance associated with the different processes is of the same magnitude and the relaxation times are not too similar can the information obtained be separated into the individual responses of the system associated with the coating and interface. However, in many cases, the ionic resistance of the coating is high and obscures other factors related to charge transfer, polarization resistance or diffusion processes of the system. Therefore, under certain conditions the parallel DC resistance technique can indicate changes at the interface at earlier times because this method is not dependent on prior breakdown of the coating before information concerning interfacial processes appear.

In addition, DC resistance measurements can be used to monitor rates of penetration of water in various salt solution environments and optical observations of the interface are made possible by the use of thin metal films deposited on glass substrates.

The results to date, although far from conclusive, give some credence to the views of Kendig (1983) that the corrosion process itself provides an environment that leads to a change in the electrical properties of the coating. The basis for this view is that the magnitude of the changes in the DC parallel resistance appears large before major changes occur in the AC impedance data. The opinions at the present time are subjective and quantitative experiments must be carried out to test the ideas of Kendig.

REFERENCES

Bacon, R.D.; Smith, J. J.; Rugg, F. M. Ind. Eng. Chem. (Ind. Division) 1948, 40, 161.

Brasher, D. M.; Nurse, T. J. J. Appl. Chem. 1959, 9, 96.

Callow, L. M.; Scantlebury, J. D. J.O.C.C.A. 1981a, 64(2), 83.

Callow, L. M.; Scantlebury, J. D. J.O.C.C.A. 1981b, 64(2), 119.

Callow, L. M.; Scantlebury, J. D. J.O.C.C.A. 1981c, 64(2), 140.

Epelboin, I.; Gabrielli, G.; Keddam, T.; Takenouti, H. In "Electrochemical and Corrosion Testing-ASTM"; Mansfeld, F.; Bertocci, U., Ed.; ASTM: Philadelphia, 1981, p.150.

Hubrecht, J.; Vereecken, J.; Piens, M. J. Electrochem. Soc. 1984, 131(9), 2010.

Kendig, M. W. Private communication, 1983.

Kinsella, E. M.; Mayne, J.E.O. Br. Polym. J. 1969, 1, 173.

Leidheiser, Henry, Jr.; Kendig, M. Corrosion 1976, 32(2), 69.

Mansfeld, F.; Kendig, M.; Tsai, S. Corrosion 1982, 38(9), 478.

Mayne, J.E.O.; Scantlebury, J. D. Br. Polym. J. 1970, 2, 240.

Mayne, J.E.O.; Mills, D. J. J.O.C.C.A. 1975, 58, 155.

O'Brien, H. C. Ind. Eng. Chem. 1966, 58(6), 45.

Piens, M.; Verbist, R. In "Corrosion Control by Organic Coatings"; Leidheiser, H. Jr., Ed.; NACE: Houston, 1981, p.32.

Rothwell, G. W. J.O.C.C.A. 1969, 52, 219.

Scantlebury, J. O.; Sussex, Graham A. M. In "Corrosion Control by Organic Coatings"; Leidheiser, H. Jr., Ed.; NACE: Houston, 1981, p.51.

Strivens, T. A.; Taylor, C. C. Materials Chemistry 1982, 7, 199.

Touhsaent, R. E.; Leidheiser, H. Jr. Corrosion 1972, 28(12), 435.

Wormwell, F.; Brasher, D. M. J. Iron & Steel Inst., Feb. 1950, 141.

Program #8

Cathodic Delamination of an Organic Coating from Phosphated Steel

Principal Investigator: Henry Leidheiser, Jr.
Prof. of Chemistry

Associate: André Sommer
Graduate Student

INTRODUCTION

Previous work, part of which is included in this report, dealt with the effects of pH and the cation of the electrolyte on a zinc phosphate conversion coating on steel. Two important conclusions drawn from those studies were: (1) The rate of phosphate dissolution increases as the pH of the electrolyte increases. (2) Sodium hydroxide dissolves the phosphate coating more rapidly than potassium, lithium, and cesium hydroxides. This latter observation will become important when interpreting the results of the cathodic delamination of organic films from a phosphated steel surface. Leidheiser and Wang [1] have shown that the delamination rate of organic coatings from bare steel surfaces increased when the cation of the electrolyte solution was changed from lithium through the alkali metals to cesium. The failure in this case was caused by the destruction of the organic coating/substrate bond. When a phosphated steel is coated, the delamination of the organic coating may occur by failure of the bonds at the organic coating/phosphate interface, at the phosphate/metal interface, or by simple dissolution of the phosphate conversion coating. If the adhesion failure is dependent on the organic coating, the cation effect that Leidheiser reported on should be seen. If, on the other hand, the adhesion failure is dependent on the phosphate, it is probable that the cation effect reported in another section of this report should be seen.

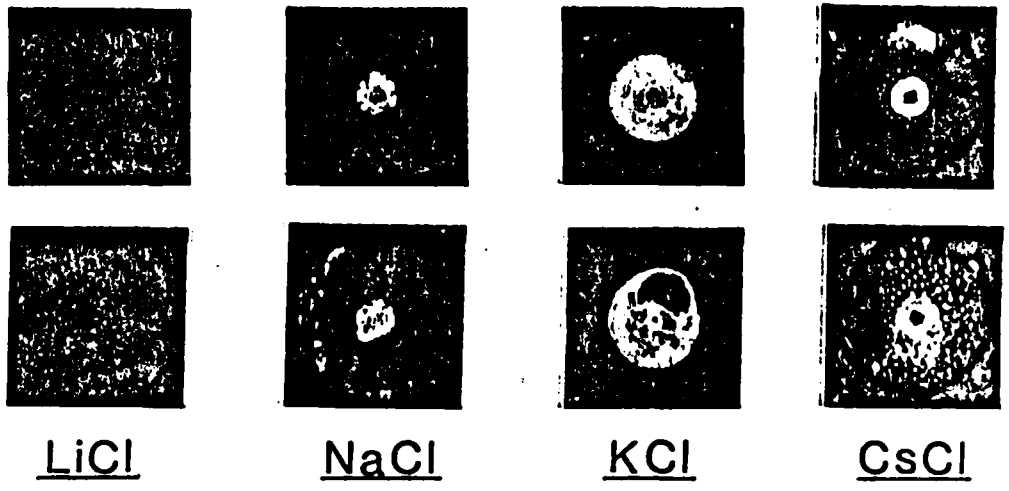

Figure 1. Macroscopic appearance of phosphated steel samples subjected to -1.5 v vs SCE in 4 halides after forming a defect in the coating.

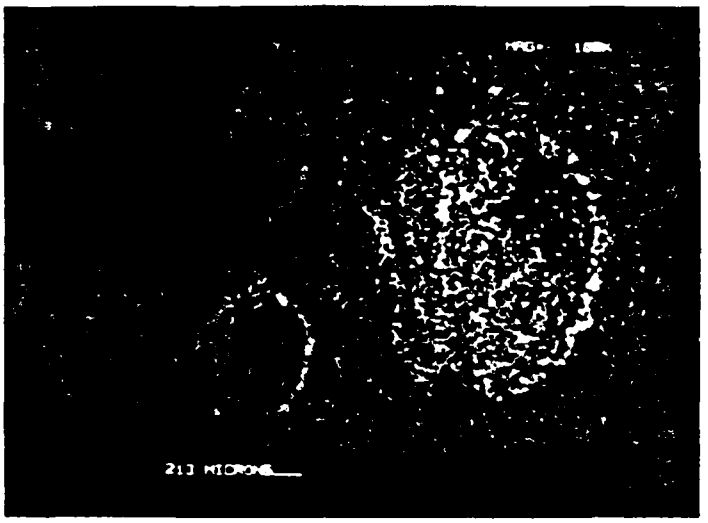

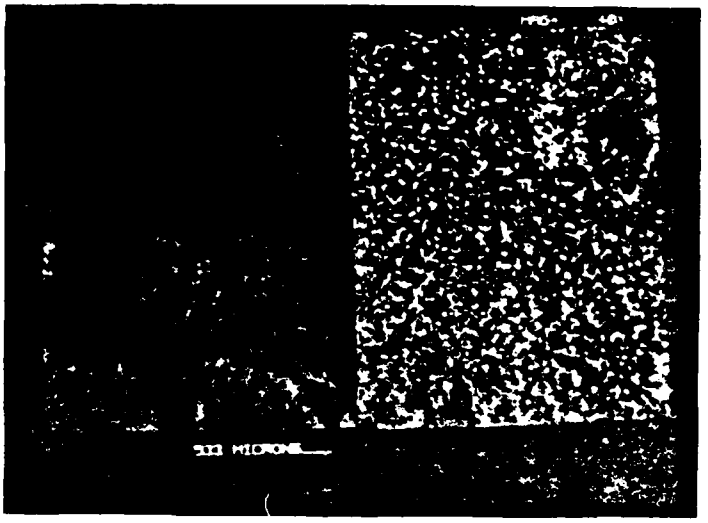

Figure 2. EDS analysis of phosphated steel subjected to cathodic treatment in lithium chloride (top) and sodium chloride (bottom) See text for details.

EXPERIMENTAL RESULTS

Zinc phosphated steel samples were coated twice with an Epanol coating by a spin coating technique. A defect was placed in the organic and phosphate coatings with a drill bit whose diameter was approximately 0.083 cm. Samples were then placed in an electrochemical cell and the sample was held at a cathodic potential of -1.5 volts vs. SCE for a period of 24 hours. At this potential, the dominant cathodic reaction at the defect is the production of hydrogen. After exposure, the samples were removed from the cell and allowed to dry. The organic coating was removed by cutting and the underside analyzed by SEM and EDS techniques. A preliminary test showed that dissolving the coating removed some of the corrosion products so this removal technique was not used. The phosphated steel samples were analyzed by laser Raman microprobe spectroscopy and electron probe microanalysis. The underside of the organic coating was analyzed only by energy dispersive spectroscopy because the fluorescence of the sample made laser Raman analysis impossible.

The physical appearance of the cathodically delaminated sample is shown in Figure 1. The delaminated coating appears as the light grey area around the defect in the center of the sample. Due to the pressure caused by evolved hydrogen and excess solution the disbonded area formed a dome. The pH of the solution beneath the coating was found to be in excess of 13 for all the samples except that exposed to lithium chloride solution. The latter sample showed no significant delamination and was therefore not tested. Figure 1 demonstrates that the rate of delamination was greatest for potassium followed by cesium and sodium.

Preliminary studies using LRMS indicated that there was little phosphate coating left on the surface of the phosphated steel. The corrosion products were randomly distributed in most cases so it was decided to record EDS maps of the areas beneath the coating. Figure 2 shows the EDS maps of the delaminated area for the sample exposed to lithium chloride (top) and the sample exposed to sodium chloride (bottom). The individual elements are mapped out on the left-hand side of the photograph. The maps on the right-hand side of the photograph are three-color composites of iron, zinc and phosphorus for which the respective colors were red, green and blue. Different colored areas such as pink, for example, indicates the presence of both iron and phosphorus. The areas colored white indicate the presence of all three elements. To use the lithium treated sample as an example for the interpretation of the other EDS maps, one can see from Figure 2 that the elements present at the defect are mostly iron and a small amount of phosphorus. Some zinc is present at the periphery of the defect indicated by the green and yellow areas. The elemental distribution shown in the map indicates that phosphorus is being removed from the phosphate coating adjacent to the defect.

The bottom half of Figure 2 shows the EDS map of the delaminated area for the sample cathodically delaminated in sodium chloride solution. Four distinct regions are visible. At the defect, which is in the upper right-hand corner, the presence of iron and phosphorus is given as the red and blue

areas, respectively. Directly above the defect the blue-green or aqua color indicates the presence of phosphorus and zinc. To the left and bottom of the defect is an area which is a mixture of all three elements depicted by the white zones and a mixture of zinc and iron depicted by the yellow zones. The fourth area located at the lower left-hand corner of the photograph indicates the presence of iron and phosphorus. This last area is at the delaminating front and shows the absence of zinc from the phosphate coating. Thus, zinc ions are removed from the phosphate at the delaminating front and deposited in the area between the front and the defect. In 1.0M NaOH (pH = 13.5) zinc ions were selectively removed from the phosphate coating. Three Raman spectra were recorded from the delaminated area, the first of which is shown in Figure 3. This spectrum was redcorded on yellow crystallites which were present over much of the delaminated area. The bands located at 1100 cm^{-1} shift and 1600 cm^{-1} shift can be assigned to carbonate and amorphous carbon, respectively. The band located at 600 cm^{-1} shift may be due to Fe_3O_4, while the band located at 350 cm^{-1} may be a zincate-type structure. The intensity of the spectrum and the breadth of the bands indicate that the species giving rise to the spectrum are present on the surface in thin layers. A second Raman spectrum was recorded from the region near the delaminating front where iron and phosphorus were found. The crystallites which gave rise to this spectrum are shown in the SEM micrograph in Figure 4 along with the Raman spectrum. Based on the elemental information and the location of the bands in the Raman spectrum, the identity of the crystallites is probably a recrystallized phosphate of iron with the vivianite structure. The third Raman spectrum shown in Figure 5 was recorded on normal phosphate crystals present at the delaminating front.

EDS maps are present in Figure 6 for the sample cathodically delaminated in potassium chloride. The map in the top photograph is at the defect, the middle photograph is in between the defect and the delaminating front, and the photograph at the bottom is at the delaminating front. Iron with a small amount of phosphorus is present at the defect. Surrounding the defect is an aqua-colored ring which indicates the presence of phosphorus and zinc. Going outward towards the delaminating front is an area in which all elements are present. The bottom photograph shows segregated areas of pure iron and areas which are rich in iron and phosphorus (yellow zones). In contrast to the sample delaminated in sodium chlordie, the delaminating front shows that little zinc is lost. Raman spectra recorded in the delaminated area are present in Figures 7-10. The first two spectra were recorded near the defect and are characteristic of a zincate structure and a carbonate as shown by the peaks at 400 cm^{-1} shift and 1063 cm^{-1} shift, respectively. The latter two spectra shown in Figures 9 and 10 were recorded near the delaminating front. The spectrum shown in Figure 9 is identical to the spectrum recorded for the cubic crystallites encountered in the exposure of zinc phosphate to KOH for four days. The bands located at 528 cm^{-1} shift and 976 cm^{-1} shift were assigned to a recrystallized phosphate of zinc and potassium. Normal phosphate crystals at the delaminating front gave the Raman spectrum shown in Figure 10.

Figure 11 illustrates the EDS map s recorded for the samples delaminated in cesium chloride. The top map was taken at the defect while the bottom map was taken at the delaminating front. The defect is again rich in iron and phosphorus as depicted by the red and pink zones. Adjacent to the defect

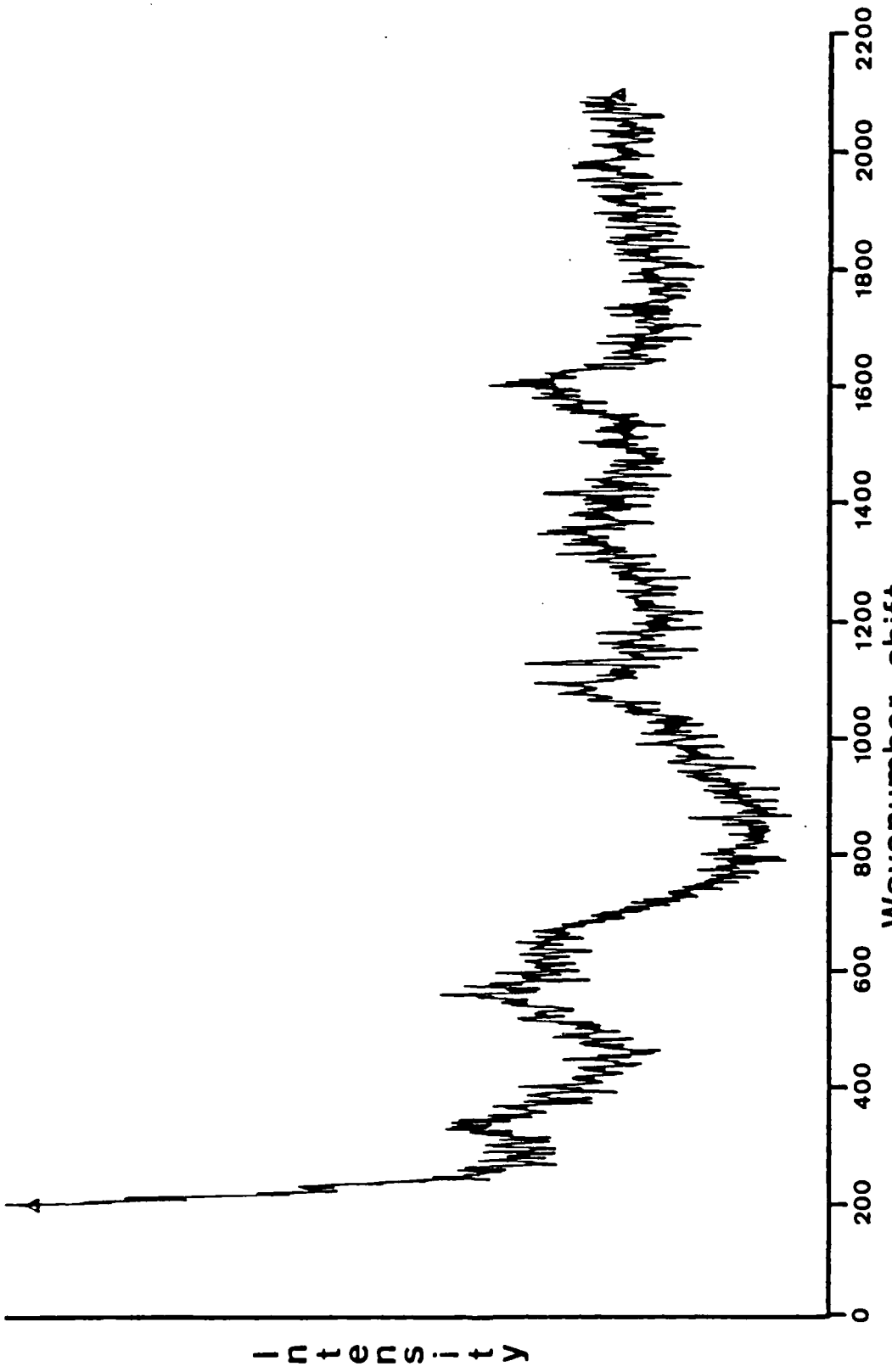

Figure 3. Raman spectrum of yellow crystallites observed in delaminated area after exposure of coated and phosphated steel to -1.5 v vs. SCE in pH 13.5 NaOH.

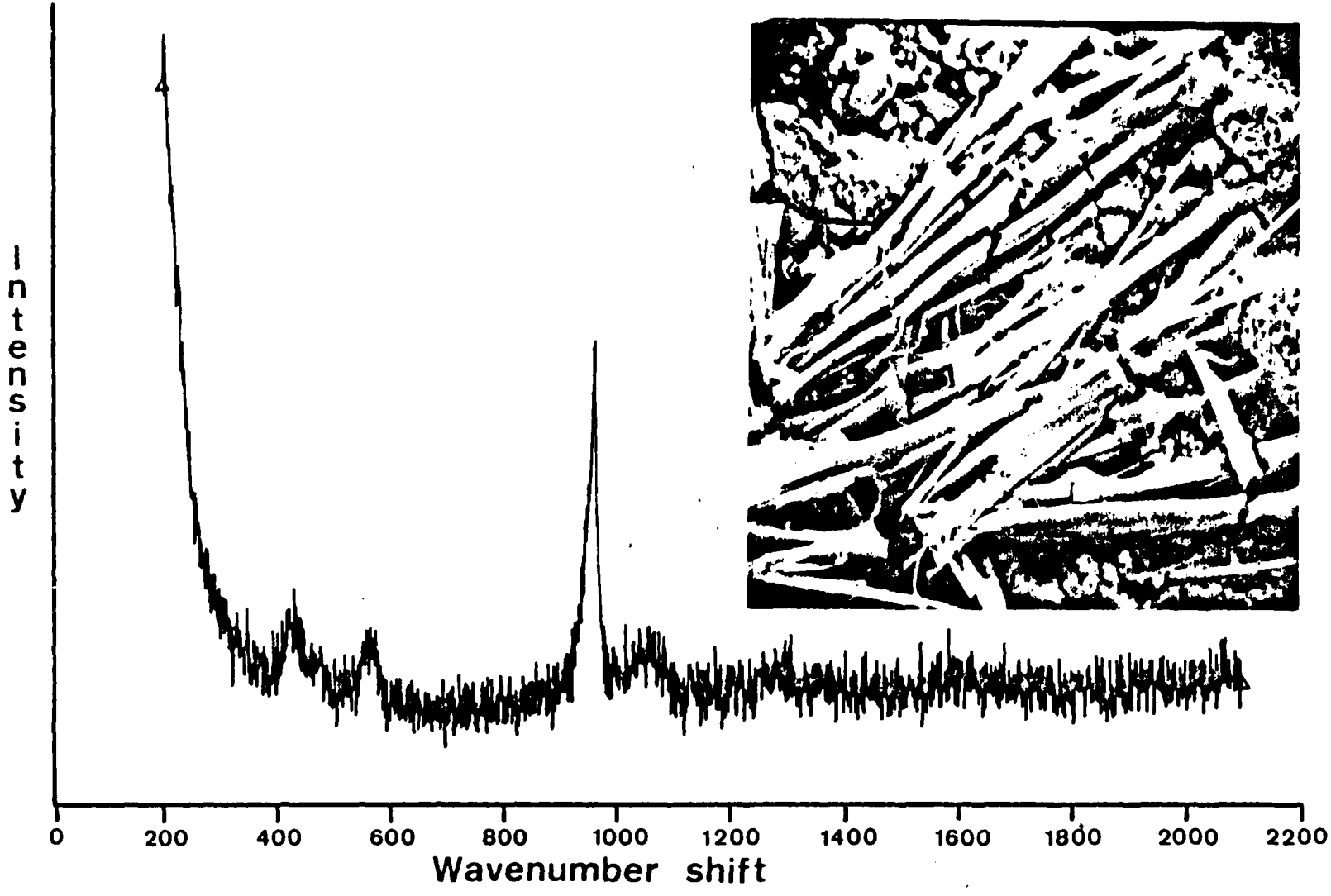

Figure 4. Raman spectrum and SEM photograph of crystallites near the delaminating front after exposure of coated and phosphated steel to -1.5 v vs. SCE in pH 13.5 NaOH.

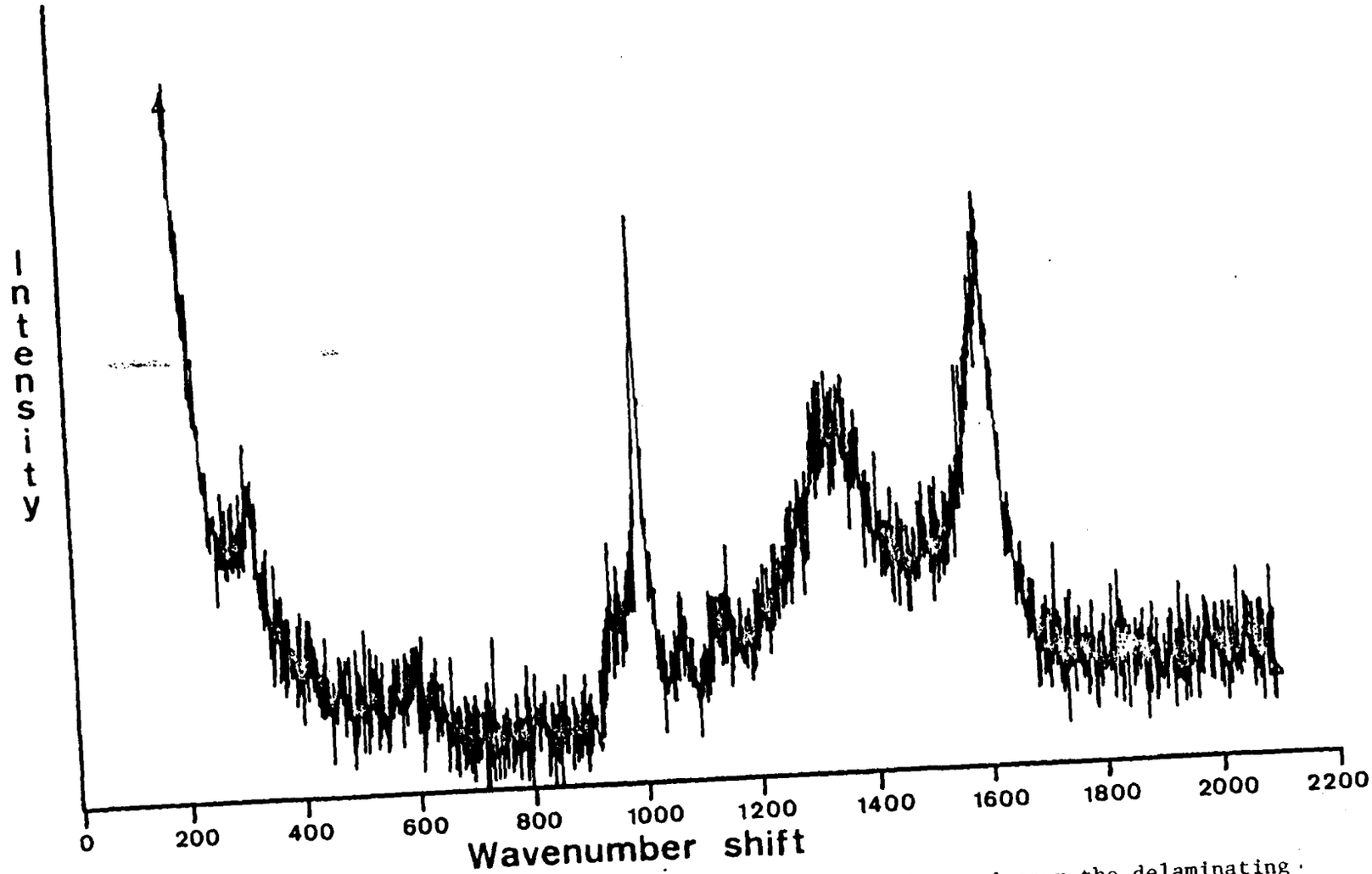

Figure 5. Raman spectrum of apparently normal phosphate crystals observed near the delaminating front after exposure of coated and phosphated steel to -1.5 v vs. SCE in pH 13.5 NaOH.

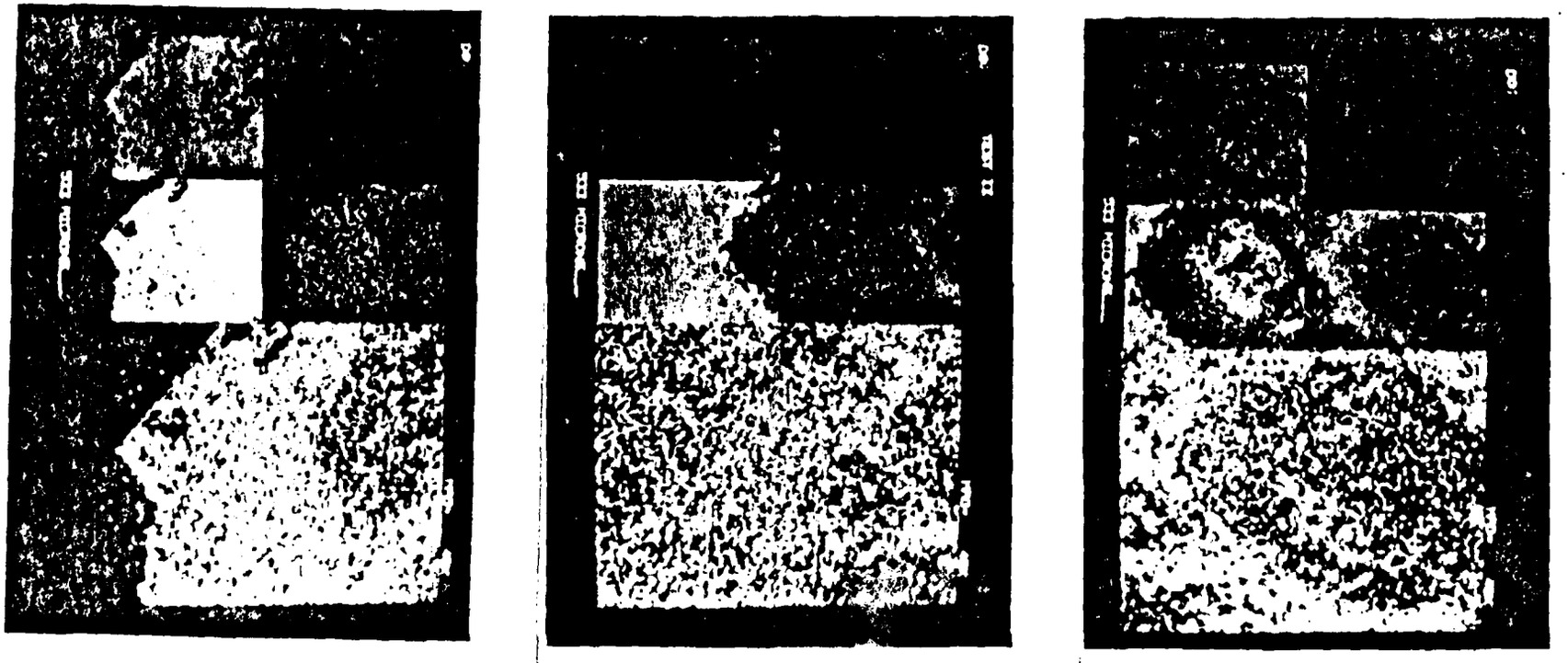

Figure 6. EDS analysis of phosphated steel subjected to cathodic treatment in potassium chloride solution. See text for details.

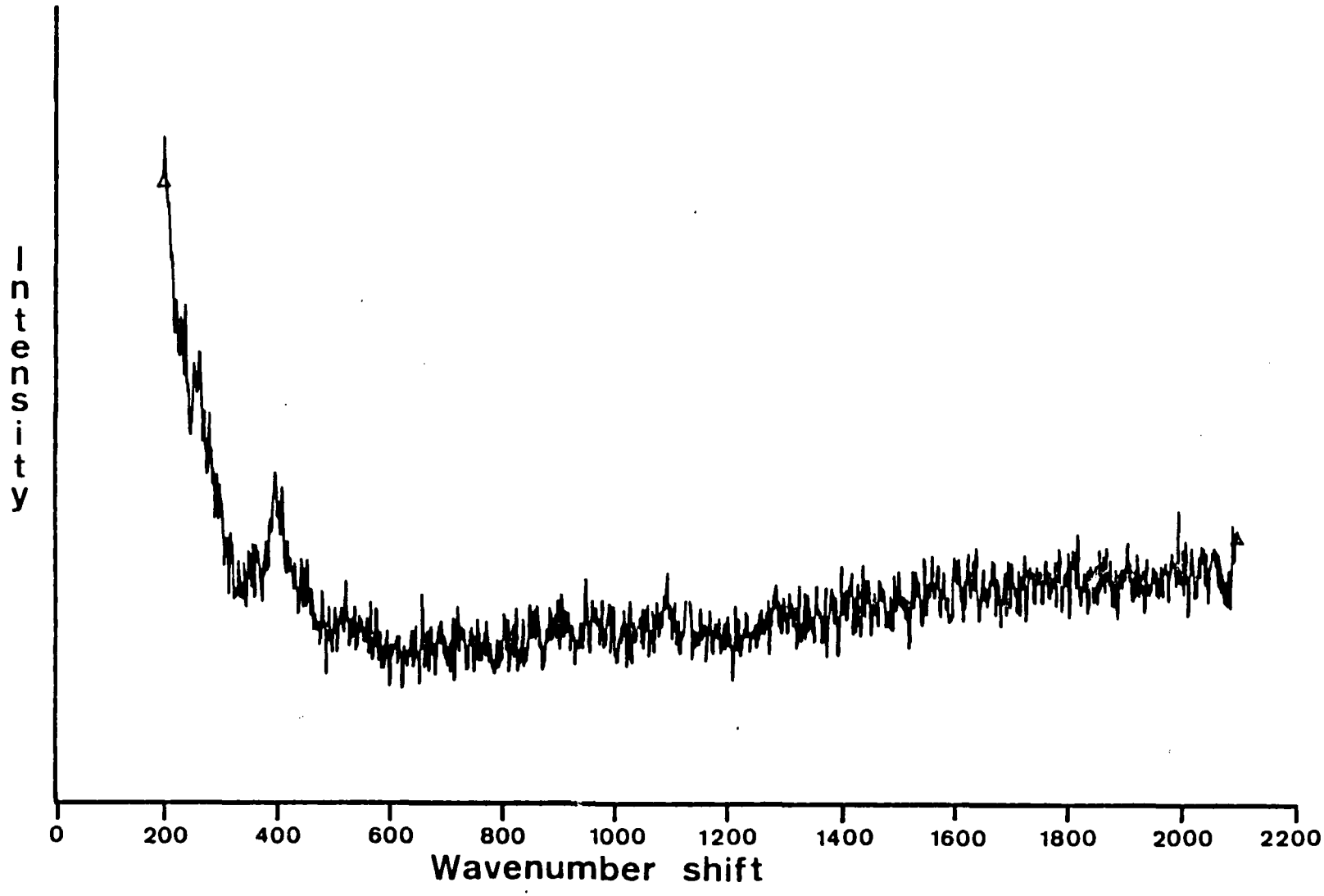

Figure 7. Raman spectrum of area near the defect after exposure of coated and phosphated steel to -1.5 v vs. SCE in potassium chloride solution.

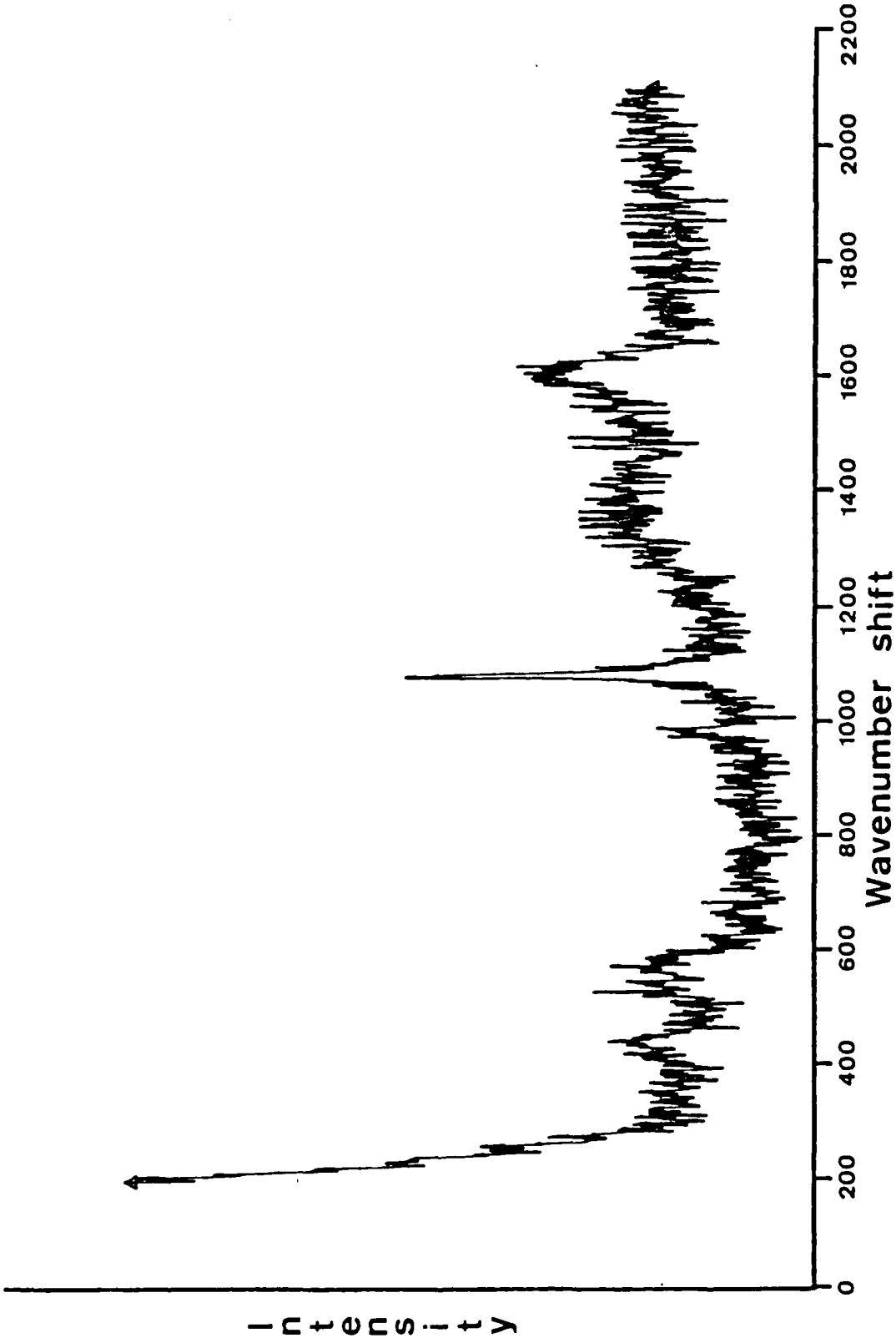

Figure 8. Raman spectrum of area near the defect after exposure of coated and phosphated steel to -1.5 v vs. SCE in potassium chloride solution.

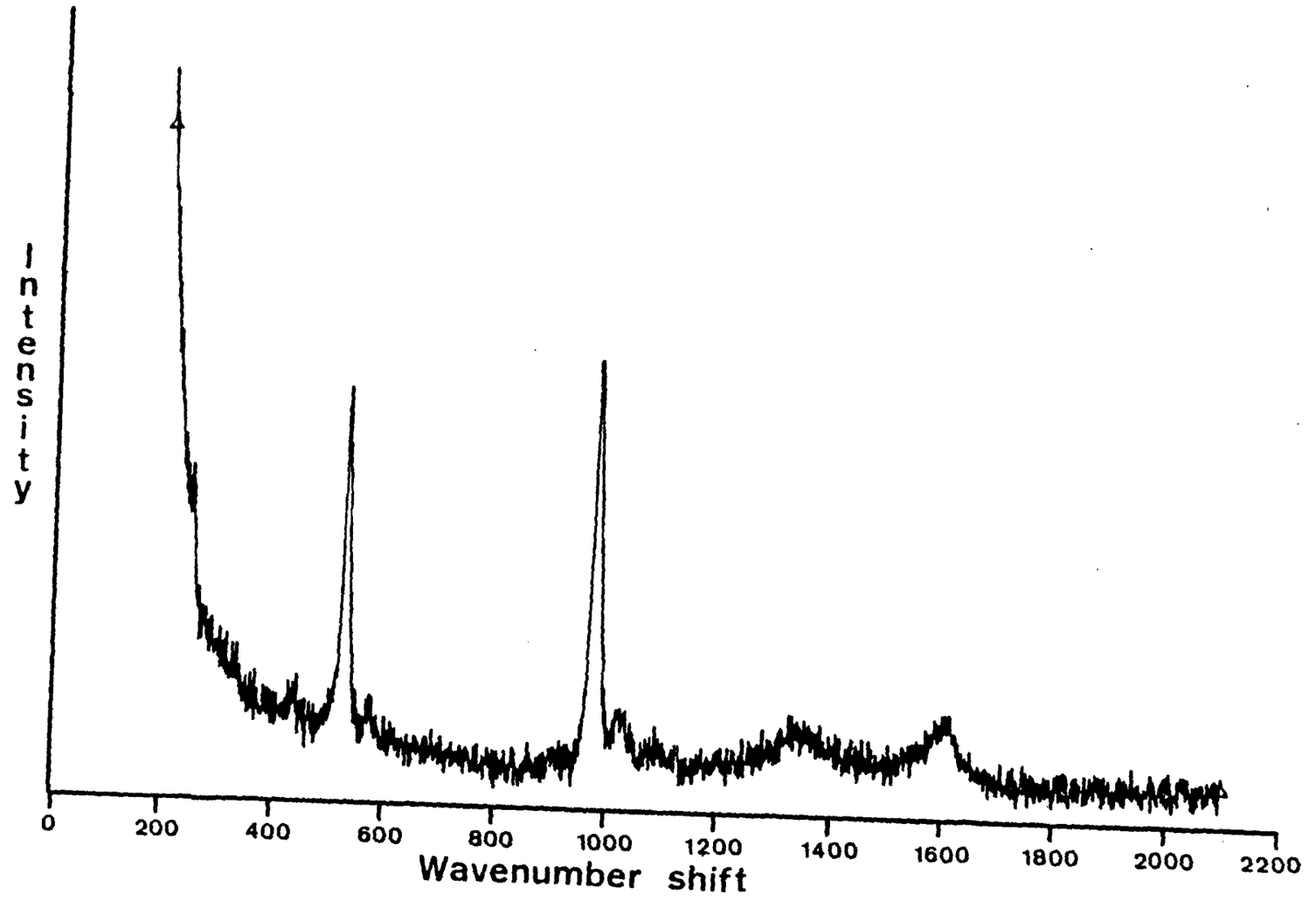

Figure 9. Raman spectrum of an area near the delaminating front after exposure of coated and phosphated steel to -1.5 v vs. SCE in potassium chloride solution.

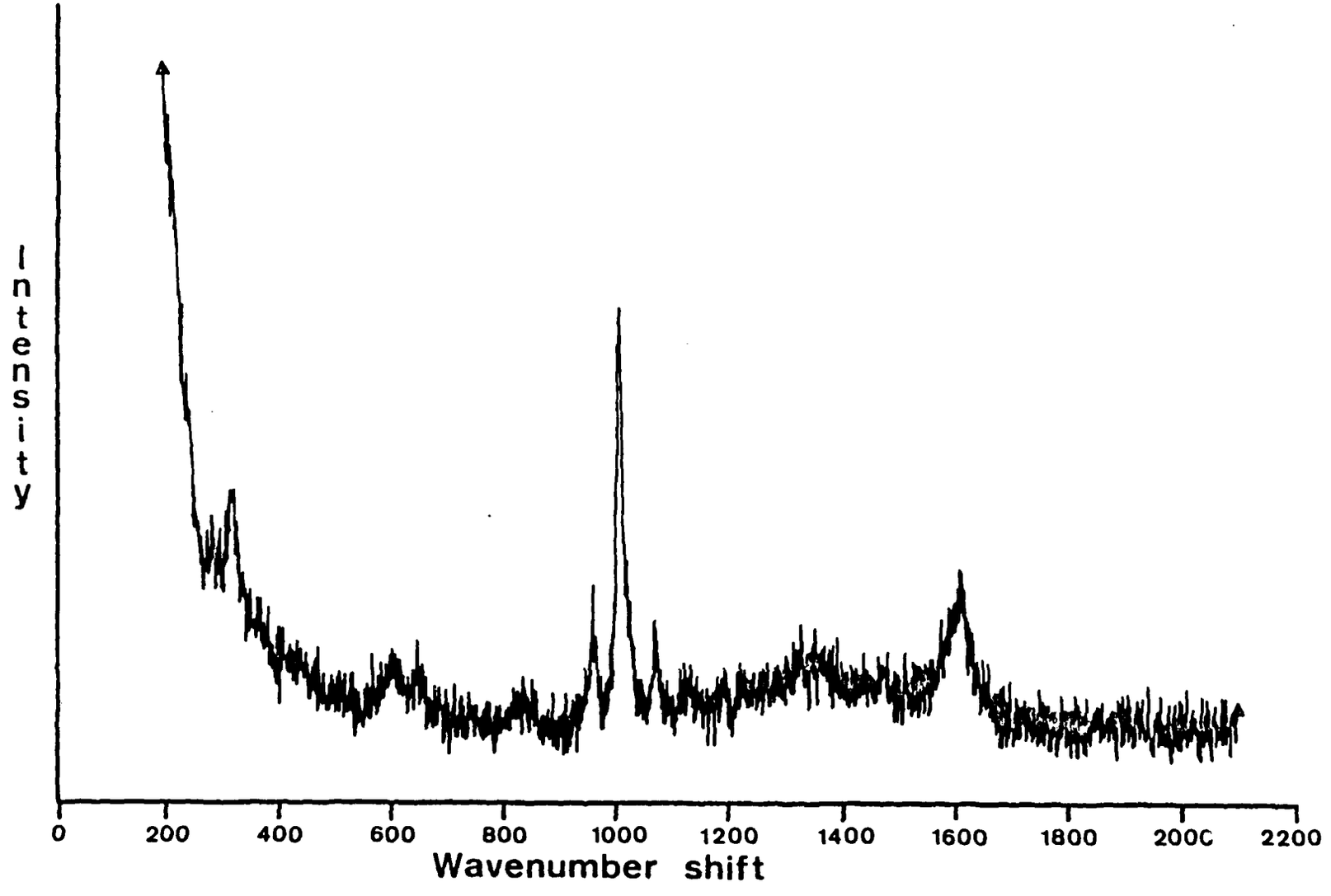

Figure 10. Raman spectrum of an area near the delaminating front after exposure of coated and phosphated steel to -1.5 v vs. SCE in potassium chloride solution.

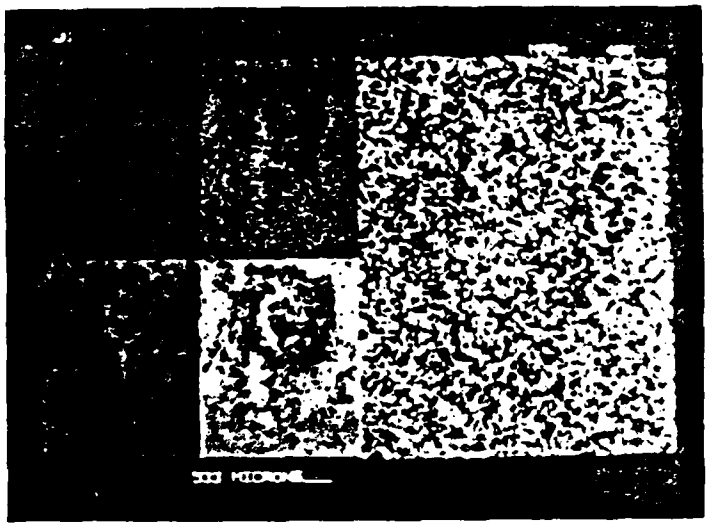

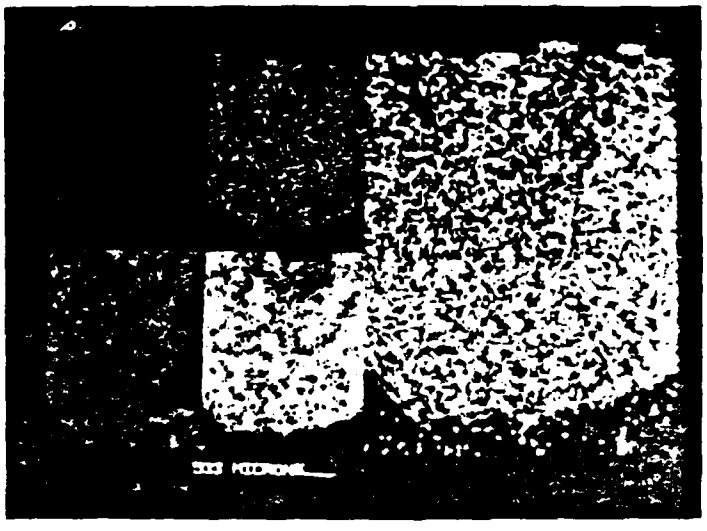

Figure 11. EDS analysis of phosphated steel subjected to cathodic treatment in cesium chloride solution. See text for details.

is an area in which all the elements are present followed by an area at the delaminating front which is devoid of zinc as indicated by the lack of the color green. Two Raman spectra were recorded from the delaminated area. The first spectrum shown in Figure 12 was recorded on a white material which evenly dispersed over the delaminated area. The band at 1063 cm^{-1} shift is again assigned to the carbonate symmetric stretching mode of vibration for a structure known as hydrozincite. The second spectrum was recorded from cubic crystals similar to tose seen in the KOH experiment. This spectrum is shown in Figure 13 with bands located at 517 cm^{-1} shift and 987 cm^{-1} shift. The location of the bands in the spectrum indicates that the crystals are a recrystallized phosphate of zinc and cesium. These cubic crystallites were found only at the delaminating front.

The organic coating at the beginning of the experiment was transparent. However, after it was cathodically delaminated, the coating became opaque. Optical microscopy showed the presence of material adhering to the underside of the coating. A preliminary analysis with LRMS proved that the coating fluoresced so it was decided to analyze the coating using EDS. The backside of the polymer film delaminated in sodium chloride solution is shown in the SEM micrograph of Figure 14 along with EDS spectra recorded at points radially outward from the defect. EDS spectra were recorded directly adjacent to the defect, midway between the defect and the edge of the coating and at the edge of the coating. The EDS spectrum recorded adjacent to the defect indicates the presence of a large amount of zinc associated with small amounts of iron and phosphorus. Midway between the defect and the coating edge, zinc, iron, phosphorus and chlorine are detected. The same elements were present at the edge of the delaminated coating. The latter two spectra are characteristic of a normal zinc phosphate associated with iron and chlorine. A similar analysis was done for the coating delaminated in potassium chloride solution for which the results are shown in Figure 15. EDS spectra were recorded for the three rings distinctly visible in the SEM micrograph. The ring adjacent to the defect was composed mostly of iron associated with small amounts of potassium, chlorine and zinc. EDS analysis of the middle region indicated the presence of a normal phosphate from the zinc and phosphorus present along with iron, chlorine and a large amount of potassium. The outer region was found to contain zinc, phosphorus and iron associated with large amounts of potassium. Figure 16 shows the SEM micrograph and EDS spectra recorded for the sample delaminated in cesium chloride. Again three distinct regions were visible. The first region adjacent to the defect was composed of zinc, iron, chlorine, phosphorus and a large amount of cesium. The second region indicated the presence of the same elements with a slight decrease in the amount of iron and phosphorus present. Finally, the third ring was characteristic of a normal phosphate associated with a large amount of cesium.

DISCUSSION

The results of the cathodic delamination experiments showed that the amount of coating disbonded from the substrate was greatest for samples delaminated in KCl solution followed by those samples delaminated in CsCl,

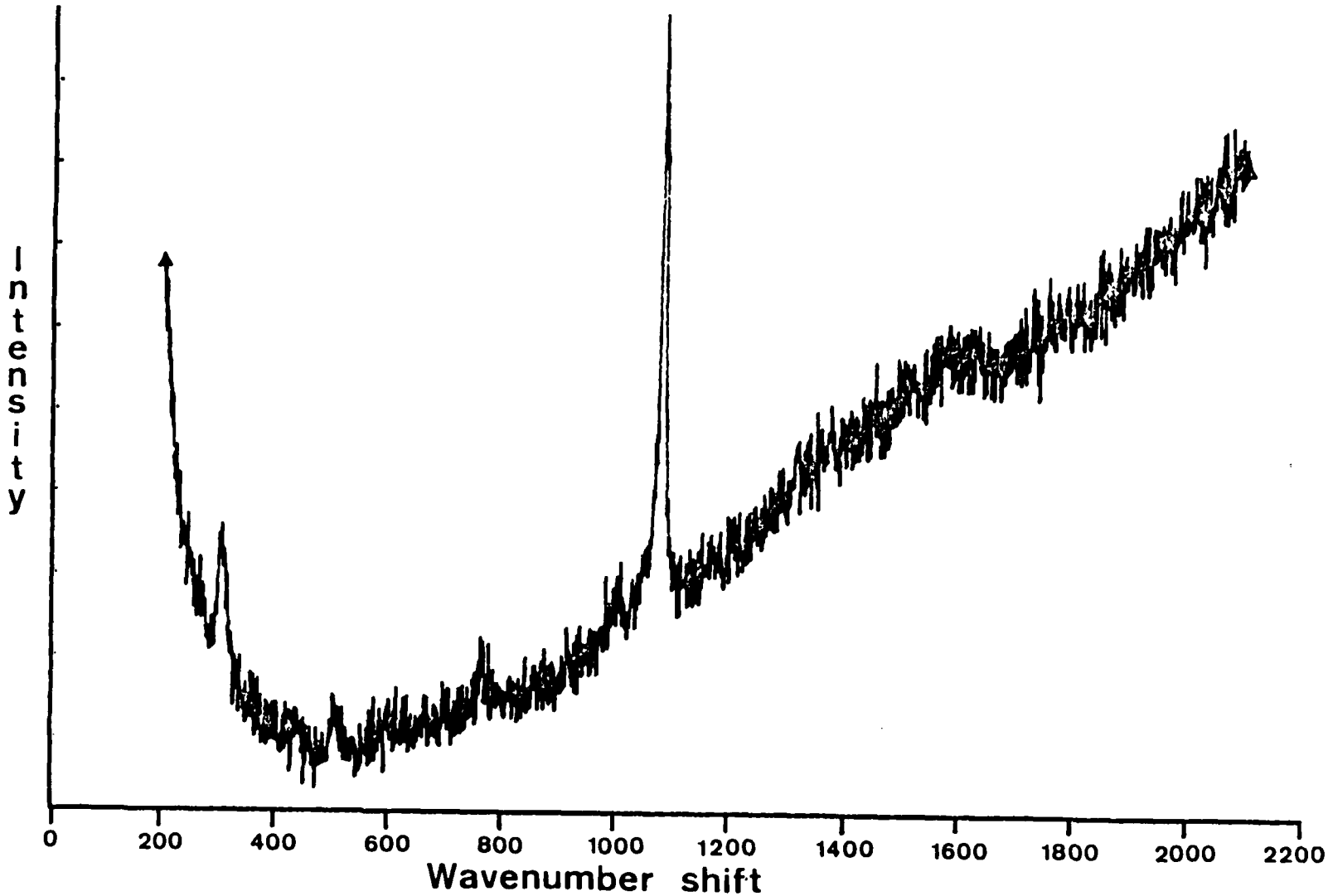

Figure 12. Raman spectrum of white material uniformly dispersed over delaminated region when a phosphated and coated steel was subjected to -1.5 v vs. SCE in cesium chloride solution.

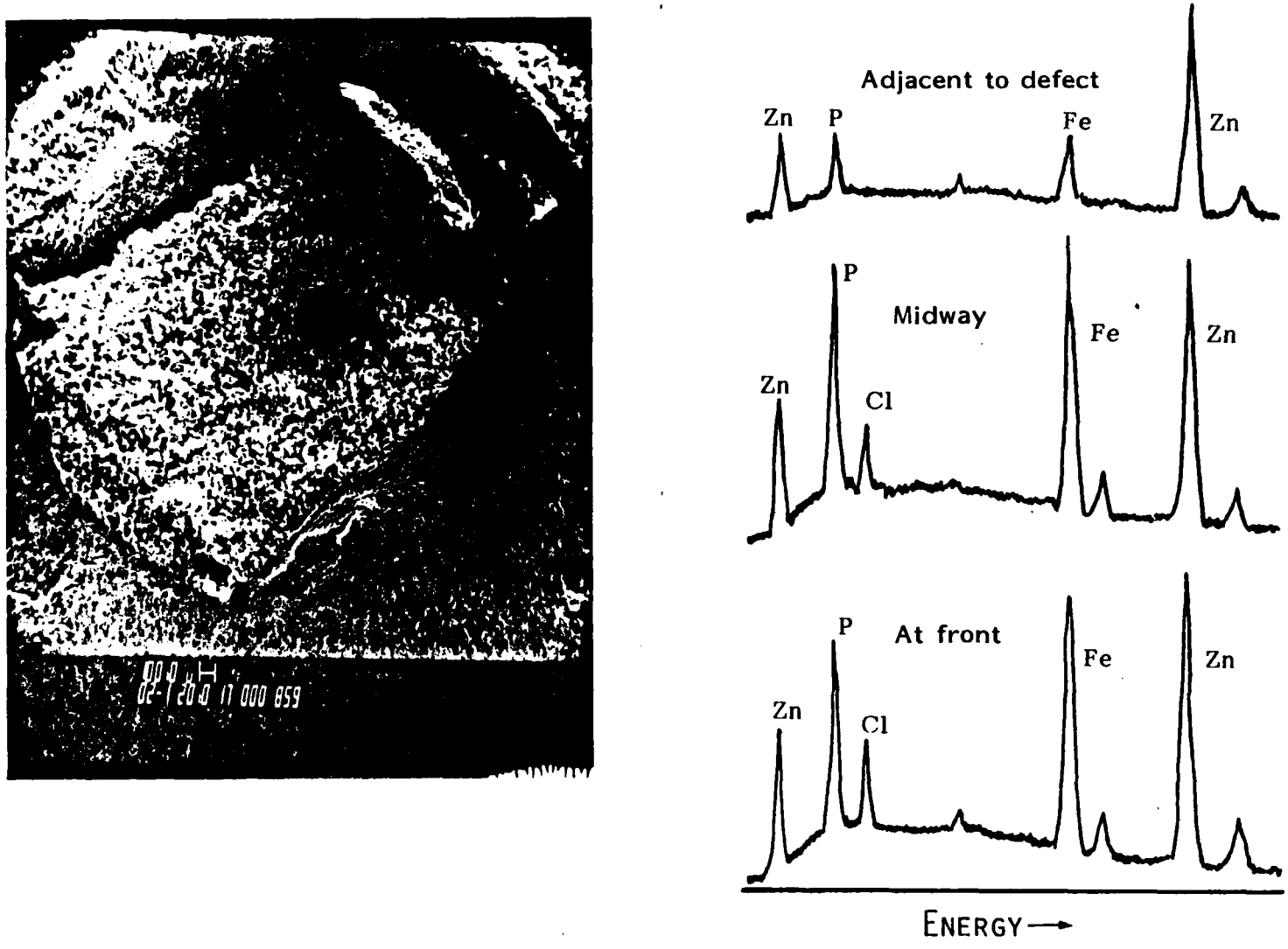

Figure 14. SEM micrograph and EDS spectra of the material adhering to the polymer coating after cathodic delamination in sodium chloride solution.

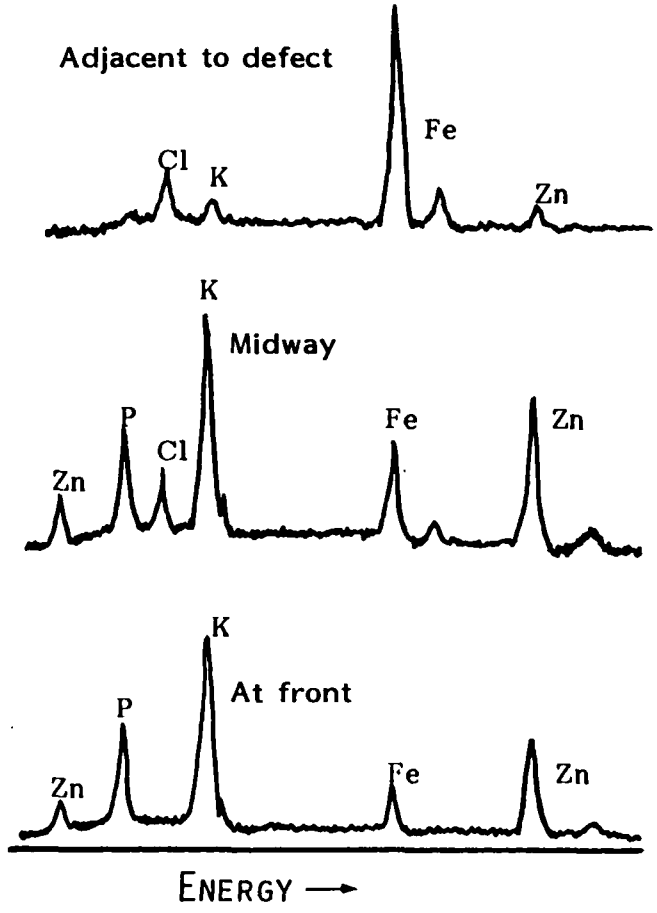

Figure 15. SEM micrograph and EDS spectra of the material adhering to the polymer coating after cathodic delamination in potassium chloride solution.

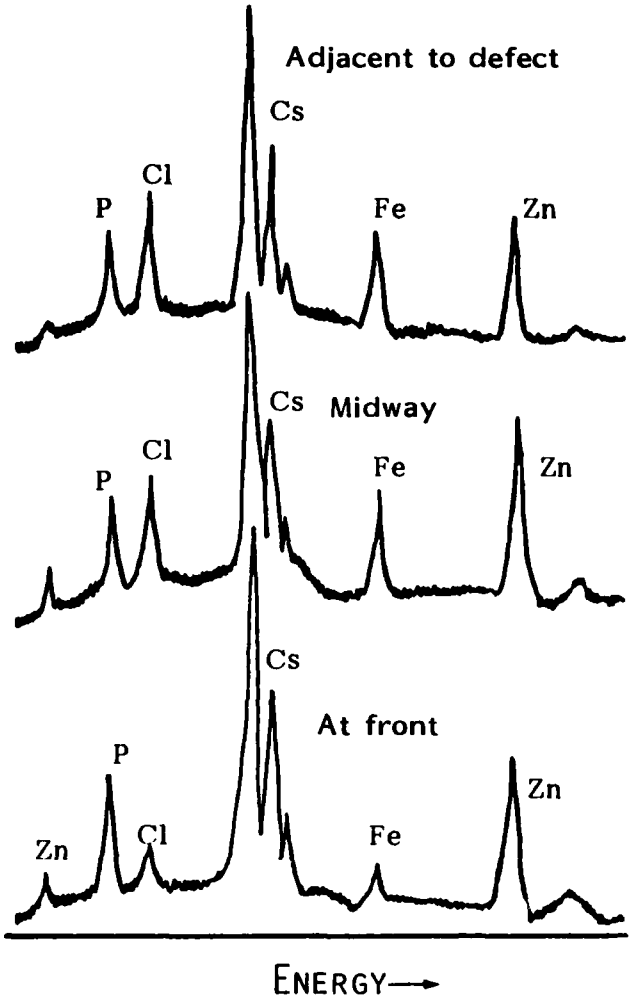

Figure 16. SEM micrograph and EDS spectra of the material adhering to the polymer coating after cathodic delamination cesium chloride solution.

NaCl, and LiCl solutions. Analysis by energy dispersive spectroscopy showed that the disbonded region for each sample delaminated in the different chloride solutions consisted of three distinct regions which included the defect, the delaminating front and the region in between. The defect was found to contain mostly iron with small amounts of phosphorus. Surrounding the defect was a region in which all the elements (Fe, P, Zn) were present. The sample delaminated in KCl was an exception in that a ring of phosphorus and zinc was present around the defect followed by the usual multi-element composition. Phosphorus and iron were the predominant elements existing at the delaminating front. This behavior was most marked for the sample disbonded in NaCl and was demonstrated to a lesser extent by the samples delaminated in CsCl and KCl. Laser Raman Microprobe analysis of the delaminated areas indicated the presence of carbonate, zincate, carbon, Fe_3O_4, normal zinc phosphate (hopeite), and recrystallized phosphate. No Raman spectra could be recorded for any of the samples at the defect since this area contained elemental iron. In the region between the defect and the delaminating front the samples disbonded in NaCl and KCl produced Raman spectra indicative of carbonate and zincate. Samples disbonded in NaCl produced Raman spectra which were characteristic of a thin amorphous coating composed of zincate, hydrozincite and carbon. Crystalline zincite and hydrozincite spectra were recorded in this region for the sample delaminated in KCl. No Raman spectra were recorded in this region for the CsCl-disbonded sample. At the delaminating front Raman spectra were recorded for each sample which indicated the presence of normal zinc phosphate and a recrystallized phosphate. Raman spectra recorded for the NaCl disbonded sample in this region were characteristic of a normal zinc phosphate associated with a large amount of carbon and a recrystallized phosphate with the vivianite structure. Both samples delaminated in KCl and CsCl gave Raman spectra characteristic of normal zinc phosphate and a recrystallized phosphate of iron, zinc and the respective alkali metal ion.

EDS analysis of the backside of the delaminated coatings showed varying amounts of all the elements adjacent to the defect. However, a short distance from the defect, spectra characteristic of normal zinc phosphate associated with a fair amount of iron were recorded. The coatings disbonded in KCl and CsCl showed that the amount of alkali metal cation present in the coating increased on going towards the delaminating front. Sodium ion could not be followed in this manner because a secondary zinc line in the EDS spectrum overlaps the primary sodium line.

The results presented show that the chemistry involved in the cathodic delamination of the Epanol coating from the phosphated steel surface is highly dependent on the cation of the electrolyte solution used. This fact is demonstrated by the different area of coating disbonded on changing the cation onf the electrolyte and the numerous molecular compounds detected by Raman spectroscopy. Although the chemistry is complex, a number of points can be made about the delamination of the organic coating from phosphated steel.

First, dissolution of the phosphate is the failure mechanism responsible for the organic coatings' loss of adhesion from the substrate. Evidence which supports this statement comes from the rates at which the coating is delaminated in different alkaline chlorides. Leidheiser and Wang [1] have

suggested that the rate controlling step in cathodic delamination is the migration of cations to the reaction zone for charge balance. The delamination rate in their experiments was greatest for cesium. The results presented in another section of this report demonstrated that sodium hydroxide dissolved a greater amount of phosphate per unit time followed by potassium hydroxide and then cesium hydroxide. The results reported in this program indicate that the rate-determining step in the cathodic delamination of organic films from phosphated steel is a combination of both dissolution of the phosphate coating and the rate at which cations migrate to the reaction zone. Rates of delamination for the phosphated steel sample were greatest for potassium chloride followed by cesium chloride, sodium chloride and lithium chloride. An explanation for this behavior follows. If cesium reaches the reaction zone more rapidly than potassium, the rate of delamination is slowed by the fact that cesium hydroxide is less destructive towards zinc phosphate than potassium hydroxide. The delamination rate is slower for sodium because, in this case, it takes longer for the sodium ions to reach the reaction zone. Thus, the delamination rate is greatest for potassium chloride solutions and slowest for lithium chloride solutions.

Second, the interface at which the failure occurs is the phosphate coating/substrate interface. Evidence which supports this statement is as follows. The cathodic reaction which generates the high pH must take place at the metal surface. The metal is the medium through which the electrons are supplied to the cathodic reaction. After the organic coating is delaminated, very little material is left on the metal substrate. A majority of Raman spectra was recorded at the delaminating front. Those spectra recorded in the region between the defect and the front were characteristic of a thin amorphous structure. The amount of carbon in the Raman spectra recorded for the delaminated region was greater than the amount shown for those spectra recorded on normal zinc phosphate. It was shown earlier that carbon is on the steel surface prior to phosphating. EDS analysis of the backside of the polymer films resulted in spectra characteristic of a normal zinc phosphate associated with a large amount of iron. The iron can only come from the substrate.

CONCLUSION

Taking into account the results presented, the following mechanism is proposed for the cathodic delamination of an organic coating from a zinc-phosphated steel surface. Figure 17 is presented to aid in the description. When a defect is initially formed in the cathodically protected coating system at high negative potentials, the dominant cathodic reaction is the evolution of hydrogen. Locally the solution around the defect attains a high pH and the phosphate is dissolved from the polymer down to the substrate in a small area around the defect. EDS spectra of the backside of the disbonded polymer film showed no phosphate in this region. As dissolution proceeds outward, the IR drop encountered decreases the effective potential at that point. Evidence for this comes from the fact that hydrogen evolution takes place only at the defect. At some point away from the defect the potential decreases to the

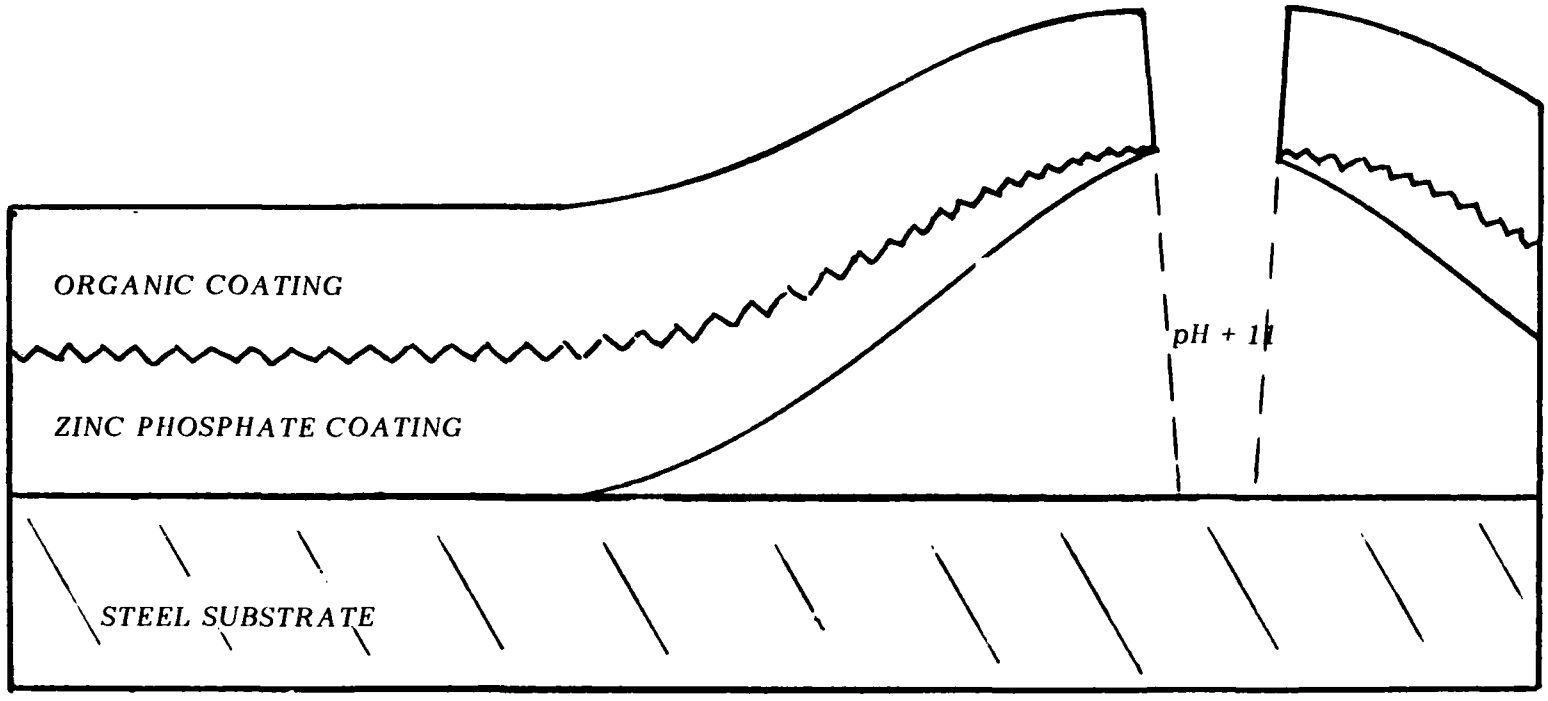

Reactions; At defect $2H^+ + 2e^- = H_2$ At the front $H_2O + 1/2O_2 + 2e^- = 2OH^-$

Dissolution of phosphate $Zn_3(PO_4)_2{:}4H_2O$ / $Zn_2Fe(PO_4)_2{:}4H_2O$ + $OH^- + CO_3^-$ = $Zn^{2+} + Fe^{2+} + OH^- + CO_3^- + PO_4^{3-}$

↓

vivianite, ferric phosphate, Fe_3O_4, zinc oxide, hydrozinzite, $ZnFe_2O_4$, and recrystallized phosphates.

Figure 17. Mechanism of cathodic delamination of phosphated steel surface.

point where the dominant cathodic reaction is the oxygen reduction reaction. From this stage on, the reaction increases the pH at the delaminating front. Cations migrate to the reaction zone and their combined effect, with the hydroxyl ions generated, dissolves the phosphate coating at the phosphate coating/interface. As delamination proceeds, the polymer film begins to blister due to the evolution of hydrogen and excess electrolyte.

REFERENCES

[1] H. Leidheiser, Jr., and W. Wang, "Corrosion Control by Organic Coatings," H. Leidheiser, Jr., Editor, NACE, Houston, p.70 (1981).

AD-A151 238 CORROSION CONTROL THROUGH A BETTER UNDERSTANDING OF THE METALLIC SUBSTRAT..(U) LEHIGH UNIV BETHLEHEM PA CENTER FOR SURFACE AND COATINGS RESE.. E M ALLEN ET AL. 3/3

UNCLASSIFIED 13 DEC 84 N00014-79-C-0731 F/G 11/3 NL

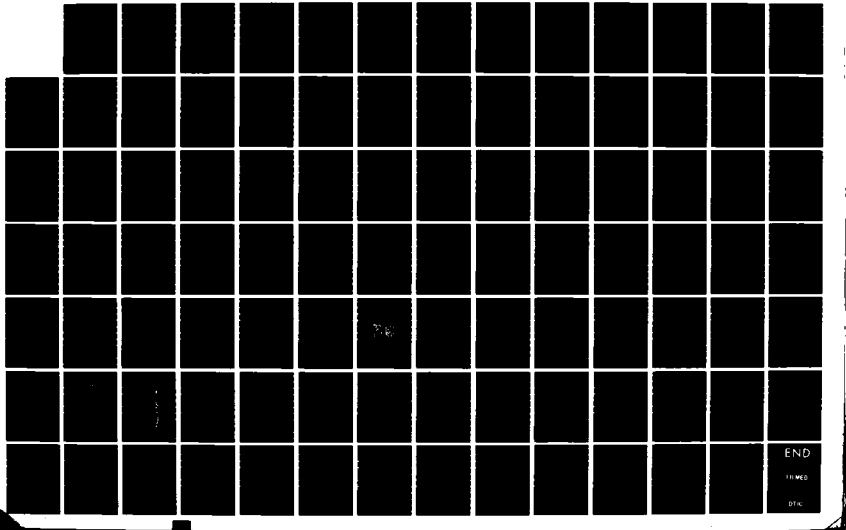

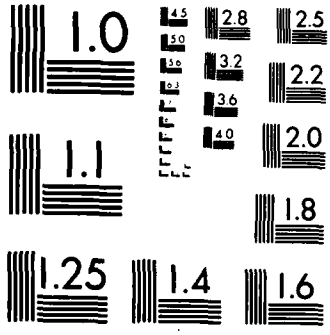

MICROCOPY RESOLUTION TEST CHART
NATIONAL BUREAU OF STANDARDS-1963-A

Program #9

Probe Molecules as a Means for Studying the Metal/Organic Coating Interface Using Raman Spectroscopy

Principal Investigator: Eugene M. Allen
Prof. of Chemistry

INTRODUCTION

It has been felt for a long time that a suitable probe molecule on a metal surface under an organic coating would provide a powerful means for the study of corrosion of the metal. Laser Raman microprobe spectroscopy is well suited to such a study because of its ability to look at microscopically small areas of the surface. But since corrosive reactions may be initiated on very thin layers on the surface, the use of one of the modern techniques for enhancing the Raman signal, such as resonance Raman spectroscopy (RRS) or surface-enhanced Raman spectroscopy (SERS), would be greatly desirable.

The RRS technique makes use of a molecule that has an absorption band which overlaps the wavelength of the laser beam. In our case, we generally use the 514.5 nm line of our laser, so in order to take advantage of RRS we would have to work with compounds that absorb strongly in the green region of the spectrum, most commonly having an orange or red shade.

The SERS effect relates to the tremendous enhancement of the Raman signal (ca. $\times 10^6$) when substances are adsorbed on certain metals, notably silver, copper and gold. The usual way of achieving adsorption is by the application of a potential to the metal immersed in a solution of the material being adsorbed. Probably the system that has received the greatest amount of study has been pyridine adsorbed on a silver electrode. The effect was first reported by Fleischmann et al., and then thoroughly studied by Van Duyne and co-workers. Van Duyne [1] provides a clearly written explanation and summary of the early work. A more recent summary of SERS is provided by Birke et al. [2].

Iron is not one of the metals that has been found to give the SERS effect. One possible way to study interfacial reactions under a coating would be to use silver as a model, and work with coated silver electrodes and a suitable probe molecule. We could study iron specifically, however, by making use of a combination of SERS and RRS, as will be discussed later.

In the present report, we describe the construction and testing of a cell suitable for use with SERS. We also present a possible RRS method using 2,2'-bipyridine as the probe molecule.

CONSTRUCTION OF SERS CELL FOR LASER RAMAN MICROPROBE

Although many electrochemical cells have been constructed for SERS, our particular laser Raman microprobe, which uses a microscope in its optical system, made it necessary to design and construct a new cell (Figure 1). The cell contains three electrodes: a working electrode, on which adsorption takes place; a reference electrode, against which the potential of the working electrode is measured; and a counter electrode, through which current flows during an electrochemical experiment.

To fill the cell, it is held vertically with stopcock A uppermost. All three stopcocks, A, B and C, are opened, the lower end of the cell adjacent to stopcock C is placed in the solution to be used, and suction is applied till the bulb adjacent to stopcock A is about three-quarters full. Stopcock C is then closed.

It is customary in SERS experiments to deoxygenate the solution in the cell with a stream of nitrogen. To do this, we continue to hold the cell vertical, connect the bottom tube to a nitrogen tank, open stopcock C, and pass nitrogen through the cell for five minutes at the fastest rate compatible with not losing any of the solution from the top. Stopcocks A and C are then closed; stopcock B is left open.

At this point, a considerable amount of nitrogen will be trapped in the cell. To get rid of all gas bubbles from the cell, we now vigorously jerk the cell downward and continually repeat that motion, always keeping the cell vertical, stopcocks A and C closed, and B open. This downward sweep will have the effect of forcing the liquid from the bulb into the cell and the gas from the cell upward into the bulb. When the cell is free of gas, we close stopcock B and detach the bulb at the ground glass joint.

The receptacle for the reference electrode functions as a salt bridge, and is filled with 5% sodium sulfate solution. The bottom of the receptacle forms a capillary, the so-called Luggin capillary, that maintains electrical contact with the cell contents while minimizing loss of salt bridge solution into the cell. The top of the cell is formed from a circular glass disk about 2.5 cm in diameter. The disk is the section that goes directly underneath the microscope objective.

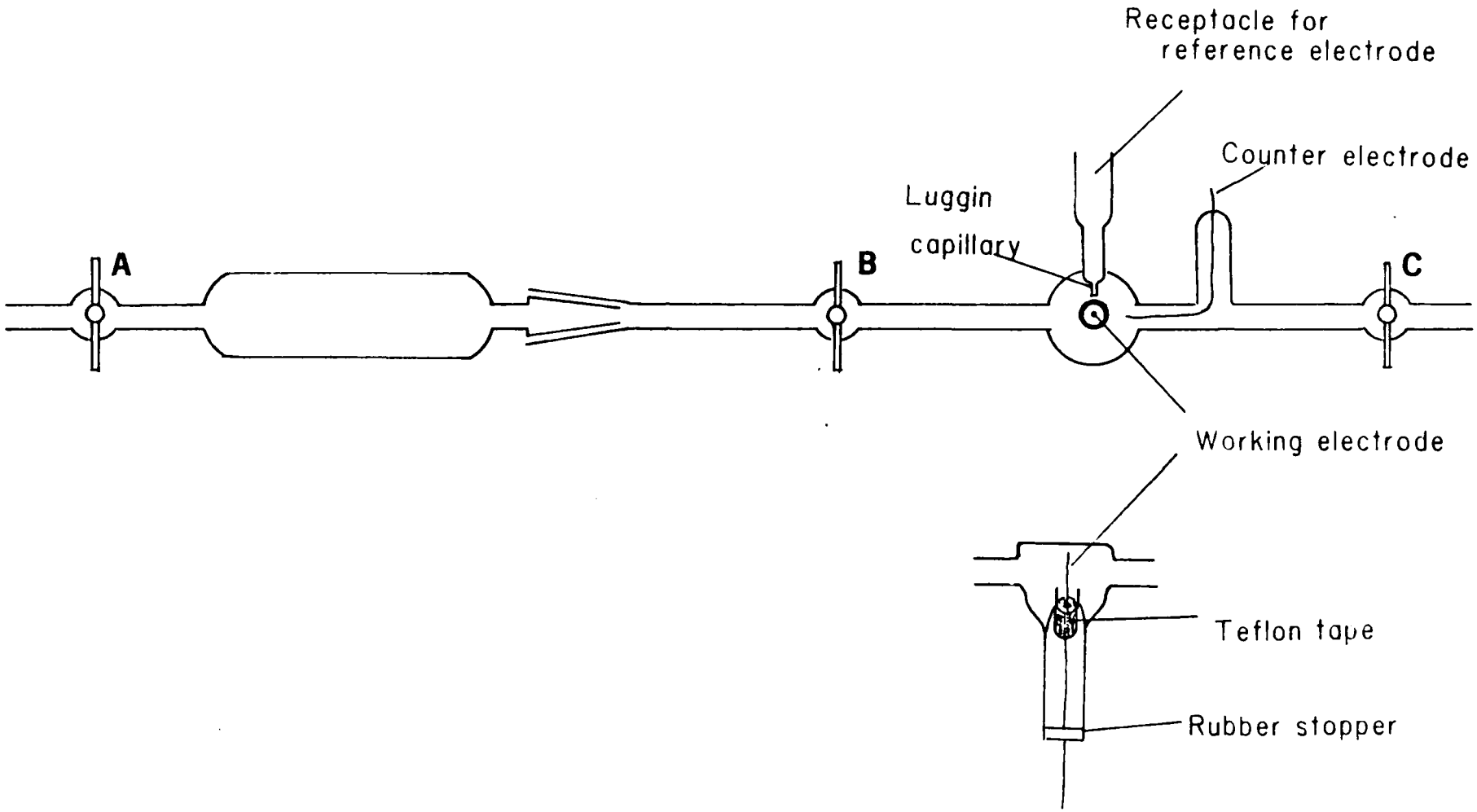

Figure 1. Cell for SERS on Laser Raman Microprobe.

The laser beam strikes one point at the end of the working electrode, which is pushed up so that it almost touches the top glass disk. A plug made of Teflon tape surrounding the electrode, as shown in the diagram, prevents the cell contents from leaking out; the electrode plus plug are held in place by a rubber stopper.

The counter electrode is a piece of platinum wire, sealed into its tube with Torr-Seal® epoxy resin.

Testing of SERS Cell

We verified that the cell was functioning properly by repeating the well-studied pyridine on silver experiment. We followed the procedure of Jeanmaire and Van Duyne [3], and used a 50 m M pyridine solution in 0.1M potassium chloride. We prepolished the silver electrode on 600 mesh abrasive, and subjected the electrode to a single, double potential step anodization procedure (-0.6 v to +0.2 v for ca. 2 sec, back to -0.6 v vs. S.C.E.) with the solution in place in the cell. We then ran Raman spectra from the surface of the electrode at -0.2 v, -0.4 v, -0.6 v and -0.8 v, confining the spectra to the region between 1000 cm^{-1} and 1650 cm^{-1}. The laser power was 500 mW at the source, and the scan rate was 50 $cm^{-1}sec^{-1}$.

The following figures show a comparison between the peaks found in the region specified above by Jeanmaire and Van Duyne [3] as compared to those found by us, both on the spectrum run at -0.6 v. We see that very good agreement has been obtained.

Jeanmaire and Van Duyne [3]	This Work
1006 cm^{-1}	1005 cm^{-1}
1035	1034
1215	1215
1594	1593

Our spectrum run at -0.6 v is shown in Figure 2.

Figure 3 displays the four spectra in order, with -0.2 v at the top and -0.8 v at the bottom. The following features found by Jeanmaire and Van Duyne are confirmed in our spectra: the increase in intensity of the 1215 cm^{-1} line from practically nothing at -0.2 v to a maximum at -0.8 v, and the increase in intensity of the 1593 cm^{-1} line from practically nothing at -0.2 v to a maximum at -0.6 v, followed by a decrease at -0.8 v.

We therefore conclude that the cell is functioning as it should and giving reliable results.

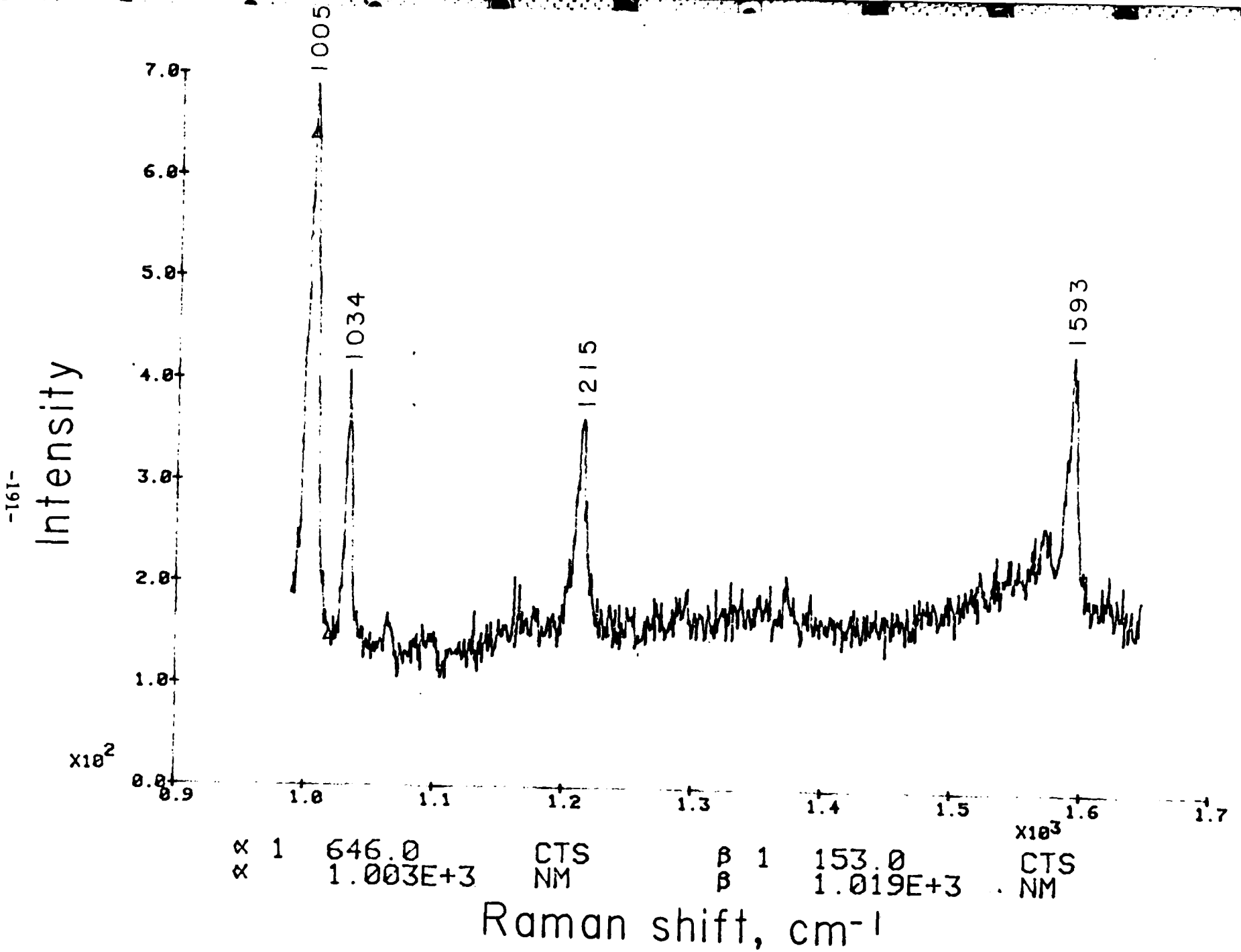

Figure 2. SERS spectrum for adsorbed pyridine on silver electrode at -0.6 volt.

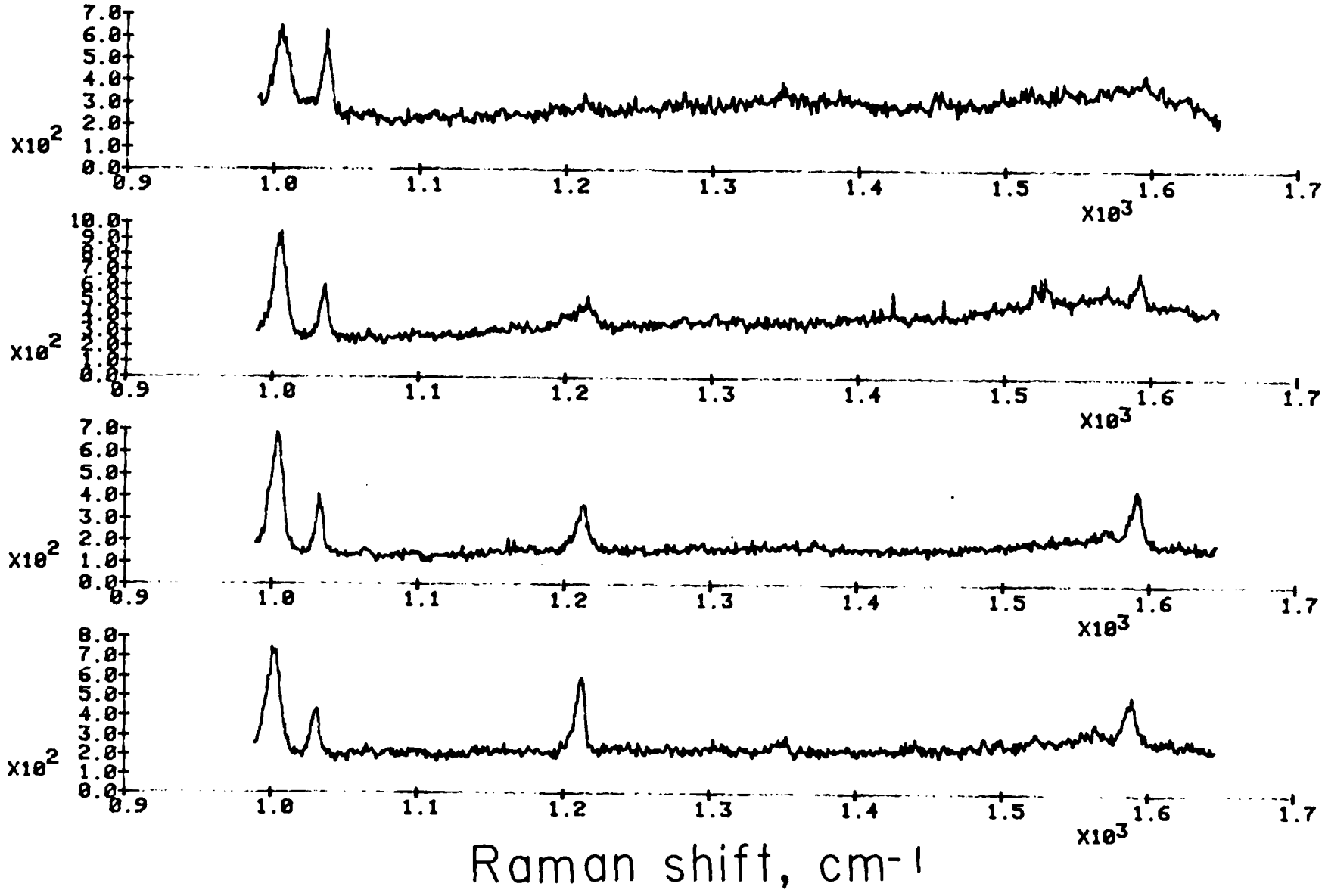

Figure 3. SERS spectra for adsorbed pyridine on silver electrode at various voltages. Top to bottom: -0.2 v, -0.4 v, -0.6 v, -0.8 v.

RRS AND SERS IN COMBINATION ON IRON

Van Duyne and Janik-Czachor [4] postulate that theoretically iron would be expected to show a SERS effect of only ca. 10^2, below that necessary to detect adsorbed monolayers. Combined with RRS, however, it might be possible to obtain meaningful spectra from monolayer-adsorbed species. To test this possibility, they worked with 1,10-phenanthroline (phen), which forms a deeply red complex with ferrous ion. Since the molar absorptivity of the complex at 514.5 nm is very high, conditions are favorable for RR.

They prepared a solution of synthesized $Fe(phen)_3^{2+}$ at 5×10^{-6}M, a concentration so low that one would not expect to obtain a Raman spectrum from solution. They then immersed a silver electrode at -0.8 v, and obtained a strong spectrum from the surface of the electrode, presumably because of both SERS and RRS working on adsorbed species.

The next step was to see if an iron electrode would give usable spectra. They prepared a solution of phen at 5×10^{-3}M, a much higher concentration, and immersed an iron electrode at -0.5 v, which is an anodic potential for iron and means that iron was being dissolved to form ferrous ion. They obtained a spectrum that was clearly identical with the one obtained from known $Fe(phen)_3^{2+}$ on a silver electrode. Evidence from depolarization ratios, however, indicated that the Raman signal probably did not arise solely from adsorbed species but bulk species (in solution) contributed an unknown amount.

We ran a similar experiment with 2,2'-bipyridine (bipy), which also forms a deeply colored red complex with ferrous ion. We prepared a 5×10^{-6}M solution of $Fe(bipy)_3^{2+}$ by mixing solutions of ferrous sulfate and bipy, and added potassium sulfate to 0.1M. We used a silver electrode which was polished and anodized as described above. We applied -0.8 v to the electrode, and ran a Raman spectrum from 900 cm^{-1} to 1650 cm^{-1} (see Figure 4). The laser power was 200 mW. Following is a comparison between the peaks we found and the known values for a bulk solution of this complex reported in a paper by Clark et al. [5]. Note: The strong peak at 1123 cm^{-1} arises from a mercury emission line coming from a fluorescent desk lamp. We keep this lamp on deliberately, so as to obtain this line on the spectrum, which we use for calibration.

Clark et al. [5]		This Work
Frequency, cm^{-1}	Intensity	Frequency, cm^{-1}
1025	med.	1026
1035	med. weak	----
1067	weak	----
1109	med. weak	----
1173	med. strong	1173
1277	med.	1278
1321	strong	1320
1490	very strong	1489
1563	strong	1561
1607	med. strong	1604

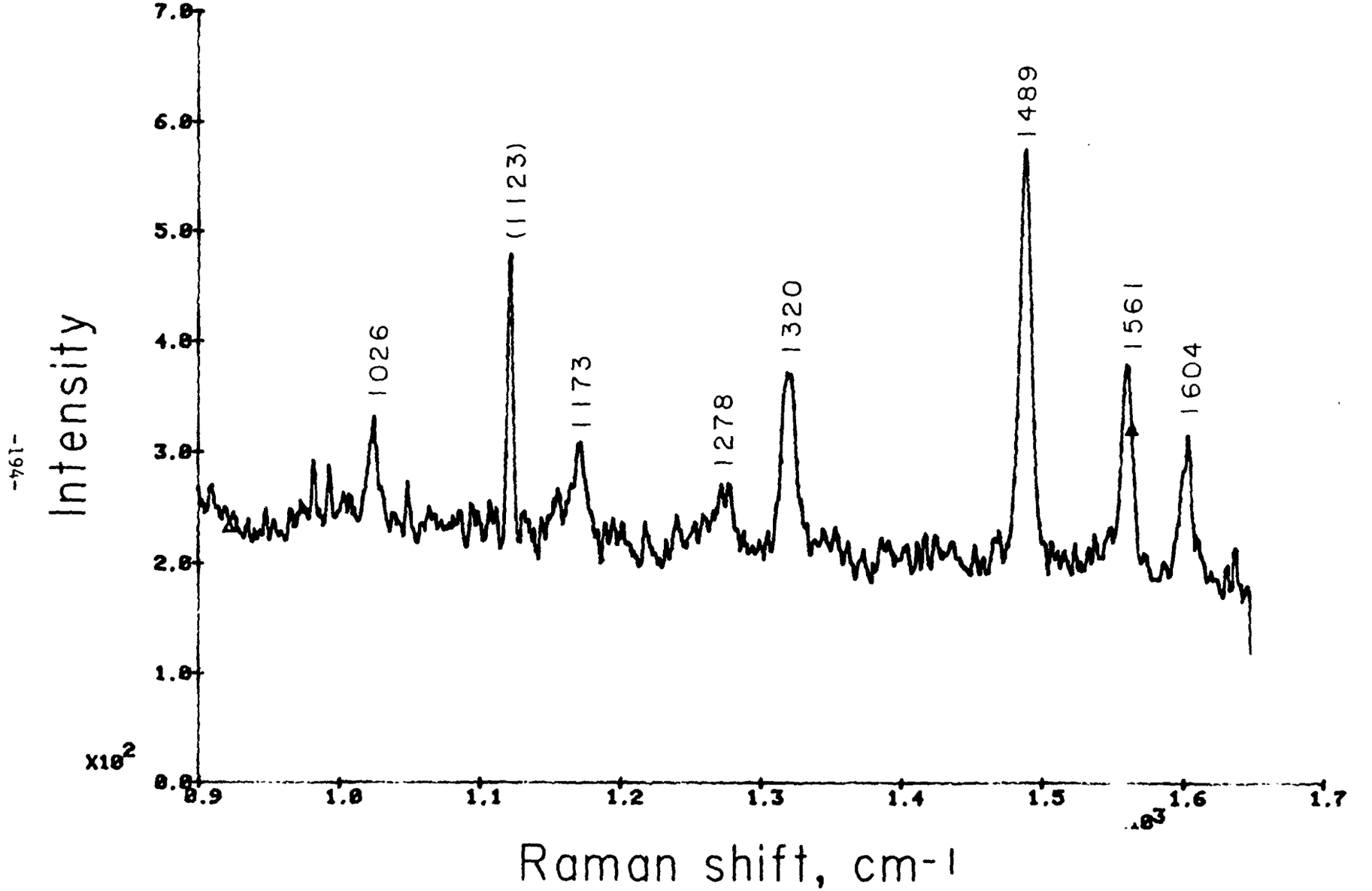

Figure 4. SERS spectrum for adsorbed $Fe(bipy)_3^{2+}$ on silver electrode at -0.8 volt.

Since the solution was presumably too weak to yield a spectrum, the strong indication is that we have a RRS plus SERS spectrum of adsorbed $Fe(bipy)_3^{2+}$ that agrees with the one reported in the literature for that ion in solution.

Further proof that the spectrum is typical for SERS is shown in Figure 5. The top spectrum is a duplication of the one in Figure 4, run at -0.8 v. The middle spectrum was run at 0.0 v, at which potential no adsorption of the complex cation would be expected [4] and, in fact, the peaks have practically disappeared. On rerunning the spectrum at -0.8 v, the peaks reappear as before (bottom spectrum).

We then prepared a solution of 1×10^{-3}M bipy in 0.1M potassium sulfate, and ran a spectrum from the surface of an iron electrode (99.999% pure). We used -0.5 v, and a laser power of 700 mW. The spectrum was noisy, but showed clearly the four strongest peaks of Figure 4. The solution was pink, however, and we found in another experiment that we could obtain a spectrum even with the potentiostat turned off. We have therefore not proved conclusively that we have obtained a spectrum from adsorbed species. This approach looks promising, however, and deserves further experimentation.

A POSSIBLE PROBE MOLECULE FOR WATER

It occurred to us, as a result of the experiments just described, that if bipy in aqueous solution, but not in the solid state, would react with iron on steel to give the red complex, which could then be detected by the Raman microprobe, we would have a very sensitive test for water under a coating. A layer of solid bipy would be applied to the surface, followed by the coating. Any water that would appear under the coating would then form $Fe(bipy)_3^{2+}$, and could be picked up by the microprobe, provided that the coating is translucent and non-fluorescent. The sensitivity of this detection would be greatly enhanced by the RRS effect.

To test this idea in a preliminary way, a Raman spectrum of solid bipy was first run, and is shown in Figure 6. We then dropped 2 ml of a solution of 25 mg of bipy in 25 ml of absolute alcohol, a little at a time, onto a steel panel, allowing each portion to evaporate. This treatment left a thin film of bipy on the panel. Then we placed two drops of water on the panel on two separate spots, and allowed the drops to evaporate over the course of one hour. After this time, we ran many spectra on various parts of the panel, confining the instrument to the region between 1440 cm^{-1} and 1510 cm^{-1} to save time. A bipy spot should give peaks at 1447 cm^{-1} and 1482 cm^{-1}, while a $Fe(bipy)_3^{2+}$ spot should give a single peak at 1489 cm^{-1}. We found bipy spots but no $Fe(bipy)_3^{2+}$ spots in the areas where there had been no water, showing that solid bipy did not react with the steel in this time. But we did find many $Fe(bipy)_3^{2+}$ spots in the areas where there had been water, showing that bipy in solution did indeed react with steel to produce the complex. In Figure 7, the top figure shows the spectrum of a typical bipy spot, the middle, of a typical $Fe(bipy)_3^{2+}$ spot, and the bottom (from the water drop area), of a bipy spot in the process of changing to a $Fe(bipy)_3^{2+}$ spot.

This approach is a very interesting one, and we will actively pursue it.

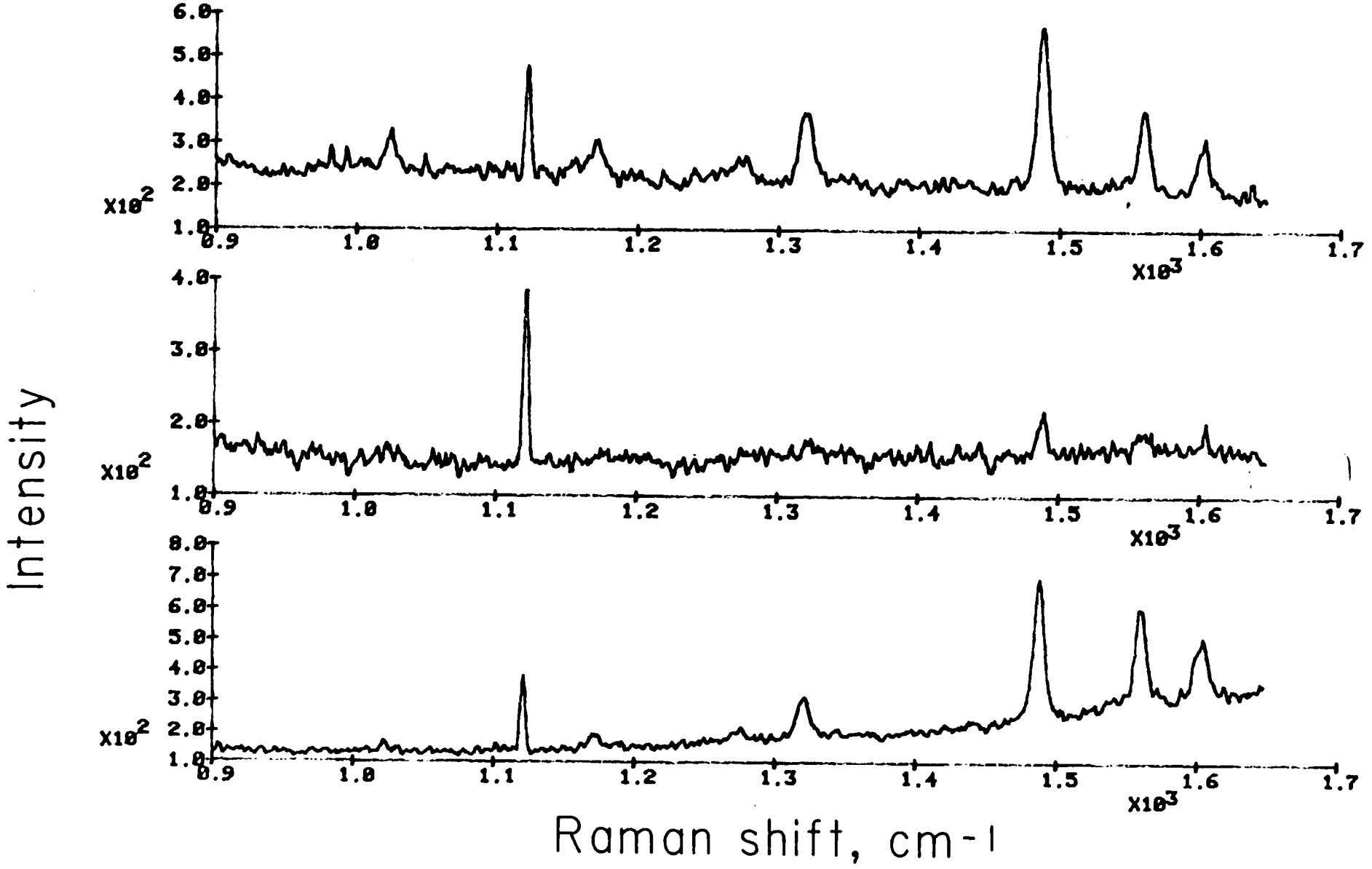

Figure 5. SERS spectra for adsorbed $Fe(bipy)_3^{2+}$ on silver electrode. Top: -0.8 volts; middle: 0.0 volts; bottom: back to -0.8 volts.

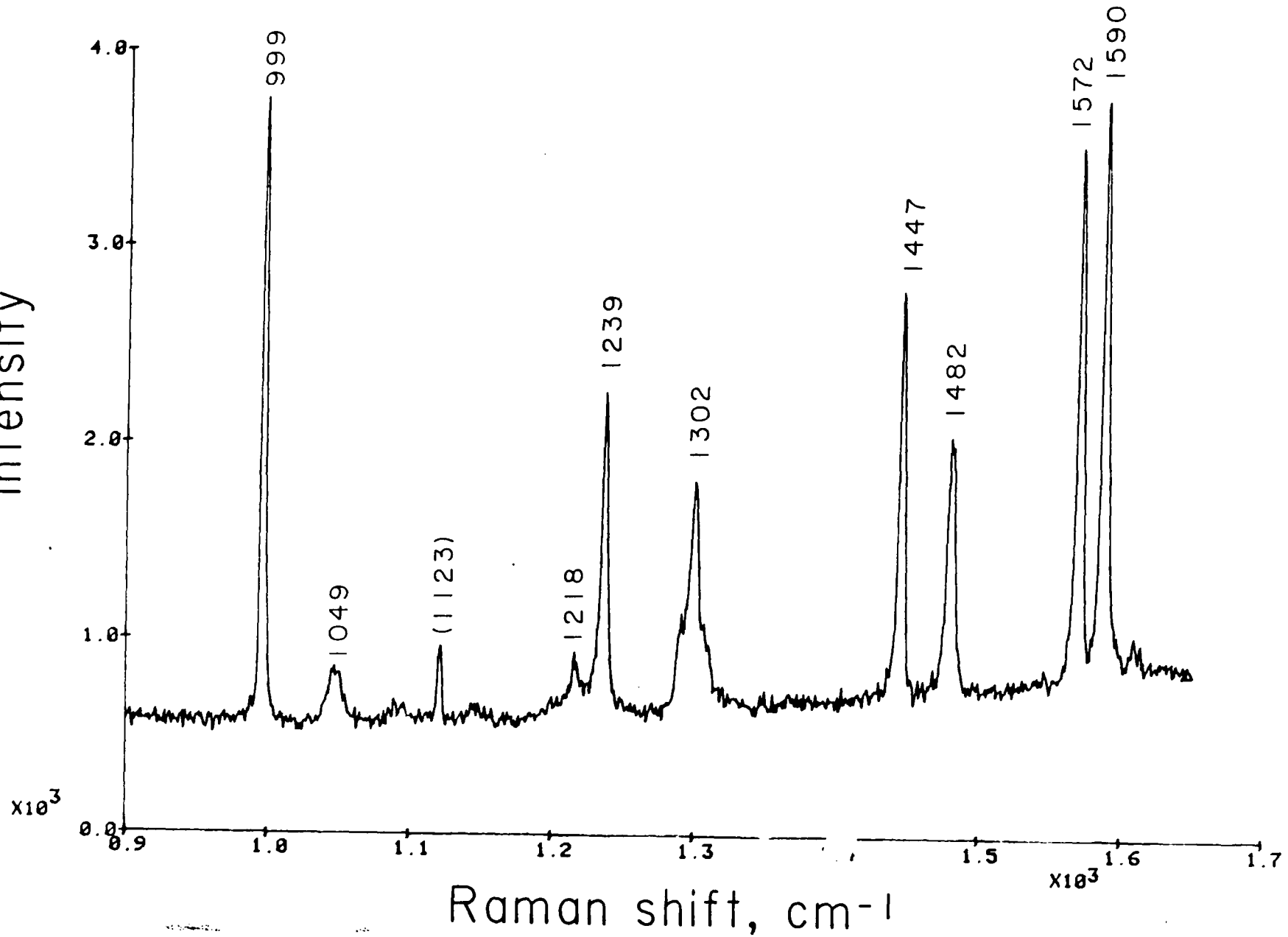

Figure 6. Raman spectrum of solid bipy.

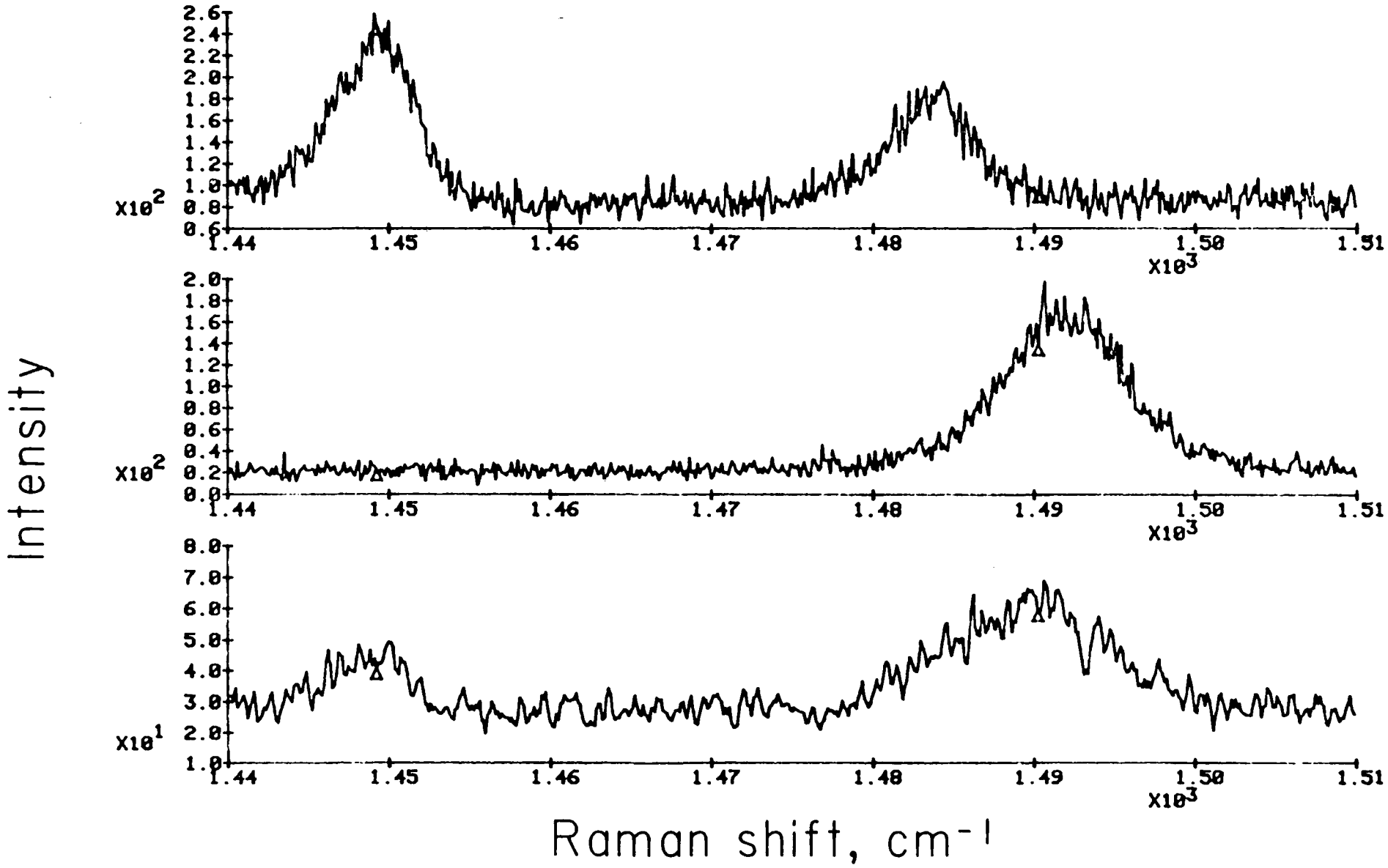

Figure 7. Raman spectra of steel panel. See text for explanation.

ACKNOWLEDGMENT

We are greatly indebted to Dr. James Sturm for his major contribution to the design of the electrochemical cell, and for constructing it.

REFERENCES

[1] R. P. Van Duyne, in "Chemical and Biochemical Applications of Lasers," C. B. Moore, ed., New York, Academic Press, 1979, Vol. 4, Chapter 5.

[2] R. L. Birke, J. R. Lombardi and L. A. Sanchez, in Advances in Chemistry Series, No. 201, "Electrochemical and Spectrochemical Studies of Biological Redox Components," K. M. Kadish, ed., American Chemical Society, 1982, Chapter 4.

[3] D. L. Jeanmaire and R. P. Van Duyne, J. Electroanal. Chem. 84, 1-20 (1977).

[4] R. P. Van Duyne and M. Janik-Czachor, J. Electrochem. Soc.: Electrochemical Science and Technology 130, 2320-23 (1983).

[5] R. J. H. Clark, P. C. Turtle, D. P. Strommen, B. Striesand, J. Kincaid, and K. Nakamoto, Inorg. Chem. 16, 84 (1977).

Program #10

High Frequency Dielectric Spectroscopy of Water in Organic Coatings

Principal Investigator: Henry Leidheiser, Jr.
Prof. of Chemistry

Associate: Douglas Eadline
(Ph.D. awarded)

INTRODUCTION

High frequency dielectric measurements have been introduced and outlined in previous reports [1]. The detailed development and application of the lumped capacitor cell are given in reference [2]. Presented in this report is the preliminary application of high frequency dielectric spectroscopy in studies of water in organic coatings.

An investigation of several organic coatings was attempted using the lumped capacitor cell. The coatings were applied to copper coupons and allowed to sorb water normally towards the metal interface. Dielectric measurements were conducted as a function of time and conclusions about the mode of water uptake are suggested.

Research indicates exposure of water to polymers in some cases has led to physical damage of the polymer [3-6]. Other results have shown the diffusion constant of water through several epoxy films to be independent of water vapor pressure [7]. The reason cited by the authors was the formation of clusters at high vapor pressure that did not contribute to the diffusion. Studies have also been performed on water diffusion through polyethylene with an applied potential [10,11]. The authors found that pretreatment (reticulation) or the presence of an electrical field did not influence water diffusion. Clustering of water within the reticulated sample was also suggested as an explanation for the sample having an increase in water content with no increase in diffusion rate. As mentioned previously, osmotic pressure can cause water to condense at the polymer-substrate interface that has been contaminated by a salt [8,9]. Thus, water may interact with polymers and with the polymer-substrate system in a variety of ways.

Sample Preparation and Method of Water Exposure

The three coating systems studied are a vinyl ester, an acrylic, and an alkyd base paint. Each coating was prepared according to the manufacturer's instructions and placed on a copper coupon 0.002 inch thick. The coatings were applied using a small paint brush because attention had to be given to the size of the coating so as not to exceed the diameter of the outer conductor of the sample cell. The coatings were exposed to water by filling a Pasteur pipette with distilled water, sealing the small end with parafilm, and placing the open end of the pipette vertically on top of the coating. The pipette was brought into direct contact with the coating to allow a constant supply of water on top of the coating.

The coatings were removed from the water and weighed before each measurement. The presence of silicon grease on the back of the sample coupon from the back pressure bolt presented a problem when weighing the sample. Even though the grease was dissolved and wiped away with toluene, the weight measurements cannot be considered an accurate indication of water uptake. An estimation of the water uptake was made after the dielectric measurements were completed. All the samples were dried in an oven and stored for several days in a vacuum desiccator. The samples were then reexposed to water as before. Weight measurements without the grease cleaning step were recorded and used as an indication of coating water uptake. The weight gain measurements are interpreted in a general sense and are only intended as a rough indication of the water uptake for the coatings tested [11].

MEASUREMENTS OF COATING SYSTEMS

The Vinyl Ester System

The vinyl ester coating was obtained from Con/Chem Inc., Hawthorne, California. The coating was prepared with a two-part promoter consisting of (a) .15% cobalt naphthenate and (b) CHP catalyst 1-2%. The coating was left at ambient conditions overnight and then baked at 60°C for two hours. Figures 1, 2, and 3 are representative results for the vinyl ester system. Table I gives a listing of the exposure time and tan δ at log frequency 8.718 Hz.

The data in Figure 1 show a significant loss is present in the sample that has not yet been exposed to water. The loss is probably due to a mechanism of the host polymer. Addition of water enhances the loss as can be seen in Figures 2 and 3. From Table I the value of tan δ increases rapidly and then levels off after about 90 hours. The water uptake data are given in Figure 4.

The results indicate that for the vinyl ester the water is initially sorbed by the polymer similar to polyvinyl acetate [1]. The vinyl ester, however, did not exhibit any physical signs that water was being sorbed. Inspection of the weight measurements in Figure 4 shows similar behavior to the dielectric data, an initial increase followed by a leveling off of the water sorption

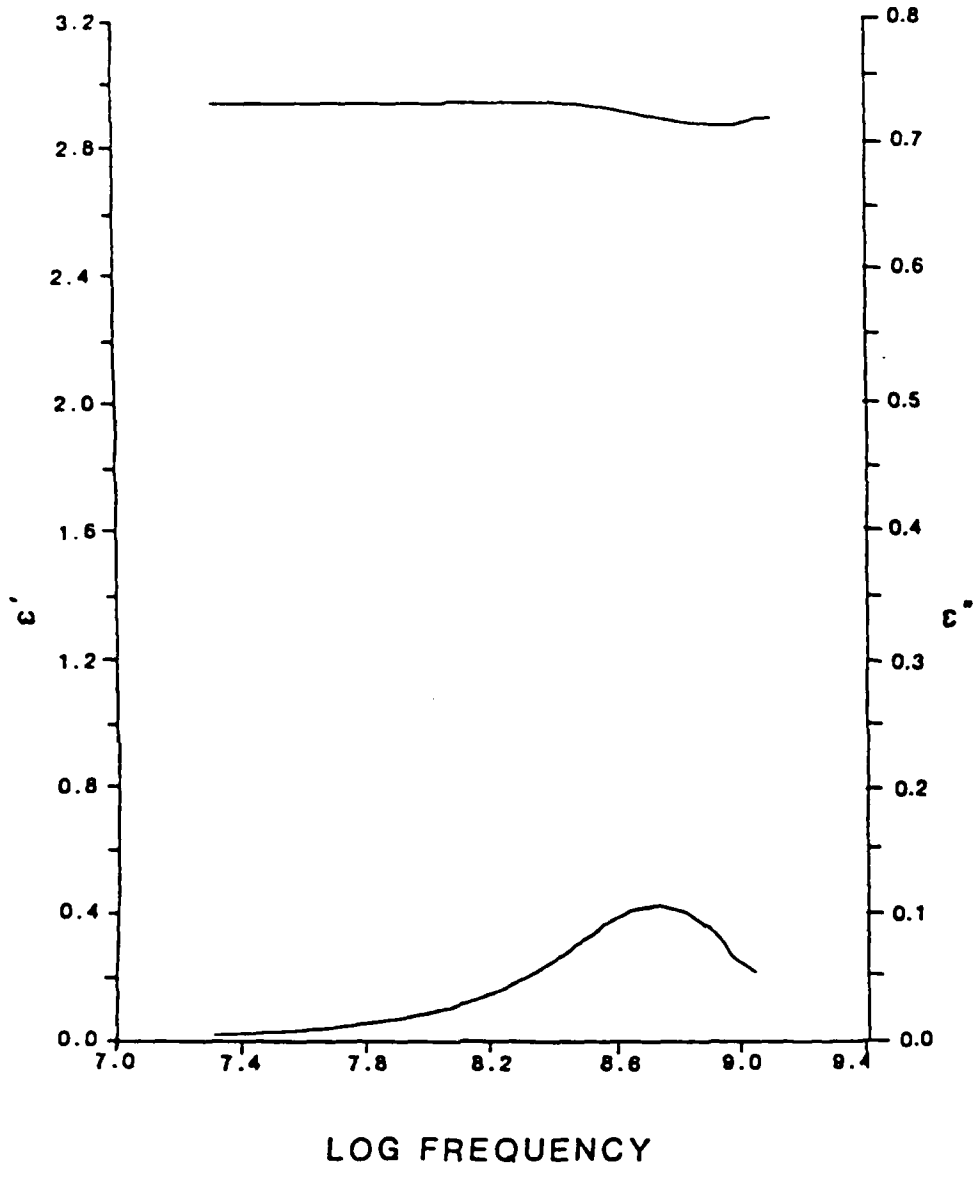

Figure 1. Dielectric response for unexposed vinyl ester sample. Sample was stored in a desiccator prior to measurement.

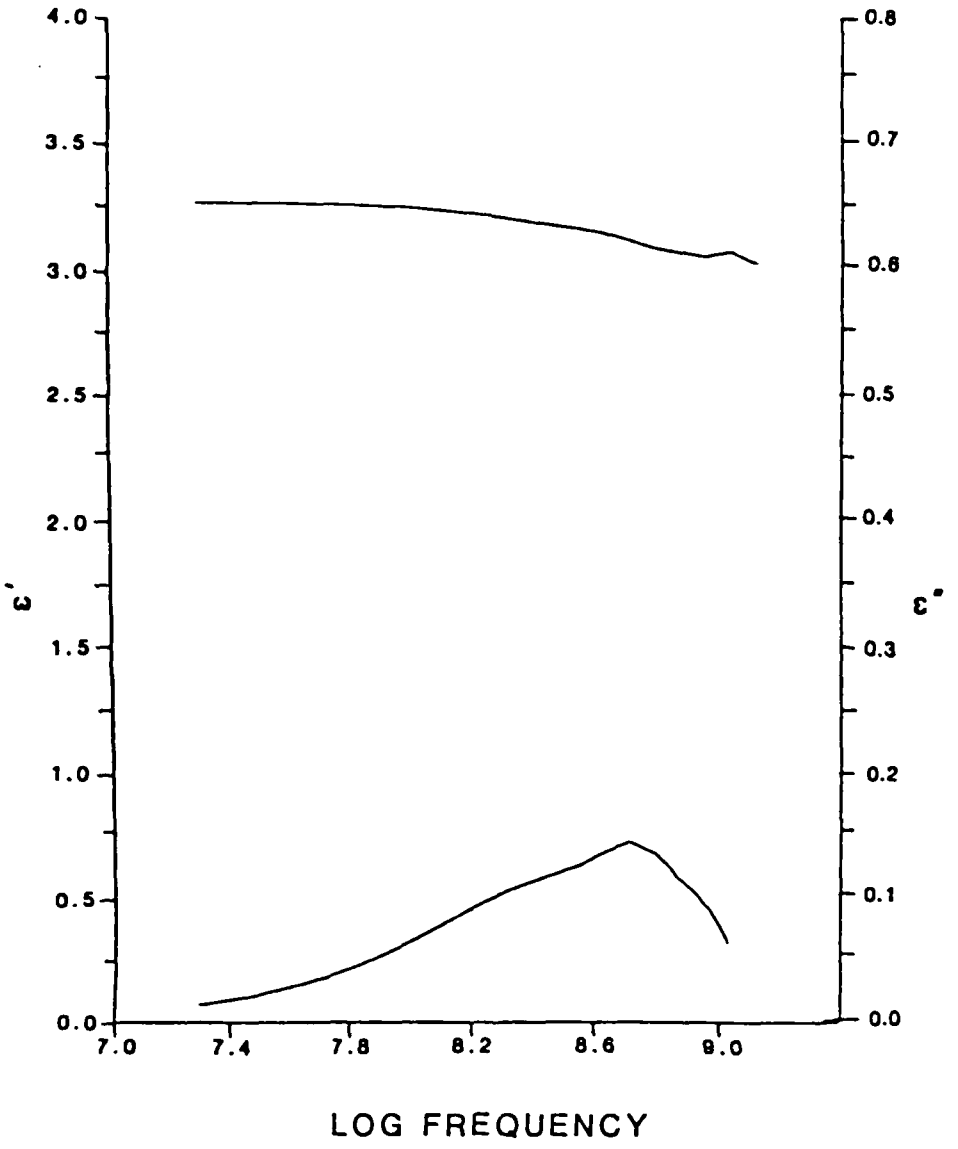

Figure 2. Dielectric response for exposed vinyl ester sample. Sample was exposed to distilled water for 141 hours.

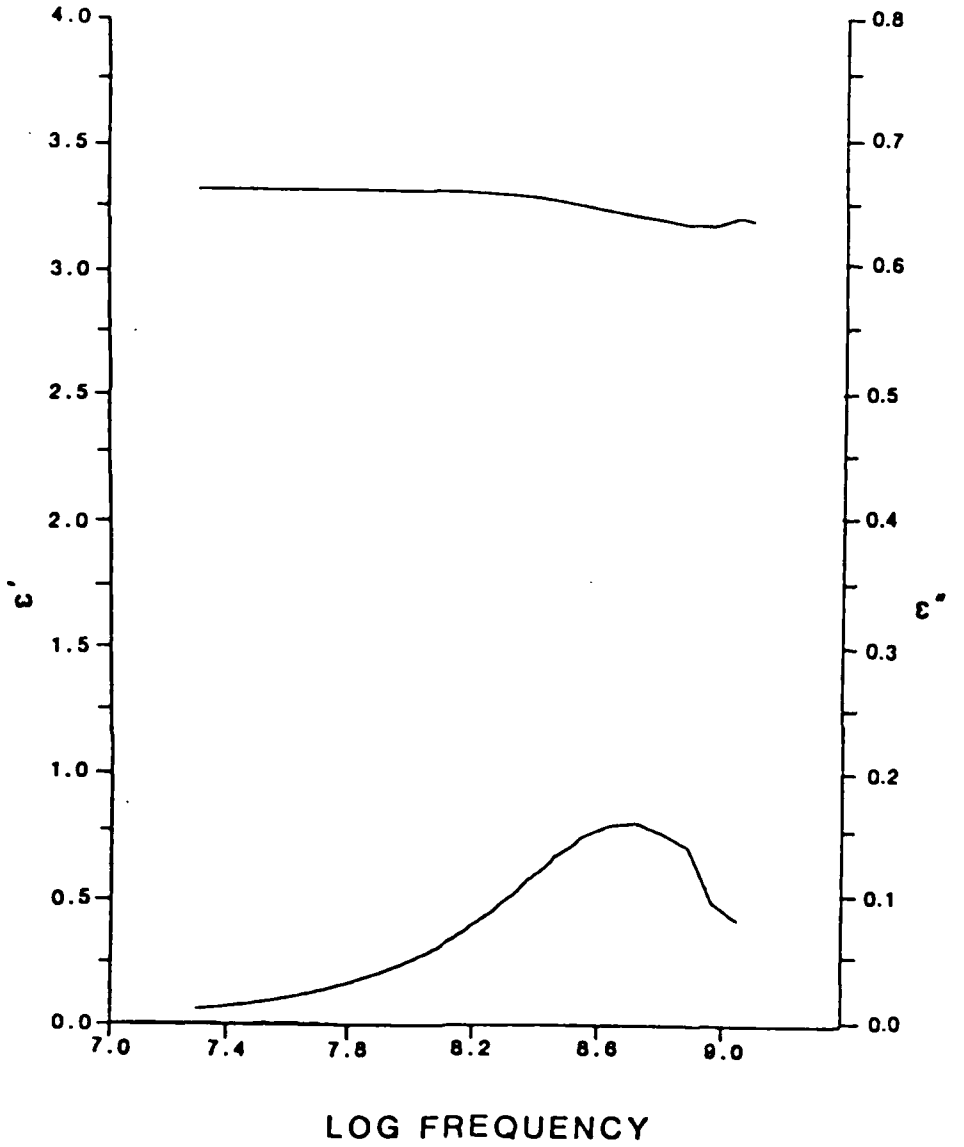

Figure 3. Dielectric response for exposed vinyl ester sample. Sample was exposed to distilled water for 254 hours.

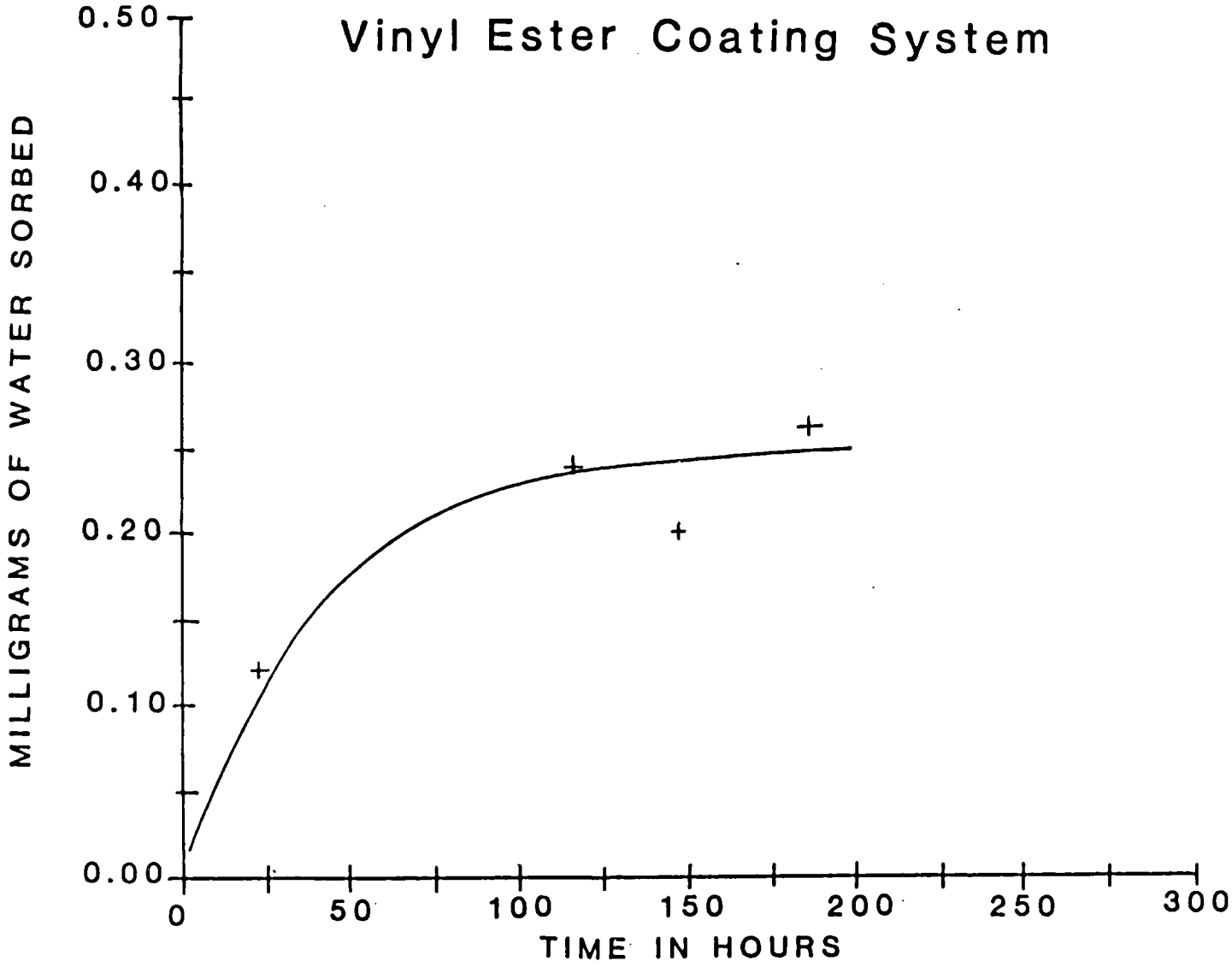

Figure 4. Gravimetric water uptake for vinyl ester coating system.

Table I

Sample	Time Between Measurements	Total Time	Tan δ at Log Frequency 8.718
*Vinyl 1	0	0	0.037
Vinyl 2	47	47	0.040
Vinyl 3	44	91	0.048
*Vinyl 4	50	141	0.047
Vinyl 5	47	188	0.046
*Vinyl 6	66	254	0.048

*Dielectric spectrum given in figures.

data. Assignment of the loss for the vinyl ester is difficult without some knowledge of the chemical structure. The coating system is a commercial product and at this point the structure is unknown.

The Acrylic System

The acrylic system is produced by Rohm and Haas under the trade name Acryloid B48N. The coating was air dried overnight and then baked for one-half an hour at 80°C. Figures 5, 6, and 7 are representative results for the acrylic system. The exposure history is given in Table II along with tan δ for log frequency 8.71 Hz.

Table II

Sample	Time Between Measurements	Total Time	Tan δ at Log Frequency 8.718
*Acry 1	0	0	0.022
Acry 2	8	8	0.025
*Acry 3	24	32	0.029
Acry 4	50	82	0.031
*Acry 5	46	128	0.034

*Dielectric spectrum given in figures.

The acrylic coating is 140 μm thick.

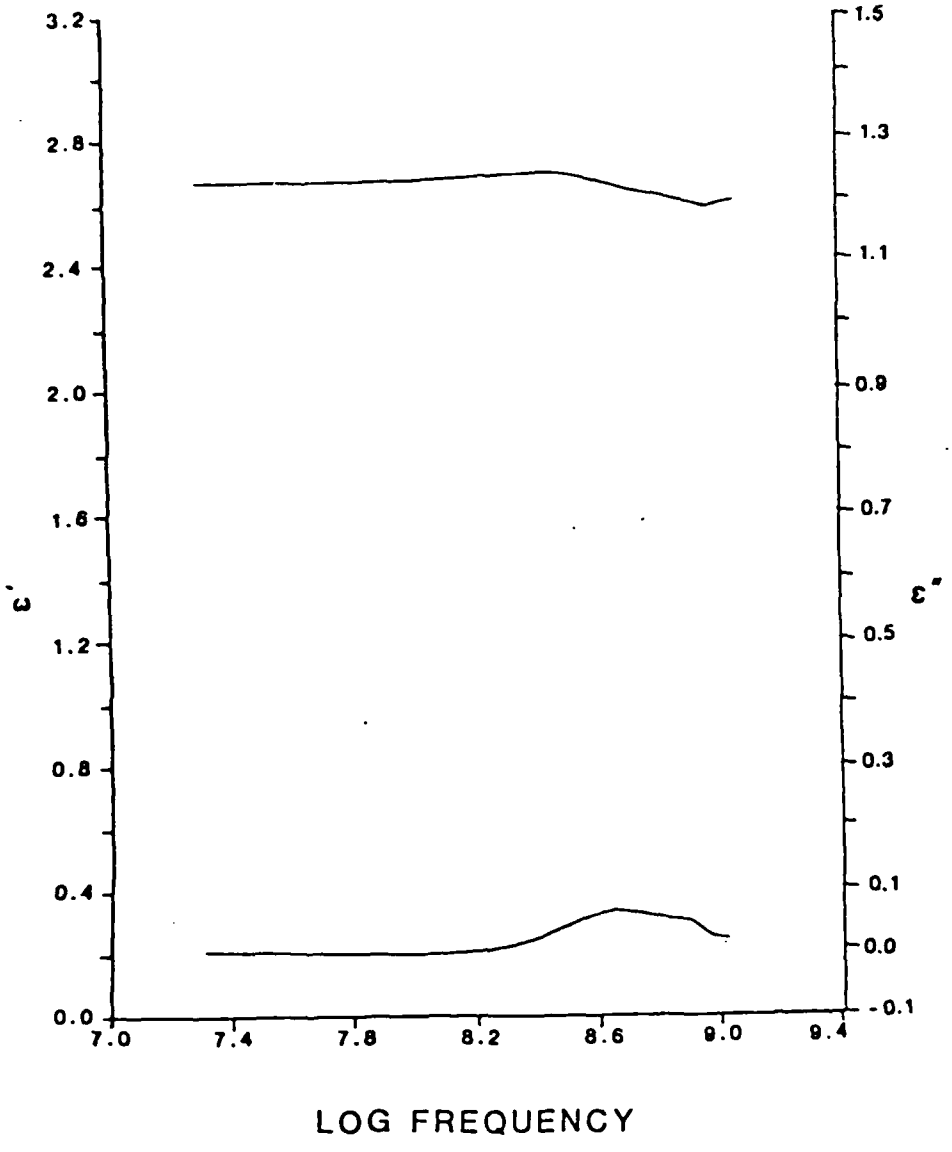

Figure 5. Dielectric response for unexposed acrylic sample. Sample was stored in a desiccator prior to measurement.

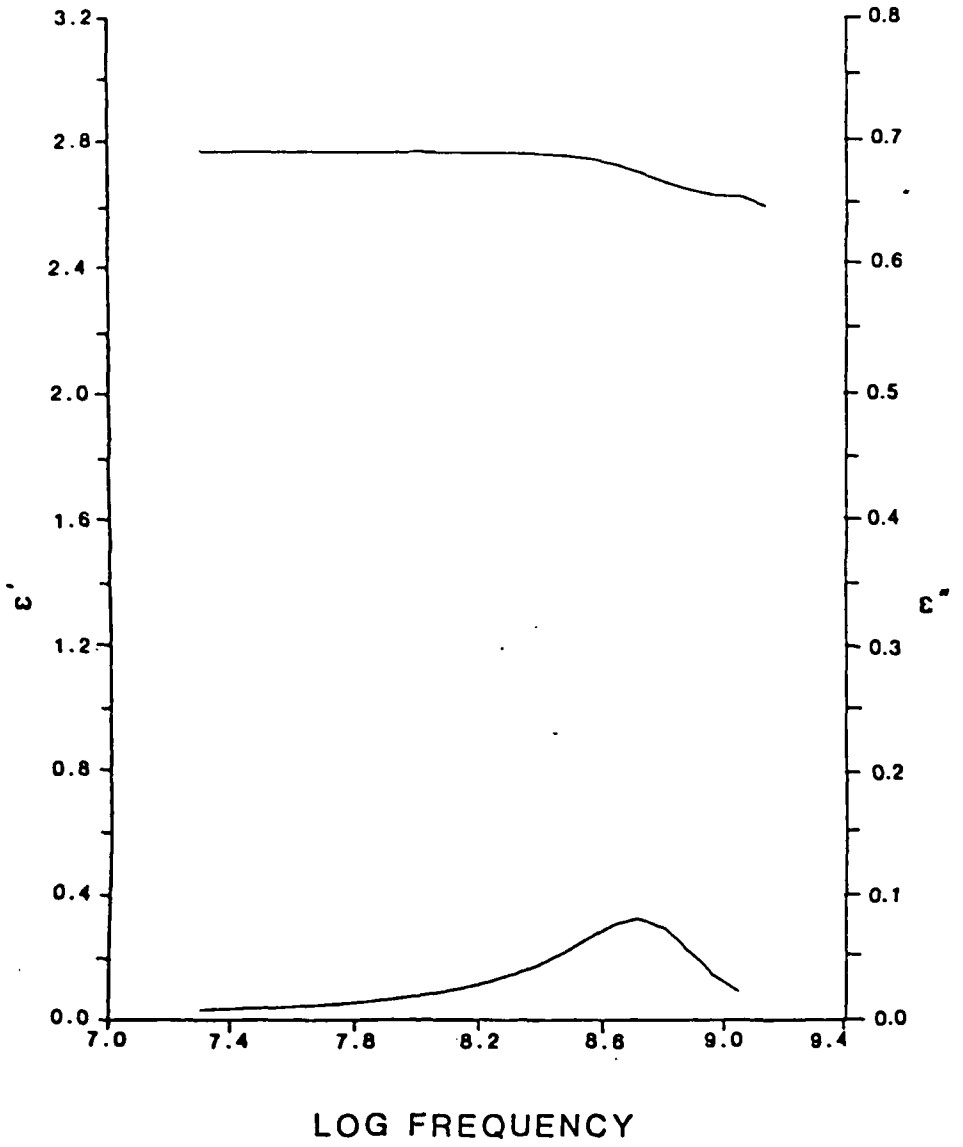

Figure 6. Dielectric response for exposed acrylic sample. Sample was exposed to distilled water for 32 hours.

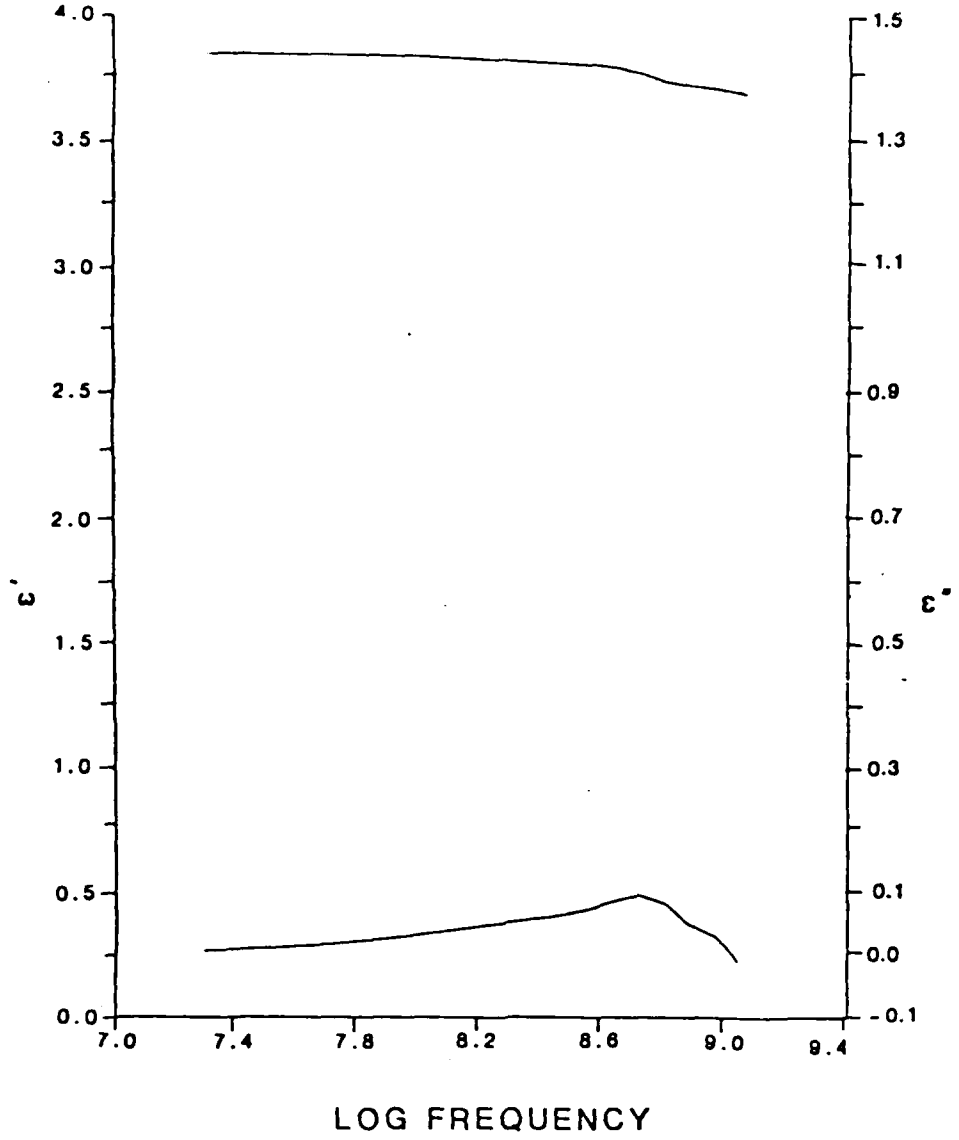

Figure 7. Dielectric response for exposed acrylic sample. Sample was exposed to distilled water for 128 hours.

The dielectric response given in Figure 5 for the acrylic system indicates a small dielectric loss. The addition of water causes an associated increase in tan δ at log frequency 8.718. Table II shows that the increase in loss intensity continued throughout the experiment. The water uptake data are given in Figure 8. The sample also became cloudy at the point of water contact after about 80 hours.

Interpretation of the dielectric response in Figure 5 is difficult because of the small amplitude of the loss. The increase in tan δ may be due to either water molecules associating with a loss mechanism of the host polymer or water collecting somewhere in the polymer with an associated loss at higher frequency. The water uptake data also tend to increase with time. Again, because the coating is a commercial product, the chemical structure is unknown, and assignment of the loss is difficult. The onset of cloudiness may indicate water is forming clusters. The dielectric data show no evidence for clustering, however.

The Alkyd System

The alkyd system used was manufactured by the Rust-Oleum Corporation, Evanston, Illinois. Two primer coats (7773 Clean Metal Primer) and two top coats (7791 Satin White) were applied to the copper substrate. Each coat was allowed to dry 12 hours and baked at 50°C for one hour. The water exposure record is given in Table III. Representative results are given in Figures 9, 10, and 11.

Table III

Sample	Time Between Measurements	Total Time	Tan δ at Log Frequency 8.384
*Alkyd 1	0	0	0.024
Alkyd 2	8	8	0.045
*Alkyd 3	24	32	0.067
Alkyd 4	50	82	--
*Alkyd 5	46	128	0.117†

*Dielectric spectrum given in figures.
†Sample became conductive.
The alkyd coating is 200 μm thick.

The results for the unexposed alkyd system in Figure 9 indicate a small dielectric loss with a maximum at log frequency 8.71 Hz. Upon exposing the sample to water, a second larger dielectric loss appears at log frequency

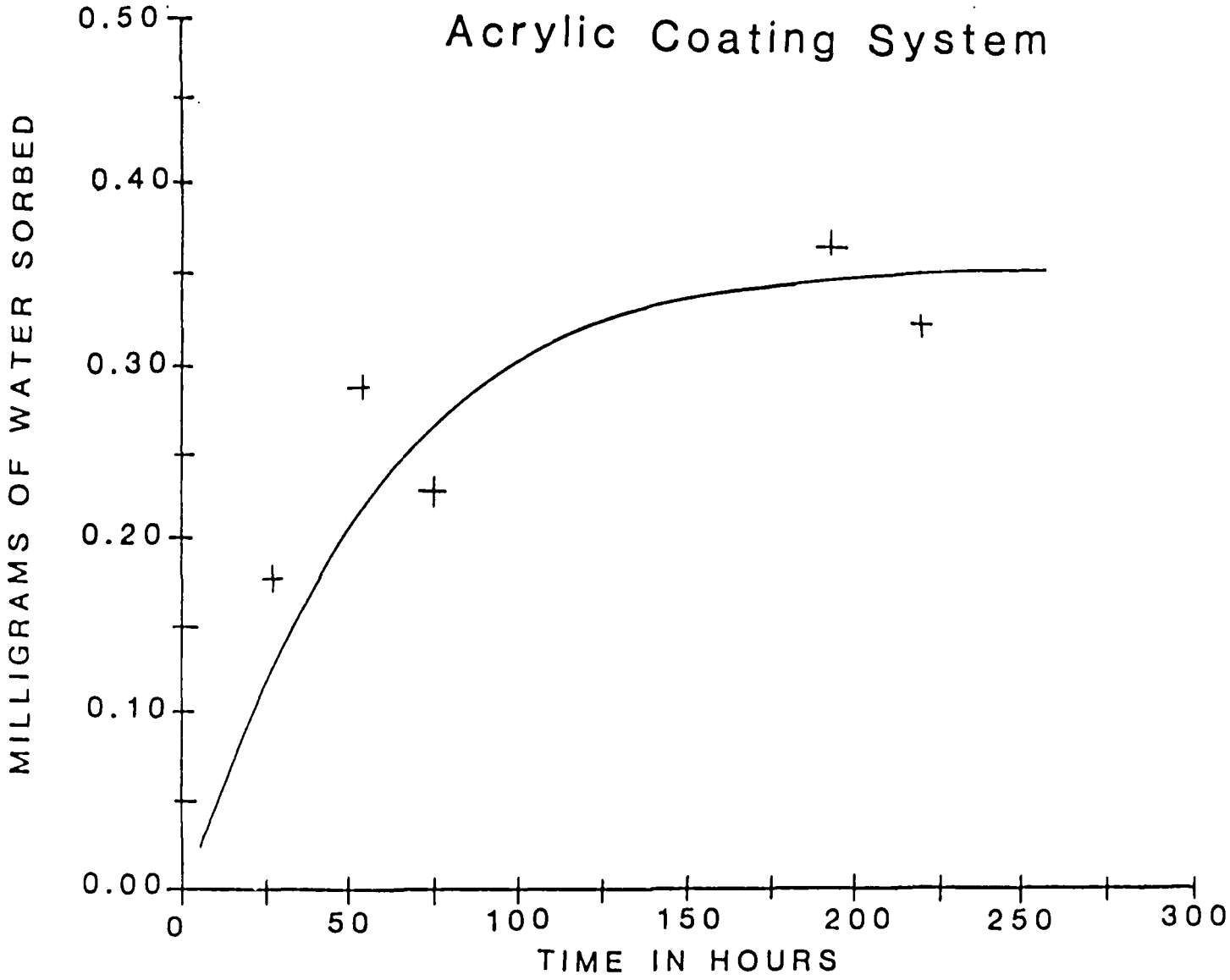

Figure 8. Gravimetric water uptake for acrylic coating system.

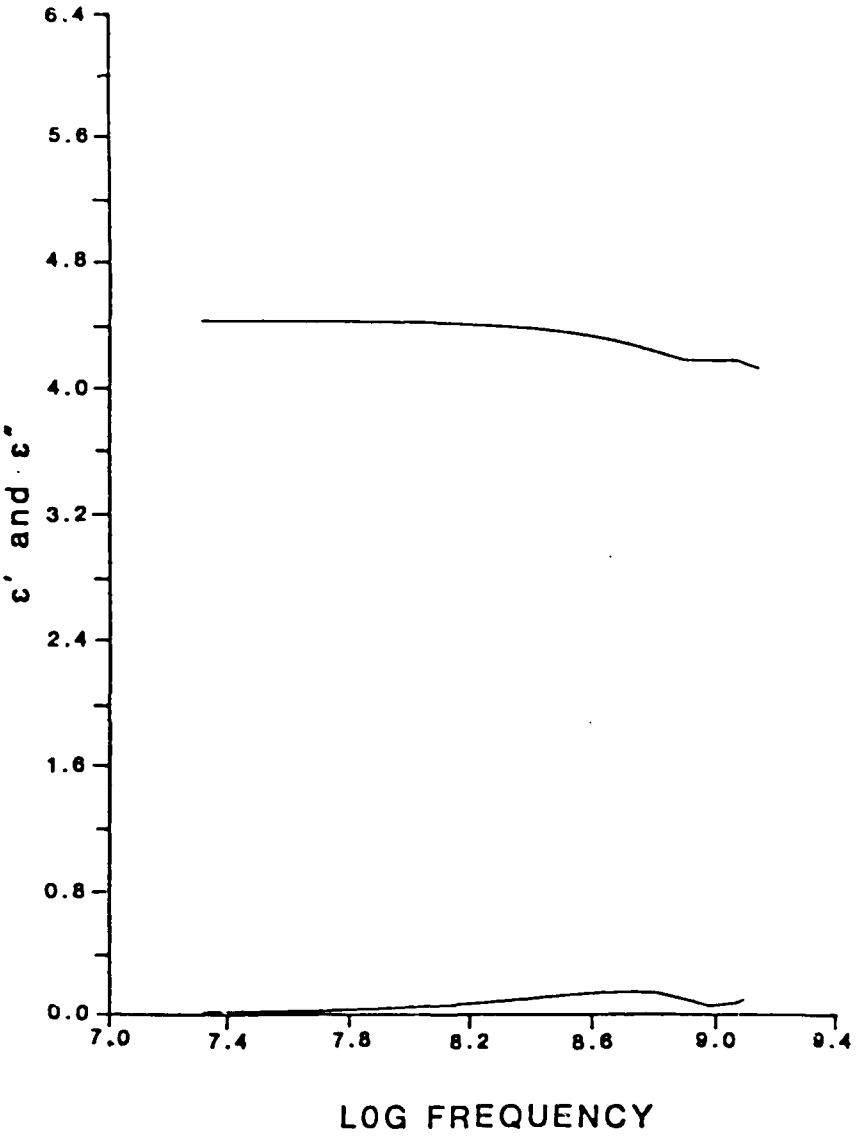

Figure 9. Dielectric response for unexposed alkyd sample. Sample was stored in a desiccator prior to measurement.

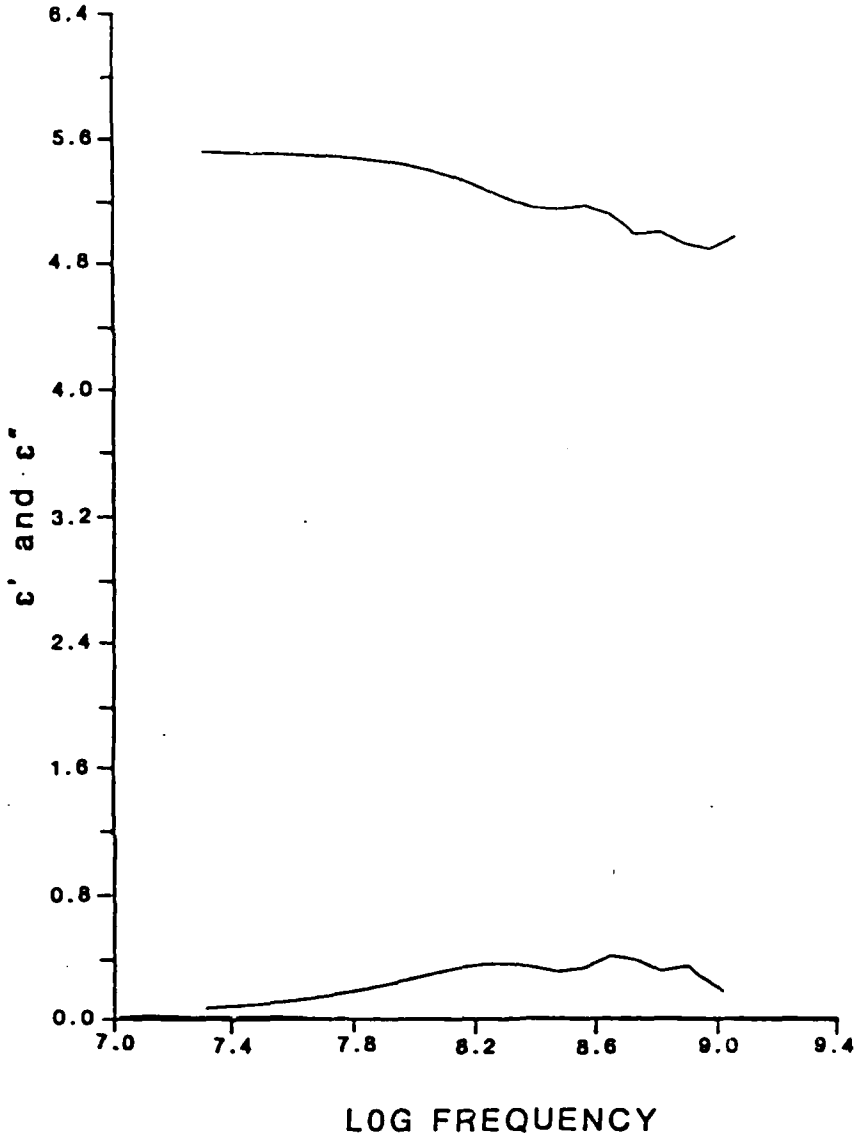

Figure 10. Dielectric response for exposed alkyd sample. Sample was exposed to distilled water for 32 hours.

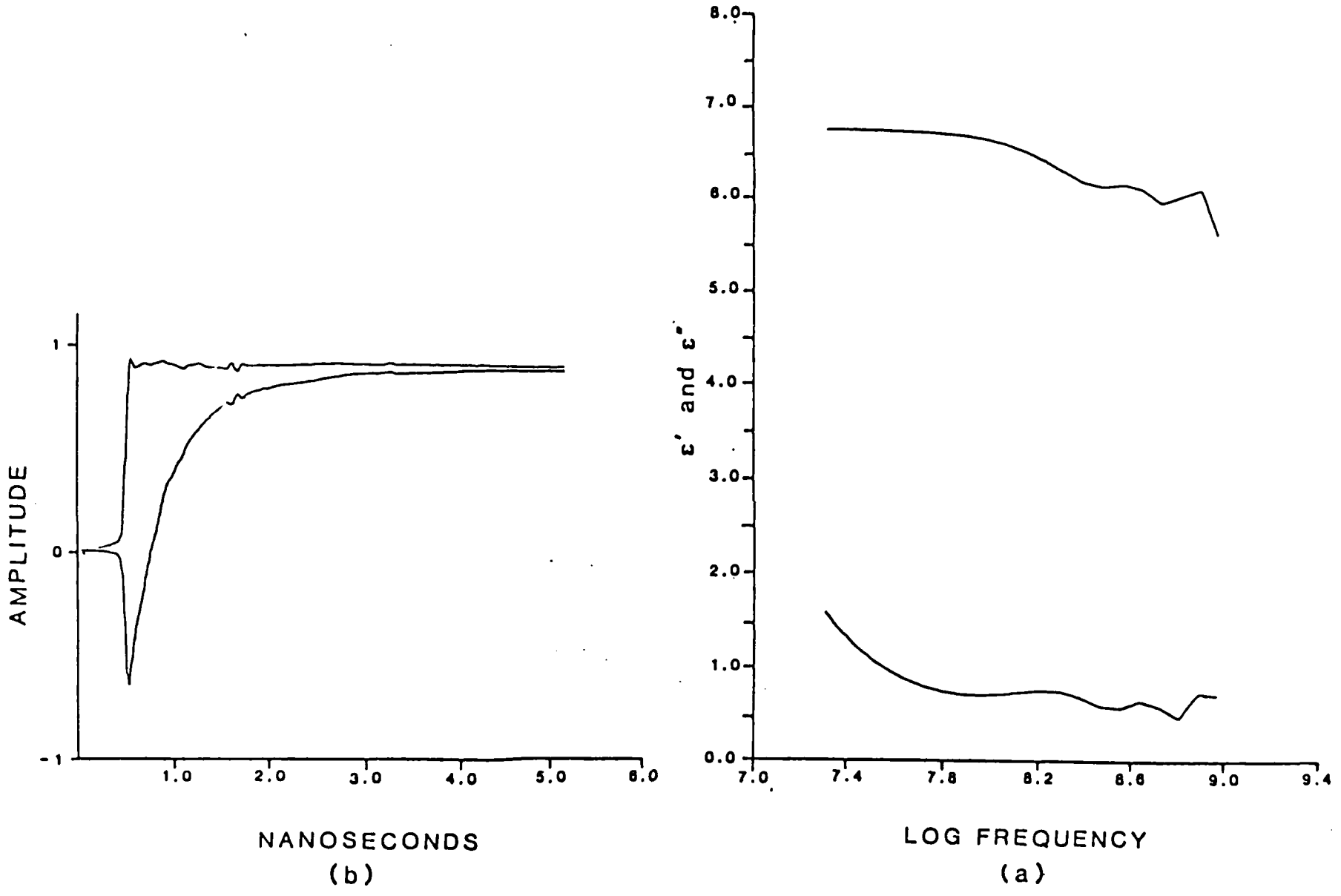

Figure 11. Dielectric response for exposed alkyd sample. Sample was exposed to distilled water for 128 hours.

8.384 Hz. The dielectric spectrum, however, is severely degraded at higher frequencies due to unwanted reflections (see Figure 10). The loss at log frequency 8.384 continues to increase with exposure until the sample finally becomes conductive. Figure 11a is the dielectric response for the conductive alkyd coating. The water uptake behavior is given in Figure 12.

Previous studies of alkyd systems [12-14] have shown water permeability to be rapid and dependent upon the pigment binder interaction. The water uptake data in Figure 12 show a rapid and substantial uptake of water. The dielectric results indicate two very interesting characteristics. First, the coating becomes conductive after about 24 hours. Second, a large loss at log frequency 8.384 appears and continues to increase as water is added.

A conductive pathway in the sample will keep the coating from completely charging back up to the amplitude of the incident pulse. The long-time amplitude of the reflected pulse will then be less than the incident pulse as shown in Figure 11b. A conductivity for the sample can be obtained by:

$$\frac{\sigma}{\varepsilon_o} = \frac{1}{C_o Z_o}\left[\frac{2}{V_o(t_\infty)} - 1\right] , \qquad (1)$$

where,

ε_o is the permittivity of free space.

C_o is the empty cell capacitance.

Z_o is the impedance of the coaxial line.

σ_o is the conductivity of the dielectric sample.

$V_o(t_\infty)$ is the amplitude of the reflected pulse at infinite time from the oscilloscope screen.

The steady state amplitude of the reflected pulse from Figure 11b can be substituted directly into Eqn. (1). The resulting conductivity is found to be 1.62×10^{-3} mho/cm, which translates to a coating resistance of 30,875 ohms for an area of 0.3 cm^2 by 200 μm. Typical resistance values for protective coatings are usually orders of magnitude higher at lower frequencies. The low value of the resistance is probably due to the absence of any low frequency polarization effects.

A three-axis plot of exposure time, ε'', and frequency is given in Figure 13. The increase of the loss at log frequency 8.384 can be seen clearly as exposure time increases. The absence of this loss in the dry sample suggests some type of Maxwell-Wagner-Sillars [15,16] effect is taking place. Indeed, the loss increases with increasing water content and is probably due to the ingress of conductive capillaries through the coating [15,16]. Sillars [15] has shown that the location of the loss maximum is dependent upon the conductivity of the dielectric within the capillaries and the magnitude of the loss is due to the penetration depth of the capillaries.

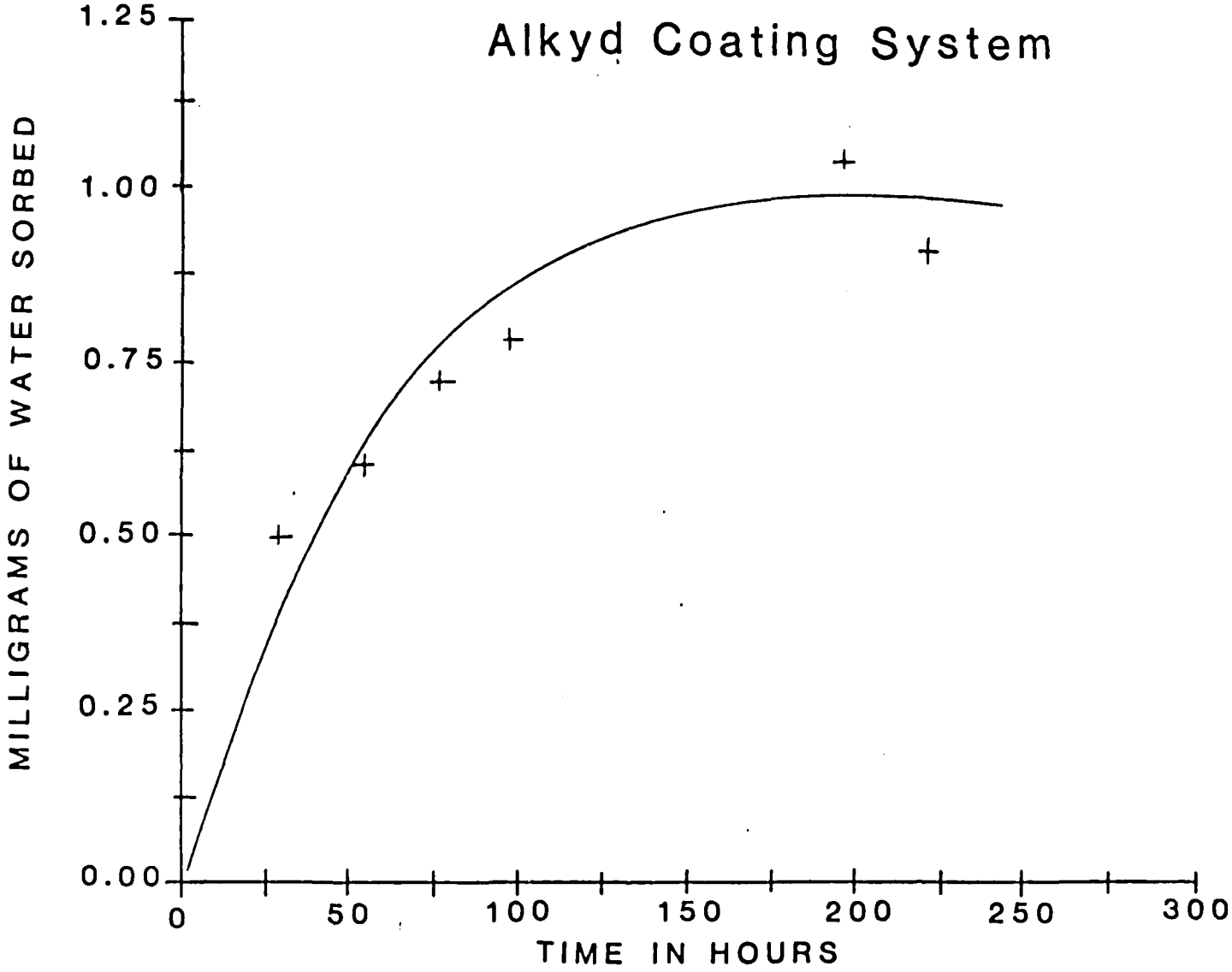

Figure 12. Gravimetric water uptake for alkyd coating system.

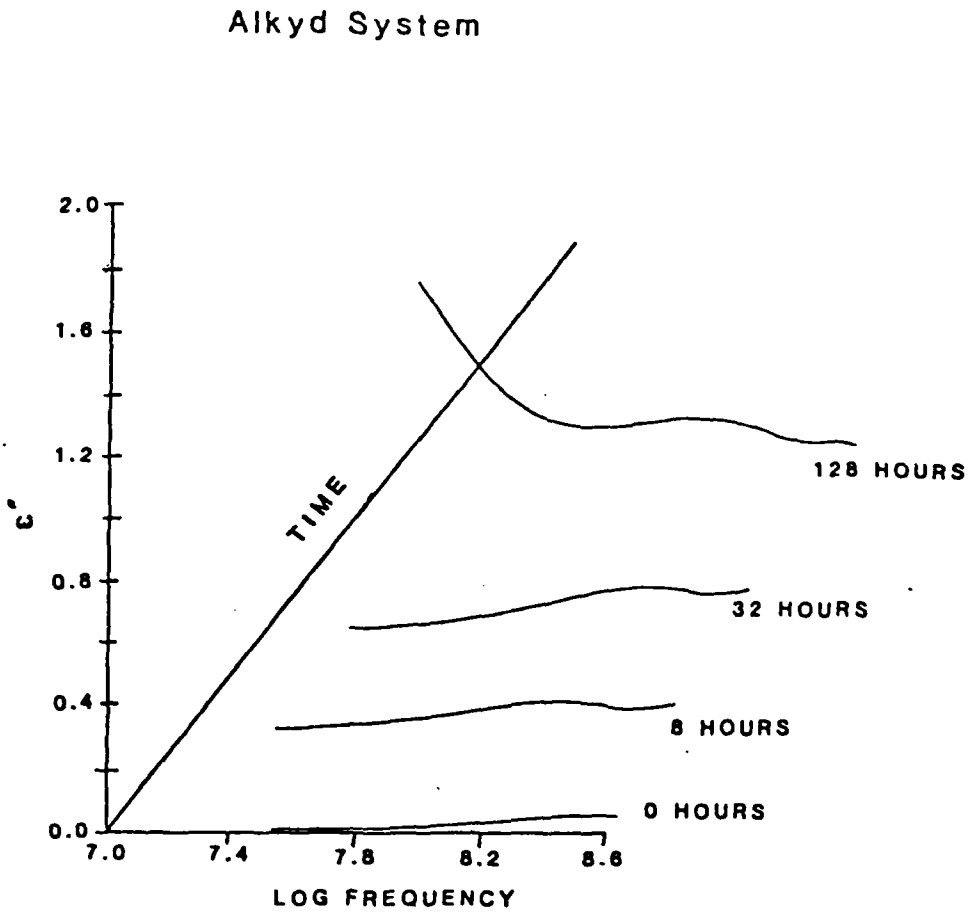

Figure 13. Water uptake as a function of ε" for alkyd sample.

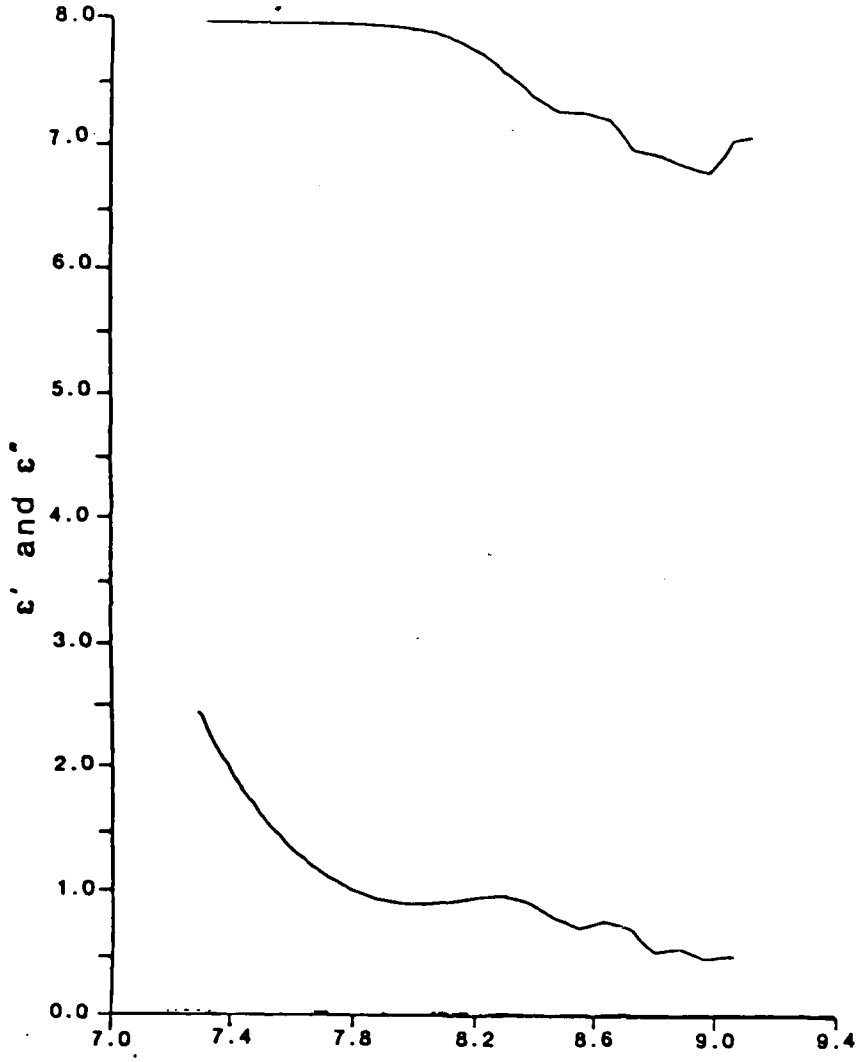

Figure 14. Dielectric response for second alkyd sample. Sample was exposed to distilled water for 254 hours.

A second sample of the alkyd system was prepared and the exposure experiment was repeated. The second sample was prepared in order to see if the presence of conductivity was due to the coating or some experimental error. Figure 14 is the response for the second sample after 254 hours of exposure. The sample also exhibited conductivity with a calculated coating resistance of 12,850 ohms for an area of 0.3 cm^2 by 200 μm. The lower resistance is presumably due to the longer exposure. Also note the presence of the suspected MWS loss peak in the dielectric response.

The reflection problem in the alkyd sample is due to the long-time response of the coating. Various reflections that were not present in the time window of previous experiments are now present in the time response.

CONCLUSIONS ON THE COATING SYSTEMS

The preliminary application of the lumped capacitor technique to several coating systems has produced mixed results. Each coating system exhibited different behavior in the exposure tests. The response varied from an enhancement of a polymer transition to a conductive alkyd system. The results indicate further experiments are needed to determine the utility of the technique in the study of coating systems.

REFERENCES

[1] D. J. Eadline, Third Annual Report, "Corrosion Control through a Better Understanding of the Metallic Substrate/Organic Coating/Interface," Office of Naval Research Agreement No. N00014-79-C-0731, January 1, 1984, p.86.

[2] D. J. Eadline, Ph.D. Dissertation, "Development and Application of High Frequency Dielectric Spectroscopy in Studies of Water in Organic Coatings," Lehigh University, Bethlehem, PA (1984).

[3] N. R. Farrar and K.H.G. Ashbee, J. Phys. Part D 11, 1009 (1978).

[4] J. Nicolas and K.H.G. Ashbee, J. Phys. Part D 11, 1015 (1978).

[5] J. L. Illinger and N. S. Schneider, Pol. Eng. and Sci. 20, 310 (1980).

[6] R. J. Morgan and E. T. Mones, Organic Coatings and Plastics Chemistry 41, 463 (1979).

[7] D. M. Brewis, J. Comyn, and J. Tegg, Polymer 21, 134 (1980).

[8] W. Funke, Prog. Organic Coatings 9, 29 (1981).

[9] L. A. Van der Meer-Lerk and P. M. Heertjes, J. Oil Col. Chem. Assoc. 58, 79 (1975).

[10] L. Gavet, B. Charbert, J. Chauchard, and J.P. Soulier, Textile Institute of France Bulletin 12 (45), 29 (1983).

[11] J. M. Parks, Third Annual Report, "Corrosion Control through a Better Understanding of the Metallic Substrate/Organic Coating/Interface," Office of Naval Research Agreement No. N00014-79-C-0731, January 1, 1984, p.199.

[12] H. Leidheiser, Jr., W. Wang, and L. Igetoft, Prog. Organic Coatings 11, 19 (1983).

[13] D. Y. Perea and P. M. Heertjes, J. Oil Col. Chem. Assoc. 54, 313 (1971).

[14] Ibid., 774.

[15] B. A. Sillars, J. Inst. Elec. Engrs. 80, 378 (1937).

[16] Progress in Dielectrics Vol. 7. J. B. Birks, Editor, Heywood Books, London (1967).

Program #11

Ionic Diffusion through Organic Coatings and Its Consequence to Corrosion

Principal Investigator: Henry Leidheiser, Jr.
Prof. of Chemistry

Associate: Jeffrey Parks,
Graduate Student

ABSTRACT

The diffusion rates of sodium, chloride and cesium ions through an alkyd topcoat, an alkyd topcoat plus primer and polybutadiene on steel were determined. Coated samples of steel were exposed to 0.5M solutions of the ions doped with trace amounts of $^{22}Na^{+}$, $^{36}Cl^{-}$ and $^{137}Cs^{+}$ and the residual radiation in the coating was measured. Diffusion coefficients were calculated for open circuit and cathodic polarization (-0.80 v vs. Ag/AgCl) conditions for the coating with and without an intentionally scribed defect. Polarization resulted in a 3- to 28-fold increase in ion uptake. The major pathway for ionic diffusion under cathodic polarization conditions was through the coating. Lateral diffusion from the defect to the delamination front appeared to be the principal transport pathway at open circuit. The ion flux through the coating was sufficient to account for the observed delamination rate at -0.80 v when certain assumptions were made.

INTRODUCTION

Paints applied to metal surfaces provide corrosion protection by introducing a barrier to ionic transport and electrical conduction. When a painted metal is exposed to electrolyte there is a gradual reduction in barrier protection as water, oxygen and electrolyte penetrate the coating.

Defects within the coating introduce direct pathways for environmental species to reach the metal substrate resulting in the localized loss of barrier protection. The corrosion of the exposed metal can be prevented by cathodically polarizing the substrate. Under these conditions, however, many coating systems have been observed to separate from the substrate radially about the defect. This so-called "cathodic delamination" of a coating from a metal is accompanied by a further reduction in barrier protection. The loss of corrosion protection due to the onset of delamination is a widely recognized problem, particularly during the cathodic protection of damaged coated metal pipelines and the electroless plating of photoresist-coated metal substrates (Leidheiser et al., in press).

Cathodic delamination has been the subject of a number of publications from this laboratory in recent years (Leidheiser, 1980, 1981; Leidheiser and Wang, 1981; Leidheiser et al., 1983), and a comprehensive mechanism for the disbondment process has been developed (Dickie et al., 1981; Koehler, 1984; Leidheiser et al., 1983; Watts and Castle, 1983). The applied cathodic potential results in the activation of the cathodic reaction immediately at the defect and at the boundary between the coating and the metal. At moderate applied potentials in aerated electrolytes, the oxygen reduction reaction, $H_2O + 1/2O_2 + 2e^- = 2OH^-$, is the dominant reaction. In deaerated solutions or at more negative potentials, the hydrogen evolution reaction occurs, $2H^+ + 2e^- = H_2$. Both reactions lead to the development of a very alkaline environment at the boundary between the coating and the metal and the bond between the coating and the metal is broken. The pH at this site may be as high as 14 (McIntyre; Ritter and Kruger, 1980).

Two important question remain unresolved. The first unresolved question relates to the mechanism by which the bond is broken and diverse views abound (Dickie et al., 1981; Koehler, 1984; Leidhesier et al., 1983; Watts and Castle, 1983). This question will not be treated in the present article. The second unresolved question relates to the route by which the charge-carrying cations reach the site where the OH^- ions are formed. It is this matter which the present study addresses.

The major purpose of this work is to determine the effect of an imposed defect and an applied potential on ionic transport through three types of organic coatings on steel. By correlating ionic transport with observed cathodic delamination rates, the question as to whether there is a sufficient number of cations penetrating the coating to support delamination is also addressed.

EXPERIMENTAL

Two cations, Na^+ and Cs^+, and one anion, Cl^-, were selected for study since convenient radiotracers of these elements are readily available in the form of ^{22}Na, ^{137}Cs, and ^{36}Cl. Half molar solutions of NaCl, doped with both ^{22}Na and ^{36}Cl, and CsCl solutions doped with ^{137}Cs only were prepared and calibration curves correlating radiotracer counts with ion concentrations

were constructed. A Nuclear Chicago Model 132A well scintillation counter was used to detect the gamma radiation form ^{22}Na and ^{137}Cs and a Nuclear Chicago Model 157 radiation detector was used to detect the beta radiation from ^{22}Na and ^{36}Cl.

The determination of ion uptake by the coated metal was carried out in the cell shown in Figure 1. A polyethylene cylinder, 1.4 cm in diameter, was secured to the flat test specimen using an epoxy cement. The doped electrolyte was introduced and the coating was exposed to the electrolyte for one hour. The electrolyte was removed, the cell was rinsed 10 times with distilled water and the surface of the coating was dried with a paper tissue. The radiation remaining in the coating was determined and the electrolyte was then returned to the cell and the procedure was repeated after each exposure period. The experiment was terminated when rust spots, blistering or severe de-adhesion was observed.

Three coating systems were selected for study on the basis of prior experience in cathodic delamination studies: (1) an alkyd topcoat (Rust-o-Leum #7791), (2) the #7791 topcoat in conjunction with a primer coat (Rust-o-Leum #7773), and (3) polybutadiene. The coatings were spin coated onto degreased and abraded cold rolled steel panels and the coating thickness was measured with a magnetic thickness gauge after curing. The alkyd coatings were cured at room temperature for no less than 1 week prior to testing. For plates with a primer coat, the topcoat was applied 24 hours after the primer. Polybutadiene was oxidatively cured at 200°C for 20 minutes, Ion uptake was studied both on coatings which were presumed to be defect free and those into which a 3 mm diameter defect had been scribed. The delamination of the samples with the defect was monitored and the rate of delamination was determined.

The delaminated area could be seen visually without destroying the sample in the case of polybutadiene because this coating is transparent. The alkyd coatings, however, were opaque and the coating had to be destroyed in each test. The method for determining the delaminated area was as follows. After removing the specimen from the electrolyte, it was dried and then stored in a desiccator for 24 hours before touching adhesive tape to the surface and determining the area that disbonded. This procedure had to be followed with the alkyd coatings because the poor wet adhesion properties allowed the entire coating to be removed by the tape and the boundary of the cathodically delaminated region could not readily be measured.

Ion uptake and delamination rates were determined both on samples which were not polarized and those which were cathodically polarized to a potential of -0.80 v using the combination counter-reference electrode depicted in Figure 1. Constant potentials were maintained using the simple potentiostat designed by Baboian et al. (1979). All potentials are given with respect to the Ag/AgCl reference electrode.

In order that experiments carried out under different conditions can be compared, approximate values of the diffusion coefficient of the ions in the coating were determined. The flux J is defined by:

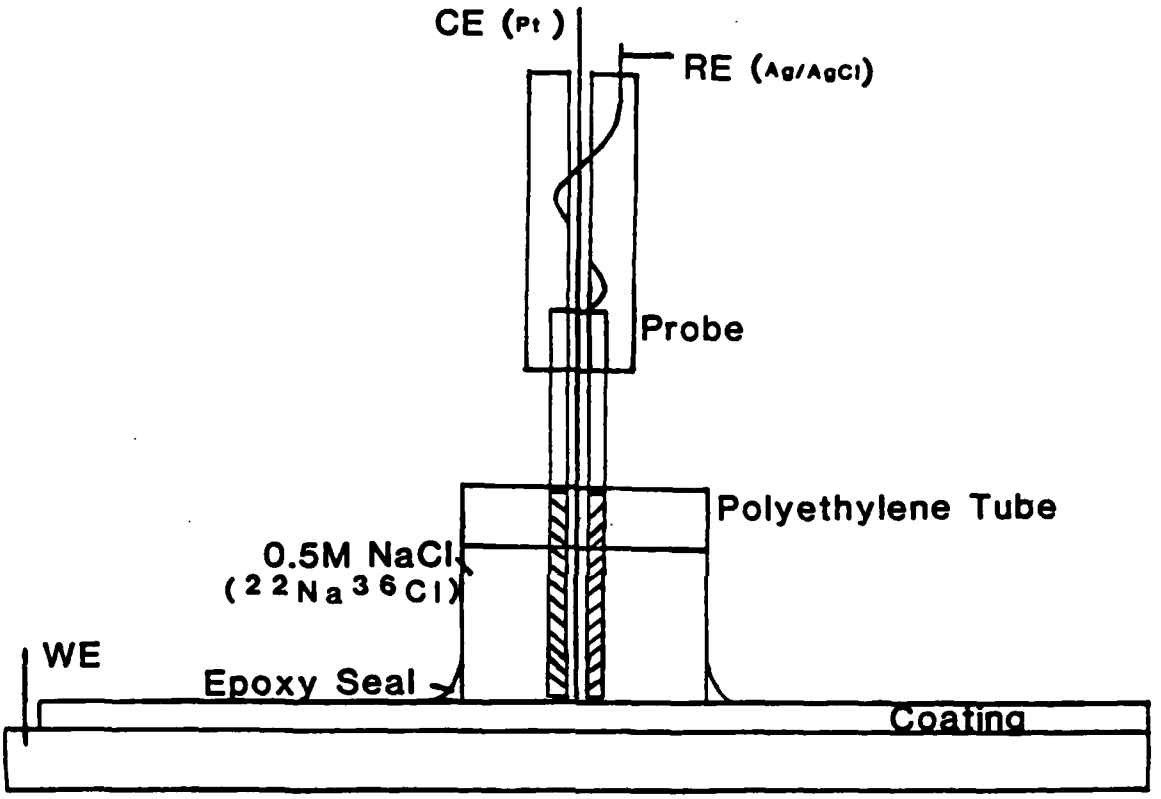

Figure 1. Cell used in the ion uptake measurements. The potential was applied between the counter electrode (CE) and the substrate working electrode (WE) and the potential was measured by means of a silver/silver chloride reference electrode (RE) compactly packaged within a probe.

$$J = \frac{1}{A} \cdot \frac{d(\text{no. moles})}{dt}$$

and the diffusion coefficient D becomes

$$D = \frac{1}{A} \frac{d(\text{no. moles})}{dt} \cdot \frac{\ell}{C}$$

where A is the area exposed, ℓ is the thickness of the coating, and C is the ion concentration in the bulk solution, 5.0×10^{-4} moles/cm^3.

RESULTS

Typical ion uptake rates for the alkyd coating systems are shown in Figures 2 and 3 and for polybutadiene in Figures 4 and 5.

The calculated diffusion coefficients for Na^+, Cs^+ and Cl^- diffusion into the three coating systems are summarized in Table I for defect-free coatings. The diffusion coefficients have been normalized with respect to coating thickness, in mils, to minimize any effects thickness might have on ion uptake. This manner of presentation has been selected as to be comparable with much diffusion data through free films as found in the literature. Table II summarizes similar data for the coatings into which the 3 mm defect was introduced.

The precision of the diffusion coefficients given in Table I and II represents the standard deviation from the mean when the coefficient was determined for a large number of samples. These values ranged from 20 to 65% of the mean. When too few samples were used to obtain a standard deviation, no precision is given and the result is a simple average value.

Data showing the rates of delamination of the three coating systems while immersed in 0.5M CsCl, both with and without an applied cathodic potential, are summarized in Figures 6, 7 and 8. The linear relationship between delaminated area and exposure time, as seen in Figures 6 and 8, is typical of laboratory measurements. The non-linear behavior with the alkyd topcoat in Figure 7 may be a consequence of the fact that this coating exhibits poor wet adhesion.

The total cation uptake as a function of delaminated area for measurements made at open circuit and at -0.8 v is summarized for the three coating systems in Figures 9, 10 and 11. It is striking that the slopes of these curves are similar at both open circuit and at -0.80 v in all three coating systems.

DISCUSSION

It is apparent from the data summarized in Table I that all three ions, Na^+, Cs^+ and Cl^-, diffuse through the three coatings when the boundary

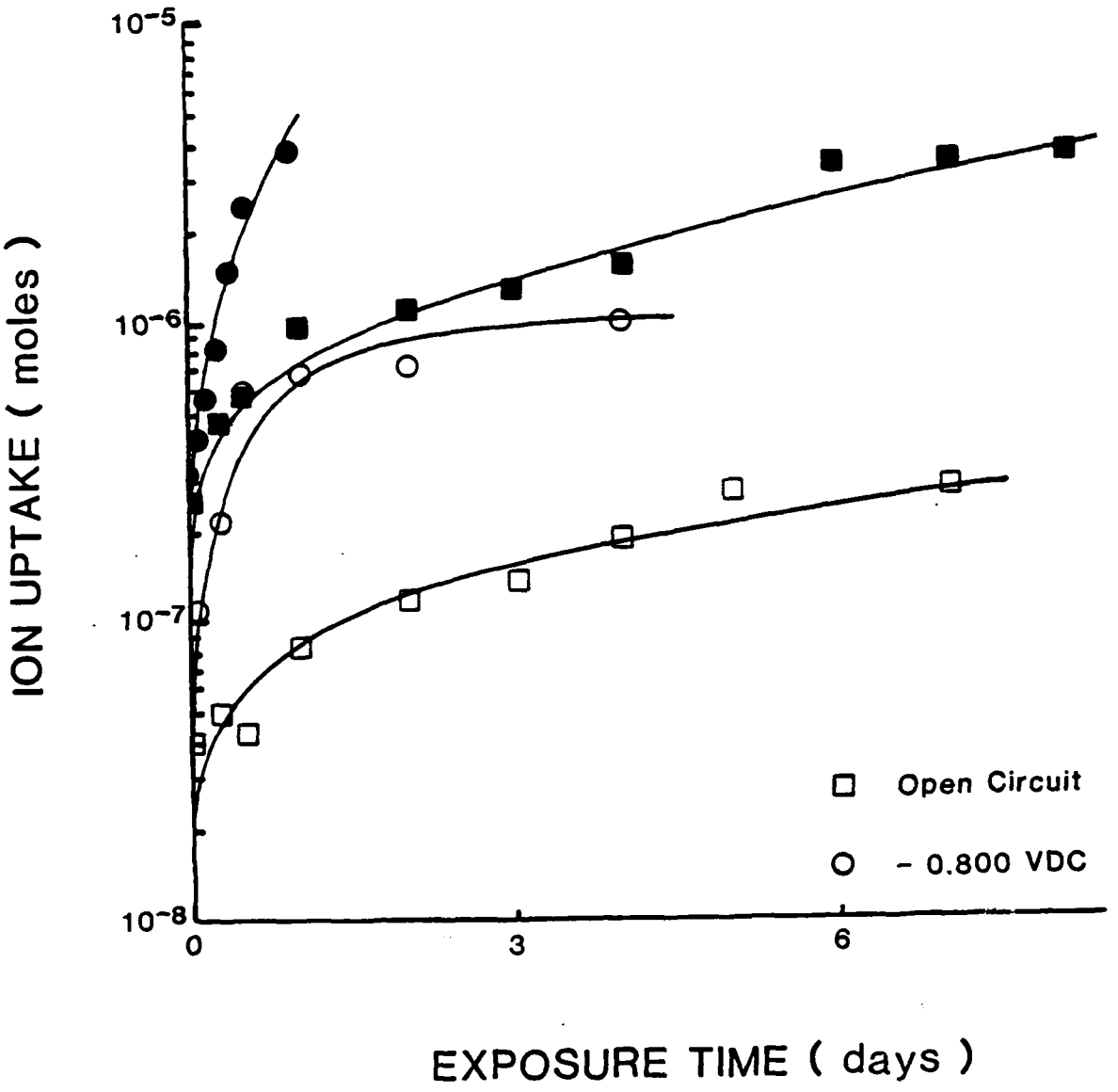

Figure 2. Representative measurements of $^{137}Cs^{+}$ uptake by an alkyd topcoat plus primer on a steel substrate during exposure to 0.5M CsCl solution. Coating thickness ranged from 57.7 to 65.9 μm. Open symbols represent defect-free coatings and solid symbols represent coatings into which a 3 mm defect was introduced. Data obtained under open circuit conditions and with an applied potential of -0.80 v are given.

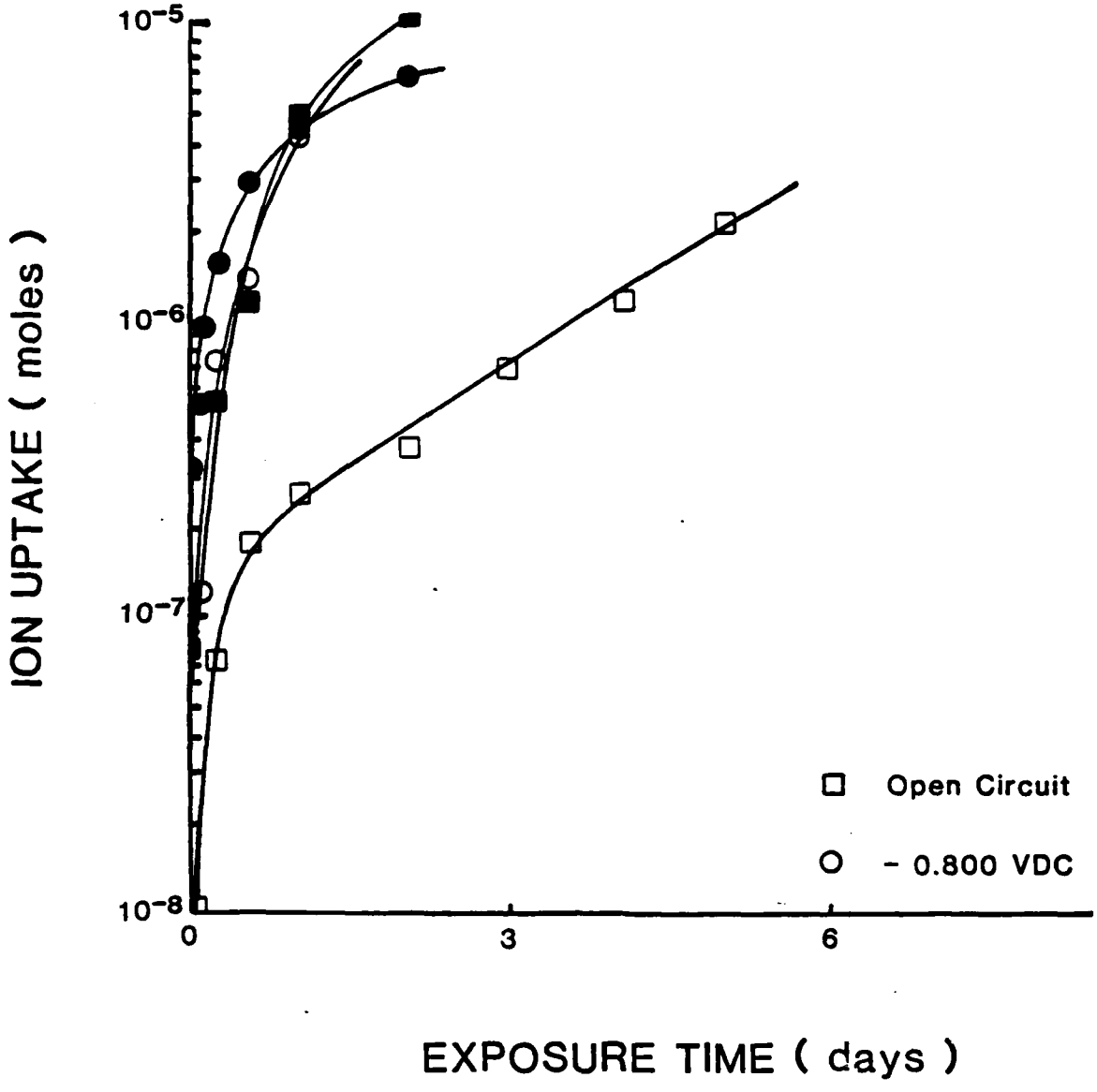

Figure 3. Representative measurements of $^{137}Cs^{+}$ uptake by an alkyd topcoat, 25.4-38.0 μm in thickness, during exposure to 0.5M CsCl solution. Open symbols represent defect-free coatings and solid symbols represent coatings into which a 3 mm defect was introduced. Data obtained under open circuit conditions and with an applied potential of -0.80 v are given.

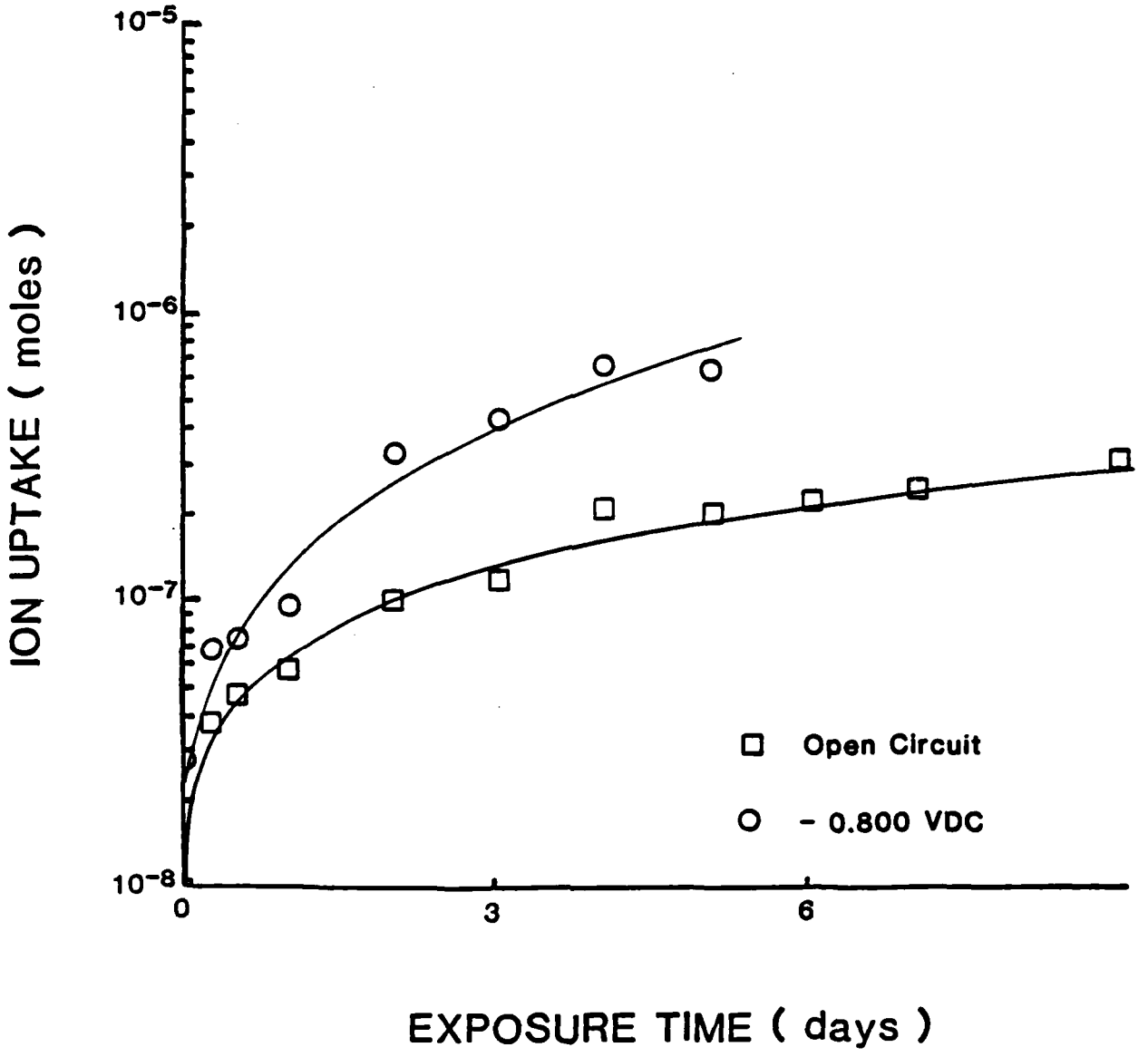

Figure 4. Representative measurement of ^{137}Cs uptake by a defect-free polybutadiene coating, 16.3 μm thick, on a steel substrate during exposure to a 0.5M CsCl solution. Data obtained under open circuit conditions and with an applied potential of -0.80 v are given.

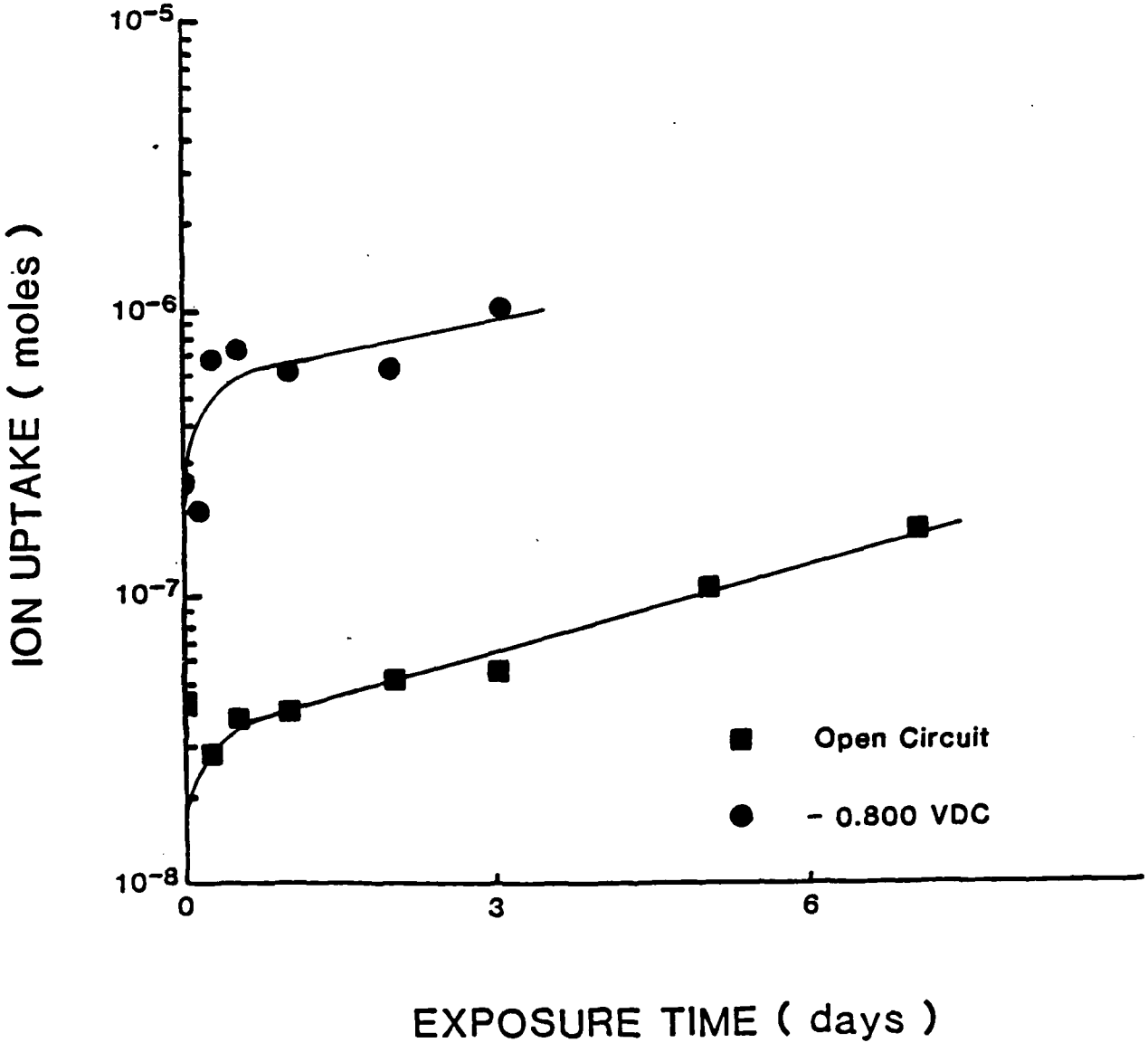

Figure 5. Representative measurement of ^{137}Cs uptake by a polybutadiene coating, 18.4-19.7 μm thick, on a steel substrate during exposure to a 0.5M CsCl solution under conditions where a 3 mm diameter defect was introduced into the coating. Data obtained under open circuit conditions and with an applied potential of -0.80 v are given.

TABLE I

Calculated Diffusion Coefficients for the Diffusion of Ions into Defect-Free Coatings on Steel

Coating System	Applied Potential	Normalized Diffusion Coefficient (cm^2/hr-mil)		
		Na^+	Cs^+	Cl^-
Alkyd Topcoat	Open Circuit	$4.6 \pm 3.0 \times 10^{-8}$	$8.9 \pm 0.6 \times 10^{-8}$	$1.5 \pm 0.8 \times 10^{-8}$
	-0.80 v	$3.5 \pm 0.7 \times 10^{-7}$	5.7×10^{-7}	$4.4 \pm 0.9 \times 10^{-8}$
Alkyd Topcoat Plus Primer	Open Circuit	$3.2 \pm 0.9 \times 10^{-9}$	2.0×10^{-9}	$7.2 \pm 1.4 \times 10^{-10}$
	-0.80 v	$4.7 \pm 2.4 \times 10^{-8}$	$3.2 \pm 0.2 \times 10^{-8}$	$1.8 \pm 0.9 \times 10^{-8}$
Polybutadiene	Open Circuit	1.8×10^{-9}	1.7×10^{-9}	5.4×10^{-10}
	-0.80 v	3.7×10^{-8}	2.0×10^{-8}	1.5×10^{-8}

TABLE II

Calculated Diffusion Coefficients for the Diffusion of Ions into Coatings on Steel in which a 3 mm Defect Was Introduced

Coating System	Applied Potential	Normalized Diffusion Coefficient (cm^2/hr-mil)		
		Na^+	Cs^+	Cl^-
Alkyd Topcoat	Open Circuit	4.5×10^{-7}	7.6×10^{-7}	1.1×10^{-7}
	-0.80 v	3.3×10^{-7}	4.6×10^{-7}	1.8×10^{-7}
Alkyd Topcoat Plus Primer	Open Circuit	$9.3 \pm 3.2 \times 10^{-8}$	$8.7 \pm 5.1 \times 10^{-8}$	3.1×10^{-8}
	-0.80 v	9.8×10^{-8}	6.3×10^{-7}	3.7×10^{-8}
Polybutadiene	Open Circuit	9.0×10^{-9}	4.4×10^{-9}	3.8×10^{-9}
	-0.80 v	6.6×10^{-8}	3.0×10^{-8}	2.5×10^{-8}

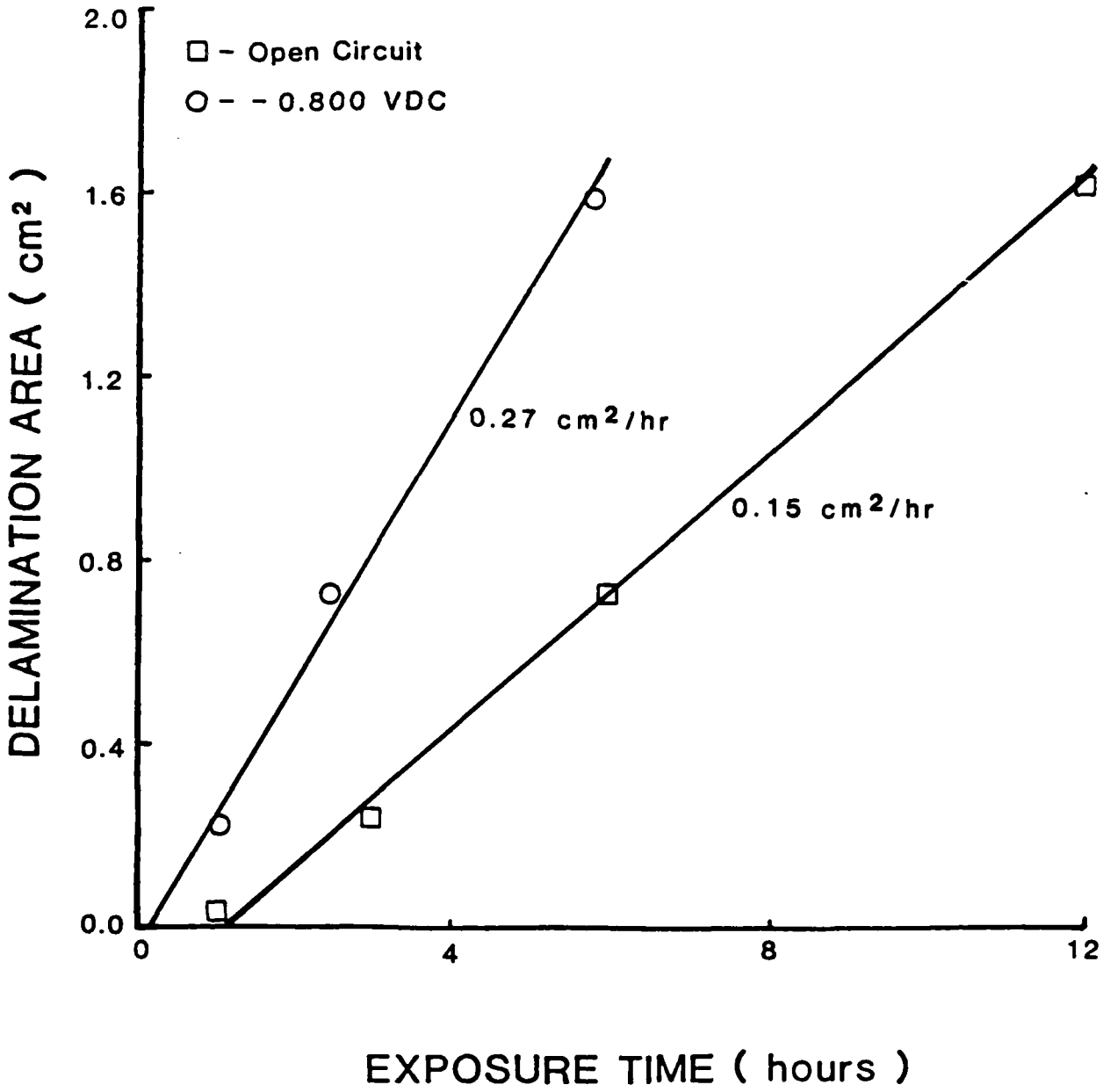

Figure 6. Delamination of an alkyd topcoat plus primer, 63.5-66 μm thick, under open circuit conditions and with an applied potential of -0.80 v while immersed in 0.5M CsCl solution.

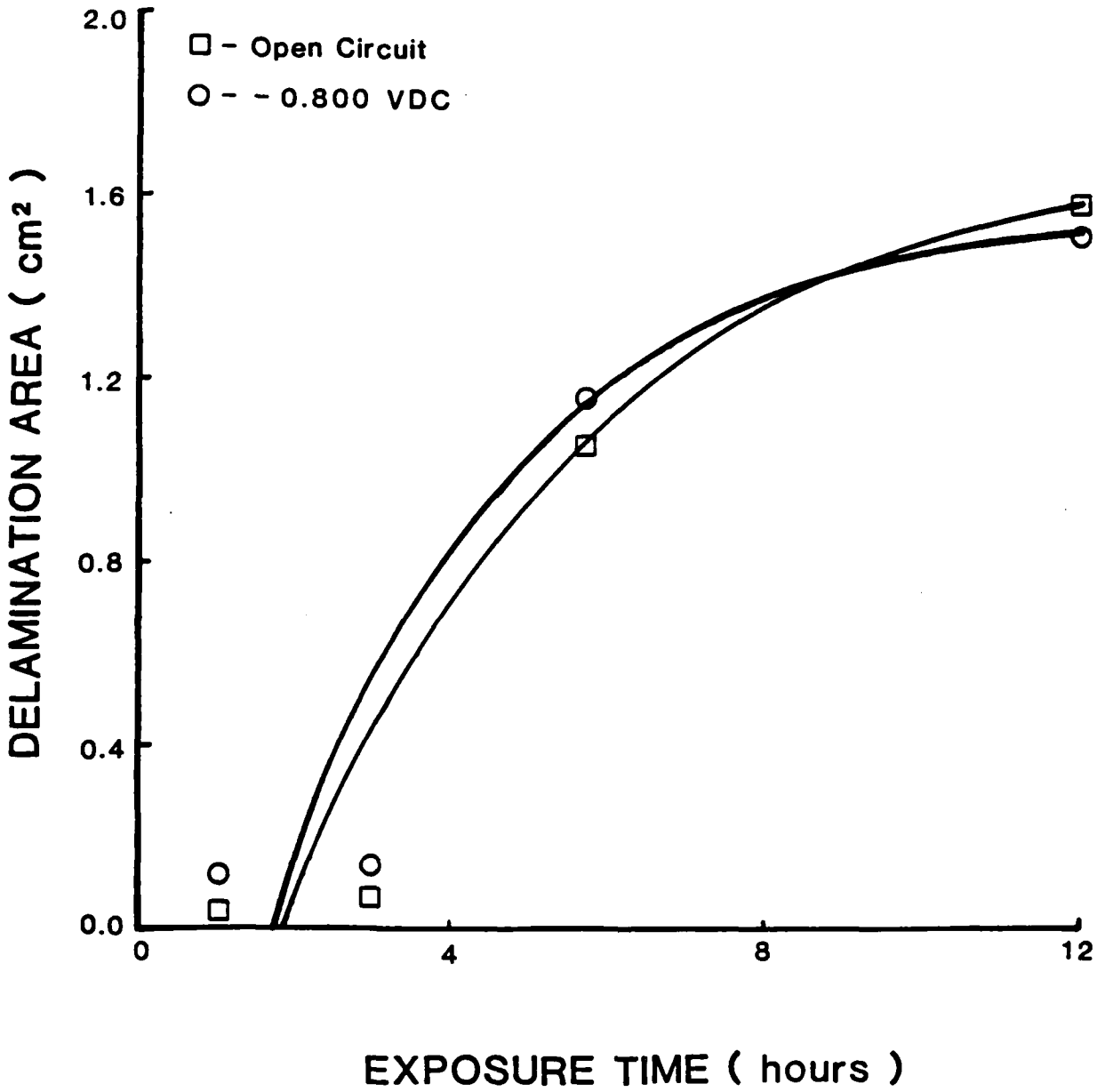

Figure 7. Delamination of the alkyd topcoat, 38.0-46.8 μm thick, under open circuit conditions and with an applied potential of -0.80 v while immersed in 0.5M CsCl solution.

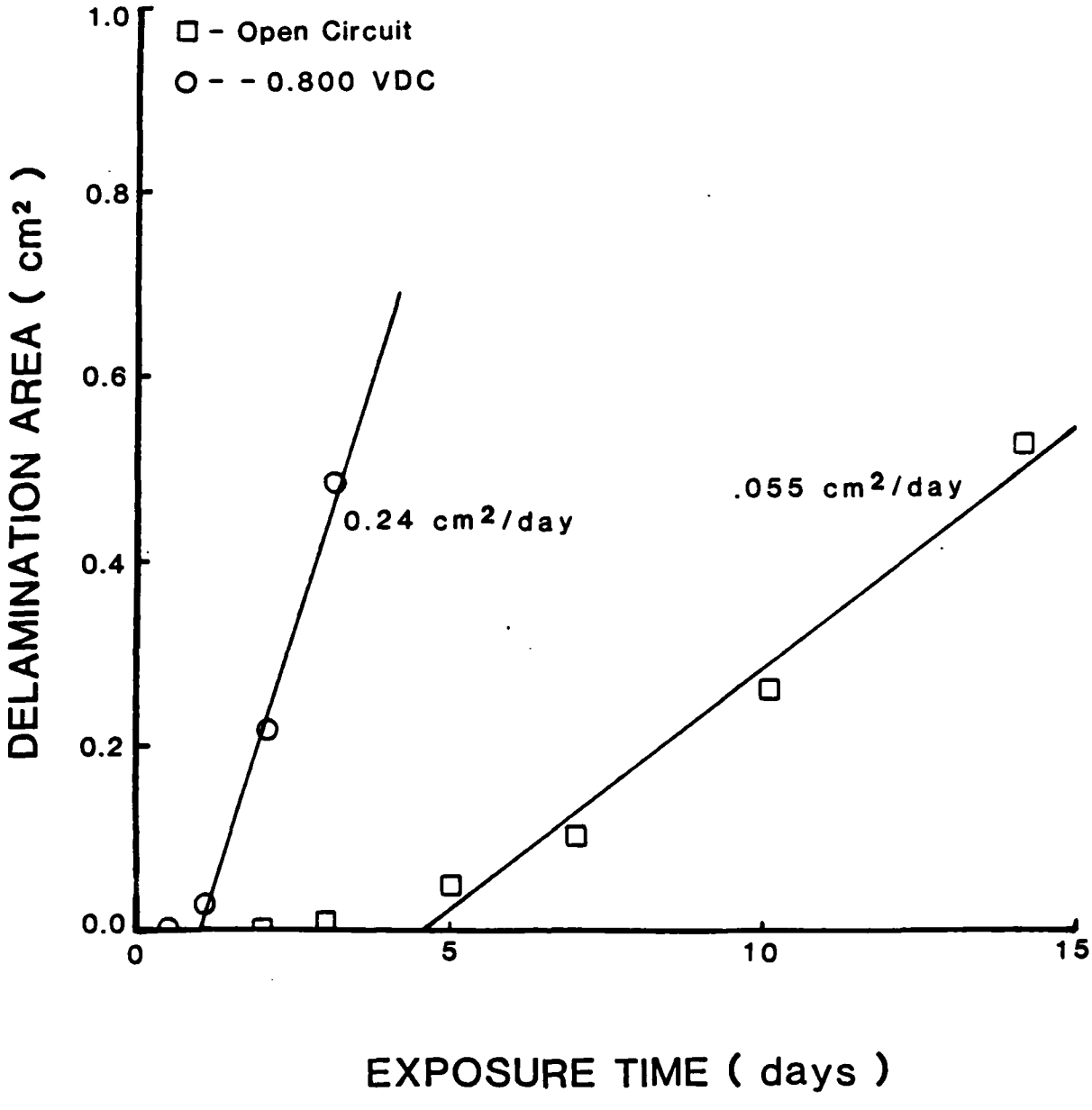

Figure 8. Delamination of a polybutadiene coating, 18.4 and 19.7 μm thick, under open circuit conditions and with an applied potential of -0.80 v while immersed in 0.5M CsCl solution.

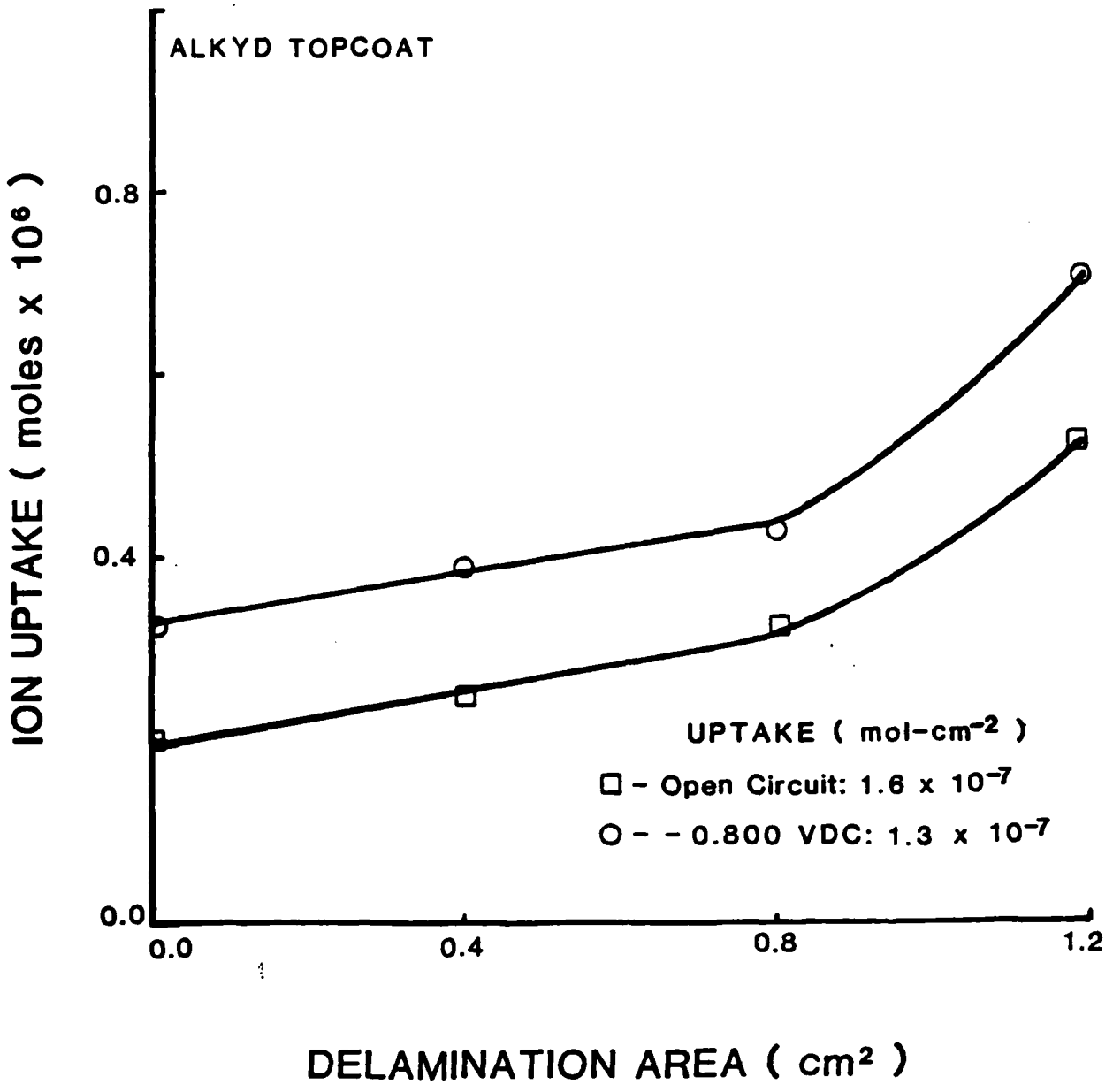

Figure 9. Total uptake of ^{137}Cs by the alkyd topcoat 38.0 μm thick, as a function of the delaminated area under both open circuit conditions and at a potential of -0.80 v.

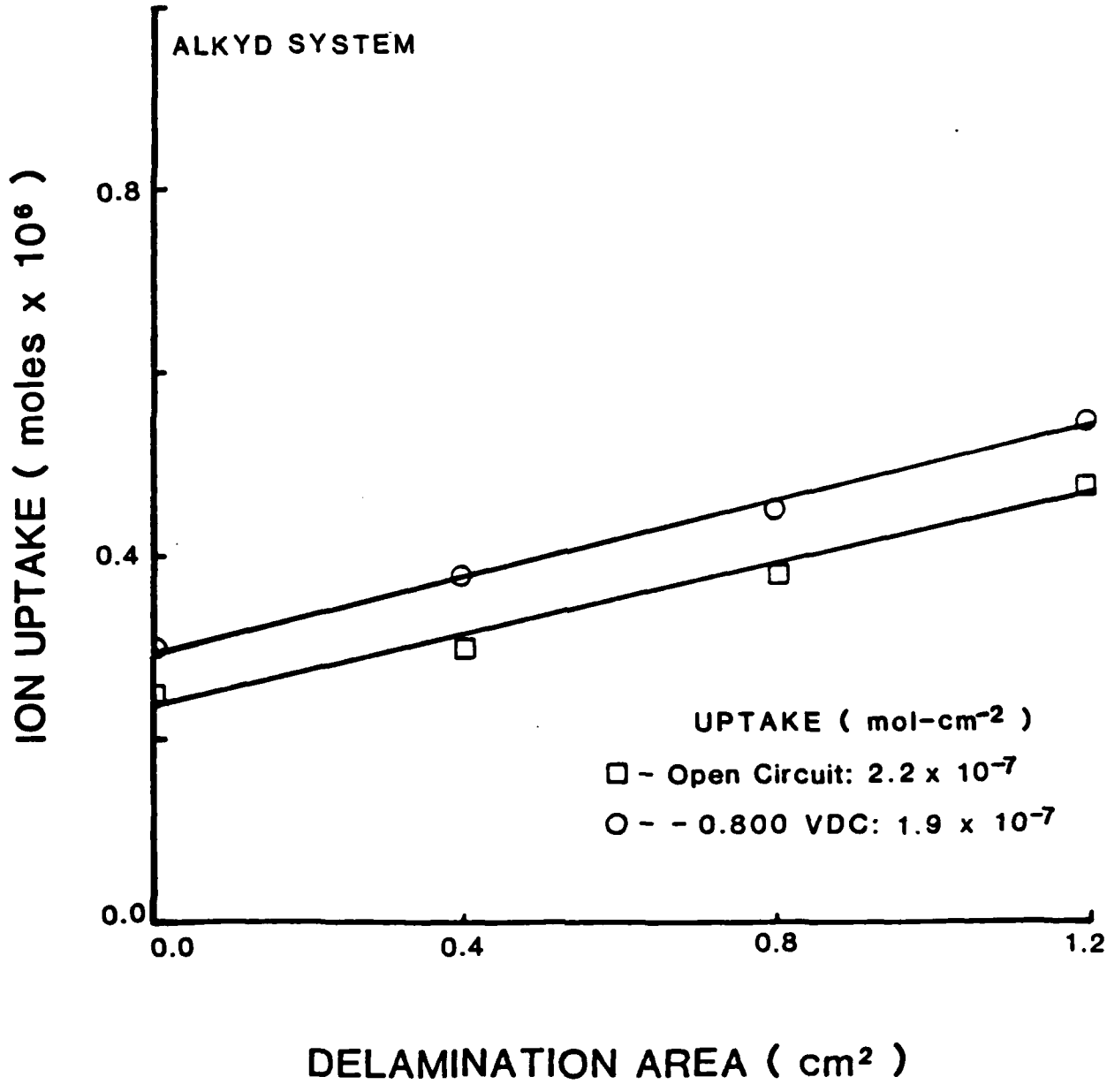

Figure 10. Total uptake of ^{137}Cs by the alkyd topcoat plus primer, 65.9 μm thick, as a function of the delaminated area under both open circuit conditions and at a potential of -0.80 v.

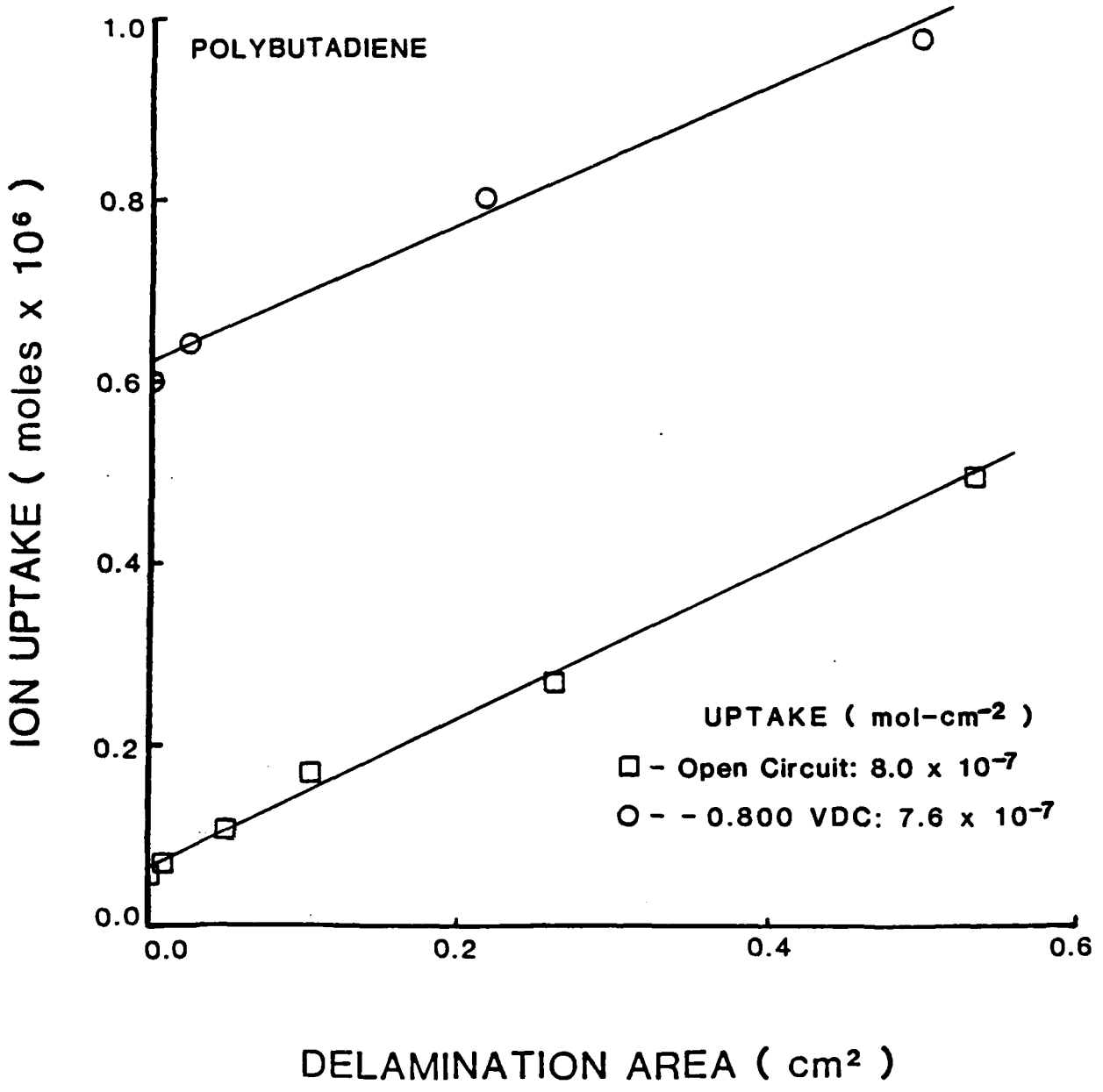

Figure 11. Total uptake of ^{137}Cs by the polybutadiene coating, 18.4-19.7 μm thick, as a function of the delaminated area under both open circuit conditions and at a potential of -0.80 v.

condition is a 0.5M solution of the alkali metal chloride. The rates under open circuit conditions yield values of the diffusion coefficient in the range of 10^{-10} to 10^{-8} cm^2/hr-mil. These values are in the same range as values obtained for the diffusion of ions through free films. For example, representative values from the literature are summarized in Table III.

The effect of polarizing the substrate to -0.80 v, a value approximately 250 mV cathodic to the corrosion potential, on the calculated diffusion coefficient is summarized in Table IV. It is apparent that the applied potential increased the rates of migration of both cations as well as the anion. The increase in the rate of cation migration is understandable in terms of the potential gradient, but the increase in the rate of Cl^- migration is a puzzle. Several possible explanations present themselves. First, the migration of the cations under the potential gradient in the absence of a cathodic reaction at the interface may result in a follow-on effect. The Cl^- may be attracted into the coating by virtue of the accumulation of a positive charge in the coating near the coating/metal interface. Second, the applied potential may enlarge the minute aqueous pathways that exist in the coating such that diffusion of all species is enhanced. Third, it is probable that both anions and cations diffuse through the coating as aquo complexes which react differently to the potential gradient than the unsolvated ion. It is known from other work based on impedance measurements (Parks) that an applied cathodic potential of -0.80 v increases the rate of diffusion of water through the same coatings used in the present study. The increase in diffusion rate of the Cl^- ion may thus be a result of the increased rate of diffusion of water under the applied potential.

A critical question which this study was designed to address is "What is the route by which the charge-carrying cations reach the site where the OH^- ions are formed?" A comparison of the data summarized in Tables I and II permits us to address this question. The data in these two tables are compared in Table V as the ratio of the diffusion coefficients obtained with and without a purposely formed defect in the coating. It is specially noteworthy that the relative diffusion coefficients are high under open circuit conditions for all three coatings, while under the influence of an applied cathodic potential the relative values of D are very low and, in seven of the nine cases, there is no major difference between the calculated diffusion coefficients with and without a defect. That the coatings with the defect take up ions much more rapidly than those in which there is no defect at open circuit is understandable in terms of the mechanism of the delamination process when there is no applied potential. Under such conditions, that cathode occurs under the coating and the anode occurs at the defect (Leidheiser and Kendig, 1976) during the corrosion process. The direction of migration of the ions is thus parallel to the surface from the defect. As the corrosion reactions occur, the delamination opens a crevice between the metal and the coating and there is free access of the solution to the interfacial zone. In the presence of an applied cathodic potential, our interpretation is that the diffusion path is largely through the coating when there is an applied cathodic potential whether or not there is a defect in the coating. We do not believe that all the ions diffuse through the coating, but we do believe that the ions which act as the counterions for the OH^- ions generated by the cathodic reaction at the delaminating front diffuse through the coating.

Table III

Representative Diffusion Coefficients for Na^+ and Cl^- Ion Diffusion through Free Films

Film	Diffusion Coefficient in cm^2/hr		Reference
	Na^+	Cl^-	
Alkyd		$7.6\text{-}40.3 \times 10^{-10}$	Sittal and Yaseen, 1978
Alkyd	8.3×10^{-10}		Svoboda et al., 1971
Cellulose Acetate	2.6×10^{-6}	6.3×10^{-7}	Glass and Smith, 1966
Epoxy-Polyamide	1.1×10^{-7}	1.7×10^{-8}	Glass and Smith, 1967
Neoprene	1.6×10^{-8}	2.4×10^{-9}	Glass and Smith, 1966
Pigmented Epoxy	3.1×10^{-9}	2.1×10^{-9}	Glass and Smith, 1966

Table IV

Values of the Ionic Diffusion Coefficients under an Applied Potential of -0.80 v Relative to Those Obtained under Open Circuit Conditions

Coating	Value of D under an Applied Potential of -0.80 v Relative to Open Circuit Conditions		
	Na^+	Cs^+	Cl^-
Alkyd Topcoat	8	6	3
Alkyd Topcoat Plus Primer	15	16	25
Polybutadiene	21	12	28

TABLE V

The Relative Diffusion Coefficients for the Ions, Na^+, Cs^+ and Cl^-, as Calculated for Coatings Having a Purposely Formed Defect and Equivalent Coatings without a Defect

Coating	Relative Values of D for Coatings Having a Purposely Formed Defect and Equivalent Coatings without a Defect		
	Na^+	Cs^+	Cl^-
Alkyd Topcoat			
Open Circuit	10	9	7
-0.80 v	0.9	0.8	4
Alkyd Topcoat Plus Primer			
Open Circuit	29	43	43
-0.80 v	2	20	2
Polybutadiene			
Open Circuit	5	3	7
-0.80 v	2	1.5	1.7

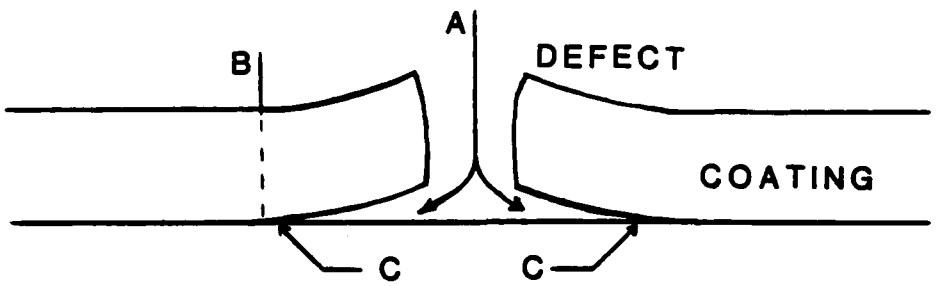

METAL

A: BULK ELECTROLYTE: M^+, X^-, H_2O

B: M^+, H_2O TRANSPORT THROUGH COATING

C: CATHODIC REACTION SITES:

$$H_2O + 1/2\ O_2 + 2e^- \rightarrow 2\ OH^-$$

REACTION LEADS TO DISBONDING

Figure 12. Schematic diagram of the two modes by which cations can reach the delaminating front.

The rationale for the diffusion of ions through the coating is elaborated on in Figure 12 which is a schematic of a defective coating on a metal substrate immersed in an electrolyte under cathodic polarization. The potential of the metal immediately under the defect is approximately equal to the applied potential whereas the potential becomes less negative at distances on the metal away from the defect because of resistance effects. The possible ionic conductance paths to the sites where the OH^- ions are generated may be within the liquid phase beneath the coating or it may be through the coating. Intuitively, the liquid path appears to be the more logical route for the ions to follow but the potential distribution is such that the cations will be electrically attracted to the region immediately at the defect where the most negative potential exists. The pathway through the coating is also a logical route because it is possible to achieve a very high pH and high cation concentration at the disbonding front without having the cation diffuse counter to the potential gradient at the metal surface. It is our conclusion based on the results summarized in Table V and the rationale above that the cations reach the disbonding site largely through the coating.

The data summarized in Figures 9-11 indicate that the number of Cs^+ cations in the coating and in the delaminated region at the interface is greater when there is an applied cathodic potential. The difference is slight in the case of the alkyd coatings but appreciable in the case of the polybutadiene coating. The similar slopes of ion uptake as a function of the delaminated area for both open circuit and an applied potential of -0.80 v suggest that the delamination mechanism is the same whether there is an applied potential or not. This conclusion is in accord with current thinking in that the delamination process is attributed to the fact that the oxygen reduction reaction occurs beneath the coating. These results also suggest that the cation transport is directly related to the disbondment process, most likely as a counter ion to OH^- ion production or bond breakage.

The question, "Is the cation flux through the coating sufficient to support the observed delamination rate?" can easily be answered provided the following assumptions are made. First, it will be assumed as an extreme case that the surface roughness factor of the steel is 10 and that every surface atom is involved in the bonding between the metal and coating. This assumption leads to the conclusion that there are approximately 10^{16} bonds per apparent cm^2 of the metal surface. Second, it will be assumed that each OH^- ion that is formed has the capability of breaking one surface bond. Third, it will be assumed that for each OH^- ion generated a cation will be available by diffusion through the coating. Let us now use these assumptions along with data generated for the diffusion of Cs^+ ions through a polybutadiene coating at an applied potential of -0.80 v. The delamination rate under these conditions is 0.24 cm^2/day as given in Figure 8. The cation flux under these conditions is approximately 10^{-7} moles/day or approximately 6×10^{-8} moles/day-cm^2 for the geometry used in the measurements as calculated from the data in Figure 4.

A flux of 6×10^{-8} moles/day-cm^2 and a delaminated area of 0.24 cm^2 leads to a required flux of 1.5×10^{-8} moles/day or 9×10^{15} ions. The number of bonds between the metal and coating, under the assumptions outlined above, that are broken per day to yield a delaminated area of 0.24 cm^2 is

2.4×10^{15}. The cation flux through the coating under an applied potential of -0.80 v is thus sufficient to provide counterions for the OH^- ions generated by the cathodic reaction.

CONCLUSIONS

We have shown that the introduction of a defect into a coating on steel, or the cathodic polarization of the substrate, results in a significant increase in the rate of ionic transport into the coating. Under open circuit conditions, the cations appear to travel along the coating/substrate interface from the defect site as delamination progresses. When a cathodic potential is applied, the primary diffusion pathway appears to be through the coating. Chloride ion diffusion is observed to accelerate under the potential gradient, probably due to one of several possible carry-along mechanisms. The ion flux has been shown to support observed cathodic delamination rates, suggesting the ions act as counter ions for the disbondment mechanism. Ion uptake-delamination area profiles for the systems studied showed almost no potential dependence, suggesting the disbondment mechanism is the same under open circuit and cathodic polarization conditions.

Literature Cited

Baboian, R.; McBride, L.; Langlais, R.; Haynes, G. Mater. Perf. 1979, 18(12) 40-44.

Dickie, R. A.; Hammond, J. S.; Holubka, J. W. Ind. Eng. Chem. Prod.Res. Dev. 1981, 20, 339-43.

Glass, A. L.; Smith, J. J. Paint Technol. 1966, 38(495), 203-09.

Glass, A. L.; Smith, J. J. Paint Technol. 1967, 39(511), 490-93.

Koehler, E. L. Corrosion 1984, 40, 5-8.

Leidheiser, H. Jr. Croat. Chem. Acta 1980, 53, 197-209.

Leidheiser, H. Jr. Ind. Eng. Chem. Prod. Res. Dev. 1981, 20, 547-51

Leidheiser, H. Jr.; Kendig, M. W. Corrosion 1976, 32, 69-76.

Leidheiser, H. Jr.; Wang, W. J. Coatings Technol. 1981, 53(672), 77-84.

Leidheiser, H. Jr.; Wang, W. In "Corrosion Control by Organic Coatings"; Leidheiser, H. Jr., Ed.; National Association of Corrosion Engineers: Houston, TX, 1981; 70-77.

Leidheiser, H. Jr.; Wang, W.; Igetoft, L. Prog. Org. Coatings 1983, 11, 19-40.

Leidheiser, H. Jr.; Granata, R. D.; Atkinson, J. M.; McBride, D. G. IBM Journal of Research and Development, Jan. 1985, in press.

McIntyre, J. Private communication.

Parks, J. Unpublished measurements.

Ritter, J. J.; Kruger, J. Surface Science 1980, 96, 364-74.

Sittal, R. R.; Yaseen, M. Pigment and Resin Technol. 1978, 2(2), 4-9.

Svoboda, M.; Kuchynka, D.; Knapek, B. Farbe u. Lack 1971, 77(1), 11-15.

Watts, J. F.; Castle, J. E. J. Materials Sci. 1983, 18, 1987-3003.

Program #12

Oxygen Diffusion through Organic Films as Influenced by the Electrolyte in Contact with the Film

Principal Investigator: Henry Leidheiser, Jr.
Prof. of Chemistry

Associate: Wayne Bilder
High School Teacher and
Part-Time Research Associate

INTRODUCTION

It has been shown previously that the delamination of organic coatings from a metal substrate radially from a defect when the coating is polarized cathodically is a function of many experimental variables [1]. Of great interest to us is the large differences in delamination rate among the alkali metal salts at equal concentration. The rate of delamination increases in the order lithium < sodium < potassium < cesium. It has also been reported re-recently [2] that the rates of blistering of organic coatings in acid media are reduced when alkali metal ions are present in the acid. In this case also the effectiveness in reducing blistering increases in the order lithium < sodium < potassium. The cathodic delamination results have been interpreted in terms of the differing rates of diffusion of the hydrated alkali metal ion through the organic coating and the blistering experiments have been tentatively associated with the competition between hydrogen ions and hydrated alkali metal ions for diffusion sites through the coating.

It occurred to us that the alkali ion effect on the rate of cathodic delamination might possibly be accounted for by interference by the alkali metal ion in the coating with the diffusion of oxygen through the coating. It is well known that the rate of cathodic delamination is a function of the oxygen concentration in solution [3] and that no delamination occurs at moderate polarizing potentials in the absence of oxygen [4]. The experiments summarized herein were thus designed to determine if the presence of alkali metal ions in an electrolyte and under a potential gradient would affect the rate of diffusion of oxygen through a coating.

EXPERIMENTAL

The rationale used in the experiments was to duplicate as much as possible the experimental conditions existing during cathodic delamination experiments. thus, both potential gradients and concentration gradients were applied across the film so as to promote the diffusion of metal cations in the same direction as the oxygen concentration gradient. The concentration and potential gradients were such as to promote the diffusion of both oxygen and metal cation from the right hand side of the apparatus to the left hand side.

The cell utilized in the measurements is shown in Figure 1. The left-hand chamber contained an oxygen probe (Lazar Dissolved Oxygen Meter DO-166) sealed in a ground glass joint and a platinum cathode. The right hand chamber was fitted with a Ag/AgCl reference electrode, a carbon rod counter electrode and a fritted glass bubbler. The tubes to each chamber were used for the addition of electrolyte solutions and the passage of argon through the system. The test film was clamped between 1-1/2" diameter holes in the two chamber walls. The entire system was closed in a climate control box and the temperature was maintained constant at 30°C.

The experimental procedure was the following. The film was mounted between the chambers and the system was flushed with argon for 1 hour. The right hand chamber was then flushed with air and the output of the oxygen meter was followed as a function of time. Many experiments enabled us to determine a standard oxygen transmission for the dry film and only those films were utilized that exhibited this standard transmission. Films with minor defects were thus excluded by this technique. Other films falling outside the standard range were discarded and another film was used. When a suitable film was detected, the system was again purged with argon, oxygen-free electrolyte was added to both chambers, and the potential of the platinum electrode was potentiostatically controlled at -1.2 v. The electrolyte in the left hand chamber was 0.005M and that in the right chamber was 0.5M.

The diffusion of oxygen through two polymer films will be reported herein. Polyethylene films with a thickness of 0.8 mils were cut from commercially available sheets. Acrylic films were prepared by coating a Teflon block with acrylic spray paint (Magicolor-clear #5513-00). The film was stripped from the block after 24 hours and was cured at room temperature for at least a week. The film thickness was 1.5 mils.

The electrolytes were KCl, NaCl and LiCl prepared from reagent grade salts.

The oxygen concentration was followed continuously by recording the meter output on a strip chart recorder. The plots thus show no datam points.

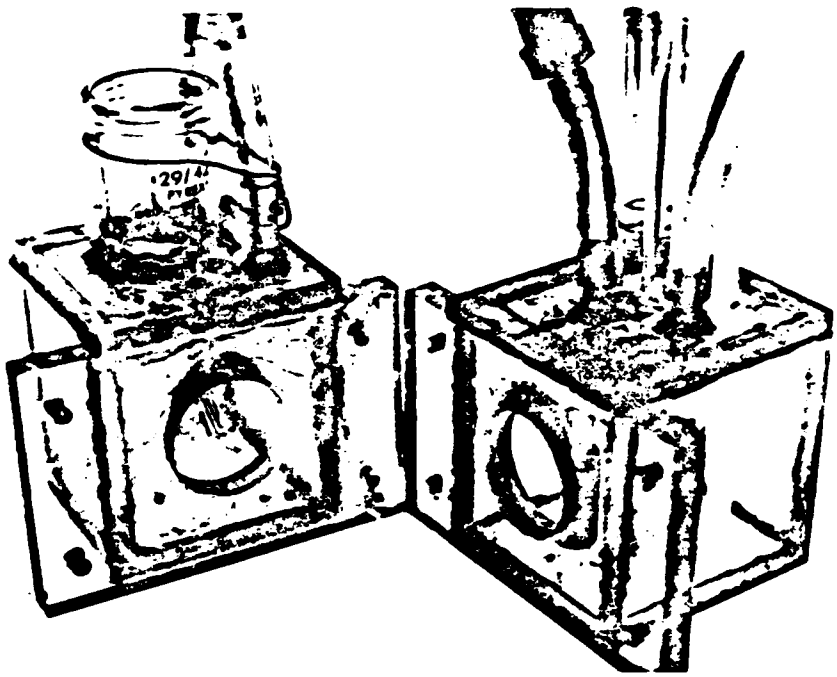

Figure 1. The unassembled diffusion cell.

RESULTS

Results typical of those observed for the polyethylene films in the absence of an applied potential are shown in Figure 2. The rates were approximately the same in the presence of the three alkali metal ions, lithium, sodium and potassium.

Results for the same three alkali metal ion solutions under conditions where the platinum cathode was maintained at a potential of -1.2 v vs. the Ag/AgCl electrode are summarized in Figure 3. The spread among the three alkali metal ions is greater than in the absence of the applied potential and the curves do fall in the same sequence as the rates of cathodic delamination, lithium < sodium < potassium. Data are summarized in Figure 4 for oxygen diffusion through 1.5 mil thick acrylic films when the cathode is maintained at a potential of -1.2 v vs. the Ag/AgCl electrode. As with the polyethylene films, the sequence is lithium < sodium < potassium.

DISCUSSION

The results summarized herein are preliminary in nature and we hesitate to draw conclusions until the data can be reproduced many times over. Differences in different pieces of the same film are a constant source of error and the making of valid comparisons requires judgment. Efforts will be made next to carry out the experiments with the different electrolytes on the same piece of film. Sufficient leaching will be required in this case to remove the electrolyte used in the prior experiment from the film.

At the present stage of the study it appears that the cations present in the electrolyte influence the rate of transmission of oxygen through the film when there is a combined potential and concentration gradient favoring the diffusion of the cation in the same direction as the oxygen.

REFERENCES

[1] H. Leidheiser, Jr., and W. Wang, J. Coatings Technol. 53, No. 672, 77 (1981).

[2] H. Leidheiser, Jr., H. Vedage, R. D. Granata and M. L. White, J. Electrochem. Soc. 131, 1460 (1984).

[3] H. Leidheiser, Jr., W. Wang and L. Igetoft, Prog. Org. Coatings 11, 19 (1983).

[4] H. Leidheiser, Jr., R. D. Granata, M. Atkinson, and D. McBride, IBM Journal of R. and D., to be published in January, 1985 issue.

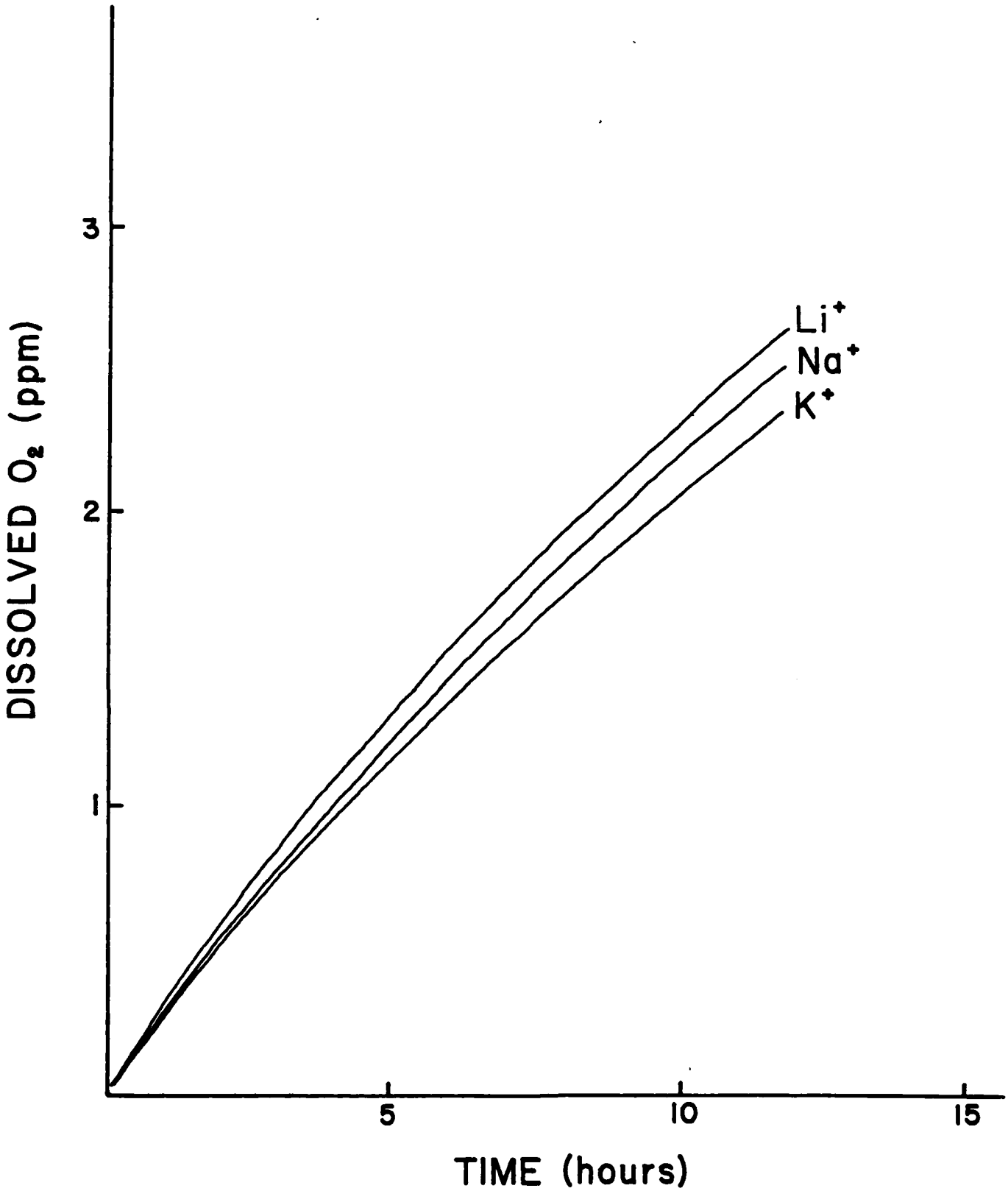

Figure 2. The transmission of oxygen through a polyethylene film in absence of a potential gradient. See text for details.

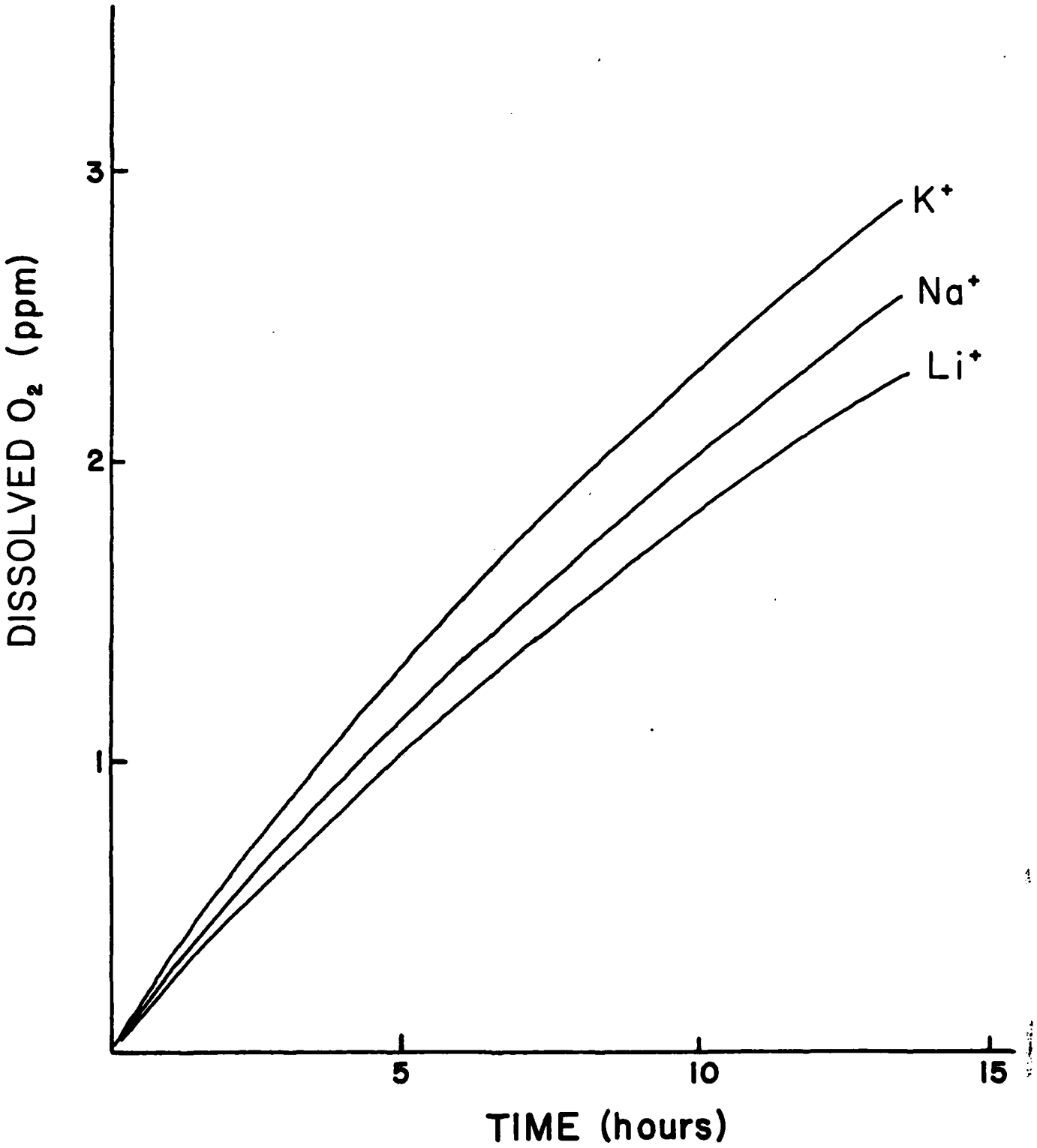

Figure 3. The transmission of oxygen through a polyethylene film in the presence of a potential and concentration gradient. See text for details.

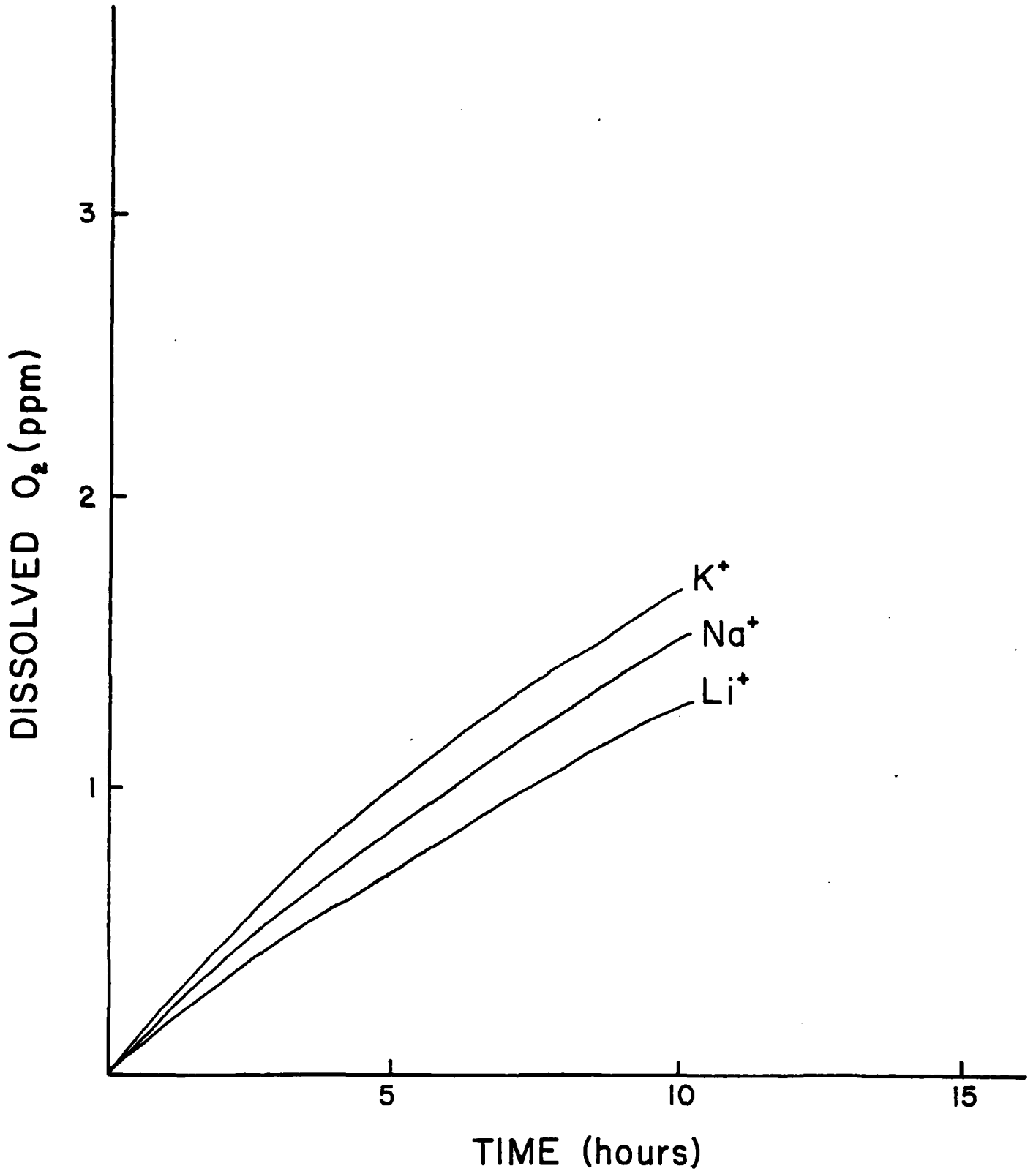

Figure 4. The transmission of oxygen through an acrylic film in the presence of a potential and concentration gradient. See text for details.

Program #13

Laser Raman Study of the Homogeneity of Epoxy-Amine Coatings

Principal Investigator: Eugene M. Allen
Prof. of Chemistry

ABSTRACT

A laser Raman microprobe is used to study the uniformity of electrodeposition of an epoxy-amine mixture. A peak ratio method tests for the mol fraction of amine in the coating; each peak is measured by a base-line technique. Unwanted fluorescence is minimized by heating the sample while running the spectrum.

In the preparation of epoxy films on steel, aqueous emulsions of Epon 1001 (diglycidyl ether or bisphenol A) and Emerez 1511 (a polyamide prepared from dimer acids and a diamine) are mixed and cathodically electrodeposited on the steel. The Emerez 1511 serves as the curing agent for the Epon 1001, presumably by reaction of the residual free amine groups of the Emerez with the epoxy groups of the Epon:

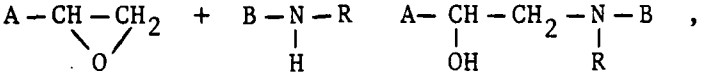

where A represents the residue attached to the epoxy group in Epon 1001, and B represents the residue attached to the amine group in Emerez 1511. The symbol R stands for either H, if the reactive amine is primary, or an organic moiety, if it is secondary.

The intent is to electrodeposit the Epon and Emerez in stoichiometric ratio, but this is very hard to achieve. The amount deposited depends strongly on the diffusion characteristics of the two reactants. One is likely to get layering and uneven film formation. We therefore wished to have a method of spot checking the deposited film, to determine whether the film is homogeneous or, if not, the degree of variation from spot to spot. Chemical analytical methods are not applicable because such methods are destructive, and too large a sample is required to furnish the required point-to-point information.

We investigated the applicability of the laser Raman microprobe to this problem, since this instrument is capable of examining areas as small as several μm^2. In order for such examination to be effective, spectra must be obtained which are capable of indicating the ratio of Epon to Emerez deposited. In this report we describe studies of films cast from solvent rather than electrodeposited, since only in this way can the ratio of the reactants be controlled easily.

MATERIALS AND METHODS

Materials. Films were cast by mixing solutions of Epon 1001 and Emerez 1511 in 1:1 methyl isobutyl ketone/toluene solvent. The mixtures were placed in aluminum evaporating dishes, and the solvent was allowed to evaporate at room temperature for several days. The samples were then heated at 150°C for one hour to complete the cure. Filings from the samples were placed on microscope slides for microprobe analysis.

Instrument. To obtain the Raman spectra, we used a "Molecular Optics Laser Examiner" (MOLE), which is the trade name for the Raman microprobe manufactured by Instruments S.A., Inc. The excitation source was 5145 Å line emitted by a Spectra Physics Model 164 Argon ion laser. In this instrument, the laser beam is focused down to a very small area of the order of several m by means of an NPL Leitz objective, and the scattered light is collected over a large angle by means of the same objective. The scattered light was detected by an RCA 31034 photomultiplier tube cooled to -30°C by means of a thermoelectric housing made by Products for Research (Model TE-104 RF).

Fluorescence Quenching. We were successful in obtaining Raman spectra of the starting materials, Epon 1001 and Emerez 1511, but found it impossible at first to get spectra of the cured reaction products. A large amount of fluorescence, generated by the laser beam, completely swamped the Raman spectra of the cured samples. We found, however, that we could quench most of the fluorescence by heating the samples to 140°-150°C while the spectrum was being run. The drop in fluorescent emission was roughly one order of magnitude, enough to make the Raman peaks easily measurable.

We used a microscope slide heater consisting of a thin plastic-imbedded heating element sandwiched between a copper block on top and an insulating

pad on bottom. The copper block was drilled for the insertion of a thermometer, and had a machined recess into which a microscope slide could be placed. We connected the heating element to a Variac transformer.

We chose a long focus objective lens of 50X magnification in the microscope, because we wished to avoid damage to the lens that might be caused by proximity to the heated microscope slide.

DEVELOPMENT OF ANALYTICAL METHOD

Raman Spectra. Figures 1, 2 and 3 show, respectively, Raman spectra of Epon 1001, Emerez 1511, and a solvent cast film (uncured) obtained by mixing stoichiometric amounts of the two reactants. (The stoichiometry was based on reacting one gram-equivalent of epoxy from Epon 1001 with one gram-equivalent of amine from Emerez 1511.) Each spectrum, of course, represents only a few μm^2 at most of the surface of each sample, but repeat spectra on different areas showed no significant differences.

A strong peak at 1609 cm^{-1} exists for Epon but is absent in the Emerez spectrum. The strongest peak in the Emerez spectrum occurs at 1442 cm^{-1}; this peak is not apparent in the Epon spectrum, although there is a minor peak close by at 1460 cm^{-1}. The 1:1 stoichiometric mixture displays the 1609 cm^{-1} Epon peak, and also a composite peak at 1448 cm^{-1} - 1461 cm^{-1} that coincides roughly with both the Emerez 1442 cm^{-1} peak and the Epon 1460 cm^{-1} peak. It is interesting, however, that the ratio of the height of the 1461 cm^{-1} peak to the height of the 1609 cm^{-1} peak is much greater for the stoichiometric mixture than for the Epon 1001 alone.

Peak Ratio Method. We investigated the ratio between the height (above base line) of the 1461 cm^{-1} peak to the corresponding height of the 1609 cm^{-1} peak as an indicator of the relative amounts of Emerez and Epon originally present before cure. Figure 4 is a diagrammatic representation of the two peaks. We took photon counts at points A (1400 cm^{-1}), B (1460 cm^{-1}), C (1500 cm^{-1}), D (1609 cm^{-1}), and E (1650 cm^{-1}). We defined the peak ratio as $\overline{BF}/\overline{DG}$, to be calculated as follows, where the lower case letters represent photon counts at the frequencies designated by the corresponding capital letters.

$$\text{Peak ratio},\% = \frac{b - [(40\underline{a} + 60\underline{c})/100]}{d - [(41\underline{c} + 109\underline{e})/150} \times 100 .$$

For these determinations, we set the slits of the MOLE at 500 μ and the power at the source of 500 mw. We scanned from 1399 cm^{-1} to 1401 cm^{-1} at a rate of 10 cm^{-1}/min, and programmed the instrument to count at 40 stations per cm^{-1}; the mean square photon count over all the counting stations was taken as the reading $\underline{a}$. We did similarly at the other four frequencies. The microcomputer associated with the instrument calculated the mean square photon count

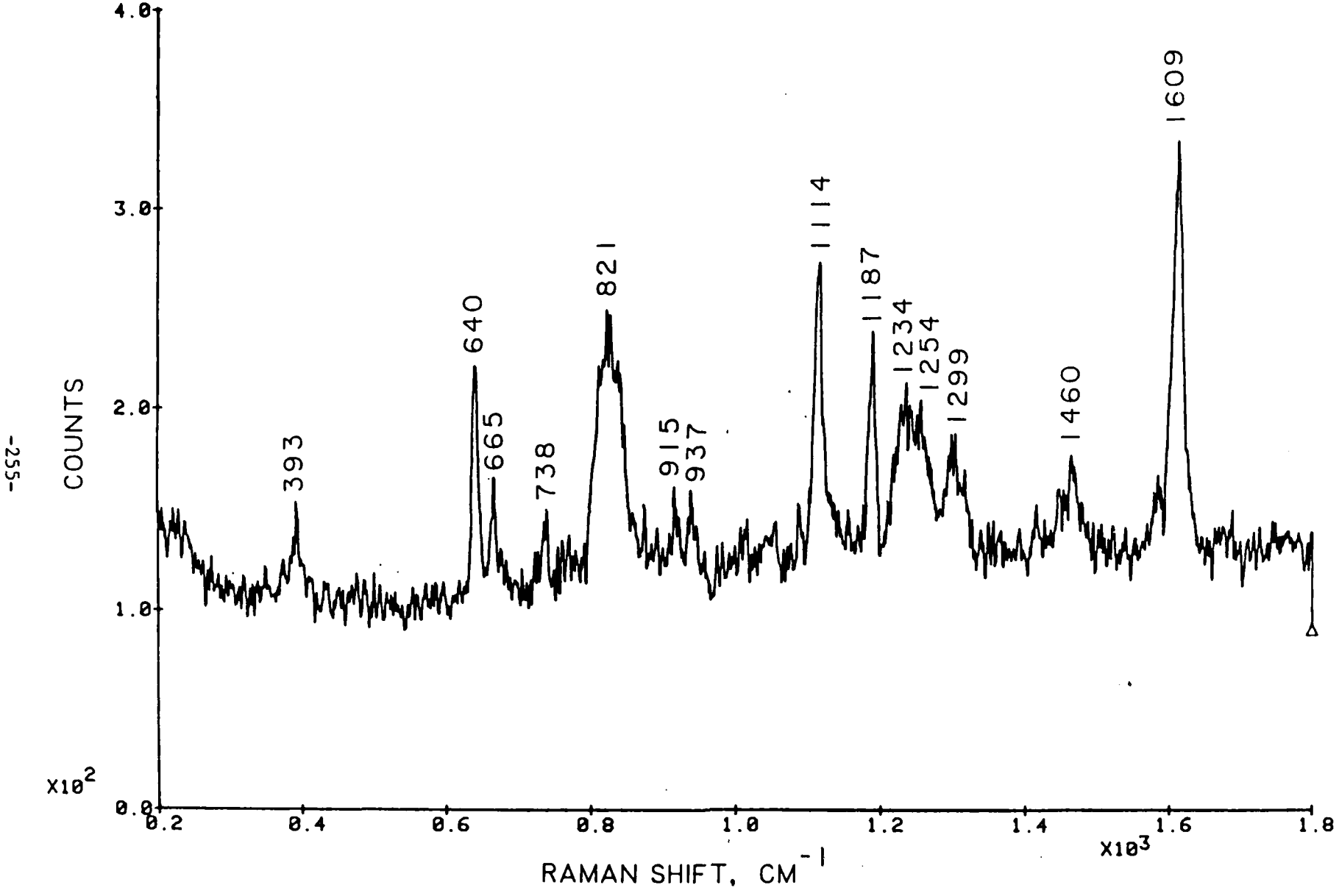

Figure 1. Raman spectrum of Epon 1001.

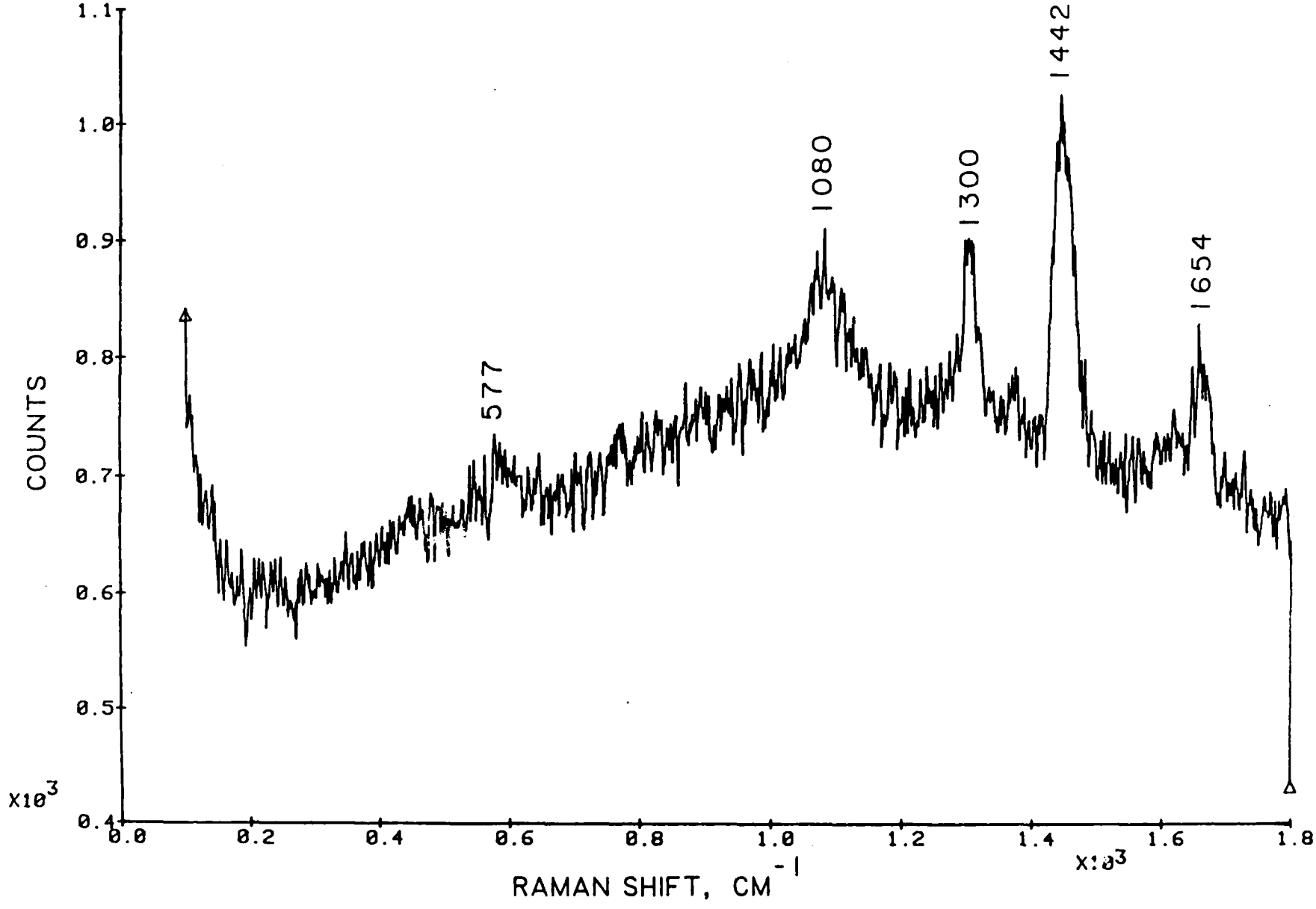

Figure 2. Raman spectrum of Emerez 1511.

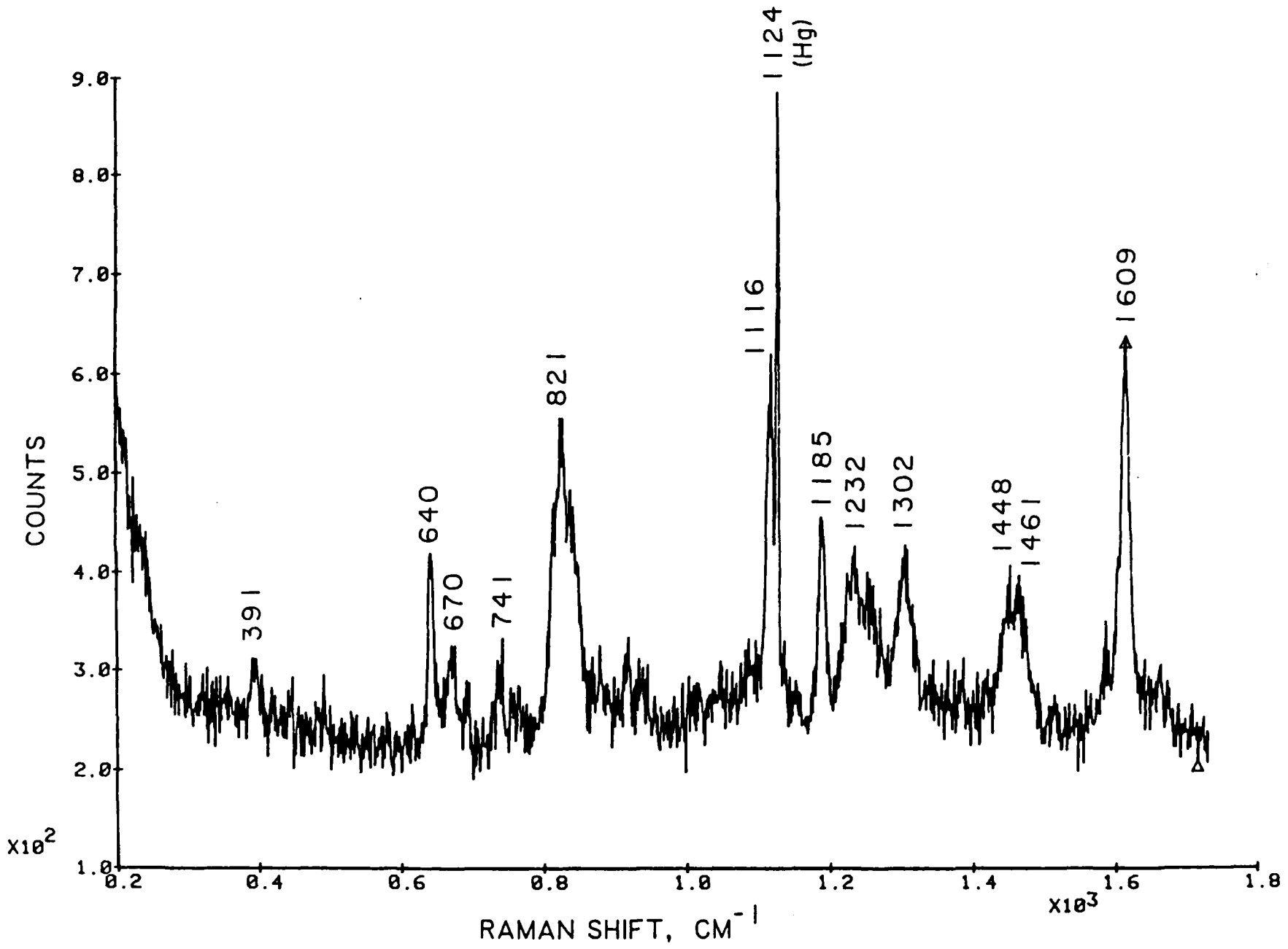

Figure 3. Raman spectrum of stoichiometric mixture of Epon 1001 and Emerez 1511.

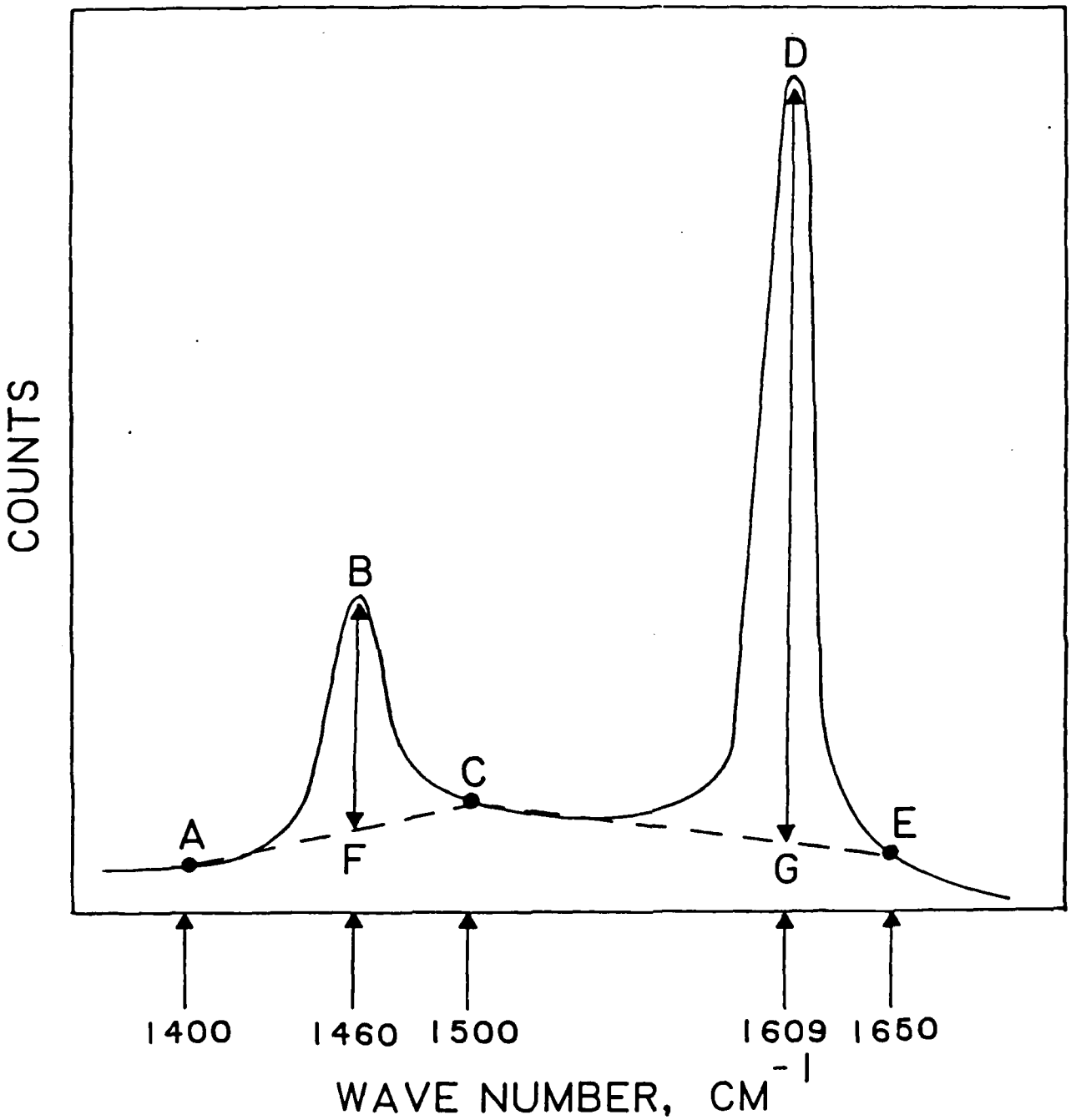

Figure 4. Schematic diagram of peak ratio method.

at each of the five analytical frequenceis, and was programmed to calculate the peak ratio by the equation given above.

RESULTS

We prepared cured samples having various stoichiometric ratios of Emerez 1511 to Epon 1001. We examined each sample at a minimum of three and usually four points on the surface, and made several peak ratio determinations at each point without disturbing the sample or the microscope. Table I shows the results.

Separate analyses of variance on each of the samples show that at the 95% level there are no significant differences between points for any of the samples. We therefore pooled all the results for each sample to calculate an overall mean and 95% confidence limits. These are given in Table I and plotted in Figure 5.

The variances of the individual samples are sufficiently homogeneous to allow of pooling all the results into a regression line. The equation of this line is:

$$P.R. = 21.38 + 21.58\ M.R. \quad ,$$

where P.R. is the peak ration and M.R. the mole ratio.

Using equations found in statistical texts [1,2], we can calculate the confidence limits of a determination of mole ratio from a given set of readings of peak ratio. If four replicate determinations on a given spot are made, the 95% mole ratio confidence limits are about ±0.4; if the number of replicates is increased to nine, the confidence limits are about ±0.3. This precision is sufficient to detect pronounced inhomogeneities in the film.

REFERENCES

[1] P. D. Lark, B. R. Craven, R.C.L. Bosworth, "The Handling of Chemical Data," Pergamom: Oxford, 1968; Chapter IV.

[2] F. S. Acton, "Analysis of Straight Line Data," John Wiley: New York, 1959.

Table I

Peak Ratio as a Function of Stoichiometric Ratio
of Emerez 1511 to Epon 1001

Stoichiometric Ratio, Emerez 1511/Epon 1001	Point 1	Point 2	Point 3	Point 4
0.25	26.34	15.47	28.83	23.82
	24.31	29.94	21.20	22.09
	31.07	21.77	34.46	35.93
	19.14	26.16	38.83	37.04
				35.33
				23.60
				14.71
Mean	25.22	23.34	30.83	27.50
Overall Mean and 95% Confidence Limits		26.84 ± 3.47		
0.50	33.22	49.70	37.71	30.55
	20.83	26.67	27.01	32.39
	47.12	21.64	23.77	26.63
	45.96	25.44	28.79	29.26
		37.70		
Mean	36.78	32.23	29.32	29.71
Overall Mean and 95% Confidence Limits		32.02 ± 4.54		
0.75	41.46	40.50	26.86	34.27
	39.12	35.74	39.70	24.74
	48.87	31.96	26.11	38.32
		50.43	35.95	29.92
Mean	43.15	39.66	32.16	31.81
Overall Mean and 95% Confidence Limits		36.26 ± 4.23		

Table I (Cont'd.)

Stoichiometric Ratio, Emerez 1511/Epon 1001	Point 1	Point 2	Point 3	Point 4
1.00	30.97	34.92	40.53	60.52
	37.92	30.55	55.00	65.26
	50.97	32.51	49.18	37.61
	42.20		63.03	44.65
Mean	40.52	32.66	51.94	52.01
Overall Mean and 95% Confidence Limits		45.05 ± 6.50		
1.50	49.04	47.55	54.38	
	56.78	52.84	58.57	
	51.50	56.18	62.51	
	44.31	47.19		
Mean	50.41	50.94	58.49	
Overall Mean and 95% Confidence Limits		52.80 ± 3.70		

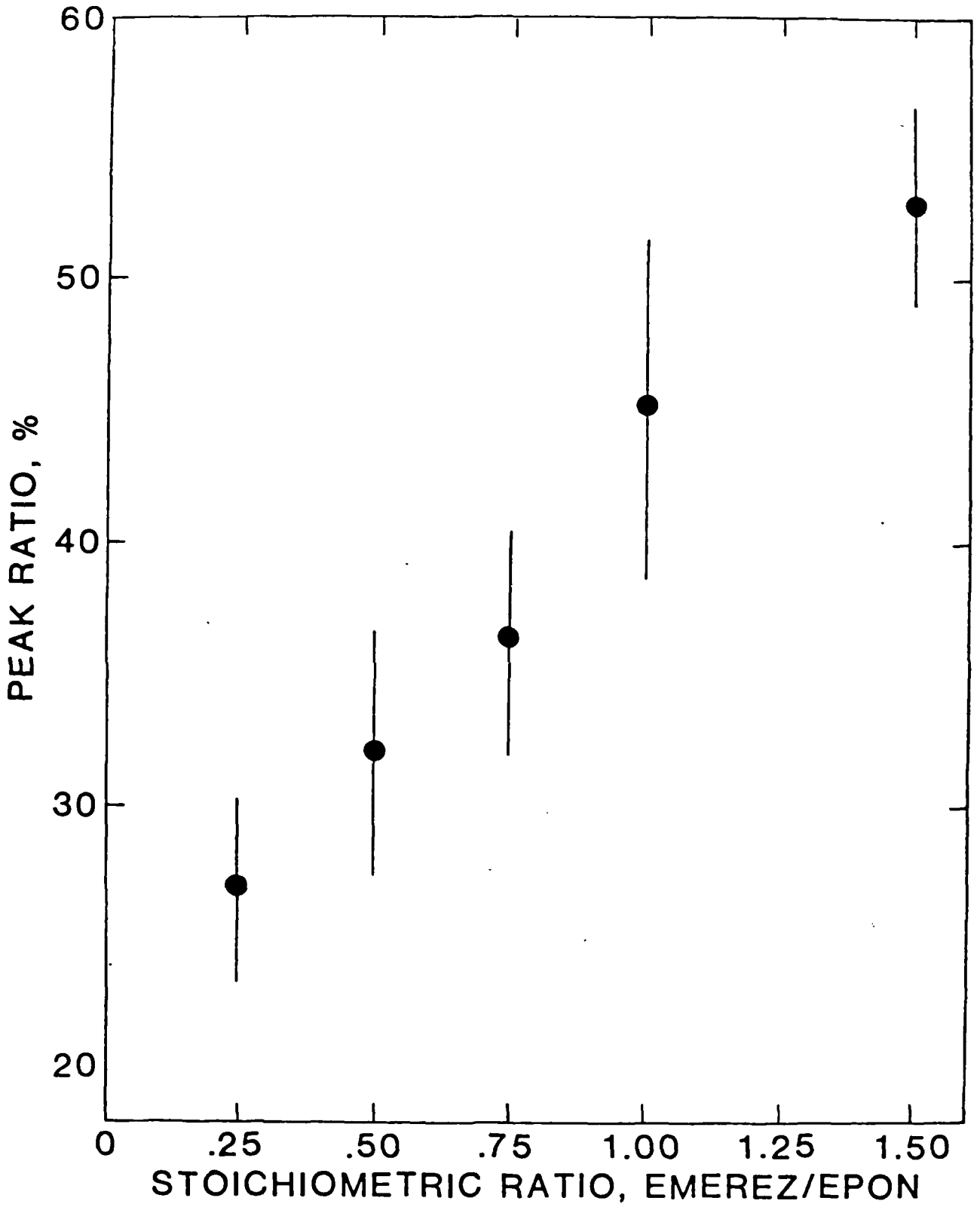

Figure 5. Means and 95% confidence limits for peak ratio determinations.

Program #14

Acid-Base Effects in Glass Bead/Phenoxy Model Coating Systems

Principal Investigator: John Manson
Prof. of Chemistry

Associate: A. Tiburcio
Graduate Student

INTRODUCTION

The goal of this research is to determine the effects of pigment(filler)-binder interaction on the permeability and other properties of model coatings for corrosion resistance. In the previous report period, the permeability to water vapor, dynamic mechanical response and solvent retention behavior of a model system comprised of glass beads as fillers (or pigments) and a linear high molecular weight phenoxy as the binder were investigated [1]. It was found that the incorporation of a high modulus filler affected these properties and that the degree of filler-matrix interaction can be interpreted in terms of acid-base (electron donor-acceptor) concepts. Emphasis on characterization by inverse gas chromatography (IGC) proved useful and showed the untreated and treated glass beads to be acidic and basic, respectively. As expected, for the electron-accepting phenoxy binder, maximum adsorption was obtained with the treated filler; a behavior consistent with electron donor-acceptor concepts. The results showed the permeability of glass bead-filled phenoxy films to water vapor to depend strongly on the degree of interfacial interaction; the greater the adhesion, the lower the permeability. In addition, the retention of the cellosolve acetate solvent was also reduced by the glass, especially with more basic glass. However, the dynamic mechanical spectrum was affected primarily through the presence of residual solvent.

During this report period, the applicability of IGC to composite systems was critically assessed, and experimental work on the glass bead-phenoxy system was continued, with emphasis on the analysis of untreated glass bead surface by IGC and on water vapor permeability at ambient temperatures. The usefulness

of Schreiber's interaction parameter, Ω [2], in characterizing the glass beads led us to extend the IGC work along more fundamental lines by relating Ω to the enthalpy of adsorption (ΔH_A). The value of the ΔH_A for a group of organic solutes (probes) was determined using an Arrhenius-type relationship, as proposed by Anhang and Gray [3]. Comparison of the ΔH_A data for acidic and basic probes enabled us to approximate the magnitude of the enthalpy of acid-base interaction, ΔH^{AB}, between the untreated glass bead filler and the basic n-butylamine probe. Furthermore, a series of experiments were conducted to show that the more basic probes were adsorbed and retained on the untreated glass surface, thus modifying the nature of the filler surface. Additional experiments provided evidence for the presence of different active sites.

To complement the permeability results of the earlier report [1], water vapor permeability measurements were conducted at room temperature. Activation energies of water vapor transport were calculated for some specimens, and comparison of the data for solvent-cast films and compression-molded samples made it possible to determine the effects of retained solvent on permeation. Also, the acquisition of a Fourier-Transform Infra-Red (FT-IR) Spectroscopy unit enabled us to confirm the presence of retained solvent in the phenoxy film, supporting gravimetric studies. Plans are being made to utilize the FT-IR to relate special shifts to the interaction between solvents and polymer.

This report briefly reviews the state-of-the-art with respect to IGC as applied to acid-base interactions, and describes and discusses progress with interfacial characterization and permeability of our model coating system.

Review: Applicability of IGC to Interfacial Characterization in Model Coatings

The application of IGC to determine physicochemical parameters involving the interaction of small amounts of volatile solutes (probes) has been reported by various investigators ever since the pioneering work of Smidsrod and Guillet in 1969 [4]. Recently, IGC was used to evaluate fillers and polymeric materials according to the acid-base concept of Fowkes et al. [2,5]. In our previous report, we utilized the normalized interaction parameter Ω (see below) proposed by Schreiber et al. [2] to characterize semi-quantitatively the overall electron donor/acceptor properties of glass-bead fillers [1]. An extension of this work along more fundamental thermodynamic lines would require the measurement of heats of adsorption of the probe on the filler. General considerations are discussed below.

Except for the reversal of roles of the solute probe and packing materials, the principle and instrumentation behind IGC is identical to that of gas chromatography (GC). In GC, the packing material serves to separate the various components of an unknown solute. In contrast, IGC utilizes specific solute probes to elucidate the interaction properties of the packing material, hence, the name "inverse gas chromatography." The retention time (t_R) of the probe molecule, the time an average molecule of solute takes to travel the length of the column, is obtained from the chromatogram. Thus an adjusted retention volume (V_R) can be computed by [6]:

$$V_R = JFt_R \qquad (1)$$

where F represents the carrier gas flow rate and J is a correction factor for gas compressibility. Since an inert molecule requires a finite amount of time simply to pass through the column, the actual retention volume or the net retention volume of the solute (V_N) can be more appropriately described by

$$V_N = V_R - V_M \tag{2}$$

where $V_M (V_M = Jt_M F)$ represents the mobile phase holdup. Finally, the specific retention volume (cm^3) characteristic of a particular combination of solute, stationary phase, and carrier gas can be computed by

$$V_g = \frac{273 V_N}{W_s T} \tag{3}$$

where W_s corresponds to the mass of stationary phase (g) present in the column and T is the column temperature (K).

Since the specific retention volumes are directly related to thermodynamic interactions [4,6], values of V_g for vapor probes that represent proton-donor or proton-acceptor types should reflect the acid-base characteristic of the packing material. Ideally, two probes that are identical in all respects except for their acceptor/donor properties should be selected. The comparison of V_g values of each probe provides a measure of the strength of the interaction between the probe and substrate. However, V_g may also be influenced by factors such as column preparation and the amount of injected solute [7]. More importantly, the value of V_g takes account of both the dispersion and acid-base interaction components of adsorption. Thus V_g does not correspond to the absolute magnitude of the adsorption energy due solely to specific donor/acceptor interactions. To minimize the contribution of the experimental variables and the dispersion component of adsorption, Schreiber et al. [2] suggested a normalized interaction parameter Ω defined as

$$\Omega = V_g(\text{Acid})/V_g(\text{Base}) \tag{4}$$

where $V_g(\text{Acid})$ and $V_g(\text{Base})$ are the specific retention volumes of the acidic and basic probes, respectively. It follows that when the two probes pass through the same column under identical operating conditions, a good estimate of Ω can be obtained by computing the ratio of the retention times of the acidic and basic probes [$\Omega = t_R(\text{Acid})/t_R(\text{Base})$].

Ideally, a neutral substrate would be expected to have Ω values of unity; for increasingly acidic or basic surfaces, Ω should tend to shift towards zero and high positive values, respectively. Thus, IGC provides a semi-quantitative way of measuring the acid-base properties of the substrate.

While the Ω parameter simplifies data interpretation, it does not explain the results along more fundamental thermodynamic lines. Several investigators (Olabisi et al. [4b], Schreiber et al. [8] and Su et al. [9],) have

used IGC data to determine χ interaction parameters for various organic solutes. Similarly, Anhang and Gray [3] have successfully applied an Arrhenius-type relation to measure the enthalpy of adsorption, ΔH_A, of non-polar probes with poly(ethylene terephthalate) (PET) as the substrate. Of the two methods, the direct measurement of ΔH_A would be more compatible with the acid-base concept because ΔH_A is related to the Drago equation [10] as adapted by Fowkes and Mostafa [11] for specific interactions at interfaces:

$$\Delta H^{AB} = C_A C_B + E_A E_B \qquad (5)$$

where ΔH^{AB} is the enthalpy of adsorption due to electron donor/acceptor interactions, C and E represent the Drago parameters which characterize the solid surface in terms of its ability to undergo specific interactions, respectively. The C and E terms reflect contributions of polarizability and electrostatic interactions, respectively.

Accordingly, Eqn. (6) represents the enthalpy of adsorption at effectively zero coverage of the surface by the solute:

$$\overline{\Delta H^{o}_{A}} = -R \frac{d \ln V_N}{d(1/T)} \qquad (6)$$

where $\overline{\Delta H^{o}_{A}}$ is the partial molar enthalpy of adsorption. This approach assumes ideal gas behavior and is most applicable to substrates on which surface adsorption dominates the solute-substrate interactions. IGC studies by Anhang and Gray [3] (using n-alkanes as probes and PET as substrate) yielded ΔH_A values that corresponded with latent heats of vaporization of the probes. This finding implies that a low degree of surface interaction between a neutral molecule and PET is predominantly due to dispersion forces, confirms the essential absence of acid-base effects, and reaffirms the validity of this approach. However, when the probe is able to participate in an electron donor/acceptor interaction, ΔH_A contains contributions from both dispersion and H-bonding:

$$\Delta H_A = \Delta H_d + \Delta H^{AB} \qquad (7)$$

where ΔH_d is the dispersion component of adsorption and ΔH^{AB} reflects the electron donor/acceptor effects of Eqn. (5). Obviously, a meaningful interpretation of ΔH_A in terms of acid-base concepts requires separation of the specific interaction from the dispersion component.

One simple approach involves the selection of a series of probes of known C and E parameters that span the range of donor/acceptor behavior, i.e., from strongly basic to neutral to strongly acidic. While this method does not measure ΔH^{AB} directly, comparison of the ΔH_A values of the various solutes provides a way to determine the relative H-bonding strength of the substrate.

In this sense, the selection of Schreiber et al. [2] of n-butylamine as the basic probe and t-butanol as the acidic probe to obtain Ω represents a special case. Since the two molecules are similar in size, the contribution of the dispersion components to ΔH_A is approximately the same. Thus the difference between the ΔH_A values for the two probes reflects the extent of electron donor-acceptor effects. For example, a basic probe will exhibit a high affinity for an acidic substrate while an acidic probe will experience repulsive forces. Since the ΔH^{AB} for the latter acceptor/acceptor pair is small, the dispersion term may very well dominate the overall energy of adsorption; a similar effect is expected for a donor/donor pair. Thus an approximate value of ΔH^{AB} is obtainable from the difference of the ΔH^{AB} of the two probes. A further check on the value of ΔH^d may be possible by comparing the ΔH_A of a neutral probe such as octane; in this case, ΔH^d should equal ΔH_A. Clearly IGC offers much promise as a convenient method for characterizing interfacial interaction in our model coatings, and in pigmented or filled coatings generally.

EXPERIMENTAL

Materials

A high-molecular-weight linear phenoxy (Union Carbide) was the binder. For fillers, glass beads of type 3000 (untreated) and 3000-CP03 (treated with an aminosilane coupling agent) were supplied by Potters Industries; particle sizes were ≤ 45 μm.

Inverse Gas Chromatography

Equipment. A Perkin-Elmer Sigma 3 Gas Chromatograph with a flame ionization detector was used for IGC measurements. Temperatures of the injection block, column, and detector cell were controlled by the instrument; the injection block and detector cell temperatures were set at 150°C. The average error in column temperature is ±1.0°C. The flow rate of the helium was controlled by the instrument.

Cu tubings, 1.22m × 0.64m O.D., were washed with acetone and methanol to remove impurities inside the column, and were then heated for a sufficient time period to ensure a "dry" column. Then 27.50 g of untreated glass beads were packed by a gentle tapping procedure into a column, whose ends were loosely plugged with glass wool, and the tubing was coiled to fit the oven chamber. Before each set of data collection the columns were conditioned by setting the column temperature above 100°C for several hours.

Probe Molecules. The selection of t-butanol as the acidic probe, n-butylamine as the basic probe, and octane as the neutral probe was based on work by Schreiber et al. [2]. For comparison, n-butanol was also used as a probe. The purities of the alcohols and n-butylamine were confirmed by FT-IR and FT-NMR. In addition, CCl_4 (essentially neutral) and $CHCl_3$ (acidic) were used as probes.

IGC Measurements. Several different chromatograms were obtained. For an isothermal run, the probe was injected into the column and passed through the column at constant temperature. Since the more basic probes were known to physisorb onto the untreated glass bead surface, it was decided to determine the presence of retained probe on the filler surface. This required a two-step process: an isothermal run followed by a "desorption run" (made by increasing the oven temperature at 10°C/min) immediately after the baseline for the isothermal measurement had stabilized. It should be emphasized that no probe was injected into the column prior to the "desorption run." Thus, the chromatogram derived from a desorption run was related to the amount of physisorbed probe during the isothermal run. A similar "heating run" was made to confirm the presence of different acidic sites on the untreated glass beads. In this case, the probe passed through a column whose temperature was increasing at a constant rate (10°C/min). Finally, three successive runs were made under isothermal conditions to investigate the effect of retained probe on V_N. The probe was injected for the second and third measurements immediately after the baseline of the previous run had stabilized.

To determine the enthalpy of adsorption of each probe with the unmodified glass beads, a series of measurements were made, at least in duplicate, from 60°C to 160°C. Sample size was kept constant at 0.5 µl and a flow rate of 30 ml/min was used for all measurements. The retention time, t_R was calculated from the point where the samples chromatogram initially deviated from the baseline. The "air peak" was obtained by determining the retention volume of methane. Inlet pressure was read directly from the instrument while the outlet pressure was assumed to be atmospheric pressure. Care was taken to flush residual solutes from the column by heating the column in between measurements.

Film Preparation

The solvent-casting procedure and formulation for the glass-bead-filled phenoxy films have been reported earlier [1]; all films were ~0.1 mm thick. The solvent-free films were made by compression-molding phenoxy pellets between Mylar sheets at approximately 180°C and 10,000 lb pressure for 3 minutes. The samples were then quenched in water and vacuum-dried to constant weight.

Permeability Testing Procedure

The permeability measurements were carried out at room temperature using the procedure described previously [1].

RESULTS AND DISCUSSION

Inverse Gas Chromatography

Using the untreated glass beads as the column packing, the temperature dependence of the IGC retention data for a number of organic probes was

obtained and plotted in Figure 1. From the slopes of ln V_N vs 1/T, the values of ΔH_A corresponding to the various solutes were calculated and are shown in Table I. The selection of n-butylamine, t-butanol, and octane as the electron donor, electron acceptor, and neutral probes, respectively, followed the work by Schreiber et al. [2] on the characterization of fillers by IGC. In addition, the adsorption behavior of two Lewis acids, $CHCl_3$ and n-butanol, and the neutral CCl_4 was investigated.

Comparison of the ΔH_A values on Table I and analysis of Figure 1 suggest that the untreated glass surface has a high affinity for the electron-donating probe; the net retention volume of n-butylamine being much larger than the other solutes throughout the whole temperature range. This high degree of interaction manifests itself in ΔH_A and Ω (Table II). As expected, Ω is less than unity, indicating a predominantly acidic surface. Ω also appears to be temperature-dependent, increasing at higher temperatures. Similarly, ΔH_A for n-butylamine is considerably greater than for t-butanol (19.1 kcal/mole vs. 6.8 kcal/mole below 100°C and 9.2 kcal/mole vs. 6.5 kcal/mole above 100°C)[1]. The n-butanol exhibits a similar adsorption behavior, reflecting the molecular similarity of the two alcohols.

Table I

Enthalpy of Adsorption of the Various Probes with Untreated Glass Beads

Probe	ΔH_A (kcal/mole)		
	60-90°C		100-160°C
n-butylamine	19.1		9.2
octane	--	7.8	--
t-butanol	6.8	--	6.5
chloroform	--	5.6	--
n-butanol	7.1	--	4.5
carbon tetrachloride	--	3.7	--

Evidently, for n-butylamine, n-butanol, and t-butanol, the strength of the interaction between the probe and substrate is greater below 100°C. Apparently, the glass bead surface contains active sites with varying degrees of acidity (see below); a similar observation was reported by McCarthy [12] for

[1] Conversion: 1 kcal/mole = 4.18 kJ/mole.

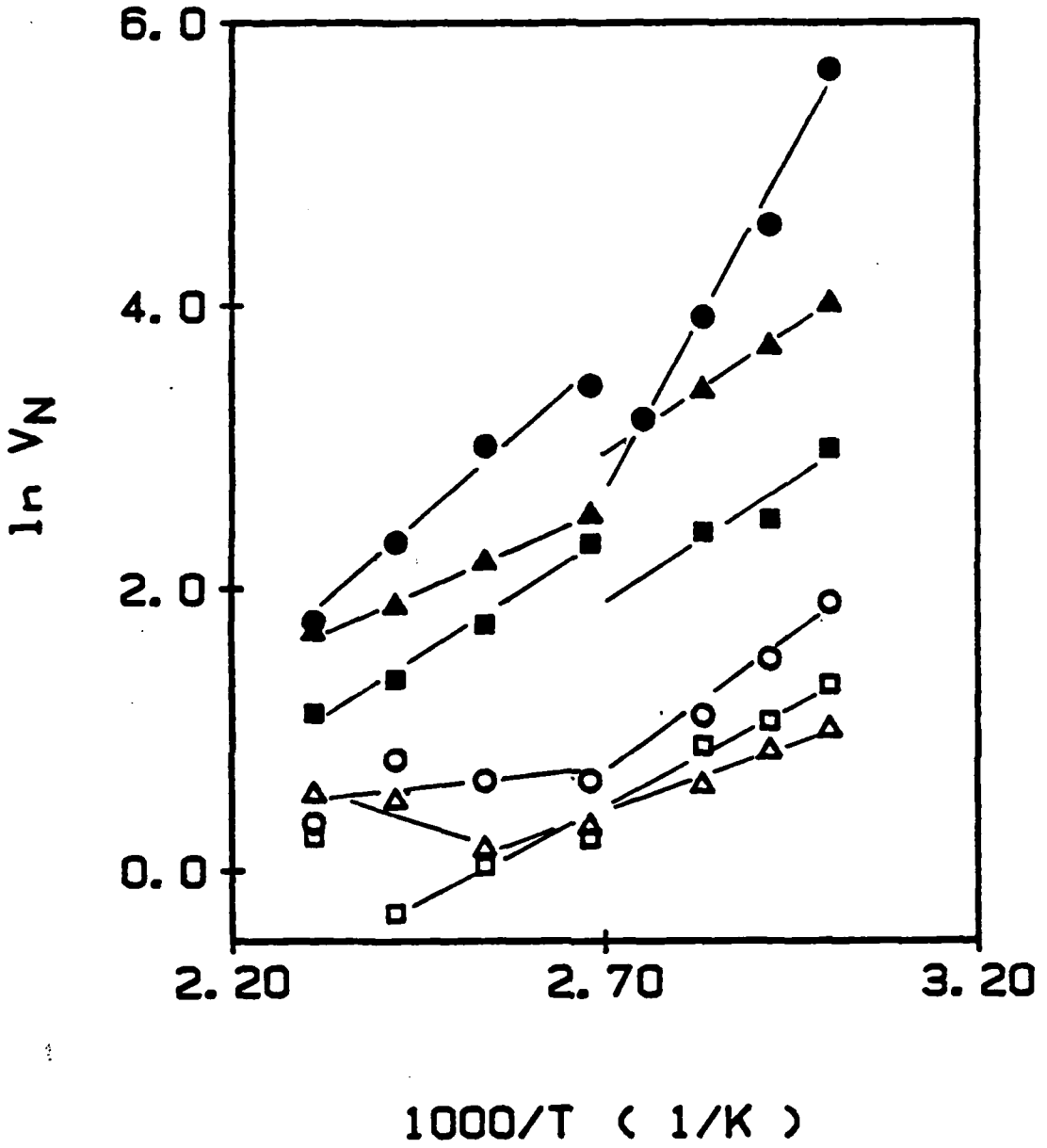

Figure 1. Retention diagram of the untreated-glass-sphere with various organic probes: ●, n-butylamine; ▲, n-butanol; ■, t-butanol; ○, octane; □, $CHCl_3$; △, CCl_4.

Table II

Interaction Parameters Ω[a] for the Untreated Glass Beads

T(°C)	Ω[b]	Ω[c]	Ω[d]
60	0.71	0.07	0.013
80	0.87	0.22	0.048
100	0.73	0.33	0.040
120	0.73	0.33	0.051
160	0.95	0.52	0.22

[a] Ω was taken to be V_N(acidic)/V_N(n-butylamine).

[b] n-butanol is the acidic probe.

[c] t-butanol is the acidic probe as proposed by Schreiber et al. [2].

[d] $CHCl_3$ is the acidic probe.

titanates. At the lower temperatures, all the sites are capable of charge transfer with the basic solute. Above 100°C, adsorption is limited to the strongest acidic sites, significantly reducing probe-substrate interaction. It is true that t-butanol and n-butanol have some basic character due to the two unshared pairs of electrons on the oxygen atom. However, the interactions are smaller than in n-butylamine because the alcohols are weaker electron donors.

The difference between t-butanol and n-butanol in Figure 1 is attributable to the relative strength of these two probes as electron acceptors. In the gas phase, n-butanol is more basic than t-butanol, explaining the higher V_N value of n-butanol throughout the whole temperature range [13]. Since the two are nearly identical in size, ΔH^d must be approximately the same. Thus, the difference in the V_N value reflects the stronger acid-base interaction between n-butanol and the untreated glass. In Table I, ΔH_A for the n-butanol is slightly higher than t-butanol below 100°C, but lower above 100°C. The reason for the lower ΔH_A for n-butanol above 100°C is not known.

Comparison of ΔH_A for octane, $CHCl_3$ and CCl_4 yields some interesting observations. Since $CHCl_3$ and CCl_4 are approximately similar in size, the magnitude of the dispersion component for both solutes should be about the same. Thus, the higher ΔH_A value for $CHCl_3$ suggests the presence of some basic sites on the glass bead surface (which is, however, known to be predominantly acidic [12]). At the same time, the higher value of ΔH_A for octane, in comparison to

CCl_4, reflects the larger London dispersion interaction of the bigger alkane molecule with the substrate. Also, it is not surprising that CCl_4, a small neutral probe, has the lowest ΔH_A. Similarly, $CHCl_3$, which is smaller and more acidic than t-butanol or n-butanol, exhibits a significantly lower degree of adsorption with the electron accepting surface of the glass beads.

Analysis of the ΔH_A values for octane, t-butanol and n-butylamine may prove useful in elucidating ΔH^{AB} for the n-butylamine/glass bead combination. Accordingly, the difference between the ΔH_A of the basic and acidic probes reflects the magnitude of ΔH^{AB}. Furthermore, the fact that ΔH_A for octane is only slightly larger than t-butanol implies that ΔH_d must be in the range of 7 kcal/mole. Thus, approximate values of ΔH^{AB} for the n-butylamine/glass bead pair are found to be 12 kcal/mole below 100°C and 2 kcal/mole above 100°C.

The discussion above establishes the relationship between ΔH_A and Ω. These findings reaffirm the usefulness of Ω to characterize the acid-base behavior of various materials. However, two factors may affect Ω: temperature and probe selection. In Figure 1, V_N for the n-butyl amine <u>decreases</u> more than V_N for the alcohol probes with increasing temperature. This is so because the kinetic energy of the probe molecules increases at higher temperatures, lowering the interaction of the stronger electron-donating n-butylamine to a greater extent than the alcohols. From Eqn. (4), it follows that Ω will increase at higher temperatures. In addition, Table II suggests that the strength of the acidic probe also affects Ω. For all three cases, the interaction parameter characterizes the surface of the untreated glass as being acidic overall ($\Omega < 1$). However, the <u>decrease</u> in value of Ω at each temperature parallels the <u>increase</u> in the relative acidic strength of the probe ($CHCl_3$ > t-butanol > n-butanol). Thus, the dependence of Ω on temperature and probe selection poses potential problems. In this sense, characterization by measuring ΔH^{AB} provides a more fundamental and general approach, but it is also more time-consuming.

As mentioned above, the discontinuities in Figure 1 for n-butylamine, t-butanol, and n-butanol suggest that the untreated-glass-bead surface may possess different active sites. The chromatograms of these probes provide further evidence for the presence of these active sites. During a "heating run" (70°C to 180°C), the n-butylamine and the alcohols exhibit three and two peaks, respectively (Figure 2). Since FT-NMR and FT-IR of the three probes confirm the purity of each solute, the multiple peaks cannot be attributable to their isomers or other impurities. Thus the multiple peaks must indicate acidic sites with different energies of interaction.

For n-butylamine, the 3-peak maxima correspond to the following temperatures: 92, 107, and 132°C; n-butanol exhibits maxima at 91 and 115°C while the t-butanol maxima appear at 77 and 111°C. These results are reproducible but the actual position of the peak maxima may vary by 2-5°C for different runs.

In contrast, a similar "heating run" for CCl_4, $CHCl_3$, and octane yields only <u>one</u> maximum. For the relatively neutral probes octane and CCl_4, the different acidic sites will not significantly affect their adsorption behavior because the interaction is predominantly due to dispersion forces. At the same time, since the acidic $CHCl_3$ undergoes repulsive interactions, adsorption will not be as strong as with the more basic probes above.

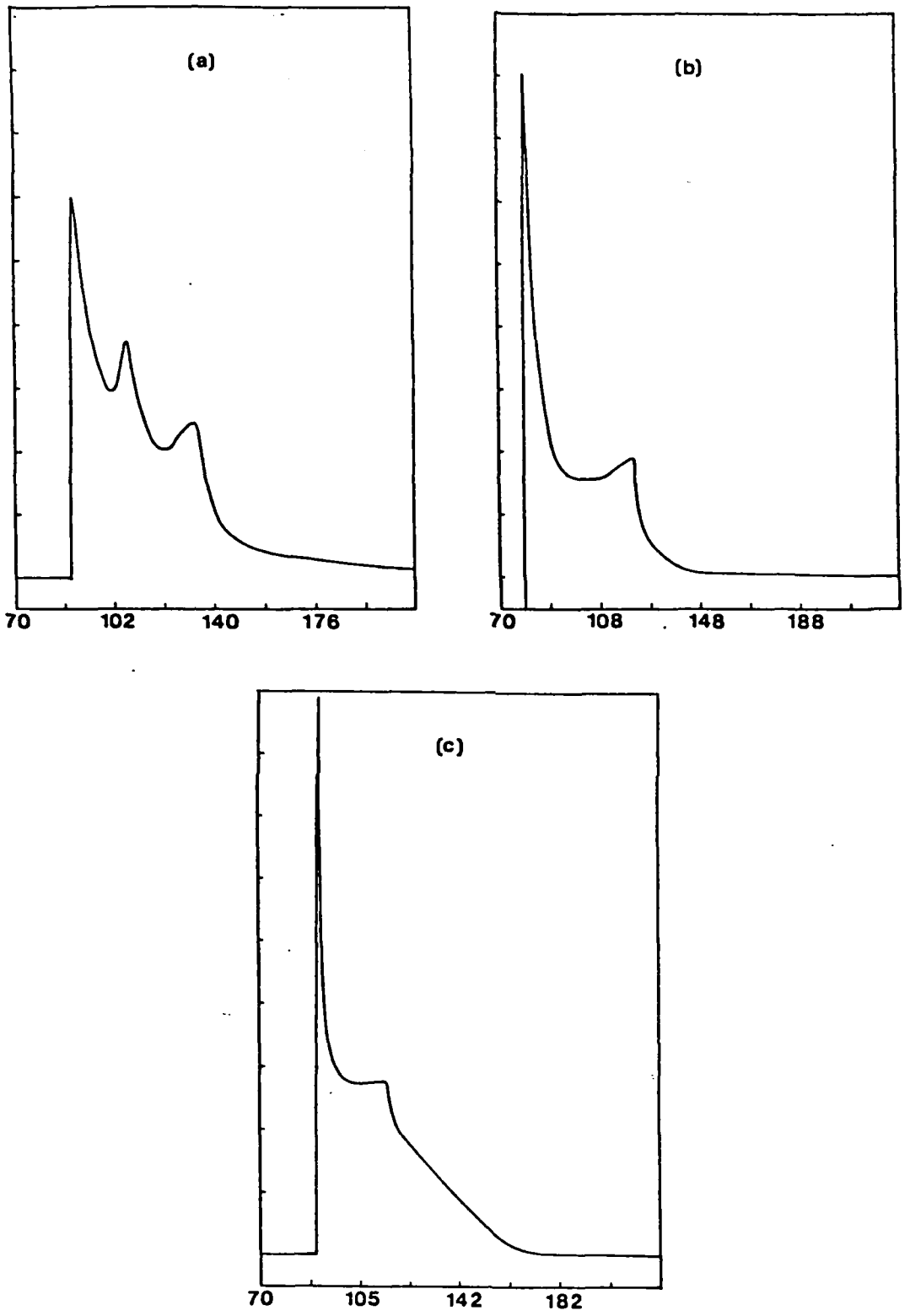

Figure 2. Heating run chromatograms of various probes at 10°C/min: (a) n-butylamine; (b) t-butanol; (c) n-butanol. Vertical axis corresponds to arbitrary units of solute concentration. Horizontal axis represents temperature (°C).

Additional experiments reinforce the correlation between the multiple peaks and different acidic sites. The selection of the initial temperatures reflects the significance of the peak maxima for n-butylamine. A similar heating run starting at 100°C produced two peak maxima for n-butylamine, but only one for t-butanol and n-butanol. Furthermore, the number of peak maxima for n-butylamine reduces to unity for a "heating run" begun at 140°C.

The temperature dependence of the peak maxima and the decrease in the number of peak maxima as the starting temperature increases suggest active sites with different acidic strengths. Below 100°C, all sites are capable of charge transfer, while above 100°C, the weaker acidic sites interact with the probe to a lesser degree, probably because the probe possesses sufficient kinetic energy to overcome the energy of interaction. The overall behavior manifests itself in the ΔH^{AB} values in Table I, where ΔH^{AB} below 100°C is greater than above 100°C.

In previous IGC experiments, it was observed that the retention time of n-butyl amine and t-butanol decreased with each successive run. The retention time of the initial run was reproduced only after the column temperature has been raised for a sufficient amount of time, in effect, the retained probe was "flushed" out of the column. These findings indicated that the residual probes remained on the filler. Confirmation of the presence of retained probe was possible by making a "desorption run." Since no probe was injected prior to the run, the appearance of a chromatogram can only be attributed to the desorption of residual probe from the filler surface. Furthermore, only n-butanol, t-butanol and n-butylamine exhibited a desorption peak, reflecting the more favorable electron donor-acceptor interactions between probe and filler. Obviously, the retained probe modifies the filler surface, reducing the degree of interaction between probe and filler.

Table III exhibits V_N of all the probes for three successive runs at three different temperatures. The selection of 70, 100 and 160°C stresses the significance of the peak maxima of n-butylamine (see above). At 70°C, V_N for the second run of the two butanol isomers and n-butylamine decreases significantly, especially for the more basic amine probe; a smaller reduction is apparent at 100°C. In contrast, V_N for $CHCl_3$, CCl_4, and octane remains essentially the same for the three successive runs at 70 and 100°C, confirming the absence of retained probe. The data at 160°C reinforces the effect of physisorbed probe on V_N. Since most of the n-butyl amine desorbs above 130°C, no significant amounts of probe should remain on the filler surface above this temperature for the other solutes, producing a relatively constant V_N for all three runs. Indeed, Table III supports this adsorption-desorption phenomenon and is consistent with the discussion above. It also emphasizes the need to remove retained probe, a procedure which cannot be neglected.

Finally, the moles of probe adsorbed per unit area filler (Γ) have been calculated from the adsorption-desorption chromatogram above. As expected, Table IV shows the value of Γ for n-butylamine, the stronger base, to be almost double the value of Γ for t-butanol.

Table III

The Effect of Retained Probe[a] on Net Retention Volume (V_N)

t(°C)	Run Series	$V_N(cm^3)$					
		CCl_4	$CHCl_3$	n-butanol	t-butanol	Octane	n-butylamine
70	1st	2.40	2.89	40.8	12.1	4.5	94.4
	2nd	2.31	2.44	25.8	10.3	4.3	32.0
	3rd	2 36	2.07	20.4	10.4	4.5	33.7
100	1st	1.18	1.26	12.4	10.4	1.94	38.6
	2nd	1.45	1.31	11.4	8.63	2.21	34.0
	3rd	1.49	1.22	11.7	8.04	1.94	15.5
160	1st	1.72	1.17	5.60	3.03	1.36	5.83
	2nd	1.72	0.81	5.47	3.03	1.58	5.88
	3rd	1.72	1.62	5.24	3.12	1.31	5.92

[a]Three successive runs.

Table IV

Physisorption of Probe by the Untreated Glass

Probe	% of Adsorbed Probe	Moles Adsorbed	$\Gamma x10^7(moles/m^2)$
		$(1x10^7)$	
n-butylamine	20	7.2	9.7
t-butanol	8.0	4.3	5.7

Permeability

In the previous report period, the permeability of glass-bead-filled-phenoxy films to water vapor at 50°C was investigated [1]. The study was repeated at ambient room conditions in order to determine the effect of temperature on water vapor transport. Also, data on solvent-cast and compression-molded specimens provided some insight to the role of solvent in permeability.

Comparison of the data at the two temperatures (Table V) clearly shows the temperature dependence of the steady state permeability coefficient, P. The decrease in P parallels two interrelating factors: a reduction in the driving force of permeant transport due to a decrease in temperature and lower free volume in the films resulting from the experimental temperature being lower than the T_g's of all the films [1]. Using the Arrhenius relationship, calculation of apparent energies of activation, E_a, was possible for some specimens (the unfilled-solvent-cast film and 0.2 volume fraction treated glass). (Of course, the values are very approximate since so far data are available for only 2 temperatures.)

Comparison of E_a values (E_a = 1.5 kcal/mole for the unfilled-solvent-cast film and E_a = 1.7 kcal/mole for the 0.2 volume fraction treated glass), with an earlier study by Manson and Chiu on a glass-bead-filled epoxy system, reveals E_a for the phenoxy system to be on the low side [14]. Furthermore, Manson and Chiu reported considerably higher activation energies above T_g than below T_g. For these phenoxy systems, the T_gs of the various films (33°C for the unfilled to ~40°C for the film containing 0.2 volume fraction filler) falls between the two experimental temperatures. Thus, a more extensive study over a wider range of temperatures should follow to supplement these preliminary results.

Following the convention of the previous report [1], Table V exhibits the relative permeabilities (P_r) of the experimental values and those predicted by theory. As expected, at the same filler content, the untreated glass exhibits higher permeabilities than the treated glass, but the treated glass is still more permeable than the behavior predicted for the limiting case of good adhesion with an impermeable filler, P_i=0. Again, it appears that interfacial channeling more appropriately models both composite systems, particularly the untreated filler [1]. A P_i/P_{PL}[1] of 40 comes close to the P_r values of the untreated glass while a P_i/P_{PL} of 10 approximates the case of the treated filler. These findings are consistent with an earlier report which showed the phenoxy binder (an electron acceptor) to strongly adsorb onto the treated glass (an electron donor) but not the untreated glass (an electron acceptor), confirming the role of acid-base filler-matrix interactions [1].

Another factor to consider is residual solvent. Judging from the amount of retained solvent in these films (as much as 40% of the weight of an unfilled solvent cast film is solvent [1]), the solvent must play a significant role in permeability. Comparison of the compression-molded samples with the unfilled-solvent-cast films may help elucidate the effects of solvent.

---

[1] P_i/P_{PL} represents the relative permeability of the interfacial region and the bulk polymer.

Table V

Steady State Permeability Constants[a] of Phenoxy Films

Volume Fraction Filler	Experimental Permeabilities $P_c(P_r^b)$		Theoretical Relative Permeabilities* P_r^b		
	Untreated Glass	Treated Glass	$P_i=0$	P_i/P_{PL}[e]$=10$	$P_i/P_{PL}=40$
0(comp. molded)	3.0[c]	3.0[c]	--	--	--
0(solvent cast)	3.3[c],4.0[d](1.0)	3.3,4.0(1.0)	1.0	1.0	1.0
0.10	7.2[c](2.2)	4.5[c](1.4)	0.86	1.1	1.8
0.20	---------	5.2,6.5(1.6)	0.73	1.1	2.6

[a]Units: $g.cm/cm^2.Pa.s \times 10^{14}$.

[b]$P_r = P_c/P$ unfilled.

[c]Ambient temperature.

[d]Temperature, 50°C.

[e]P_i/P_{PL} represents the relative permeability of the interfacial region and the bulk polymer.

*See Reference [15] for the calculation of theoretical P_r.

There are two opposing points of view. On the one hand, considering the strength of interaction between solvent and binder, the solvent may act as an inhibitor to water vapor transport [1,15]. At both temperatures, the unfilled solvent-cast film has lower P values than the glass-bead-filled films, even with treated glass. On the other hand, Table V indicates that the solvent-cast film has a slightly higher P value than the compression molded samples, but within experimental error. As mentioned in a previous report [1], the very high amounts of retained solvent plasticize the polymer and may in effect provide a continuous capillary network in the polymer phase, explaining the lower P value of the compression-molded sample.

An additional factor to consider is free volume. Since the compression-molded sample has a higher T_g than the solvent-cast films (74° vs 26°C), the compression-molded sample has a lower free volume at ambient temperatures. These results partly support both points of view and emphasize the importance of understanding the role of solvent in permeation. Study of the displacement of residual solvent by water vapor will also be timely, especially on how

displacement affects the amount of residual solvent and the transport properties of the film.

Application of FT-IR

Figure 3 shows the FT-IR spectra of three specimens: a solvent-cast film, a compression-molded sample, and the cellosolve acetate solvent. The band region from 1700 cm^{-1} to 1760 cm^{-1} corresponds to the carbonyl vibrational frequency of the cellosolve acetate. Since the pure phenoxy resin contains no carbonyl group, the presence of a carbonyl peak in this region is attributable to retained solvent. The assignment of the absorption band in this region for the compression-molded sample is not known, but comparison between the two phenoxy samples will confirm that the compression-molded sample band cannot be due to the carbon-oxygen double bond. Firstly, the band for the compression-molded specimen is split into two peaks, the more prominent peak appearing at a lower wavenumber. Secondly, the compression-molded sample is thicker than the solvent cast film, but the solvent-cast sample displays a greater degree of absorption, in contradiction to Beer's law. Thus, the solvent-cast band corresponds to carbonyl groups that are present in the phenoxy matrix, confirming the earlier gravimetric studies on retained solvent.

The use of FT-IR to measure acid-base energies of enthalpies of adsorption and to analyze the bonding scheme at the interface between filler and matrix is applicable to this work. Fowkes et al. have related the spectral shifts of carbonyl containing solvents and plasticizers interacting with a polymer to electron donor/acceptor interactions [16]. Similarly, Ishida and Koenig have studied the interfacial bonding between fiber filler and polymer matrix [17]. Plans are being made to incorporate these approaches to future work.

CONCLUSIONS

IGC Study

1. IGC results establish the relationship between the interaction parameter Ω and the enthalpy of adsorption. Ω values of less than unity for untreated glass complement the ΔH^{AB} for n-butylamine, characterizing the surface as being acidic overall.

2. Application of the Arrhenius relationship to IGC data was successful in determining ΔH_A.

3. The temperature dependence of Ω may limit its application to semi-quantitative characterization, but the method is sound and experimentally convenient.

4. The glass bead filler surface possesses different acid sites.

5. Physisorption of probe molecules significantly affect IGC measurements, reinforcing the importance of the removal of retained probe.

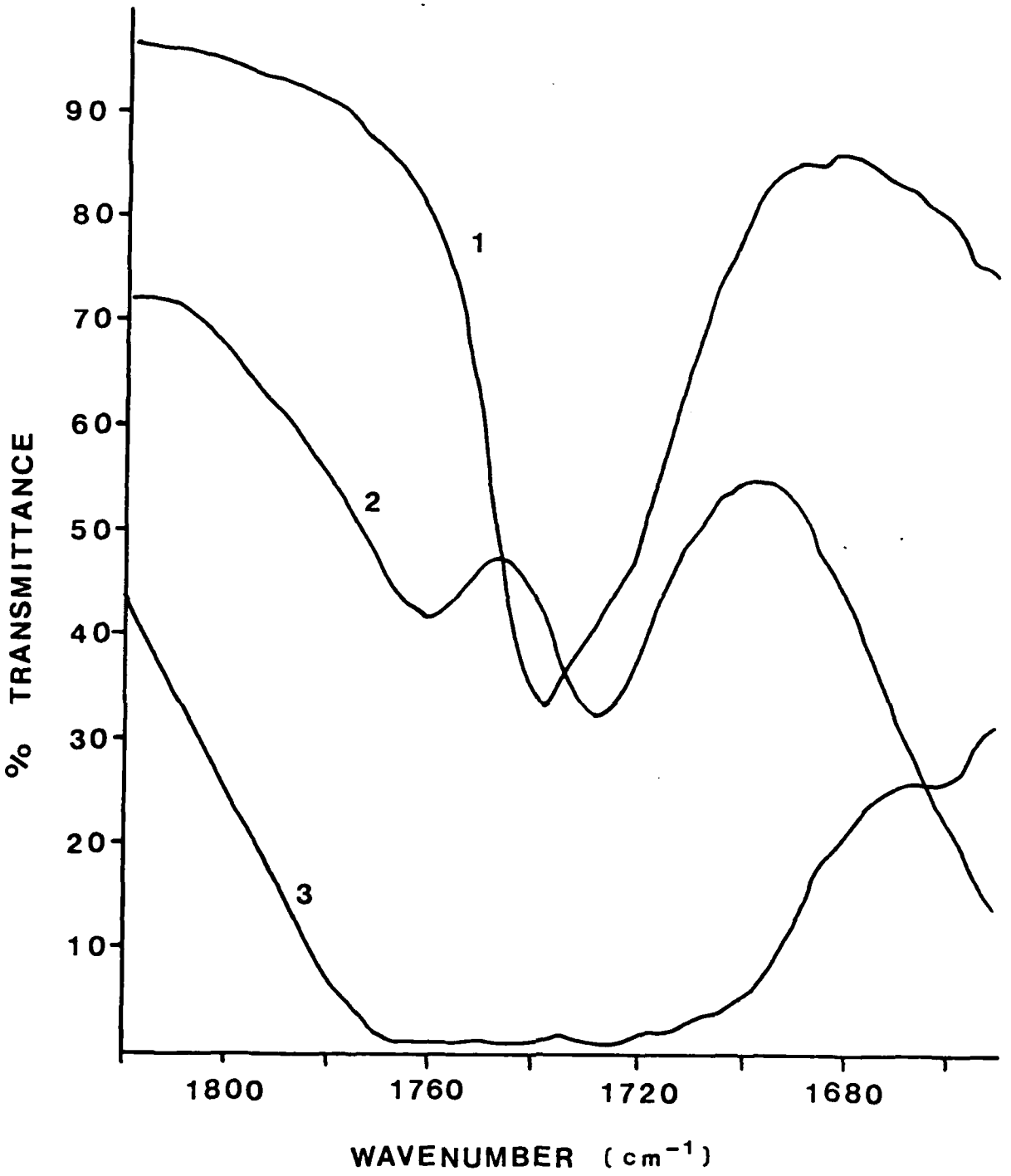

Figure 3. FT-IR spectra of: 1, solvent-cast phenoxy film; 2, compression-molded phenoxy (no solvent); 3, cellosolve acetate solvent.

Permeability

1. The treated glass is less permeable than the untreated glass at ambient temperature. Calculation of E_a for the phenoxy system exhibits values less than expected.

2. Solvent appears to play some role in permeability of water vapor through films.

FUTURE PLANS

The goals for the next year's studies are:

1. A continuation of the IGC work to determine C and E constants for the glass beads and the phenoxy matrix.

2. Use of FT-IR to study the interfacial bonding between filler and polymer matrix.

3. Completion of studies of the effect of temperature on permeability over a wider range of temperatures with various acid-base combinations, and estimation of apparent energies of activation for permeation from the slopes of the permeability vs 1/T.

4. Use of FT-IR techniques to study the displacement of residual solvent by water vapor.

5. Continuation of dynamic mechanical studies to determine complex modulus and glass transition temperature.

REFERENCES

[1] Annual Report, this project, 1983.

[2] a) H. P. Schreiber, M. R. Wertheimer, and M. Lambla, J. Appl. Polym. Sci. 27, 2269 (1982).

b) H. P. Schreiber, Org. Coat. Appl. Polym. Sci. 45, 22 (1982).

[3] J. Anhang and D. G. Gray, J. Appl. Polym. Sci. 27, 71 (1982).

[4] a) O. Smidsrod and J. E. Guillet, Macromolecules 2, 272 (1969).

b) O. Olabisi, L. M. Robeson, and M. T. Shaw, "Polymer-Polymer Miscibility," Academic Press, New York 1979.

[5] a) C. S. Flour and E. Papirer, Ind. Eng. Chem. Prod. Res. Dev. 21, 666 (1982).

b) C. S. Flour and E. Papirer, J. Coll. Int. Sci. 91(1), 69 (1983).

[6] J. R. Conder and C. L. Young, "Physicochemical Measurement by Gas Chromatography," John Wiley & Sons Ltd., New York, NY, 1979, Chapter 2.

[7] M. Galin and M. C. Rupprech, Polymer 19, 506 (1978).

[8] H. P. Schreiber, Y. B. Tewari, and D. Patterson, J. Polym. Sci.: Polym. Phys. Ed. 11, 15 (1973).

[9] C. S. Su, D. Patterson, and H. P. Schreiber, J. Appl. Polym. Sci. 20 1025 (1976).

[10] R. S. Drago, G. C. Vogel, and T. E. Needham, J. Am. Chem. Soc. 93, 6014 (1971).

[11] F. M. Fowkes and M. Mostafa, I&EC Prod. Res. Dev. 17(1), 3 (1978).

[12] D. C. McCarthy, Ph.D. Dissertation, Lehigh University (1984).

[13] J. E. Bartness, J. A. Scott, and R. T. McIver, Jr., J. Am. Chem. Soc. 101, 6046 (1979).

[14] E. H. Chiu and J. A. Manson, Org. Coat. and Plast. Preprints, ACS 32, 162 (1972).

[15] A. C. Tiburcio and J. A. Manson, Submitted, 1984.

[16] F. M. Fowkes, D. O. Tischler, J. A. Wolfe, L. A. Lannigan, C. M. Ademu-John and M. J. Halliwell, J. Polym. Sci.: Polym. Chem. Ed. 22, 547 (1984).

[17] a) H. Ishida and J. L. Koenig, J. Polym. Sci.: Polym. Phys. Ed. 17, 1807 (1979).

b) S. R. Culler, H. Ishida, and J. L. Koenig, Appl. Spect. 38(1), 1 (1984).

END

FILMED

4-85

DTIC